KINETIC ROUGHENING PHENOMENA, STOCHASTIC GROWTH, DIRECTED POLYMERS AND ALL THAT

Aspects of multidisciplinary statistical mechanics

Timothy HALPIN-HEALY[a,b], **Yi-Cheng ZHANG**[c]

[a] *Physics Department, Barnard College, New York, NY 10027-6598, USA*
[b] *Isaac Newton Institute, Cambridge University, Cambridge CB3 0EH, UK*
[c] *Institut de Physique Théorique, Université de Fribourg, Fribourg CH-1700, Switzerland*

ELSEVIER

AMSTERDAM – LAUSANNE – NEW YORK – OXFORD – SHANNON – TOKYO

ELSEVIER

Physics Reports 254 (1995) 215–414

PHYSICS REPORTS

Kinetic roughening phenomena, stochastic growth, directed polymers and all that. Aspects of multidisciplinary statistical mechanics

Timothy Halpin-Healy [a,b], Yi-Cheng Zhang [c]

[a] *Physics Department, Barnard College, New York, NY 10027-6598, USA*

[b] *Isaac Newton Institute, Cambridge University, Cambridge CB3 0EH, UK*

[c] *Institut de Physique Théorique, Université de Fribourg, Fribourg CH-1700, Switzerland*

Received August 1994; editor: I. Procaccia

Contents:

SSDI 0370-1573(94)00087-5

Abstract

Kinetic interfaces form the basis of a fascinating, interdisciplinary branch of statistical mechanics. Diverse stochastic growth processes can be unified via an intriguing nonlinear stochastic partial differential equation whose consequences and generalizations have mobilized a sizeable community of physicists concerned with a statistical description of kinetically roughened surfaces. Substantial analytical, experimental and numerical effort has already been expended. Despite impressive successes, however, there remain many open questions, with much richness and subtlety still to be revealed. In this review, we give an unorthodox account of this rapidly growing field, concentrating on two main lines – the interface growth equations themselves, and their directed polymer counterparts. We emphasize the intrinsic links among the topics discussed, as well as the relationships to other branches of natural science. Our aim is to persuade the reader that multidisciplinary statistical mechanics can be challenging, enjoyable pursuit of surprising depth.

1. Introduction

Consider a wheat field of dark golden hue and densely planted in level ground, being roughly rectangular in shape, but rather large in extent, and stretching lazily toward the distant horizon. On a cool, but calm August evening, with nary a breeze about, the edge of the field is ignited, in preparation for leaving the soil fallow the following season. The propagating fire front, initially straight by virtue of its birth along the edge, evolves in a kinetic, violent fashion and heads mercilously into the bulk of the field. Burning shafts of wheat communicate the conflagaration locally to their neighbors, and the narrow, bright, and tortuously shaped fire line, an interface separating the blackened region from the portion of the field soon to be consumed, becomes increasingly rough as random elements, such as local inhomogeneities in the moisture content or density of the wheat, begin to have a large scale cumulative effect.

Rather, consider a Petri dish filled with agar, amply nutritious, upon which is very carefully placed a stretched string, infested with common bacteria. Because the nutrient is present in abundance, the growth proceeds at a furious pace, being reaction rather than diffusion limited, with the *in situ* population doubling every half-hour. Soon, the consequences are observable on a scale visible to the naked eye- the bacterial colony has spread laterally on the surface of the agar and exhibits a self-affine, rough growth front that has progressed several millimeters from the string. In the days that follow, the colony morphology behind the front has become extraordinarily complex, with greedy microorganisms saving themselves and going dormant because of the sudden paucity of food, while others permit self-sacrifice with the assistance of piggy-back viruses that destroy the individual bacterium, but pass on its genetic material for the greater good of the colony. Nevertheless, at the front, things are simple – it's eat, eat, eat,... the propagating edge of the colony becoming increasing rough due to local variations in the food concentration and reproduction rate.

Or finally, consider a random, very dense and essentially two-dimensional packing of tiny glass beads (roughly, but not uniformly, sand grain size, though entirely transparent), sandwiched between two rectangular glass plates that are sealed along opposite long edges. Because the bead pack is geometrically and compositionally disordered, it serves quite nicely to realize a random, but porous medium. Water is introduced along the entire length of an open edge and is forced through the broad, but very narrow channel by means of a pump. As water displaces air in the pores of the random bead pack, the interface separating these two phases, easily seen from above, pushes ahead getting kinetically roughened, thanks to local inhomogeneities in the random medium.

The above physical processes, apparently unrelated, nonetheless share an important common feature. Each produces a kinetically roughened edge, whose geometrical complexity can best be understood, perhaps, within the nuance-stricken discipline of nonequilibium statistical mechanics. In recent years, much analytical, numerical and experimental effort has been expended by investigators seeking a greater understanding of the statistical properties of such self-affine edges. The theoreticians pushed the field into a mature phase of sorts with the development, in the mid-eighties, of a small industry devoted, in part, to the explication of the noise-driven Burgers' equation [B74], which was made popular following the work in the interface context [KPZ86]. This stochastic partial differential equation, incorporating effects of surface relaxation, locally normal growth (i.e., parallel propagation of the front), and the incessant peppering of stochastic noise, has come to represent a crucial step in eliciting Nature's secrets of kinetic roughening phenomena. This review uses the KPZ equation, as well as its immediate antecedents, as a point of departure, but soon focusses its attention on more re-

cent interdisciplinary developments concerning anomalous kinetic roughening, where the phenomena, though patently governed in some measure by the essential nonlinear mechanism of parallel transport of the surface, nevertheless exhibit a self-affine roughness that exceeds naive predictions.

In retrospect, it was hardly thinkable a few years back that the explication of such simple physical processes would necessitate the bulk of the material touched upon here. Nonetheless, subsequent research endeavors diffused far beyond the original intentions; e.g., recent suggestions concerning interfacial growth and the structure of the universe [BF94]! Admittedly, such matters are more for scientific curiosity than for practical applications. But in a subtle way, they form an integrated part to our understanding of the original problem. Along the way, the reader will soon find himself amidst a new branch of statistical mechanics that involves an impressive array of concepts drawn from contemporary physics. Let us now have a glimpse at that list: stochastic differential equations, dynamic and functional renormalization groups, Langevin and Fokker-Planck equations, fluctuation-dissipation theorem, Bethe ansatz, infinite matrix products, Burgers equation for shock waves, Kuromato-Sivashinski equation for flame propagation, passive scalars in turbulent fluids, self-organized criticality, spin glasses, replica symmetry breaking, ultrametricity, intermittent biological evolution, ground-state instability, global optimization, pattern formation and directed percolation. These interdisciplinary matters may sometimes appear to be deceivingly simple and easy, for anyone can turn on his personal computer to do a little simulation. Indeed, if he plays in the right corner, he will probably discover something worth reporting to the Physical Review. Yet, very seasoned players can still find interesting challenges in the same community. Indeed, some of the finest contemporary minds still consider the problems of sufficient subtlety to merit their time. Even so, we shall see that this interdisciplinary branch is not just a theorist's paradise. Many aspects directly concern experiments: fire propagation on paper or in a forest, ink imbibition, solid state surfaces, chemical corrosion, electrochemical deposition, sputter-etching, Schwoebel instability, rock porosity, geomorphology and the erosion of earth's surface, vortices in ceramic superconductors, blown fuse networks, oil recovery through porous media, etc.

In crafting this review paper, it was our main purpose to inspire the reader, assumed here to be at advanced graduate student or postdoctoral fellow, scanning the horizon for a worthy field of endeavor, whom we exhort to pause briefly and gaze upon the many intriguing avenues of research available within and beyond the realm of the kinetic roughening. The immediate goal was to furnish a primer of sorts – introducing the basic grammar, spelling out the essential details, passing on a few tricks of the trade, and calling attention to some technical features of interest. We make no pretense of completeness and though roughly equal time is accorded numerical, analytical and experimental aspects, the careful reader will rightly sense a slight propagandistic thread favoring traditional methodologies (typically involving pencil and paper...) over approaches dependent upon brute processing power. Indeed, it is our strong prejudice that members of the community redouble their efforts on the analytical front, despite much appreciated difficulties, since tiny chinks in the wall may suddenly yield large scale breakthroughs! We shall adopt the style to present the physics in simple language, using a rather liberal format. Intuitive reasoning is preferred over formal approaches. We do not pretend this field to be a well established one, but endeavor to expose wherever possible the pitfalls and cracks in theory. Many loose ends are emphasized as they may lead to new research directions. In any case, since the field of nonequilibrium kinetic roughening is undergoing rapid development, any treatment purporting to be comprehensive would become obsolete even before the ink had dried upon the pages. Rather, we suspected that a pedagogical, though entirely informal

introduction to kinetic roughening phenomena might be more appropriate, especially for beginning research students or physicists in other areas who may simply want a quick glimpse of the subject. Of course there are already several good reviews available on this subject, two of which are particularly worth mentioning, [KrS91r] and [FV91r]. The latter contains a reprint collection, including many of the important original papers, while the former is a very careful presentation of many early analytical and numerical aspects of surface growth related phenomena. Furthermore, a timely review paper [M93r] on rough surfaces and computer-implemented stochastic growth models, written by an expert in the field, has just appeared in this series. The reader is urged to consult this as the source for many recent developments, particularly with regard to numerical matters. Finally, a short, but handy summary [KV94r] of the dynamic scaling properties of self-affine surfaces will soon be available, as well.

For our own part, we discuss various topics in an admittedly idiosyncratic manner. Starting with a brief discussion of the early models of stochastic growth, we hit the numerics with a brief investigation of self-affine roughness and the apparently universal dynamic scaling properties of Eden clusters, ballistic deposits and RSOS surfaces. We quickly move on, however, to various nonlinear stochastic PDEs relevant within the kinetic roughening context, touching lightly upon renormalization group methods, but inevitably pay homage to the almighty MIP. Next, we contemplate the subtle beauty of the Fokker-Planck approach, and follow with complementary exact solutions via the nonequilibrium statistical mechanics of driven lattice-gases. Next, we consider a complete, though somewhat strong-armed, characterization of the strong coupling fixed point, addressing important issues of universality. The chapter on nonlinear surface growth closes with a surprising, but important link to the Kuramoto-Sivashinski equation, a toy model of spatio-temporal chaos, and a brief look at an intriguing deterministic, but singular interface equation. Subsequently, we address experimental manifestations of anomalous kinetic roughening, as well as variations upon our essentially theme, including power-law, correlated, and quenched varieties of noise. Directed percolation makes its way through the back door, thanks to the viscous imbibition experiments, followed by a quick detour to the self-organized depinning model. Our kinetic roughening discussion then concludes with a brief, somewhat speculative, interlude on MBE-relevant surface diffusion models. The remainder of the review, constituting nearly half its bulk, concentrates on the equilibrium statistical mechanics of directed polymers in random media (DPRM), a rich, but baby-version of the spin-glass problem that addresses broad issues of global optimization and is one of the very few tractable systems in ill-condensed matter.

As this new branch of multidisciplinary statistical mechanics nears its golden age, it is apparent that there are many "left-over" unsolved problems, even for the topics which may be considered well understood. These tiny loose ends may will lead to new surge of research activities and define new directions. In order to actively engage a diligent reader, we have inserted some exercises along the way. Some of these are really just exercises; i.e., straightforward extensions of the discussion in the text. By contrast, some are not that simple, and to solve them out may amount to a small research project. Nevertheless, we felt it would serve the community to sketch out a handful of problems for which we had only a modest idea concerning outcome; their inclusion is meant to challenge the reader, who is left to make the distinction between these different classes of problems.

Lastly, we mention just a few of the many topics we did not have time to include within these notes. For example, directed polymers on various hierarchical lattices offer many elegant analytical problems where considerable mathematical prowess can be exercised. This rather compact subject,

developed by Derrida and Spohn and coworkers, merits, perhaps, a mini-review in its own right. Even so, it has already been nicely touched upon in the past by Krug and Spohn [KrS91r], as has been the topic of driven lattice-gases [SZ95r], a favorite of the more mathematically-minded members of the statistical mechanics community. The wonderful connections between driven lattice-gases, kinetically roughened surfaces and the DPRM are fertile, indeed, for the resourceful researcher. Much work can be done via these ties. As an indication, the reader need only glance at the recent efforts of Tang and Lyuksyutov [TLv93], who investigate the DPRM delocalization from extended defects, a matter relevant to the wandering of elastic vortex lines in disordered superconductors plagued with columnar defects or grain boundaries, by simulating inhomogeneous KPZ stochastic growth! Similarly, Krug and Tang [KrT94] have uncovered novel shock phenomena of open boundary driven lattice-gases by studying the DPRM analog: disorder-induced unbinding in confined geometries. Unfortunately, we had insufficient stamina to present subtle issues of replica symmetry breaking for directed polymers and manifolds in random media, as elucidated by Mézard and Parisi within their variational approach [Pa90,MP91]. The reader is encouraged to scout out these matters directly; likewise, the dynamics of driven lines [Hwa92,EK92], the importance of rare versus typical DPRM fluctuations [Méz90,HF94], as well as the difficult subject of kinetic roughening within the MBE context with its associated instabilities [KrPS93], pattern formation and coarsening phenomena [John94,Ern94,SP94]. Hwa and Fisher [HF94] have reformulated the DPRM using rigorous functional methods, their work is a mini-review per se and gives particular insight into the ground state instability problem. Note, too, the recent renormalization group study [Mi94] concerning overlap distributions for the many-dimensional DPRM. Again, for a systematic discussion of the huge body of simulation work done in the past few years, we defer to Meakin [M88r,M93r]. After submission of this manuscript, we learned that Barabasi and Stanley [BS94] have nearly completed an inspired, useful elementary book on fractal interface growth, while Maritan et al. [Ma95] are preparing a comprehensive review on similar matters. The reader is urged to consult all for completeness.

2. Early models of local stochastic growth

2.1. Eden model [E58,E61]

The classic model of stochastic growth was proposed by Eden, several decades back, as a gross simplification of the biological growth process exhibited by cancerous cells [E58,E61,WB72]. Its essential ingredients are easily appreciated – take a sheet of graph paper and shade in the small central square. Now, with equal probability, darken one of this seed's 4 immediate neighbors. The resulting two-particle cluster possesses 6 perimeter squares. Again, with equal probability, one of these is chosen as the growth site and occupied, yielding a three particle cluster, and so on, see Fig. 2.1a. This very simple stochastic growth algorithm, trivially implemented on the computer, is iterated repeatedly giving rise to an Eden cluster that is compact, nonfractal in the bulk, but with intriguing surface roughness properties – Fig. 2.1b. Surprisingly, even for such a straightforward model, it proves highly nontrivial to gain substantial analytical insights.

Some limited progress was achieved early on by exactly solving the model in infinitely large dimensionality [PZ84]. The idea is to count exactly all the possible cluster configurations and then to take the ensemble average of the physical quantity of interest – in our case, the gyration radius,

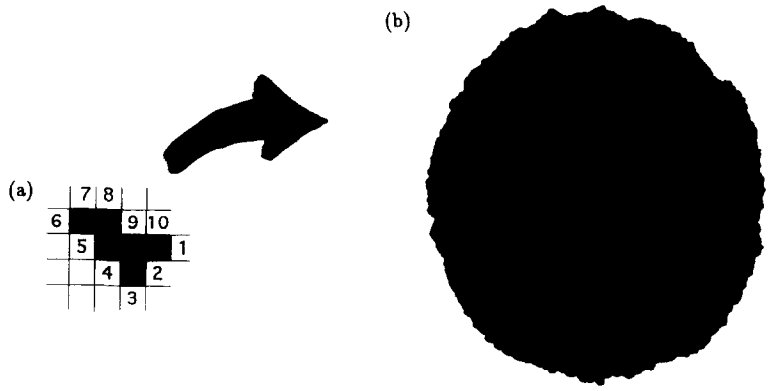

Fig. 2.1. (a) Stochastic growth rule defining the basic Eden model, (b) Resulting cluster, shown here after incorporating 60 000 particles, reveals a bulk geometry that is nonfractal in character, but with an interesting, kinetically roughened surface.

a measure of the mean size of the Eden cluster. Unfortunately, counting everything may not be possible in practice, even for the fastest computers available today working on clusters of rather modest size. Nevertheless, we can work out by hand a few of the first order terms, say clusters built successively from one, two, three,... particles. Doing this we unearth an induction rule; that is, we realize an analytical relation between the nth and $(n+1)$th order, provided the physical space is infinite dimensional or on a Cayley tree. For finite, but large d, the systematic corrections can be found

$$\lim_{n\to\infty}\langle R_n^2\rangle = 2\ln n\left(1+\frac{3}{2d}+\frac{30}{4d^2}\right) \tag{2.1}$$

where n denotes the number of constituent particles and d the dimensionality. The first-order correction in (2.1) is easily obtained [PZ84], while the second requires a bit more calculational stamina and is due to Friedberg [RF86]. On a Cayley tree of coordination number q, it can be shown [PZ84]

$$\lim_{n\to\infty}\langle R_n^2\rangle = 2\ln n\left(\frac{q-1}{q-2}\right) \tag{2.2}$$

A Cayley tree is a special lattice which avoids the complication of the real space by not having loops. Note that in infinite d, all particles of the cluster are peripheral; in other words, Eden bulk and Eden surfaces are essentially the same. In the interface context, Derrida and Spohn [DS88] found exact solutions on a Cayley tree, also for large d, using more systematic methods. From related considerations, we may deduce that in large dimensions, the surface fluctuations are characterized by a logarithmic behavior. Nevertheless, these approaches are difficult to extend to finite dimension (this, despite the fact that the $1/d$ corrections can be found exactly!), because of subtleties associated with the fact that the two limits $d\to\infty$ and $n\to\infty$ do not commute with each other [RF86,D85].

2.2. *Reggeon field theory [PZ85]*

With the hope of systematically treating the kinetically roughened surface of Eden clusters, as well as related models to be discussed shortly, such as ballistic deposition and RSOS, it is desirable

to formulate a continuous, partial differential equation that captures the important features of the growth process, while ignoring irrelevant microscopic details. An early proposal, due to Parisi and Zhang [PZ85], relied upon a Reggeon-like field theory, an approach which was previously known to be useful for other dynamical processes, notably the directed percolation problem [CS80]. Indeed, we will see that the directed percolation mechanism makes an appearance during our discussion of viscous imbibition, in Section 4.5, where experiments observe anomalous kinetic roughening. In short, the full growth equation can be expressed in the form,

$$\dot{\rho}(\boldsymbol{x}, t) = \nabla^2 \rho + \rho - \rho^2 + \rho\eta(\boldsymbol{x}, t) \tag{2.3}$$

where $\boldsymbol{x}$ is the position vector in a d-dimensional space and ρ is the density of the cluster. If $\rho(\boldsymbol{x}, t) = 1$, the site $(\boldsymbol{x}, t)$ is occupied by the cluster, 0 implies the site is unoccupied. The initial condition is that $\rho = 0$ everywhere, except at some starting point, which we label the origin. The noise term, being non-negative but random, mimics the probabilistic nature of growth, which is present everywhere and at any time. Thus, the initial seed evolves into a growing cluster, expanding into unoccupied space. Since the occupied cluster represents the "stable" phase, and the unoccupied is in the "unstable" phase, there is a rather sharp interface region ($0 < \rho < 1$) that naturally arises from the above equation. Although the noise is, in principle, present everywhere, in fact it is only effective at the interface region. This is because within the cluster proper, the factor $\rho - \rho^2$ strongly suppresses any perturbation deviating from $\rho = 1$, thereby rendering noise negligible; in the unoccupied region ($\rho = 0$) the noise has null effect by construction. Lastly, it is apparent that the diffusion term $\nabla^2\rho$ is only effective in the interface region, since the bulk phases are essentially homogeneous.

The above equation can be regarded as a faithful, field-theoretic description of the Eden cluster as well as the surface. It shares all the essential ingredients of the interface-based descriptions which are emphasized in this review. Unfortunately, this full equation proves much too difficult for analytical treatment. The technical problem can be traced to the *simultaneous* presence of a nonlinear term, as well as multiplicative noise. On the other hand, for Eden growth processes, a full description is apparently redundant since the cluster's interior is known to be compact, there being no need to treat it and the surface on the same footing.

Exercise: *Numerically solve the above equation and investigate the dynamic scaling properties of the surface fluctuations and compare with the results of the interface-only description in Chapter 3.*

2.3. Edwards-Wilkinson equation [EW82]

The above approach, motivated by Reggeon field-theoretic ideas, was far too ambitious in its attempt to describe the bulk cluster, as well as its kinetically roughened surface. Considerably greater progress can be made by focussing our attention upon the interface proper, trying to extract its essential dynamic scaling properties. Edwards and Wilkinson [EW82] made an important first step in this direction in their endeavor to understand the inherently probabilistic process of paricle sedimentation within a liquid. Concerned with competing effects of gravitational relaxation, which tends to smooth the surface, and the incessant peppering of stochastic noise, EW derived a continuum partial differential equation appropriate to such sedimentary kinetic roughening. The EW equation, an important player throughout the remainder of the review, reads

$$\dot{h}(\boldsymbol{x},t) = \nu\nabla^2 h(\boldsymbol{x},t) + \eta(\boldsymbol{x},t) + c \tag{2.4}$$

where $h(\boldsymbol{x},t)$ is the surface's position, $\boldsymbol{x}$ is a coordinate in the $(d-1)$-dimensional base space, η the space and time-dependent stochastic noise, while c is the constant average velocity of the propagating surface. In the simplest scenario, the noise is assumed spatially and temporally uncorrelated and gaussian, with variance $\langle\eta(\boldsymbol{x},t)\eta(\boldsymbol{x}',t')\rangle = 2D\delta(\boldsymbol{x}-\boldsymbol{x}')\delta(t-t')$.

Being linear, the EW equation is readily solved via Fourier methods. A central quantity of interest is the width w of the fluctuating interface, given by $w^2(L,t) = \langle L^{-(d-1)}\int_0^L d^{d-1}x[h(\boldsymbol{x},t)-\bar{h}]^2\rangle$ where the angular brackets denote averaging over samples and $\bar{h}$ is the mean height. Direct integration shows that the surface roughness w has the following scaling behavior

$$w^2(L,t) \sim \frac{D}{\nu}L^{\chi} f_{EW}(\nu t/L^2) \tag{2.5}$$

where $\chi = (3-d)/2$ is the EW *saturation-width* exponent, while the universal scaling function f_{EW} for the surface width,

$$f_{EW}(x) = \frac{K_d}{(3-d)(2\pi)^{3-d}}\left(1 - e^{-8\pi^2 x} + (8\pi^2 x)^{(3-d)/2}\int_{8\pi^2 x}^{\infty} y^{(3-d)/2}e^{-y}dy\right)$$

with $K_d = 2^{d-2}\pi^{(d-1)/2}\Gamma((d-1)/2)$, has been worked out explicitly by Nattermann and Tang [NT92], who also discuss more generally the analytical properties of the height-height correlation function $\langle h(\boldsymbol{x},t)h(\boldsymbol{x}',t')\rangle$. In fact, it is straightforward to determine the temporal evolution of the full probability functional describing the height fluctuations of the EW surface; e.g., in $d = 2$, the Fourier modes h_k are distributed as,

$$P(\{h_k\},t) \sim \exp\left(-\frac{\nu}{2D}\int dk \frac{k^2}{1-e^{-2\nu k^2 t}}h_k h_k^*\right) \tag{2.6}$$

which tracks the crossover between two distinct gaussian forms in the small and large time limits, see Yu, Pang and Halpin-Healy [YPHH94]. Returning to the steady-state exponent, we note that χ has value $1/2$ for $d = 2$; that is, for a kinetically roughened EW edge we simply retrieve the famous random walk exponent, a fact recently pursued with a vengeance [FZ94]. In $d = 3$, w has logarithmic dependence on L, while for $d > 3$, the surfaces are essentially flat. These results are probably not surprising. Although there is, in (2.4), a constant velocity c added to mimic the average progress of the interface, it can be absorbed by redefinition $h \to h - ct$. This reduces the EW equation to a perfectly *equilibrium* problem, where it is known, see, e.g., [MF86r], that the roughening exponent $\chi = (3-d)/2$, as above. We will see in later sections that surface growth is typically a genuinely irreversible process that cannot be reduced to an equilibrium problem.

2.4. *Pinned interfaces and quenched noise [BA84,KL85]*

Motivated by a rather different physical situation, Bruinsma and Aeppli [BA84] proposed the first truly irreversible nonlinear, stochastic partial differential equation appropriate to the description of kinetic roughening processes. These authors were concerned with the dynamical properties of driven domain walls in RF Ising magnets. Under the influence of an externally applied magnetic field, the

original equilibrium position of such a domain wall becomes unstable and the interface starts to move. Due to the presence of quenched random magnetic disorder, however, the domain wall can be locally pinned. Even so, if the applied field is sufficiently strong or the disorder weak enough, there remains the possibility that the interface will move in an incessant fashion. Their equation, using our notation, reads

$$\dot{h}(x,t) = F + \nabla^2 h + \eta(x,h) \tag{2.7}$$

where F is a uniformly applied field, the noise term η accounts for the *quenched* disorder, which is fixed in space and depends on the basal coordinate x, as well as the precise interface position h, but not explicitly on t. Since the noise term is a function of h itself, this equation is highly nonlinear and, in sharp contrast to the EW equation above, unyielding to traditional analytical tacks. This notwithstanding, we will, because of its resemblance to (2.4), refer to (2.7) as EW with quenched noise. Note that this equation can be cast in the Langevin form, $\dot{h} = -\delta H/\delta h$, but with the noise tucked into the hamiltonian

$$H_{BAKL} = \frac{1}{2}\int dx(\nabla h)^2 - \int dx \int^{h(x)} dh'\eta(x,h'). \tag{2.8}$$

Subsequently, Koplik and Levine [KL85], then working for Schlumberger Co., realized that the very same equation was of relevance to the oil industry, who habitually rely upon pressurized water to drive the black gold upwards through porous sedimentary stone, which acts as a random medium with quenched disorder. Koplik and Levine performed extensive, but essentially nonconclusive analytical work on this stubborn nonlinear equation. Years later, Koplik, Levine and Tu [KLT91] produced much more refined simulations of the EW equation subject to quenched noise. In section 4.4, we will discuss their important numerical work in the context of recent experiments on forced fluid flow through porous random media.

Exercise: *Determine whether for large t the "quenched" interface equation* $\dot{h}(x,t) = \nabla^2 h + \eta(x) + c$ *leads to a time independent solution, i.e. a rigid interface moving with a constant velocity. Note, here, that the noise has no explicit nor implicite time dependence.*

2.5. Simulation matters

Contemporary with these early analytical developments can be found a veritable cornucopia of simulation work on the surface growth problem. The initial assault in this domain might be rightly considered as a spin-off of the huge activity a decade ago focussed on diffusion limited aggregation (DLA) and other self-similar, fractal growth processes [WS81]. Much progress has been achieved in understanding the DLA-like fractal growth mechanism, although mainly by means of numerical simulations, since analytical efforts are generally hindered by the non-local nature of DLA; as an indication of recent endeavors, see [HL92]. For readers interested in making a serious foray into the subject of self-similar, as well as the self-affine fractals germane to this review, we might recommend the book by Feder [F88r]. In any case, thanks to concerted and rather large-scale simulations, the statistical physics community soon realized that if the growth mechanism were strictly *local*, only the surface of a cluster merited attention. For this reason, it was soon appreciated that local

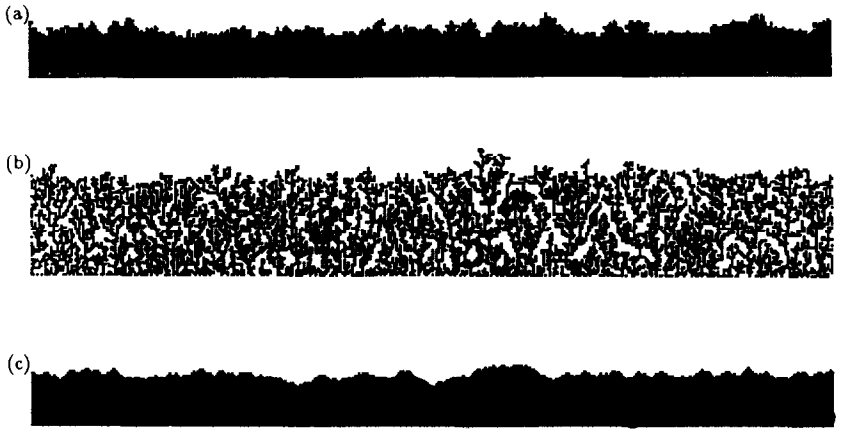

Fig. 2.2. Snapshots illustrating surface and bulk properties of three distinct stochastic growth models: (a) Eden cluster, (b) ballistic deposit, and (c) RSOS solid. All belong to the KPZ universality class [HH93].

growth mechanisms were interesting in their own right and, moreover, might have wide applicability in understanding kinetic roughening phenomena observed in Nature. Among the many simulation models relevant to our present task can be found: random deposition with surface diffusion [F86,MJ87], ballistic deposition [FV85,MRSB86], different variations of the Eden model [JB85ab,MJB86,JM87] – including various noise reduction schemes [WK87ab,KW88], RSOS models [KK89], single-step [MRSB86,PRL87] and polynuclear growth [G84,KrS89]. A complete account can be found in the recent book [FV91r] and some well-written reviews [KrS91r,M93r]. These models have one thing in common – they are all exceedingly simple to define, yet produce rich and rather different geometrically complex structures on microscopic scales. The effort to understand the large length scale surface fluctuations has led to an evolving sequence of stochastic partial differential equations. We propose to the reader some illustrative examples, stressing in the end the essential and underlying universality in their kinetically roughened surfaces.

2.5.1. On growth and form: Eden clusters, ballistic deposits, and RSOS surfaces

Numerical algorithms aim directly at simulating the cluster growth mechanism; although the various growth rules do not bear any resemblance at all to the continuous equations highlighted in this paper, we will see that if some basic features such as symmetry and locality are respected, the dynamic scaling behavior will not depend on many of the microscopic details. Conversely, to establish links with the continuum equations on the microscopic level is not easy, see, for example, Sections 3.7 and 3.8 in this review. In any case, consider the three stochastic growth algorithms delineated below, implemented in the so-called "strip geometry" on a square lattice of horizontal width L, with periodic boundary conditions imposed in the lateral directions, and of infinite vertical extent. The resulting structures are drawn in Fig. 2.2:

(i) *Eden model.* A row of seed particles is placed at the base and a cluster is grown by randomly choosing one of the perimeter sites.

(ii) *Ballistic deposition.* Here, a column $i \in 1, ..., L$ is picked at random, a particle is dropped vertically in that column and sticks upon first contact with the evolving deposit. In the code, the update rule would read: $h(i, t+1) = \max[h(i-1), h(i)+1, h(i+1)]$, where the surface position h and space coordinate i assume integer values. After many interations, it produces a

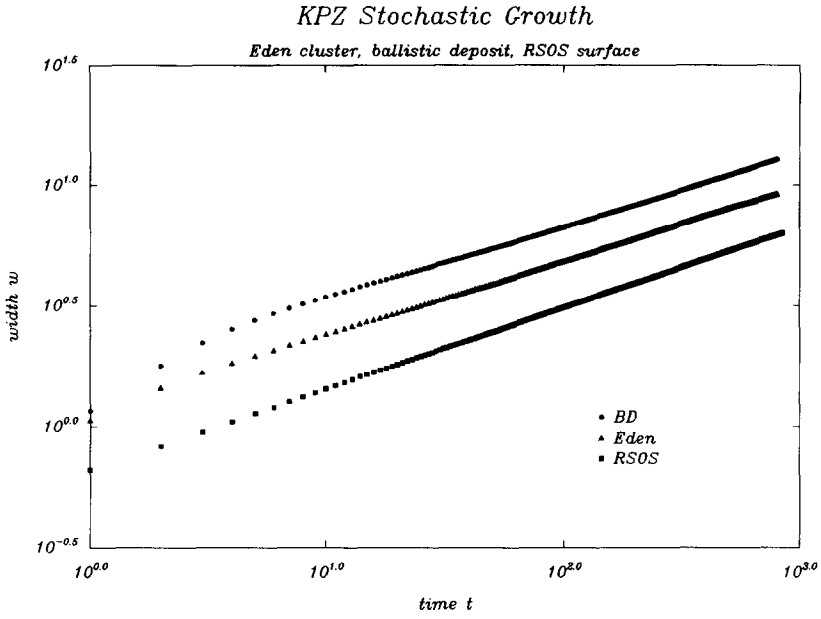

Fig. 2.3. *Early-time* roughness exhibited by Eden clusters, ballistic deposits, and RSOS surfaces. The numerically determined exponents are β=0.31, 0.31, 0.33, respectively. 800 layers were deposited on very wide substrates, $L = 5000$ (Eden – tough memory constraints in my working man's version!) and $L = 10000$ (BD, RSOS) [HH93].

highly porous, but nonfractal bulk structure of uniform density; the surface, however, is a not too distant relative of the Eden profile, an assertion made quantitative below.

(iii) *RSOS.* In this stochastic growth algorithm, a column is chosen at random and the height variable at that location augmented by unity, $h_i \rightarrow h_i + 1$, provided the restricted solid-on-solid condition, $\Delta h \leq 1$, is not violated. This height difference restriction results in entirely compact clusters without vacancies and overhangs, with hills of unit slope. Here again, despite the rather different bulk property, the RSOS model exhibits a kinetically roughened surface akin to that characteristic of Eden clusters and ballistic deposits.

Note that all three models are defined in a rather ad hoc manner. Fig. 2.2, of course, emphasizes that the bulk morphologies of Eden clusters, ballistic deposits, and RSOS solids are rather distinct. A quick glance at the corresponding edges also suggests, somewhat disconcertingly, differences rather than similarities.

In order to make quantitative our analysis of the kinetic roughening phenomena exhibited by these microscopically different stochastic growth models, we focus our attention on the temporal behavior of the surface width. Experience shows that for a given value of L, a numerical simulation in the strip geometry yields a surface roughness that initially grows algebraically with time, $w \sim t^{\beta}$, but eventually, thanks to finite-size effects, crosses over and plateaus at some sample-dependent saturation width that scales as L^{χ}. Shown in Fig. 2.3 are scaling plots from a 1+1 dimensional simulation of Eden, BD, and RSOS, used to extract the *early-time* roughness exponent β for these models. In each case, the scaling index is roughly $\frac{1}{3}$, firm evidence corroborating KPZ universality. Note, however, that the models vary greatly in their apparent willingness to exhibit clean scaling behavior; for example, RSOS was, in the stochastic growth model context, genetically engineered by Kim and Kosterlitz

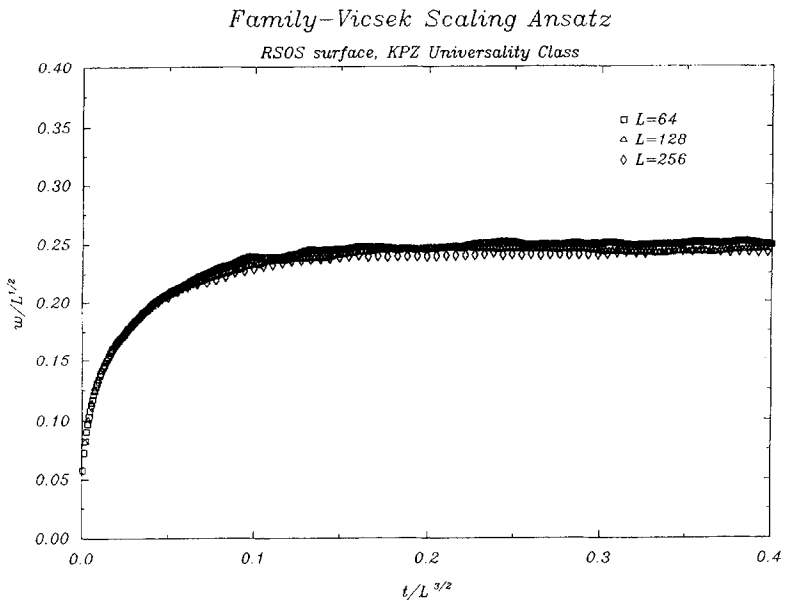

Fig. 2.4. Dynamic scaling hypothesis confirmed for RSOS edge, member of the KPZ universality class [HH93].

[KK89] to reach the scaling regime very quickly with minimal statistical noise, whereas ballistic deposits and Eden clusters are a bit more leisurely in their approach to asymptopia. Nevertheless, the somewhat surprising evidence supporting a common value $\beta = 1/3$ is quite strong. Presently, we understand that the different models suffer to varying degrees involuntary crossover effects, which makes the initial scaling model-dependent. We believe, however that by going to very large length and time scales, all three models are truly described by the same kinetic roughening exponents.

2.5.2. *The dynamic scaling hypothesis [FV85,JB85b]*

Numerical studies have provided the kinetic roughening community with substantial insight into the scaling nature of the surface growth problem. In fact, motivated by the exact results obtained for the Edwards-Wilkinson equation, Family and Vicsek [FV85], as well as Jullien and Botet [JB85b], proposed the following ansatz for the surface roughness

$$w \sim L^{\chi} f_{KPZ}(t/L^{z}) \tag{2.9}$$

where χ is the familiar saturation-width exponent, z the so-called *dynamical* exponent, and the KPZ scaling function $f(x)$ behaves asymptotically as $x^{\beta=\chi/z}$ for small argument and approaches a constant for large argument. Fig. 2.4 illustrates the convincing data collapse following from the dynamic scaling hypothesis, with the appropriate values, $\chi = 1/2$ and $z = 3/2$, assumed for the RSOS edge in two dimensions. In the above expression $\chi < 1$ is assumed. Kinetically roughened surfaces having the above scaling relation are called self-affine fractals, which are anisotropic and globally flat with a well-defined mean-height, since $w/L \to 0$ as $L \to \infty$. Throughout these notes we will see that self-affine edges arise naturally from local stochastic processes initiated from a line source.

Exercises:

1. *Consider a variant of the Eden model in which we keep track not of the unoccupied perimeter sites (Version A), but rather maintain a list of occupied perimeter sites. The new growth algorithm involves randomly selecting one of these occupied sites and then choosing one its unoccupied neighbors (Version C), see [JB85ab] for details. Convince yourself that this rule greatly reduces the number of vacancies temporarily left waiting in the bulk.*

2. *Version H of the Eden model, created by Hasmik Diratzouian, a Barnard biophysics major, keeps the running list of unoccupied perimeter sites, as in version A, but the growth rule involves 1) selecting such a site, 2) randomly picking an occupied neighbor, and then 3) searching its neighbors for an unoccupied eligible growth site. Does version H exhibit asymptotic scaling sooner than version A? How does it fare regarding vacancies compared to model C?*

3. *Can you cook up a model that scales better than KK's RSOS? To do so, you must appreciate the shortcomings, if any, of the RSOS model!*

4. *Determine the analytic form of the universal KPZ scaling function. For educated guesswork, see [AHK92].*

5. *In anticipation of our discussion of power-law noise within the context of anomalous kinetic roughening, see Section 4.2, perform a ballistic deposition simulation in which the particle size is not uniformly one pixel, but rather is distributed according to a power-law. Compare to [BHK91].*

3. Nonlinear surface growth equations

3.1. Call for the nonlinear term

We would like to have a valid description of kinetically roughened surfaces based upon a stochastic partial differential equation. In the preceding discussion we have been apprised of the fact that although we may have a correct equation describing the full growing cluster, capable of reproducing the growing interface as well as bulk properties, there are insurmountable technical difficulties preventing us from drawing useful information.

A good starting point is to examine anew the Edwards-Wilkinson (EW) equation in an effort to determine what modifications may be necessary to make it an adequate equation for the description of irreversible growth processes. Neglecting for a moment the additional effects associated with the diffusion and noise terms in the equation, a surface advances according the EW by the mechanism of *uniform* translation. Consider, for example, Fig. 3.1a where a typical segment of surface is drawn. We advance the segment a small distance forward by a uniform translation, as shown also in Fig. 3.1b. Alas, in the full fledged equation, the additional terms incur distortions in the pure translated shape; nevertheless, the uniform translation mechanism still prevails.

Imagine for a moment that the segment illustrated were to represent the boundary of a propagating fire alluded to in the introduction; it is very unlikely that the fire line propagates *only* in the forward direction, as that implied by the uniform translation mechanism. The systematic bias inherent in uniform translation is clearly betrayed in Fig. 3.1b, where the *lateral* growth is underestimated. Elementary geometric considerations reveal this bias to be proportional to the local slope of the

segment. The steeper the slope, the larger the bias. Indeed, since the fire front segment does not realize where we have set our mathematical axis (forward), nor is it aware of the average overall slope of the kinetic interface, common sense dictates that the fire is most likely to propagate along the direction of the local normal. The *effective* global forward translation is only the result of the locally normal propagation. To compensate the local bias of the uniform translation mechanism, it is easy to see that an extra term should be added to the surface equation. From Fig. 3.1c, we note that the *locally* normal propagation must be projected on the forward axis to represent the effective advance in the equation. This amount is proportional to $\sqrt{1+(\nabla h)^2}$.

As is traditional, we keep only the first leading nonlinear contribution in the equation. Assuming $(\nabla h)^2$ small, the above expression can be expanded as $1+1/2(\nabla h)^2+\cdots$, and the constant term can be dropped, as in the EW case. In this way we arrive at the nonlinear, stochastic interface equation first reported and analyzed in a paper by Kardar, Parisi and Zhang [KPZ86], which later became referred to in the literature as the KPZ equation. In the following, we shall for convenience adhere to this popular terminology. The reader should bear in mind though, this equation was known implicitly to quite a few people. A systematic RG study was already conducted by Forster, Nelson and Stephen [FNS77], though in the hydrodynamic context. A more proper name, "noise-driven Burgers' equation" [B74] somehow did not make into large circulation. The equation reads,

$$\dot{h}(\boldsymbol{x},t)=\nu\nabla^2 h+\frac{\lambda}{2}(\nabla h)^2+\eta(\boldsymbol{x},t) \tag{3.1a}$$

with noise correlator

$$\langle\eta(\boldsymbol{x}',t')\eta(\boldsymbol{x},t)\rangle=D\delta(\boldsymbol{x}'-\boldsymbol{x})\delta(t-t') \tag{3.1b}$$

Note that this equation, nothing more than EW supplemented by a nonlinearity, looks much simpler than Eq. (2.3) for the full Eden cluster, since noise is additive rather than multiplicative. Nevertheless, the two are intrinsically equivalent.

As a digression, we note that despite the naturalness suggested by the preceding remarks, the first derivation of (3.1) was much more painful, unaware of the earlier efforts of Burgers and FNS, relying upon purely formal mathematical considerations. One observes that the EW equation with

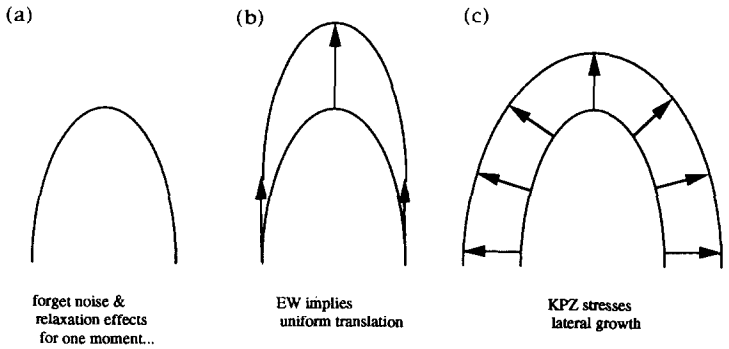

Fig. 3.1. (a) Piece of kinetically roughened surface, advances, on average, (b) via uniform translation according to the Edwards-Wilkinson equation, whereas (c) the more natural assumption is that of locally normal growth, involving a correction term $\sqrt{1+(\nabla h)^2}$ [KPZ86].

quenched noise can be expanded in the perturbative Feynman diagrams and that its leading orders are equivalent to those of KPZ [PZ86].

Before tackling the above equation, several remarks are in order. Firstly, the equation is not symmetric; i.e., if $h \to -h$, it is not invariant. This feature immediately sets Eq. (3.1) in sharp contrast to its equilibrium counterpart, the EW equation. The absence of time-reversal invariance implies that Eq. (3.1) distinguishes, in an essential manner, the two regions separated by the interface. The + sign in front of the nonlinear term is appropriate for growth (e.g., ballistic deposition, as discussed in Section 2.5), though it can be replaced by the − sign for erosion-like processes, such as those involving acid-rain, where the surfaces retreat.

Even so, (3.1) looks like a Langevin equation. In such situations, however, there usually exists a Hamiltonian H such that the Langevin equation can be expressed as

$$\dot{h}(\boldsymbol{x}, t) = -\frac{\delta H}{\delta h} + \eta(\boldsymbol{x}, t) \tag{3.2}$$

where $\delta/\delta h$ denotes functional differentiation. For instance, the EW equation can be reproduced using the Hamiltonian

$$H_{EW} = \frac{\nu}{2} \int d\boldsymbol{x}\, (\nabla h)^2 \tag{3.3}$$

The non-existence of an equilibrium hamiltonian for the KPZ equation shows that it is a *genuinely dynamical* equation, appropriate for the description of irreversible processes, and cannot be reduced to an effective equilibrium description.

The above difficulty can be overcome, at least formally, by a more careful consideration of the Langevin equation. In general dynamical interface studies, Bausch et al. [Bau81] (also private comm., A. Maritan) have noted that the above Langevin equation, (3.2), cannot be correct as it stands. To amend it, we must project both $\dot{h}$ and η in the normal direction; i.e., divide by the appropriate factor: $\sqrt{1 + (\nabla h)^2}$. Consequently, it is $\dot{h}/\sqrt{1 + (\nabla h)^2}$ and $\eta/\sqrt{1 + (\nabla h)^2}$ that should appear in Eq. (3.2) rather than simply $\dot{h}$ and η. This is because they represent physical quantities, velocity and noise, in the direction normal to the interface – the physical pushing force $-\delta H/\delta h$ is already in the normal direction. Therefore, the hamiltonian actually exists and is given by,

$$H_{KPZ}(h) = \nu \int d\boldsymbol{x} \sqrt{1 + (\nabla h)^2} - \lambda \int d\boldsymbol{x} h(\boldsymbol{x}) \tag{3.4}$$

the first term on the right hand side represents the surface contribution, while the second concerns the bulk (the bulk comes back, recall the discussion following Eq. (2.3)!) contribution, arising from the volume below the interface. Substituting the above $H_{KPZ}(h)$ into (3.2), we obtain

$$\dot{h} = \frac{\nu \nabla^2 h}{1 + (\nabla h)^2} + \lambda \sqrt{1 + (\nabla h)^2} + \eta. \tag{3.5}$$

By keeping the leading order, we recover Eq. (3.1). Note, however, that the above $H_{KPZ}(h)$ is not a hamiltonian in the traditional sense, since it is not bounded. In other words, h would like to be at infinity right away. The physical meaning, on the other hand, is clear: we are dealing with a time-dependent process, so the initial condition is important. Suppose at a given time, h is finite; we know that h would like to gain energy by virtue of Eq. (3.4), but this must happen in a gradual way – no unconnected jumps are allowed!

The careful reader might suggest that the above considerations should apply to the EW case, as well. Thus, the EW hamiltonian ought to be Eq. (3.4) with $\lambda = 0$, i.e. no bulk contribution. It then follows that all the terms have the same factor, therefore it drops out and we recover the EW equation. From the above discussions, the original derivation of the EW equation with quenched noise [BA84,KL85], should also be subject to scrutiny. Indeed, the hamiltonian (2.8) should be replaced by

$$H_{BAKL} = \frac{J}{2}\int dx\sqrt{1+(\nabla h)^2} - \lambda \int dx \int^{h(x)} dh'[\eta(x,h') + F/\lambda] \tag{3.6}$$

it differs from the "KPZ Hamiltonian" only by the last term. Should the quenched landscape be flat $\eta = \text{const}$, the two would be the same. Repeating the steps leading to Eq. (3.1) [GZ94], we found that it is unavoidable to add the nonlinear term to the EW equation with quenched noise; i.e., the correct version of this equation should read, instead of (2.7),

$$\dot{h}(x,t) = -\frac{\delta H}{\delta h} + F + J\nabla^2 h + \lambda(\nabla h)^2 + \eta(x,h). \tag{3.7}$$

In short, the equation for a driven interface should always contain the nonlinear term, no matter whether the noise be stochastic or quenched. Now the constant F can no longer be absorbed by a redefinition of h, since quenched noise violates the translation invariance in h. Later, we will see that the presence or absence of the nonlinear term makes a big difference in scaling behaviors for the case of quenched noise case. Note that these concerns regarding the nonlinear term in the context of driven interfaces turn out to have far broader implications; for example, in other driven systems such as charge density waves, the nonlinear term is traditionally overlooked.

Eq. (3.1) enjoys a subtle local symmetry: Galilean invariance. This symmetry has its origin in the fact that if we tilt the mathematical coordinate system slightly by an infinitesimal angle $\boldsymbol{\epsilon}$, our dynamical equation should remain invariant, since the physics remains manifestly so. We can see this by means of the following coordinate transformation,

$$h \to h + \boldsymbol{\epsilon}\cdot\boldsymbol{x}, \quad \boldsymbol{x} \to \boldsymbol{x} + \lambda\boldsymbol{\epsilon}t \tag{3.8}$$

which leaves Eq. (3.1) invariant. As a consequence of this local symmetry there is a characteristic identity (for detailed reasoning see [MHKZ89]) between the two fundamental scaling exponents, χ and z, which reads

$$\chi + z = 2. \tag{3.9}$$

Eq. (3.1) also has other important applications in disguise. If we consider a new variable $\boldsymbol{v} = \nabla h$, then the equation satisfied by $\boldsymbol{v}$ is

$$\dot{\boldsymbol{v}} = \nu\nabla^2\boldsymbol{v} + \lambda\boldsymbol{v}\cdot\nabla\boldsymbol{v} + \boldsymbol{f}(\boldsymbol{x},t) \tag{3.10}$$

where the noise term $\boldsymbol{f} = \nabla\eta$. Here again the nonlinear term owes its origin to geometry. Suppose we consider the simplest linear equation

$$\dot{\boldsymbol{v}} = \nu\nabla^2\boldsymbol{v} + \boldsymbol{f}(\boldsymbol{x},t), \tag{3.11}$$

but in the moving frame this equation cannot be correct. Instead of the partial derivative $\partial/\partial t$, the total derivative should be used $d/dt = \partial/\partial t - \lambda \mathbf{v}\cdot\nabla$, with λ being a unfixed constant between the space and time scales. Thus we are naturally led to (3.10). In the absence of noise, equation (3.10) is referred to as the Burgers' equation, whose applications and analysis, relevant to the discussion of shock wave asymptotics, are dealt with in great detail in the slender volume [B74]. With the noise term, (3.10) is the so-called noisy Burgers' equation, which has been used to model vortex-free fluids, as done systematically by Forster, Nelson and Stephen [FNS77] almost a decade before the efforts of KPZ to understand the kinetic roughening phenomena characteristic of stochastic growth. The resemblance between (3.10) and the Naviers-Stokes equation of fluid dynamics is evident, except that we have $\nabla \times \boldsymbol{v} \equiv 0$ by construction, so that the applicability of the noisy Burgers' equation is limited to vortex-free situations (e.g., shocks propagating down a tube). In a discretized version where a fluid is replaced by a host of hard particles in a pipe, we are lead rather naturally to the one dimensional driven lattice gas, a system which was studied independently by van Beijeren, Kutner and Spohn [BKS85]; for additional details connecting to the kinetic roughening context, see [KrS91r,KrT94].

Another important substitution, the so-called Hopf transformation,

$$W(\boldsymbol{x}, t) = \exp\left(\frac{\lambda}{2\nu} h\right) \tag{3.12}$$

converts Eq. (3.1) into an entirely different looking beast:

$$\dot{W} = \nu \nabla^2 W + \eta(\boldsymbol{x}, t) W. \tag{3.13}$$

We see that the above equation is linear, at the price of introducing multiplicative noise. Recall the earlier difficulties with the presence of both nonlinear term and multiplicative noise in Eq. (2.3). Linearizing (3.1) to (3.13) does not make the problem easier, but it does present us with a completely new perspective, as well as opening the door to a vast new field in the equilibrium statistical mechanics of ill-condensed matter.

Observe that (3.13) looks like a Schrödinger equation, except the time t is imaginary and that the stochastic noise in Eq. (3.1) has taken on a new role as a time-dependent random potential. It is particularly instructive to study the problem in the path integral formalism. In the spirit of Feynman, we can reformulate our Schrödinger problem in terms of its functional path integral solution:

$$W(\boldsymbol{x}, t) = \int_{(0,0)}^{(\boldsymbol{x},t)} D\boldsymbol{x}' \exp\left\{ -\int_0^t dt' \left[\frac{\nu}{2} \left(\frac{d\boldsymbol{x}'}{dt'} \right)^2 - \eta(\boldsymbol{x}', t) \right] \right\} \tag{3.14}$$

Note the imaginary time formalism makes the above amplitude real, thus permitting us to interprete it as statistical weight, or Boltzmann factor. Later, in chapter 5, we will devote much discussion to this problem, where such Feynman paths are relevant to the statistical mechanics of *directed polymers in random media.*

3.2. Dynamic RG analysis [KPZ86,MHKZ89]

The standard manner of treating a non-linear stochastic PDE such as (3.1) is the renormalization group approach for dynamical processes, developed some two decades ago. The essential idea is to

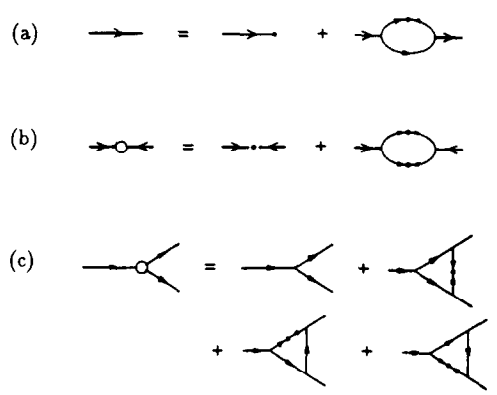

Fig. 3.2. Diagrammatics associated with the 1-loop perturbative dynamic RG analysis of Eq. (3.1). First-order correction to the (a) propagator, (b) noise correlator, and (c) vertex. Light and heavy lines represent h_0 and h, respectively. Lines with arrows represent propagators G_0 and G.

write the KPZ equation in Fourier-transformed fashion. Thus, following space and time transformations, we have,

$$h(\boldsymbol{k},\omega) = h_0(\boldsymbol{k},\omega) - \frac{\lambda}{2} G_0(\boldsymbol{k},\omega) \int_{q,\Omega} \boldsymbol{q}\cdot(k-q)h(\boldsymbol{q},\Omega)h(\boldsymbol{k}-\boldsymbol{q},\omega-\Omega) \tag{3.15}$$

where $h_0(\boldsymbol{k},\omega) = G_0(\mathbf{k},\omega)\eta(\boldsymbol{k},\omega)$, the free propagator $G_0(\boldsymbol{k},\omega) = (-i\omega+\nu k^2)^{-1}$, and the noise correlation function $\langle \eta(\boldsymbol{k},\omega)\eta(\boldsymbol{k}',\omega')\rangle = 2D\delta^d(\boldsymbol{k}+\boldsymbol{k}')\delta(\omega-\omega')$. The strategy of the dynamic RG is a ruthless utilization of the iterative structure of Eq. (3.15). The normal procedure of perturbative dynamic RG is to replace the h inside the integral above by (3.15) itself, and repeat this to the desired order. For book-keeping purposes, the series can be represented graphically, representing the terms pictorially and momentarily supressing unimportant details regarding differentiations, integrals and vertex factors. In the actual calculation, all we need do is keep track of proper vertex factors and momentum integrations. Physical observables are noise-averaged quantities or correlation functions. For instance, if we want to obtain the wave function renormalisation, we pick up the correlation function $\langle h\eta\rangle$. h is a series in η in ascending order, the average is done by pairing up the η's. For the gaussian distribution of η's all correlations break into products of pairs, i.e. $\langle\eta\eta\rangle$. To lowest orders the wave function renormalisation is represented graphically by Fig. 3.2a, the noise correlation function renormalization $\langle hh\rangle$ by Fig. 3.2b and the vertex $\langle h\eta\eta\rangle$ by Fig. 3.2c. The guiding principle of the momentum shell RG scheme entails integrating out momenta in the range of $e^{-l}\Lambda < |\boldsymbol{k}| < \Lambda$. When l is sufficiently small, the renormalization corrections to the bare value can then be expressed by differential equations. The individual differential flow equations for the phenomenological parameters ν, D and λ read as follows,

$$\frac{d\nu(l)}{dl} = \left(z-2+\frac{2-d}{4d}K_d\bar{\lambda}^2\right)\nu(l), \tag{3.16}$$

$$\frac{dD(l)}{dl} = \left(z-d-2\chi+K_d\bar{\lambda}^2/4\right)D(l) \tag{3.17}$$

and

$$\frac{d\lambda(l)}{dl} = (\chi + z - 2)\,\lambda(l) \tag{3.18}$$

where $\bar{\lambda}^2 = \lambda^2 D/\nu^3$ and we note the important fact that the diagrams contributing to the renormalization of λ (vertex) cancel at this order; in fact, they cancel at succeeding orders as well, a consequence of the Galilean symmetry which dictates the fundamental exponent equality $\chi + z = 2$. We are thus led to the evolution equation of the effective coupling constant $\bar{\lambda}^2 = \lambda^2 D/\nu^3$,

$$\frac{d\bar{\lambda}}{dl} = \frac{2-d}{2}\bar{\lambda} + K_d \frac{2d-3}{4d}\bar{\lambda}^3, \tag{3.19}$$

where $K_d = S_d/(2\pi)^d$ and S_d is the surface area of a unit sphere in d dimensions. The desired exponents χ and z are defined through

$$z = 2 - K_d \bar{\lambda}^2 \frac{2-d}{4d}, \quad \chi = 2 - z. \tag{3.20}$$

The renormalization group algorithm requires that in the scaling region the right hand side of (3.19) should vanish; i.e., it is independent of scale.

The renormalization group flow equation $d\bar{\lambda}/dl = 0$ has different solutions in various dimensions. For $d = 1$, we obtain $K_1\bar{\lambda}^2 = 2$. Thus from equation (3.20), we have $z = 3/2$, and $\chi = 1/2$. Note that $d = 2$ is a special case, since the first term in (3.19) is zero. This is usually called the marginal dimension in equilibrium statistical field theories, where only logarithmic corrections to the mean field solutions ($\bar{\lambda} = 0$) are expected. However, in the present case $\bar{\lambda} = 0$ is not a stable solution, since an infinitesimal value of it will diverge according to (3.19). We conclude, therefore, that the renormalization group analysis fails to yield physical predictions for $d = 2$, as (3.19) indicates that physics cannot be probed by a perturbation theory. The perturbative results, nevertheless, hint at the existence of a strong coupling region, though the theory cannot make more precise predictions. For $d > 2$ the situation is somewhat different than that of $d = 2$. Since the first term of (3.19) reverses its sign with respect to that of $d < 2$, the fixed point $\bar{\lambda} = 0$ becomes the stable one. However, for large initial values of $\bar{\lambda}$ the cubic term dominates and (3.19) implies a divergence of $\bar{\lambda}$, revealing once again the existence of a strong coupling region.

We conclude that, according to the one-loop result, there is a unique fixed point for $d = 1$ and the scaling exponents can be found. Interestingly, the one-loop RG gives a result coinciding with the exact one, so the reader may wonder what happens when higher order contributions are considered. In fact, the higher order contributions must give the same result, by virtue of a fluctuation-dissipation theorem in this dimensionality [HHF85]. For $d = 2$ there may be a unique fixed point, but the perturbative dynamic RG approach cannot probe the strong coupling region. For $d > 2$, two distinct regions exist: a weak coupling region where the mean-field, Edwards-Wilkinson ($\lambda = 0$) results ($z = 2, \chi = 0$) hold and the interface is flat, as well as a strong-coupling region that cannot be reached via any scheme perturbative in the nonlinearity. We will see these conclusions are corroborated by the non-perturbative results of directed polymers in random media, where one uses the existence of bound-states as the criterion, see Section 5.9.2.

In retrospect, we may say that the success of the RG for 1+1 KPZ case is fortuitous: there is the FDT guaranteeing that nothing goes wrong in perturbative series. Exact solutions in various forms exist – this also makes the above perturbation approach superfluous. Generally speaking, since we do

not know how good is the convergence rate, RG results have to be cross-checked by other means. Blindly applying the RG to other stochastic differential equations is like sailing in uncharted waters, at your own risk and peril. Thus, despite its elegant, seducing appearance there is little control once the RG machinary is turned on. Even so, its allure is strong: Frey [F94] has recently reported results for a 2-loop calculation of the dynamic RG, confirming several features, including (i) persistence of FDT-induced cancellations in 1+1, even at second order, which permit retrieval of the exact exponents, (ii) likewise, the continued nonrenormalizability of λ, maintaining the fundamental KPZ identity, and (iii) a dynamic exponent $z_c = 2$ at the transition between weak and strong coupling in $d > 2 + 1$, as predicted by Doty and Kosterlitz [DK92]. However, much was anticipated by the Weizmann group [LLPP93] who using formal Feynman diagrammatics in their endeavor to establish an equivalence between KS and KPZ equations, prove that to *all* orders in perturbative expansion these exponents remain exact. Thus, as far as to the two scaling exponents (z, χ) are concerned, we may consider the RG structures of 1+1 KPZ equation a closed case.

Exercise: *It is believed and numerically confirmed that when the nonlinear term in KPZ equation is replaced by* $|\nabla h|^\alpha$, $\alpha \geq 1$, *the same universal scaling exponents will stay; that is, the renormalized equation always recovers* $(\nabla h)^2$. *Show this using RG techniques. If this proves to be too difficult, turn to your PC. Discuss also if a upper limit of* α *exists, above which the nonlinear term is irrelevant.*

Remark: *Recently, Schwartz and Edwards [SE92] introduced a new RG approach to tackle the KPZ equation in 2+1 dimensions. Their approach consists in truncating the infinite perturbative expansion using a Dyson-Schwinger trick, which was successfully employed for the Navier-Stokes equation earlier by Edwards [E64]. Using a plausible ansatz, they were able to find the exponent* $z \simeq 1.69$, *very close to the numerical value* $z \simeq 1.6$ *of the most recent simulations. Bouchaud and Cates [BC93] followed suit with similar ideas, but using a different approach and an easier language. They found the exponent* $z \simeq 1.67$, *close again to the physical value.*

A question naturally arises – why the apparently very different ansätze by the two groups all converge towards the presumed physical value? It is our conjecture that both ansätze are arbitrary – symmetries permitting. In fact, when we examine all possible allowed ansätze we should find the convergence towards the physical value always good. We may attribute this rapid convergence to some hidden small parameter in the 2+1 KPZ problem which makes the Dyson-Schwinger an excellent approximation scheme (Procaccia and Zhang, unpublished).

3.3. A worthy detour: kinetic roughening with conservation law [SGG89]

In an informative variation upon the basic theme, Sun, Guo and Grant [SGG89] considered the effects of constraining the dynamics of a stochastically growing interface by imposing a *global conservation of total mass*. Their investigations, based upon an analytical dynamic RG, as well as a complementary numerical simulation, unearthed several unappreciated matters, but more importantly inspired many later KPZ-related efforts towards a working theory of molecular-beam epitaxy, see Villain's pedagogically-inspired paper for a handy introduction to such matters [V91]. In any case, the inquiries of the Canadian group were motivated by two fundamental questions,

- What features are responsible dictating the universality class of a particular kinetic roughening process?

- Given the rather general considerations that led to the scaling relation, $\chi + z = 2$, are there growth processes for which this equation does not hold?

Motivated by dynamic critical phenomena, where it is known that universality classes for nonequilibrium systems are determined by a variety of factors beyond the symmetry of the order parameter and the spatial dimensionality (e.g., the presence or absence of conservation laws, mode-coupling terms, etc.), these authors generalized the inherently *nonconservative* KPZ to the following conserved model:

$$\dot{h}(\boldsymbol{x}, t) = \nabla^2 \left[\nu \nabla^2 h + \frac{\lambda}{2} (\nabla h)^2 \right] + \eta(\boldsymbol{x}, t) \tag{3.21a}$$

where

$$\langle \eta(\boldsymbol{x}, t) \eta(\boldsymbol{x}', t') \rangle = 2D \nabla^2 \delta(\boldsymbol{x} - \boldsymbol{x}') \delta(t - t'). \tag{3.21b}$$

The important point here is that total h is conserved since the right hand side of this equation can be written, noise term included, as the divergence of a current. Physically, some aspects of the conservation law can be understood within a scenario where relaxational effects via surface diffusion are crucial; indeed, as Villain has carefully discussed, the presence of the laplacian squared term owes precisely to this. Nevertheless, the insistence upon conserving the total number of atoms keeps the model somewhat distant from true MBE processes.

Fourier transformation of (3.21) leads to a dynamic RG perturbative in the vertex $-\frac{1}{2}\lambda k^2 \boldsymbol{q} \cdot (\boldsymbol{k} - \boldsymbol{q})$, resulting in the following 1-loop differential flow equations for the phenomenological parameters:

$$\frac{d\nu(l)}{dl} = \left(z - 4 + \frac{4 - d}{4d} K_d \bar{\lambda}^2 \right) \nu(l), \tag{3.22}$$

$$\frac{dD(l)}{dl} = (z - 2 - d - 2\chi)\, D(l) \tag{3.23}$$

and

$$\frac{d\lambda(l)}{dl} = (z + \chi - 4)\, \lambda(l) \tag{3.24}$$

where $\bar{\lambda}^2 = \lambda^2 D / \nu^3$ is the usual reduced coupling constant, and K_d is the geometric angular factor from before, resulting from the momentum shell integration. All this is highly reminiscent, apparently, of the original Eq. (3.1), aside from several crucial differences:

(i) the bare propagator is of the form $G_0(\boldsymbol{k}, \omega) = (-i\omega + \nu k^4)^{-1}$, which implies a classical exponent $z = 4$,

(ii) because the vertex possesses an extra factor of k^2, as compared to the standard case, all diagrams contributing to the renormalization of D have prefactors proportional to powers of k^4, resulting in their demise as we consider the infrared, long wavelength limit $k \to \infty$. Such diagrams simply correspond to higher derivatives in the original noise spectrum and are therefore irrelevant on large length scales. Hence, SGG note the great simplification that (3.23) is exact, D remaining *unrenormalized* to all orders of perturbation theory. Consequently, we are led immediately to the exponent identity

$$z - 2\chi = d + 2 \tag{3.25}$$

an exact result that can be derived by more general arguments and is appropriate to all situations where the deterministic dynamics is conserved [Kr91b]; e.g., surface diffusion models relevant to molecular beam epitaxy – see end of chapter 4.

(iii) Though the conservation law imposed by SGG destroys the characteristic Galilean invariance (which implied $\chi + z = 2$), their conserved model possesses a symmetry of its own. If one makes the transformation,

$$h \to h + \boldsymbol{a} \cdot \boldsymbol{x}, \quad \boldsymbol{x} \to \boldsymbol{x} - \lambda t \boldsymbol{a} \nabla^2 \tag{3.26}$$

it is apparent that the form of the original equation is preserved. As before, the explicit presence of the parameter λ in the prescription for the transformed coordinates requires that it suffer no renormalization; there being diagrammatic cancellation at each order of perturbation theory. Thus, SGG obtained the exponent relation

$$\chi + z = 4 \tag{3.27}$$

for their version of the conserved equation.

The unrenormalized nature of D and λ thereby fix, directly, the strong coupling, nonclassical scaling indices for this model: $z = (10 + d)/3$ and $\chi = (2 - d)/3$, indicating the only nontrivial case to be that of one substrate dimension, where we find

$$z_{SGG} = \tfrac{11}{3}, \quad \chi_{SGG} = \tfrac{1}{3}. \tag{3.28}$$

Interestingly, SGG performed the necessary numerical simulations themselves, using an RSOS model in which the local interface height was increased by unity at the expense of decreasing it elsewhere by the same amount (conservation of total particle number!). In their extensive simulations, they extracted an early time exponent $\beta = \chi/z = 0.091 \pm 0.002$, which was in excellent agreement with the dynamic RG prediction $\beta = 1/11$, while their estimate for the saturation roughness of the conserved RSOS interface, a more difficult numerical matter given the unusually large value of z, gave $\chi = 0.35 \pm 0.03$. Together, these independent determinations of the exponents imply $\chi + z = 4.2 \pm 0.4$, providing good evidence for their novel index relation, as well as the existence of a new SGG universality class. Despite this apparent success, strong objections regarding the validity of this microscopic model have been raised by Rácz and coworkers [RSLP91]; later, a second advertised SGG model was summarily dismissed [WVZ93]. Regardless, Krug [Kr94u] has recently simulated a truly SGG lattice model, confirming the expected early-time behavior. Krug's SGG rule is particularly simple:

1. Pick a site i at random.
2. Check if $h_{i+1} > h_i$ or $h_{i-1} > h_i$; if yes, pick another site.
3. If no, move the particle at i to a randomly chosen nearest neighbor.

The reader is encouraged to test this algorithm and, while the machine is running, read up surface diffusion currents [KrPS93] for relevant insider tips.

3.4. Stochastic Burgers equation: keeping the faith [AF90,MW92,MW94]

It cannot be stressed sufficiently that the utility of the dynamic RG is restricted almost entirely to the one-dimensional case, where its success, though impressive, is completely reliant upon a serendipitous

symmetry in that dimension, in addition to our being privy to somewhat arcane Feynman graphical matters. Given that many readers may be unfamiliar with renormalization group techniques, as well as the troublesome constraints of their limited utility within the realm of interface growth, the reader's faith in the noisy Burgers equation as the correct stochastic PDE to describe the dynamic scaling behavior and kinetic roughening of Eden clusters, ballistic deposits, and RSOS surfaces, recall Section 2.5, can be rather firmly established by simply integrating Eq. (3.1) by brute force numerical methods. This straightforward procedure, which is completely *nonperturbative* in nature and simply involves studying the statistical properties of the fluctuating variable $h(\boldsymbol{x}, t)$, was first successfully implemented in a convincing fashion by Amar and Family [AF90], who used a Connection Machine facility to determine the scaling properties of KPZ at the marginal dimension. To implement the method, minimizing the amount of excess baggage, we make a change of scale $h = y\sqrt{2D/\nu}$ and $t = \tau/\nu$, with the result that Eq. (3.1) takes the form

$$\partial y(\boldsymbol{x}, \tau)/\partial \tau = \nabla^2 y(\boldsymbol{x}, \tau) + \sqrt{\epsilon}|\nabla y|^2 + \xi(\boldsymbol{x}, \tau) \tag{3.29}$$

where $\langle \xi(\boldsymbol{x}, \tau)\xi(\boldsymbol{x}', \tau')\rangle = \delta^d(\boldsymbol{x} - \boldsymbol{x}')\delta(\tau - \tau')$ and $\epsilon = \lambda^2 D/2\nu^3$, the coupling constant from above is the important tunable phenomenological parameter which gauges the strength of the nonlinearity. The only freedom remaining concerns the choice of integration scheme (the simple finite-difference method works just fine) and the manner of creating the short-ranged stochastic noise. In the simulations, we consider a discrete spatial grid of linear dimension L, so that in 2+1 dimensions, this equation becomes

$$\begin{aligned} y_{\tau+1}(i,j) &= y_\tau(i,j) \\ &+ \Delta\tau([y_\tau(i,j+1) + y_\tau(i+1,j) + y_\tau(i-1,j) + y_\tau(i,j-1) - 4y_\tau(i,j)] \\ &+ \sqrt{\epsilon}/4([y_\tau(i+1,j) - y_\tau(i-1,j)]^2 + [y_\tau(i,j+1) - y_\tau(i,j-1)]^2)) \\ &+ \sqrt{\Delta\tau}\xi(i,j;\tau) \end{aligned} \tag{3.30}$$

where $\xi(i,j;\tau)$ corresponds to independent Gaussian noise (in fact, using a uniform distribution typically presents no difficulties and is numerically faster) while $\Delta\tau$, the small finite-time step, must be varied depending upon ϵ to obtain optimal convergence.

In Fig. 3.3 are shown the results for the *early-time* width in low dimensional simulations of the KPZ equation. For $d = 1$, $L = 10000$, $\Delta\tau = 0.005$, and $\epsilon = 5.0$, an average over 100 runs took 10 hours on a fully committed Sparc 2 and gave an exponent $\beta = 0.33 \pm 0.02$, in excellent agreement with the exact value 1/3. In $d = 2$, with $L = 250$, $\Delta\tau = 0.001$, $\epsilon = 25.0$ and 100 runs, the computational time on the same machine was considerably longer, some 15 days [HH92]. The straight lines in the figure have slopes 1/3 and 1/4, respectively, the latter thanks to the Kim-Kosterlitz conjecture [KK89],

$$\beta_{d+1} = 1/(d+2) \tag{3.31}$$

which was motivated empirically by findings from a cleverly implemented RSOS growth algorithm. Though correct in d=0,1, the KK value is now known to be good, though only approximate estimate more generally. Large scale simulation of Eq. (3.1) by Amar and Family [AF90] has produced the estimate $\beta_{2+1} = 0.24 \pm 0.01$, a value confirmed by the more recent, elegant numerical integration efforts of Moser and Wolf [MW92], who cut the uncertainty in half.

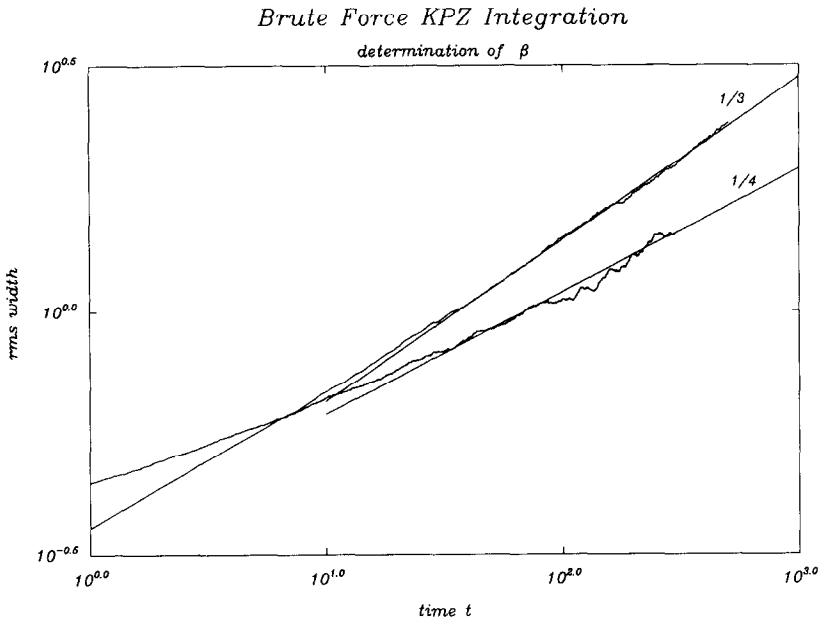

Fig. 3.3. Determination of the *early-time* roughness exponent β, in low dimensions, via direct integration of Eq. (3.1).

Extraction of the *saturation-width* exponent in this dimensionality can be plagued by unfortunate crossover effects if ϵ is chosen too small, since the unstable EW fixed point momentarily holds sway. Nevertheless, in their best case scenario, $\epsilon = 25$, [AF90] found $\chi_{2+1} = 0.39 \pm 0.01$, which compares favorably with the refined estimate 0.385 ± 0.005 of Forrest and Tang [FT90,TFW92] for an evaporation/deposition growth model within the 2+1 KPZ universality class. Forrest and Tang also measured the early-time exponent in their stochastic growth simulation, finding $\beta_{2+1} = 0.240 \pm 0.001$, putting a definitive nail in the coffin of the sadly short-lived KK conjecture. For additional nails, see [AV94], who report $\beta_{2+1} = 0.240 \pm 0.002$ from a refined scaling analysis [AHK92] of 2+1 RSOS results, as well as [AHKV93], who indicate, for the same model, $\beta_{3+1} = 0.180 \pm 0.002$, which should be compared with the earlier Forrest-Tang [FT90] value 0.180 ± 0.005 and the recent KPZ integration of Moser and Wolf [MW94] giving 0.181 ± 0.007, probably the best estimates to-date. Results in still higher dimensions [AHKV93], based simply upon the asymptotics of the rms width, give $\beta_{d+1} \approx 0.135$, 0.11, 0.10, 0.08 in $d = 4$, 5, 6, 7, suggesting the absence of any accessibly finite UCD for the strong coupling regime.

3.5. *Fokker-Planck approach: steady-state surface fluctuations*

There are quite a few analytical methods available to solve the KPZ equation for the scaling exponents χ and z. Besides the dynamic RG approach discussed earlier, which is the most straightforward, there are also the mode-mode coupling method [BKS85], an exact solution via clever transformation [D87], as well as the Bethe ansatz technique [Kard87a] in the directed polymer context. However, the simplest and the most elegant means of attack is based upon the Fokker-Planck approach, which permits us to calculate directly the probability the distribution of steady-state height fluctuations. This

approach was developed previously by many people, under different disguises [HuHF85,KrS89r,Pa90, and Zhang, unpublished].

Let us recall some basic facts in stochastic dynamics. From standard textbooks, we know that for a set of dynamic variables $y_i(t)$, $i = 1, \ldots, n$ of a stochastic system, the time evolution of the fluctuating variables is governed by the Langevin equation

$$\dot{y}_i = A_i(y) + \eta_i(t) \tag{3.32}$$

where each $A_i(y)$ can have nonlinear dependence on $\{y\}$, while $\eta_i(t)$ is the gaussian noise with correlator $\langle \eta_i(t)\eta_j(t')\rangle = 2\Gamma\delta(t-t')\delta_{ij}$. Denote by $P(y,t)$ the distribution function of $\{y\}$, at time t, it is usually true that each Langevin equation has a corresponding Fokker-Planck equation. Thus the very same system can be described by

$$\frac{\partial P(y,t)}{\partial t} = -\sum_{i=1}^{n} \frac{\partial}{\partial y_i}[A_i(y)P] + \Gamma \sum_{i=1}^{n} \frac{\partial^2 P}{\partial y_i^2}. \tag{3.33}$$

From a practical point of view, two descriptions are equivalent and we may choose one at will that better serves our purpose.

A moment's reflection reveals that we may regard Eq. (3.1) of stochastic growth as a generalized Langevin equation, in which the variables $y_i(t)$ are replaced by $h(\boldsymbol{x}, t)$. In other words, where the discrete index i becomes a continuous label for each point $\boldsymbol{x}$. For this case functional notation is necessary. If we denote by $P[h(\boldsymbol{x}); t]$ the distribution functional of the surface position function $h(\boldsymbol{x})$, the corresponding Fokker-Planck equation is

$$\frac{\partial P[h;t]}{\partial t} = -\int d\boldsymbol{x} \frac{\delta}{\delta h}\left\{\left[\nabla^2 h + \frac{\lambda}{2}(\nabla h)^2\right] P\right\} + \int d\boldsymbol{x} \frac{\delta^2}{\delta h^2} P. \tag{3.34}$$

The above equation admits a time-independent solution for $d = 1$; i.e., $\partial P[h;t]/\partial t = 0$, for

$$P = \exp\left[-\frac{1}{2}\int_0^L dx(\nabla h)^2\right]. \tag{3.35}$$

Incidentally, this is the solution when the nonlinearity is absent; *i.e.,* the solution for EW equation as well. The presence of the nonlinear term does not, apparently, alter the steady-state solution. With the definition $\delta h(x)/\delta h(x') = \delta(x - x')$, it is straightforward to verify that (3.35) satisfies (3.34): the first term in (3.34) has contributions independent of λ after carrying out the $\delta/\delta h$ operation, these cancel exactly the second term of (3.34). The λ-dependent contribution is proportional to

$$\frac{\lambda}{2}\int dx(\nabla h)^2 \nabla^2 h \tag{3.36}$$

which is identically zero and this is readily seen by an integration by parts. The reader should stop, now, to verify this point explicitly.

The time-independent solution is applicable at the long time limit where a dynamic surface is believed to be in a stationary state. Thus, we conclude that in the stationary state, the surfaces described by the EW and KPZ equations have the equivalent distribution and the static exponent

$\chi = 1/2$ is the same for both cases. In a sense, the KPZ and EW equations are only different in temporal scaling, at least for $d = 1 + 1$.

Exercises:

1. *Show that the above equivalence is only true for $d = 1$, for any other d the cancellation mentioned above is not complete. Indeed, stationary solutions for $d \neq 1$ have not been found. However, you may cook up a few ansätze for P to convince yourself that only $d = 1$ is a lucky case.*

2. *Repeat the above steps to show that if the nonlinear interaction were $(\nabla h)^4$, instead of $(\nabla h)^2$, the solution to the Fokker-Planck equation would be exactly the same. Convince yourself that this is true for any $(\nabla h)^k$, where k is a positive integer and for any linear combination of them (e.g. $\sqrt{1 + (\nabla h)^2} = \ldots$). Thus we learn that d=1 is a special case where the stationary distribution is very robust. Try to exhaust the whole class of nonlinear interactions that leave the steady-state height distribution function invariant.*

3. *Consider the equation $\dot{h}(x,t) = -\nabla^4 h + \eta(x,t)$ and show that the static solution similar to Eq. (3.35) is $P = \exp[-\frac{1}{2}\int_0^L dx(\nabla^2 h)^2]$.*

From the full probability distribution, calculation of the height fluctuations is straightforward. Eq. (3.35) yields for the variance, $\langle w \rangle \sim L^{\chi}$, with $\chi = 1/2$.

A few remarks are in order: The functional approach using Fokker-Planck equation is particularly powerful, no approximation is involved and we obtain the full steady-state distribution for the height fluctuations, which turn out to be gaussian. This method is to be compared to others, where usually only the second moment of the distribution is available. Note that the dynamic RG, an entirely perturbative approach, also gives the exact result $\chi = 1/2$, but only after laborious work. This still leaves untamed higher loops at large. The natural question that arises – how come we strike lucky at the first order RG approximation? The answer to this puzzle lies in the fact that the higher order Feynman diagrams do not alter the scaling exponents, though the fixed points may change. A deeper understanding is summed up in the so-called fluctuation-dissipation theorem, explained in great detail by Dekker and Haake [DH75]. The Fokker-Planck equation, however, bypasses these subtleties since it works in the configuration space and no loop expansion is necessary.

Of course, the steady-state height distribution is only part of the story. For a dynamically evolving KPZ surface, we are also interested in the exponent z, which characterizes the time evolution. Unfortunately, the early-time behavior of height distribution is a very tough nut to crack; indeed, we have to follow a completely different approach, based upon a replica scaling analysis [Z90d] of the directed polymer problem and the successes are limited so far. Here, we simply quote the main result, referring the interested reader to the original reference for details, though we do touch base on this matter in Sections 3.7.3 and 5.4.3. In any case, it was possible to show that if we start from a flat configuration, i.e., $h(\boldsymbol{x}) = 0$, denoting by $\bar{h}$ the mean position of the surface at time t, then the probability of finding the surface at h is

$$P(h) \sim \exp\{-[(h - \bar{h})/t^{1/3}]^{\eta_+}\}, \quad \text{for} \quad h > \bar{h} \tag{3.37}$$

where $\eta_+ = 3/2$. That the above expression is only valid for $h > \bar{h}$ can be traced to the fact that height fluctuations of the KPZ surface correspond to free energy fluctuations in the directed polymer

context, where we need to calculate quenched disorder averages of arbitrary *positive* moments, $\langle Z^n \rangle$, of the DPRM partition function.

The guiding principle was the familiar notion of probability theory that knowledge of all its moments permits us to reconstruct the full distribution function. Unfortunately, though calculation of $\langle Z^n \rangle$ may be straightforward for *positive* integer n, it is essentially impossible for *negative* integers; the gentle reader being reminded, for example, that $\langle Z^{-1} \rangle \neq \langle Z \rangle^{-1}$. Hence, it was only possible to determine the analytical form of the distribution for "half" of the variables h, whence the condition $h > \bar{h}$. This corresponds to the forward portion, the "peaks" and "tips" of a growing surface, which is, in any case, believed to dominate the temporal scaling; whereas the statistics governing the valleys and grooves of the surface that lag behind prove much difficult to obtain, since it requires knowledge of the *negative* moments. Nevertheless, numerical work [KBM91a] shows that for $h > \bar{h}$, $\eta_+ = 1.6 \pm 0.2$, which compares favorably with Zhang's theoretical prediction 3/2; for $h < \bar{h}$, η_- seems to be ≈ 2.5. The numerical evidence is consistent with our expectation that (3.37) cannot be a symmetrical function for early times, the peaks and valleys playing very different roles during the early growth.

In short, we have come a long way to extend the dynamic scaling hypothesis, recall Section 2.5.2, which concerned only second moments. Therefore,

$$w \sim L^{\chi} f(t/L^{z}) \tag{3.38}$$

is generalized to

$$P(\Delta h) \overset{t \gg L^z}{\simeq} \exp\left[-(\Delta h)^2/L\right], \tag{3.39}$$

$$P(\Delta h) \overset{t \ll L^z}{\simeq} \exp[-(|\Delta h|/t^{1/3})^{\eta_\pm}], \quad \eta_+ = 3/2, \quad \eta_- \simeq 2.5. \tag{3.40}$$

Now we know the whole distribution!

Based upon the Fokker-Planck approach and replica scaling analysis, we have a complete understanding of the steady-state gaussian height probability distribution, as well as a preliminary handle on the *skewed* early-time distribution. These results, based upon delicate analytical tools, allow us to make very strong statements about the surface fluctuations exhibited by a kinetically-roughened surface, since they specify all the moments and also the shape of the distributions. Clearly, it would be desirable to have a more systematic numerical verification directly from growth models. We pick up some of these threads in the next section, where a variety of intriguing issues are addressed.

3.6. Fully asymmetric exclusion process: aka single-step model

In the following, we outline two other analytical solution approaches to solve the same surface growth problem. The reader will see they vary greatly from the "direct" approaches we are reporting so far, in appearance as well as in techniques. Yet at the end of the day we still recover the standard scaling behavior. These two examples may offer some glimpse into other treasures of the field.

3.6.1. Solution via Bethe ansatz [D87,GS92]

In an intriguing one page note, Dhar [D87a] announced the exact solution, via Bethe ansatz, of a stochastic growth model in the 1+1 KPZ universality class, characterized by the steady-state and

dynamic exponents $\chi = 1/2$ and $z = 3/2$, respectively. Unfortunately, aside from an abbreviated conference paper[D87b], further details of Dhar's work never made their way into circulation; subsequently, however, Gwa and Spohn [GS92a] derived his results in a much more general context dealing with vertex models, roughened surfaces and asymmetric Heisenberg spin chains. Here, thanks to some additional notes supplied by the author, we follow Dhar's intuitive line of thought, referring the interested reader to later calculationally explicit work [GS92b] for the final say.

Our starting point is Dhar's growth algorithm, very much akin to the single-step model [MRSB86, PRL87], the interface being a line, characterized by a single-valued height coordinate $h(x,t)$, overhangs and holes strictly forbidden. Starting from a flat configuration, the discrete stochastic evolution proceeds via a parallel updating scheme. At odd (even) times t, $h(x,t)$ increases by 1 at odd (even) sites x with probability p if $h(x\pm1,t) = h(x,t)$, and otherwise with probability 1. Periodic boundary conditions and a finite system size L are assumed. Note that this stochastic growth rule favors the formation of flatter interfaces by leaving them unchanged; in particular, for small p, the steady-state surface consists of long stretches of flat regions, with infrequent height changes.

Since the local evolution rules are dictated by height *differences*, rather than the heights themselves, it makes sense to use them as the basic variables. Moreover, it follows from Dhar's microscopic algorithm that the height differences are restricted to the values 0,+1,-1. In fact, defining the variable

$$n(x,t) = h(x+1,t) - h(x,t) + \sin^2\frac{\pi}{2}(x-t) \tag{3.41}$$

it is apparent that $n(x,t)$ can take only the values 0 and 1. This follows because $h(x+1,t) - h(x,t) = -1$ only when $(x-t)$ is odd, and if $h(x+1,t) - h(x,t) = +1$, then $(x-t)$ is necessarily even. Consequently, we naturally interpret $n(x,t)$ as occupation numbers of a lattice gas on a ring, there being a unique configuration of the lattice gas for each surface profile. The stochastic evolution rules are simply translated in terms of these occupation variables: if $n(x,t) = 1$ and $n(x+1,t) = 0$, the lattice gas particle at x jumps one step to the right with probability $(1-p)$. Thus, Dhar's growth model is equivalent to a model of biassed diffusion of hard spheres on a ring, a problem referred to in the probability literature as the *asymmetric simple exclusion process* [L85]. Such driven diffusive systems have a long venerable history; for a review see [Sch90]. Their specific relevance is elaborated upon by Krug and Spohn [KrS91r]. Recent work within the statistical physics community concerns phase transitions incurred by open boundaries [Kr91c,DDM92], including analytically calculated steady-state density profiles, correlation functions and diffusion constants [DEHP93,DEM93]; see next section.

If $P(c,t)$ denotes the probability that at time t, the lattice gas configuration is c, then in the limit $p \to 1$, we can write down a continuum master equation for the time evolution of $P(c,t)$, given by

$$\frac{d}{dt}P(c,t) = \sum_{c'} H(c,c')P(c',t) \tag{3.42}$$

where c' are configurations differing from c by at most one jump. The matrix $H(c,c')$ can be written, in second quantized notation, as

$$H = \sum_i (1 - a_i^\dagger a_{i+1}) a_{i+1}^\dagger a_i \tag{3.43}$$

where the a's are standard Pauli operators and their relation to the surface variables is through (3.41), n_i being the number operator $n_i = a_i^+ a_i$. The nonhermitian matrix H is similar in structure to the nearest neighbor Heisenberg chain with anisotropic interactions. Nevertheless, it is a hamiltonian that conserves particle number and can be diagonalized exactly via Bethe ansatz. The ground state eigenvector describes the steady state. In this state, all allowed configurations of $L/2$ particles on the ring are equally likely, from which it follows trivially that the variance of h is proportional to L. That $\chi = 1/2$ via such considerations for the single-step model was appreciated very early [MRSB86,PRL87,LP88]. Regarding the first excited state, Dhar found the decay rate to vary as $L^{-3/2}$, indicating the dynamical exponent $z = 3/2$.

Here we discuss, finally, the strategy underlying Dhar's diagonalization of H, sending the reader part way down the road to an explicit determination of z. The trick is to consider, initially, small numbers of particles on the ring, which reveals the structure of the full Bethe solution. Consider the case $N = 1$; i.e., one particle on the ring. If $P(R,t)$ denotes the probability that the particle is at site R at time t, the master equation reads $\partial_t P(R,t) = P(R-1,t) - P(R,t)$, which has the trivial eigenfunctions $\psi = e^{ikR}$, with eigenvalue $\lambda_1 = e^{-ik} - 1$. Simple enough. How about the two-particle sector, $N = 2$? There the eigenvalue equation is

$$\lambda_2 \psi(R_1, R_2) = \psi(R_1 - 1, R_2) + \psi(R_1, R_2 - 1) - 2\psi(R_1, R_2) \tag{3.44}$$

for $|R_1 - R_2| > 1$, while for next neighbor sites,

$$\lambda \psi(R, R+1) = \psi(R-1, R+1) - \psi(R, R+1) \tag{3.45}$$

Note that this equation is of the same form as the previous one, provided ψ satisfies the constraint, $\psi(R, R+1) = \psi(R, R)$, for all R. Now, we make the Bethe ansatz

$$\psi(R_1, R_2) = e^{ik_1 R_1 + ik_2 R_2} + A_{21} e^{ik_2 R_1 + ik_1 R_2} \tag{3.46}$$

for all $1 \le R_1 \le R_2 \le L$. This is an eigenfunction with eigenvalue

$$\lambda_2 = e^{-ik_1} + e^{-ik_2} - 2. \tag{3.47}$$

Imposing the wavefunction constraint gives

$$A_{21} = -\frac{e^{ik_2} - 1}{e^{ik_1} - 1} \tag{3.48}$$

while periodic boundary conditions, with suitably permuted arguments of ψ, require

$$\psi(R_1, R_2 = L + 1) = \psi(1, R_1) \tag{3.49}$$

for all R_1, which demands

$$e^{ik_1 L} A_{21} = 1, \quad e^{ik_2 L} = A_{21}. \tag{3.50}$$

Note that (3.49) can be rewritten as $z_{1,2} = e^{-ik_{1,2}}$, with z_i being roots of the equation

$$z^{L-2}(1 - z)^2 = -\eta^2 \tag{3.51}$$

where

$$\eta^2 = (z_1^{-1} - 1)(z_2^{-1} - 1) \tag{3.52}$$

which indicates already the general form of things to come. For the three-particle sector, $N = 3$ the wavefunction $\psi(R_1, R_2, R_3)$ satisfies the equation

$$\lambda_3\psi(R_1, R_2, R_3) = \psi(R_1 - 1, R_2, R_3) + \psi(R_1, R_2 - 1, R_3) + \psi(R_1, R_2, R_3 - 1) - 3\psi(R_1, R_2, R_3) \tag{3.53}$$

for $|R_i - R_{i+1}| \neq 1$. This equation can be made to hold for all R_1, R_2, R_3, if we impose the constraint that $\psi(R_1, R_2, R_2 + 1) = \psi(R_1, R_2, R_2)$, cyclic variations holding as well. The Bethe ansatz for $N = 3$ reads

$$\psi(R_1, R_2, R_3) = \sum_p A_p \exp\left[i\sum_{j=1}^{3} k_{p(j)}R_j\right] \tag{3.54}$$

where the sum is over all permutations p, which send the index j to the index $p(j)$, while the eigenvalue is, not surprisingly,

$$\lambda_3 = e^{-ik_1} + e^{-ik_2} + e^{-ik_3} - 3. \tag{3.55}$$

In general, for N particles, we impose the (now very natural) constraint condition,

$$\psi(R_1, R_2, \ldots, R_i, R_{i+1} = R_i + 1, \ldots, R_N) = \psi(R_1, R_2, \ldots, R_i, R_{i+1} = R_i, \ldots, R_N), \quad \text{for all } i. \tag{3.56}$$

This is valid for all $R_1, \ldots, R_N$, only if

$$A_p e^{ik_{p(i+1)}} + A_{t(i,i+1)p}e^{ik_{p(i)}} = A_p + A_{t(i,i+1)p} \tag{3.57}$$

where $t(i, i+1)$ is the transposition operator which exchanges i and $i+1$. This equation has the solution

$$A_{t(i,i+1)p} = -\frac{e^{ikp(i+1)} - 1}{e^{ikp(i)} - 1}A_p \tag{3.58}$$

The (permuted) periodic boundary condition reads

$$\psi(R_1, R_2, R_3 = L + 1) = \psi(1, R_1, R_2), \quad \text{for all } R_1, R_2 \tag{3.59}$$

which can be written in the form

$$e^{ik_1 L} = \frac{(e^{ik_1} - 1)^2}{(e^{ik_2} - 1)(e^{ik_3} - 1)} \tag{3.60}$$

with two similar equations holding for e^{ik_2}, e^{ik_3}. Writing $z_i = e^{-ik_i}$, it is easy to see that in the general case, the z_i's are N distinct roots of the equation

$$z^{L-N}(1 - z)^N = (-1)^{N-1}\eta^N \tag{3.61}$$

where η is a complex parameter determined by the self-consistency condition

$$\eta^N = \prod_{j=1}^{N} \left(\frac{1}{z_j} - 1 \right) \tag{3.62}$$

and the eigenvalue is given by

$$\lambda_N = \sum_{j=1}^{N} (z_j - 1). \tag{3.63}$$

These equations are used to generate the spectrum of our original nonhermitian Hamiltonian H. Starting with the flat initial condition, $h(x, t = 0) = 0$, corresponds to the sector $N = L/2$. Recall that the slowest relaxation occurs for the first excited state. Assuming N odd, with $n \equiv L/2 = N$, we have the equation,

$$z^n (1 - z)^n = \eta^n \tag{3.64}$$

which has $2n$ roots,

$$z_j = \tfrac{1}{2} + \sqrt{\tfrac{1}{4} - \theta e^{2\pi i j/n}}, \quad z_{j+n} = \tfrac{1}{2} - \sqrt{\tfrac{1}{4} - \theta e^{2\pi i j/n}} \tag{3.65}$$

with $j = 1, \ldots, n$. To find an arbitrary energy level, we make a choice of n integers between 1 and $2n$. This gives us n roots, via Eqs. (3.65). Then we must vary η continuously so that the self-consistency condition is satisfied, recall (3.62). Finally, from (3.63), we obtain the associated eigenvalue. If we choose the roots to be $z_1, z_2, \ldots, z_n$, it is straightforward to see that the self-consistent choice corresponds to $\eta = 0$. To get the first excited state, we create a "single particle-single hole" excitation outside this Fermi sea of filled single particle levels. Then solving the self-consistent equations for large n perturbatively, using a systematic expansion – for complete details, including subtle contour integrations, see Sections IV and V of [GS92b], we find

$$\eta = \tfrac{1}{4} + \mathcal{O}(1/n) \tag{3.66}$$

which implies, ultimately from (3.63),

$$\lambda_n \propto n^{-3/2} \tag{3.67}$$

so that the dynamic exponent is 3/2, as advertised.

3.6.2. Alternative matrix method [DEHP93,DEM93]

As mentioned earlier, recent work on the fully asymmetric exclusion model has focussed on elucidating the phase diagram of this driven lattice gas subject to open boundary conditions, as well as calculating correlation functions and density profiles [DEHP93]. Furthermore, for the case of periodic BC, an exact determination of the diffusion constant has been achieved [DEM93]. Much of this progress owes to the introduction by Derrida and collaborators of a novel matrix method [for a summary, see DE94], complementary to the Bethe ansatz just discussed. In particular, the matrix technique permits easy access to the dynamic exponent $z = 3/2$. Moreover, it may provide the key to a complete understanding of the steady-state properties of kinetically roughened edges in the KPZ universality class. Here, we briefly sketch the method and touch upon the important results.

The starting point is the driven lattice gas on a one-dimensional chain of N sites. At each site is a variable τ_i=0 (1) indicating whether the site is empty (occupied). The dynamics of fully asymmetric exclusion allow a hop to the right if the neighboring site is empty; in addition, particles are fed in (pulled out) from the left (right) with a probability proportional to α (β). The great utility of the matrix method follows from the fact, suggested and proved by [DEHP93], that the relative probability of finding a particular steady-state configuration $\{\tau_1, \tau_2, \ldots, \tau_N\}$ is given by

$$f_N(\tau_1, \tau_2, \ldots, \tau_N) = \langle W| \prod_{i=1}^{N} [\tau_i D + (1 - \tau_i) E] |V\rangle \tag{3.68}$$

where the matrices D, E (generally noncommuting and infinite-dimensional) and state vectors $\langle W|$, $|V\rangle$ (suggestive bra, ket notation borrowed from quantum mechanics) satisfy the algebraic constraints:

$$D|V\rangle = \frac{1}{\beta}|V\rangle, \quad DE = D + E, \quad \langle W| = \frac{1}{\alpha}\langle W| \tag{3.69}$$

which, aside from freeing us from worries concerning explicit representations (possible via sparse, shift matrices, see [DEHP93]), also permit convenient calculation of physically interesting quantities. For example, the density profile is given via the formula

$$\langle \tau_i \rangle_N = \frac{\langle W|C^{i-1}DC^{N-i}|V\rangle}{\langle W|C^N|V\rangle} \tag{3.70}$$

with $C = D + E$, while the current $J = \langle \tau_i(1 - \tau_{i+1}) \rangle$ through the bond $i, i+1$ is

$$J = \frac{\langle W|C^{i-1}DEC^{N-i-1}|V\rangle}{\langle W|C^N|V\rangle} = \frac{\langle W|C^{N-1}|V\rangle}{\langle W|C^N|V\rangle} \tag{3.71}$$

since $C = DE$, as well. In fact, all we need know in practice are the matrix elements associated with arbitrary powers of C, which has been shown [DEHP93] via the commutation rules (3.69) to be

$$\frac{\langle W|C^N|V\rangle}{\langle W||V\rangle} \sum_{p=0}^{N} \frac{p(2N-1-p)!}{N!(N-p)!} \frac{\beta^{-p-1} - \alpha^{-p-1}}{\beta^{-1} - \alpha^{-1}}. \tag{3.72}$$

With this result in hand, we are in business; an analysis of the asymptotics reveals three distinct phases, corresponding to different expressions for the current, see Fig. 3.4, which is precisely the phase diagram predicted by mean field theory [Kr91b,DDM92].

Derrida, Evans and Mukamel [DEM93] have extended the method to calculate steady-state properties beyond equal-time correlation functions. In their inaugural effort, they determine exactly, in the fully asymmetric case, the diffusion constant for a system of M particles on a ring (periodic BC assumed) of N sites. Denoting Y_t the number of hops performed by an arbitrarily tagged particle between times zero and t, they find

$$\lim_{t\to\infty} \frac{\langle Y_t \rangle}{t} = v, \quad \lim_{t\to\infty} \frac{\langle Y_t^2 \rangle - \langle Y_t \rangle^2}{t} = A \tag{3.73}$$

where the drift velocity v and diffusion constant A are given by

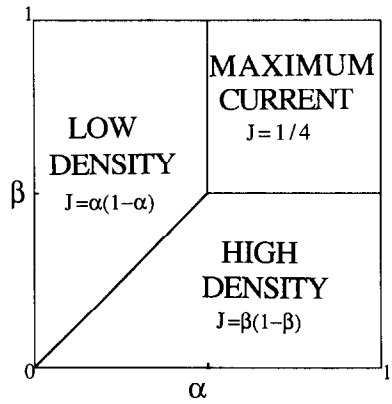

Fig. 3.4. Phase diagram in the $\alpha - \beta$ plane for the hard-core, driven lattice gas with open boundaries. Particles fed in at left end of system with probability proportional to α, pulled out from the right end at rate β. The phases are distinguished by different behaviors of the steady-state current J. Calculations via mean-field [DDM92] and exact matrix methods [DEHP93] yield the same diagram.

$$v = \frac{N-M}{N-1}, \quad A = \frac{(2N-3)!}{(2M-1)!(2N-2M-1)!}\left[\frac{(M-1)!(N-M)!}{(N-1)!}\right]^2. \tag{3.74}$$

Heading for the thermodynamic limit, but keeping the particle density $\rho = M/N$ fixed, leads to the asymptotic expression,

$$A \approx \frac{\sqrt{\pi}}{2}\frac{(1-\rho)^{3/2}}{\rho^{1/2}}\frac{1}{N^{1/2}}. \tag{3.75}$$

The dynamic exponent in 1+1 dimensions follows in a simple manner from this result. Thanks to the mapping between fully asymmetric exclusion and single-step growth models, we associate the movement of a lattice-gas particle with a surface height increment of one unit. Thus, the variance of the height fluctuation at time t, or surface roughness, must scale as $[\langle Y_t^2\rangle - \langle Y_t\rangle^2] \sim N^{-1/2}t$. Yet we know for stochastic growth subject to finite system size, this variance does not increase without bound, but rather saturates at a value $\propto N$. Consequently, the time at which this crossover occurs scales as $N^{3/2}$. So there we have it, $z = 3/2$. Other results for the fully asymmetric exclusion process admit immediate translation into exactly computable properties of the kinetically roughened edges [DE93], particularly for inhomogeneous growth processes involving a localized excess/deficit in the shot noise [WT90]; see, in particular, the recent efforts of Krug and Tang [KrT94]. Finally, it seems possible to employ the matrix method to calculate temporal correlations [DE94] in the steady-state. In this regard, comparison with numerics [KrMHH92] and theory [HF91] in the growth model context would be most welcome.

3.7. Amplitude universality at the strong coupling fixed point [KrMHH92,AF92]

Bolstered by the exact information available concerning the surface fluctuations in the steady state via Fokker-Planck and other approaches in 1+1 dimensions, researchers have recently attempted a complete characterization of the strong coupling fixed point. This program goes well beyond simple knowledge of the critical exponents and has concentrated on numerically pinning down various universal amplitudes in the transient regime, as well as the full probability distribution of the height

fluctuations, including the temporal evolution of the skewness. The motivations for doing so are several. Firstly, it is a natural and thorough extension of all matters relating to the Family-Vicsek dynamic scaling ansatz. Secondly, in experimental contexts, it is crucial to understand how amplitude prefactors depend on system parameters, in order to be able to assess the range in which to expect asymptotic scaling (see, e.g., Section 3.7.2). Thirdly, it is possible by brute force numerical methods to establish the rather broad collection of growth models that fall within the KPZ universality class – found among the membership are Eden, ballistic deposition, RSOS models, and various single step models [MRSB86,PRL87], with generalizations due to Gates and Westcott [GW88], as well as polynuclear growth [G84,KrS89]. This section concentrates on the analytical and numerical tricks employed in extracting truly universal quantities within the realm of interface growth.

3.7.1. Determining model-dependent parameters

Implicit in the Family-Vicsek scaling ansatz is the existence of two distinct asymptotic scaling regimes. Since we desire to characterize the full probability distribution of the height fluctuations, we can define a set of amplitudes associated with the *transient regime* $t \ll L^z$,

$$a_n = \lim_{t\to\infty} \lim_{L\to\infty} t^{-n/3} \langle [h(x,t) - \langle h(x,t)\rangle]^n \rangle_c \tag{3.76}$$

where $\langle X^n \rangle_c$ denotes the n^{th} cumulant of the random variable X, while $\beta = 1/3$ is the relevant scaling index, and another set associated with the *stationary regime* $t \gg L^z$,

$$b_n = \lim_{L\to\infty} \lim_{t\to\infty} L^{-n/2} \langle [h(x,t) - \langle h(x,t)\rangle]^n \rangle_c \tag{3.77}$$

where $\chi = 1/2$ is the familiar saturation-width exponent. A secondary quantity of interest is the leading correction to the asymptotic growth rate

$$v_\infty = \lim_{t,L\to\infty} \langle \partial h/\partial t \rangle. \tag{3.78}$$

For kinetically roughened surfaces, Krug and Meakin [KrM90] have established the existence of a scaling form,

$$\langle \partial h/\partial t \rangle - v_\infty = L^{-1} f(t/L^z) \tag{3.79}$$

where the function f asymptotically approaches a constant for large arguments, and scales as $f(y) \sim y^{-2/3}$ as $y \to \infty$. Hence, inspired by the dictim that more may be better, we are naturally lead to define the growth-correction amplitudes,

$$a_v = \lim_{t\to\infty} \lim_{L\to\infty} t^{2/3} (\langle \partial h/\partial t \rangle - v_\infty) \tag{3.80}$$

and

$$b_v = \lim_{L\to\infty} \lim_{t\to\infty} L (\langle \partial h/\partial t \rangle - v_\infty) \tag{3.81}$$

Note, however, because of the special structure of the one-dimensional problem, all the above static amplitudes are trivial. By contrast, the dynamic amplitudes, once freed of nonuniversal model-dependent parameters, contain essential information about the strong coupling fixed point. In particular, with the standard phenomenological parameters ν, λ and D, see Eq. (3.1), the Fokker-Planck approach reveals that the stationary height fluctuations are gaussian with variance

$$\lim_{t\to\infty}\langle|h(k,t)|^2\rangle = \frac{D}{2\nu LK^2} \tag{3.82}$$

for the discrete Fourier modes $h(k,t), k = 2\pi m/L, m = -L/2,\ldots,-1,1,\ldots,L/2$, independent of the nonlinearity, so that the static (stationary, equal-time) correlation functions are readily computed. Thus, the stationary height-difference correlation function in an infinite system is

$$C_h(r) = \lim_{t\to\infty}\langle[h(x+r,t) - h(x,t)]^2\rangle = Ar \tag{3.83}$$

for large r, with

$$A = D/2\nu \tag{3.84}$$

while the saturation-width of the interface in a finite system with periodic boundary conditions is

$$\lim_{t\to\infty}\xi(t,L) = (A/12)^{1/2}L^{1/2} \tag{3.85}$$

for large L. The latter result implies $b_2 = A/12$ and the gaussian character of the stationary distribution causes all higher cumulants to vanish, $b_n = 0$ for all $n > 2$.

Regarding the finite-size correction to the asymptotic growth rate in the steady state regime, it can be shown simply from (3.82) that

$$b_v = -\frac{\lambda}{2}\langle(\nabla h)^2\rangle = -\lambda A/2. \tag{3.86}$$

From a practical point of view, the results (3.82), (3.85) and (3.86) for the static amplitudes provide us with a simple method to determine numerically the values of A and λ for any growth model of interest. In addition, λ can be determined directly from the inclination dependence of the growth rate; imposing a small tilt $h(x,t) \to h(x,t) + \epsilon x$ in Eq. (3.1) and computing the response in the average growth rate, it is revealed that

$$\lambda = v''_\infty(0). \tag{3.87}$$

An altogether different method for determining λ, utilizing inhomogeneities in the deposition rate, has been suggested and very successfully implemented by Wolf and Tang [WT90].

Knowledge of the parameters A and λ are central to the present endeavor because in the transient regime, where the Fokker-Planck approach cannot help us, simple dimensional considerations require (3.82) to take the dynamic scaling form

$$\langle|h(k,t)|^2\rangle = \frac{D}{2\nu LK^2}g[(\lambda^2 A)^{1/3}kt^{2/3}] \tag{3.88}$$

where g is a universal, model-independent nontrivial scaling function. The height fluctuations in this transient regime are not gaussian and hence the higher moments are not related to the variance (3.88) in any simple way. Most important, since the nonlinear term in KPZ breaks $h \to -h$ symmetry, odd moments may become nonzero, evidence of a nonvanishing skewness. Nevertheless, the higher moments are expected to satisfy scaling relations similar to (3.88), so that the general form of the transient amplitudes is

$$a_n = (|\lambda|A^2)^{n/3} c_n \tag{3.89}$$

and

$$a_v = (|\lambda|A^2)^{1/3} c_n \tag{3.90}$$

where the absolute values of c_n and c_v are expected to be universal numbers. Note that the signs of c_n (for $n > 2$) and c_v are not fixed a priori, but it is clear from the symmetry of Eq. (3.1) that they are fixed by the model-dependent sign of λ. In particular, it is known that c_v and λ have opposite signs. The bottom line regarding the strong coupling fixed point is that all amplitude prefactors can be expressed in terms of only two model parameters, the spatial correlation function amplitude A and the nonlinear coefficient λ. In the context of the KPZ equation, this implies that the phenomenological parameters ν and D appear only in the combination D/ν. The nontrivial dynamic amplitudes (3.89) and (3.90) are governed by the single scaling parameter

$$\theta = A^2|\lambda| \tag{3.91}$$

In particular, the nth cumulant diverges as $(\theta t)^{n/3}$ in the transient regime, with a universal prefactor c_n.

3.7.2. Extracting universal prefactors

As discussed above, determination of universal amplitudes at the strong coupling fixed point necessitates pinning down the parameters A and λ for the model at hand. The strategy is straightforward; in this section we present some representative data from a numerical simulation of an RSOS model, see Fig. 3.5. Finding A involves studying (i) the height-difference correlation function $C_h(r)$, see equation (3.83), or (ii) finite-size dependence of the saturation width $\xi(t \to \infty, L) = \sqrt{AL/12}$. In Fig. 3.5a, is shown the height-difference correlation function with the asymptotic behavior $C_h(x) \sim x$ divided out. The simulation was performed on a substrate of size $L = 2^{18} = 262144$ and the correlation function is shown at six different stages during the deposition process. The dashed horizontal line indicates the value estimated for A. The coefficient λ is ascertained by (i) measuring the finite-size correction to the asymptotic growth velocity in the steady state regime, or (ii) directly monitoring the tilt dependence of the average growth velocity, since $\lambda = v''_\infty(0)$. Fig. 3.5b shows the stationary growth rate as a function of inverse system size for the same RSOS simulation. The dashed line represents a least-squares fit to the data (each point represents between 2×10^7 and 2×10^8 attempted depositions), the slope of which yields our estimate for the stationary growth-rate correction amplitude $b_v = -A\lambda/2$. Note that the positive slope implies a negative coefficient, here $\lambda = -0.81$. An independent determination of this quantity via the second method gave $\lambda = -0.75$, which yields a fair measure of the uncertainty in these procedures. With the model parameters thus fixed, we have $\theta_{RSOS} = A^2|\lambda| \simeq 0.53$. To give an indication of the variation within the KPZ universality class, we have $(A, \lambda, \theta) = (2.46, 1.54, 9.37)$ and $(6.76, 1.21, 55.4)$ for NN and NNN ballistic deposition. Single-step and Gates-Westcott models typically have $\theta \simeq 0.1 - 1$, while smaller values of the scaling parameter are possible within polynuclear growth models, where it can be shown [KrS89] that for small nucleation rates $p \ll 1$, $\theta = A = \lambda^{-1} = \sqrt{2p}$. Having found θ for a variety of models, we can get down to the business of measuring transient amplitudes and extracting universal quantities characteristic of the strong coupling fixed point. In Fig. 3.6a are exhibited the second and third moments of the early time height fluctuations in the discrete time PNG model with $p = 0.001$. Note that

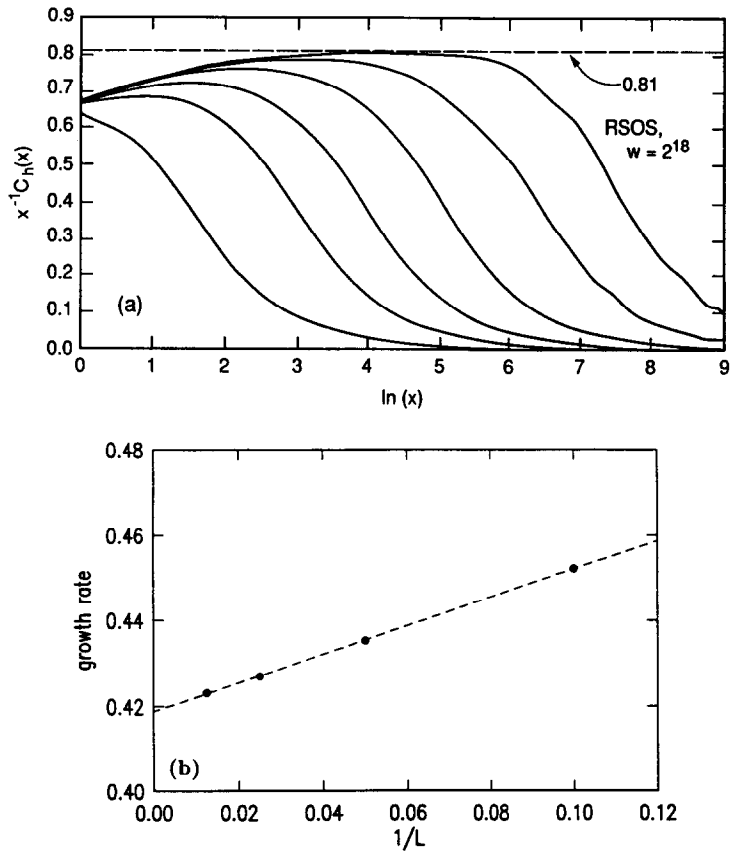

Fig. 3.5. Determination of the static amplitude A and the nonlinearity λ for the RSOS model of Kim and Kosterlitz via (a) height-difference correlation function, (b) finite-size dependence of the stationary growth rate [KrMHH92].

the predicted time dependence has been divided out and that the statistics of the second moment are considerably better than the third. A glance at the figure reveals $a_2 \simeq 0.051$ and $a_3 \simeq 0.0033$ which, with $\theta \simeq 0.0447$, see (3.91), implies $c_2 \simeq 0.405$ and $c_3 \simeq 0.074$. The former should be compared to the estimate in the literature for this universal quantity,

$$c_2 = 0.404 \pm 0.013 \tag{3.92}$$

obtained by studying many different models over nearly four decades in the scaling parameter θ, see Fig. 3.7. This plot stands as a strong testament to the broad collection of models that fall within the purview of KPZ universality. The point is driven home by Fig. 3.8, which shows the actual measured values of a_2, $|a_3|$, and a_v in a log-log plot, confirming the anticipated power-law scaling with θ. From the data, it is estimated that

$$|c_v| = 0.193 \pm 0.013 \tag{3.93}$$

a value easily appreciated by examining Fig. 3.6b, which shows the early-time correction to the average growth rate $\langle h \rangle / t$ vs $t^{-2/3}$ obtained from the PNG simulation discussed earlier. Here the slope of the dotted line, $a_v = c_v \theta^{1/3} \simeq -0.46/0.20 = -0.23$, is negative, consistent with the general rule-of-thumb that c_v, the amplitude prefactor detailing the leading correction to the asymptotic growth

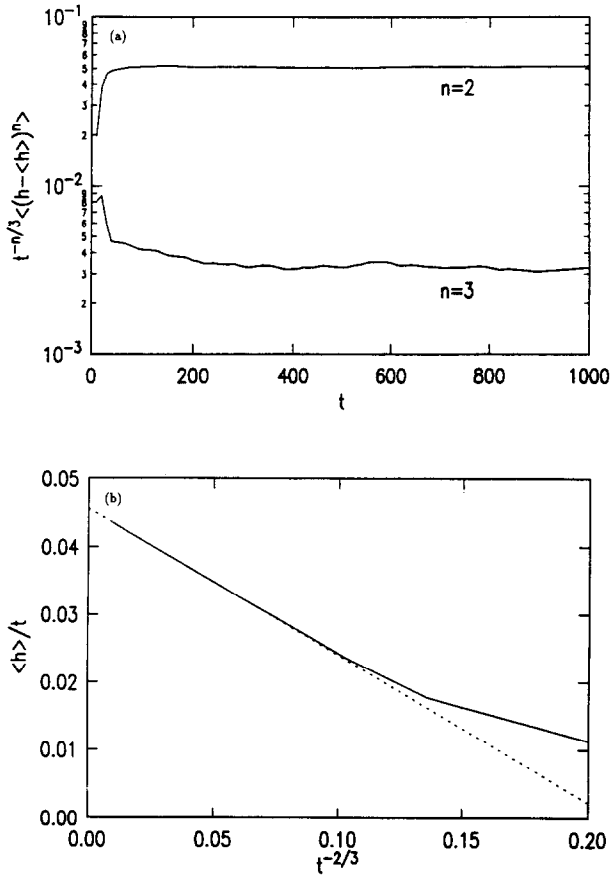

Fig. 3.6. PNG simulation data used to extract transient amplitudes [KrMHH92]. (a) 2nd and 3rd height fluctuation cumulant, with predicted time dependence divided out, (b) approach to asymptotic growth rate in the early-time regime.

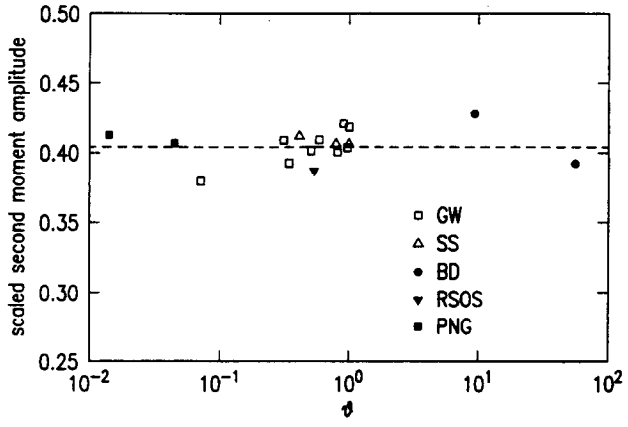

Fig. 3.7. Numerical results for the universal amplitude prefactor of the 2nd cumulant of the height fluctuations, obtained from a veritable cornucopia of stochastic growth models, including Gates-Wescott (GW), single-step (SS), ballistic deposition (BD), RSOS, and PNG, the last being evolved with nucleation probability $p = 0.0001, 0.001$. For details, see [KrMHH92].

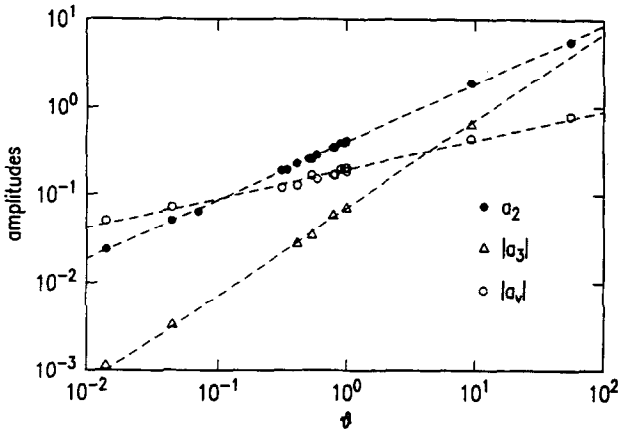

Fig. 3.8. Summary plot of the numerical estimates for the height cumulant and finite-size correction amplitudes. The dashed lines indicate the anticipated slopes [KrMHH92].

rate, and λ, the nonlinear coefficient, have *opposite* signs. By contrast, the sign of c_3 is observed to be equal to the sign of of λ in all cases, with magnitude, see Fig. 3.6a,

$$|c_3| = 0.071 \pm 0.005 \tag{3.94}$$

indicating that our rough estimate above for the PNG simulation wasn't all that bad. Note the sign. Finally, because of the difficulties associated with generating sufficiently good statistics, it is presently fruitless to go beyond the fourth cumulant of the early-time height fluctuations, for which Krug, Meakin and Halpin-Healy [KrMHH92] estimate the universal amplitude

$$c_4 = 0.02 \pm 0.002 \tag{3.95}$$

extracted from a simulation of the single-step model at zero tilt. It should be stressed that in each instance the value quoted above for the universal amplitude prefactors $c_{2,3,4}$ and c_v in the kinetic roughening context is in complete accord with that obtained for free energy fluctuations of directed polymers in random media [KBM91a,HH91,KrMHH92], see Section 5.4.4. In the hopes of establishing relevance to actual physical systems, such are the tasks necessary to fully document KPZ universality.

3.7.3. Skewness of the height fluctuation probability distribution

As mentioned earlier, whereas the steady-state height fluctuations are gaussian, at early times the related probability distribution is asymmetric, possessing nontrivial higher moment. This peculiar feature manifests itself most strongly at the level of the third cumulant, the sign of which, just discussed, is intimately tied to that of the coefficient λ. A useful measure of the asymmetry of the height fluctuation distribution is the *skewness* [W87,KrS88], defined as

$$s = \frac{\langle (h - \langle h \rangle)^3 \rangle}{\langle (h - \langle h \rangle)^2 \rangle^{3/2}} \tag{3.96}$$

which is estimated, in the transient regime, to take the value [KrMHH92]

$$|s| = 0.28 \pm 0.04 \tag{3.97}$$

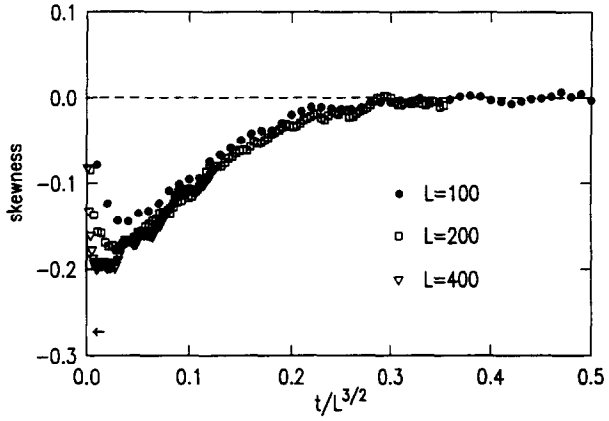

Fig. 3.9. Skewness of the height fluctuation probability distribution in the SS model for small system sizes. The arrow indicates the universal value for this quantity, obtained in the limit of infinite system size – see text.

a value in fine agreement with the skewness noted for the free energy probability distribution for directed polymers in random media, reported as

$$s_{DPRM} = -0.296 \pm 0.028 \tag{3.98}$$

by the same authors,and corroborated by the independent, rather thorough DPRM study of [KBM91a], which yields -0.29 ± 0.02. Because the skewness of the height fluctuation distribution is a *transient effect*, absent for $t \gg L^{z=3/2}$ where the height fluctuations are gaussian in nature, it is natural to conjecture a scaling form for the skewness,

$$s(t, L) = f_s(t/L^{3/2}) \tag{3.99}$$

where $|f_s(0)| \approx 0.28 - 0.29$ and the function f_s vanishes for large arguments. Fig. 3.9 shows the data collapse supporting such a conjecture where, in spite of severe finite-size effects which prevent the skewness from reaching the early-time maximum value gleaned in separate simulations, there is clear evidence of the above dynamic scaling form.

3.8. Inverse method for interface growth [LS93a]

In Eq. (3.1), the nonlinearity λ is model-dependent but unrenormalized, whereas ν and D are, individually, running phenomenological parameters, being functions of the observation length scale l. In fact, these two parameters scale as l^{χ} and in Section 3.7.2, we have discussed a technique for extracting their ratio $A = D/2\nu$, as well as the value of λ specific to particular models within the KPZ universality class. Taking an altogether different tack, Lam and Sander [LS93a] have subsequently proposed an inverse method that documents the individual scaling behaviors of these quantities. Their trick, very much in the spirit of a Monte-Carlo RG approach involving renormalized block-spins, but adapted to the continuum dynamical context, is to calculate directly the renormalization group flow of the KPZ equation itself by comparing to the evolution of single-step and BD surfaces coarse-grained on the scale l. This is done by examining successive, but appropriately averaged, snapshots $h(x, t + \Delta t)$ of the surface profile in the steady-state following time intervals Δt, and minimizing the mean square deviation from the assumed, though discretized description to determine λ, ν, and

D. Allowing a constant contribution to the growth rate, $\partial_t h = c + \nu\partial^2 h + \lambda(\partial h)^2 + \cdots$ introduces an additional phenomenological parameter c. In fact, the authors include the possibility of various higher order contributions to the minimal KPZ equation, such as $\partial^4 h$, $\partial^2(\partial h)^2$, $\partial h \partial^3 h$, etc., but large statistical uncertainties and finite-difference effects prevent them, unfortunately, from reporting conclusively that the relevant coefficients are vanishingly small, as expected. Nevertheless, it is reassuring that they first test their method on the EW universality class, finding the measured λ to be zero with high precision, lending much creedence to the technique.

We limit our discussion here to the Lam-Sander analysis of c, ν, λ, and D for the simplest single-step model (SS I), in which one attempts to add particles of height two atop the aggregate, without violating the constraint that nearest-neighbor height differences be ± 1. The great advantage of the SS model is that the steady-state probability distribution for the surface fluctuations is known exactly in 1+1 dimensions [MRSB86], so typical configurations can be generated directly (permitting an uncharacteristically large system size: $L = 32\,768$), a feature which Lam and Sander exploit with a vengence, their work focussed entirely on the steady-state. Beyond the probability distribution, much more is known about this special model; in particular, for finite-system size l, the the nonlinearity parameter, as well as the constant contribution to the growth rate approach their asymptotic values in a manner that is known exactly [KrM90], given by $\lambda = -[1-(l-1)^{-1}]^{-1}$ and $c = \frac{1}{2}[1-(l-1)^{-1}]^{-1}$, respectively. In Fig. 3.10, we reproduce both the exact (dotted curve) and numerically determined length scale dependence of c and λ for various values of the time difference Δt. Note that for $\Delta t \geq l^z$, where $z = 3/2$ in 1+1 dimensions, the finite-time difference approximation incurs deviation from the exact results observed in the large-l limit for all cases considered. Because of the the large system size simulated, Lam and Sander were able to cover more than two decades in the resolution scale l, an important ingredient to their success. In Fig. 3.10 are also shown data for the running, renormalized parameters ν and D, where it is evident that, for large l, these quantities saturate at well-defined values that scale with Δt. In fact, the numerics reveal $\nu/\Delta t^{1/3} \approx 0.413$ and $D/\Delta t^{1/3} \approx 0.399$, which yields a scale-independent ratio $D/\nu \approx 0.966$, in reasonably good agreement with the known exact result of unity [KrM90], though slightly smaller due to a systematic underestimation of the noise strength D, intrinsic to the method. Because of the restriction to a finite observation time Δt, rather than the long-time limit characteristic of dynamic RG calculations [MHKZ89], Lam and Sander were obliged to test, independently, the scaling form

$$\nu(l, \Delta t) = l^{\chi} f_1(\Delta t/l^z) = \Delta t^{\beta} f_2(\Delta t/l^z) \tag{3.100}$$

assumed in their analysis. Nevertheless, a plot of $\nu/\Delta t^{\beta}$ vs. $l/\Delta t^{1/z}$ produced excellent data collapse for critical exponents $\beta = 0.33 \pm 0.01$ and $z = 1.50 \pm 0.04$, confirming the validity of their method. Finally, calculation of the the fixed point value of the dimensionless coupling constant, suitably adapted to the method, produced the value $\bar{\lambda}^2(\Delta t) = [\lambda^4 D^2/\nu^5)\Delta t]^{2/3} \approx 5.66$ for the SS I model. Similar calculations for a second single-step model with parallel updating, as well as two variants of ballistic deposition produced 5.68, 5.30, and 5.45, respectively, leading the authors to quote $\bar{\lambda}^2(\infty) = 5.5 \pm 0.2$ as the first numerical estimate for this universal quantity in 1+1 dimensions.

3.9. Kuramoto-Sivashinsky equation

Familiar from a variety of different physical contexts such as chemical turbulence [K84], flame front propagation [S77], and the dynamics of liquid films subject to gravity [S80], the Kuramoto-

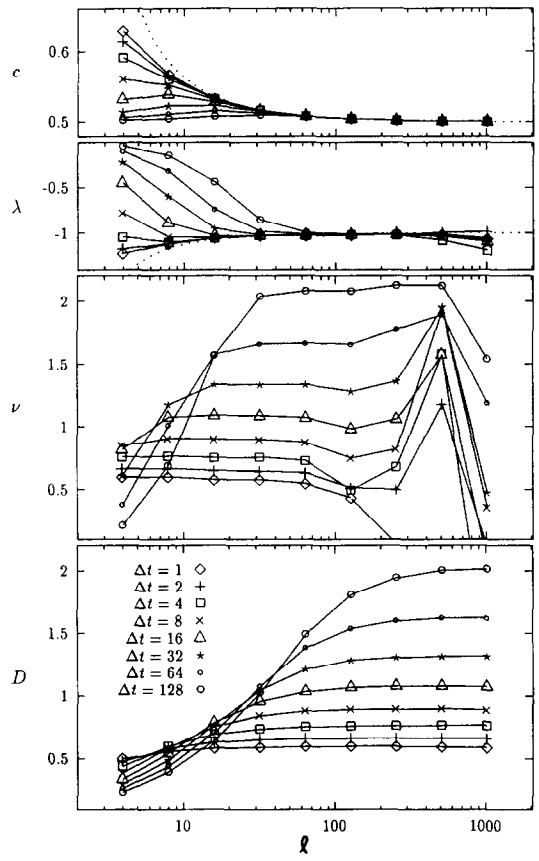

Fig. 3.10. Numerically extracted the parameters c, λ, ν, and D as functions of length scale l and time-increment Δt, as determined for the single-step model (SSI) in 1+1 dimensions [LS93a].

Sivashinsky (KS) equation

$$\frac{\partial h}{\partial t} = -\nabla^2 h - \nabla^4 h + (\nabla h)^2 \tag{3.101}$$

has become an object of intense inquiry as a toy model of spatially extended chaos, with a particular emphasis on the manner in which it engenders large-scale stochastic behavior. Here, the scalar field $h(\boldsymbol{x}, t)$ refers, for example, to the local phase of the cyclic chemical reaction or the height of the evolving flame front, while all dimensionful phenomenological parameters have been absorbed into definitions of h, $\boldsymbol{x}$, and t. Observe that although a flat interface, h = const., is the trivial solution to this entirely deterministic equation, a linear stability analysis reveals it to be unstable, thanks to the negative Laplacian which allows small-q perturbations to grow at a rate $\omega(q) = q^2 - q^4$, giving rise to a cellular local structure of wave-vector peaked at $q_0 = 1/\sqrt{2}$. As shown by Pomeau, Pumir and Pelce [PPP84], the KS equation produces at large times a turbulent, chaotic steady state, characterized by a situation in which fluctuations generated by the instability are transferred by the nonlinear term to larger q, where they are dissipated by the stabilizing fourth-order derivative. In fact, as first conjectured by Yakhot [Y81] following a mode-coupling analysis of Fujisaka and Yamada

[FY77], but only dealt with recently in the numerical studies of Sneppen et al. [Sne92] and Hayot, Jayaprakash and Jossand [Hay93]. The large-time, long wavelength properties of the deterministically chaotic KS equation are now understood to be controlled, at least in the case of 1+1 dimensions, by the strong and weak coupling fixed points of the stochastic KPZ equation

$$\frac{\partial h}{\partial t} = \nu\nabla^2 h + \lambda(\nabla h)^2 + \eta \tag{3.102}$$

where $\nu > 0$ and $\eta(x,t)$ is the Gaussian white noise with covariance $\langle \eta(x,t)\eta(x',t')\rangle = D\delta(x - x')\delta(t - t')$, discussed earlier – see Section 3.1. Note that in order for these two quite dissimilar PDEs to yield the same long-time, large length-scale behavior, two rather extraordinary events must take place. The fluctuations inherent in the KS equation must not only renormalize the coefficient of the Laplacian, rendering it positive (in which case the fourth order derivative becomes irrelevant in the RG sense and one is left with a positive interface tension ν), but must also effectively create from within, so to speak, a stochastic driving force with short-range correlations! That this, indeed, is the state of affairs, was established by Zaleski [Zal89], who employed a constructive, Wilsonian RG to explicitly integrate out degrees of freedom, his numerical work on the KS equation indicating a large, but positive, effective interface surface tension. Ironically, as shown by several authors [Sne92,Hay93], who based their numerical studies on results of Krug, Meakin and Halpin-Healy regarding the universal amplitudes [KrMHH92], the large positive renormalized ν characteristic of the KS equation is, unfortunately, responsible for an extended crossover regime in which the dynamic scaling properties of the interfacial fluctuations are governed by the Edwards-Wilkinson exponents of the weak-coupling fixed point, where $\lambda = 0$. Eventual crossover to the strong-coupling region ($\lambda \neq 0$), where the nonlinearity is omnipotent yielding a dynamic index $z = \frac{3}{2}$, is long delayed – a fact which early investigators [M81,Zal85,Hy86] of the KS equation came to appreciate all too well.

As alluded to previously, the RG studies of the KPZ equation in 1+1 dimensions make rather explicit predictions concerning dynamic correlations in a kinetically roughened interface, as it relaxes into the steady state starting from a flat initial configuration, $h = 0$. In particular, the scaling form for this transient relaxation has Fourier components that obey

$$\langle |h(q,t)|^2 \rangle = \frac{A}{Lq^2} g_{tr}(q^z t) \tag{3.103}$$

where L is the system size and a fluctuation-dissipation theorem [HuHF85] reveals that $A = D/2\nu$ is fixed by the linear theory ($\lambda = 0$). The transient scaling function g_{tr} has the limiting properties that $g_{tr}(0) = 0$ and $g_{tr}(\infty) = 1$. In their seminal work, Sneppen *et al.* numerically integrated the KS equation by brute force methods and measured the dynamic exponent via the interface width, which behaves in the large system limit $L \to \infty$) as

$$\xi(t)^2 = \langle (h - \langle h \rangle)^2 \rangle \sim t^{2\beta} \tag{3.104}$$

where $\beta = 1/2z$. In the labored intermediate scaling regime where the EW fixed point dictates the scaling, $z = 2$ and $\beta = \frac{1}{4}$. Sneppen et al. estimate the time scale for the onset of the asymptotic regime with $z = \frac{3}{2}$ and $\beta = \frac{1}{3}$, by computing the interface width in the absence of the nonlinearity,

$$\xi^2_{\lambda=0}(t) = \frac{D}{\sqrt{2\pi\nu}} t^{1/2} \tag{3.105}$$

and then comparing it to known result for the complete KPZ equation,

$$\xi^2_{KPZ}(t) = c_2(A^2\lambda t)^{2/3} \tag{3.106}$$

where $c_2 \approx 0.40$ is a universal number characteristic of the strong-coupling fixed point [KrMHH92], recall Section 3.7.2 and Fig. 3.7. These considerations yield the crossover time scale

$$t_c = \frac{2^5}{\pi^3 c_2^5}\frac{\nu^5}{D^2\lambda^4} \approx \frac{252}{\nu g^2}. \tag{3.107}$$

Here, $g = \lambda^2 D/\nu^3$ is the standard coupling constant, familiar from previously discussed RG analysis.

A glance at this last equation reveals the following important features. Firstly, for the case at hand of one spatial dimension, g has units of inverse length, so that $t_c \sim 1/\nu g^2$ is clear from dimensional considerations. Nevertheless, the presence of the large prefactor, with its damaging implications for numerical simulations of the KS equation, could be appreciated only after the universal amplitude c_2 had been pinned down. Secondly, determination of the precise value for the crossover timescale necessitates knowledge of the phenomenological parameters ν, λ, and D appropriate to KS kinetic roughening. The systematics of pinning down these effective, macroscopic coefficients for a given lattice simulation has been codified by Krug, Meakin, and Halpin-Healy [KrMHH92]. Finally, observation of the asymptotic regime is possible only if t_c is small compared to the saturation time induced by the finite system size L. This requirement renders manifest the serious computational demands of the task, for an estimate of the saturation time can be had by equating (3.105) or (3.106) with the saturation width

$$\xi^2_\infty(L) = \frac{AL}{12} \tag{3.108}$$

obtained by summing over the long-time limit of the Fourier modes (3.103). The resulting criterion for the accessibility of the asymptotic regime is $L \gg L_c \approx 152/g$. Since Sneppen et al. discovered the KPZ coupling constant $g \approx 0.060 \pm 0.016$ which implies $L_c \simeq 2500$, it is not at all surprising that early numerical work [Hy86,Zal89], using fairly modest system sizes, remained stuck in the intermediate scaling regime. This value of g, as well as the phenomenological parameters ν, λ, and D, were determined for the KS simulation as follows [Sne92]:

(i) Using (3.108), but accomodating the large intrinsic width [KW88] arising from the local cellular structure of the KS flame front, the static amplitude $A = D/2\nu$ can be estimated by studying the finite size dependence of the saturated width. Alternatively, see Fig. 3.11, one can extract this quantity by examining the small-q behavior of the stationary Fourier spectrum. Sneppen et al. obtained $A = 0.158 \pm 0.009$ employing this procedure, a value that was entirely consistent with their estimate $A \approx 0.154$, obtained by the former method. Unfortunately, despite the two means of attack, it is this quantity, compared to the others to be discussed, that suffers the greatest uncertainty, the order of 6%.

(ii) By focussing their attention on the time dependence of the interface width in the intermediate scaling regime, see Fig. 3.12 and Eq. (3.105), these authors were able to establish another relation between the phenomenological parameters, $D/\sqrt{2\pi\nu} = 0.397 \pm 0.001$. This result, taken with the previous one for the L-dependence of the saturation width, imply the effective parameters, $D_{KS} = 3.2 \pm 0.1$ and $\nu_{KS} = 10.5 \pm 0.6$, the last being an explicit confirmation of Zaleski's large, positive interfacial tension.

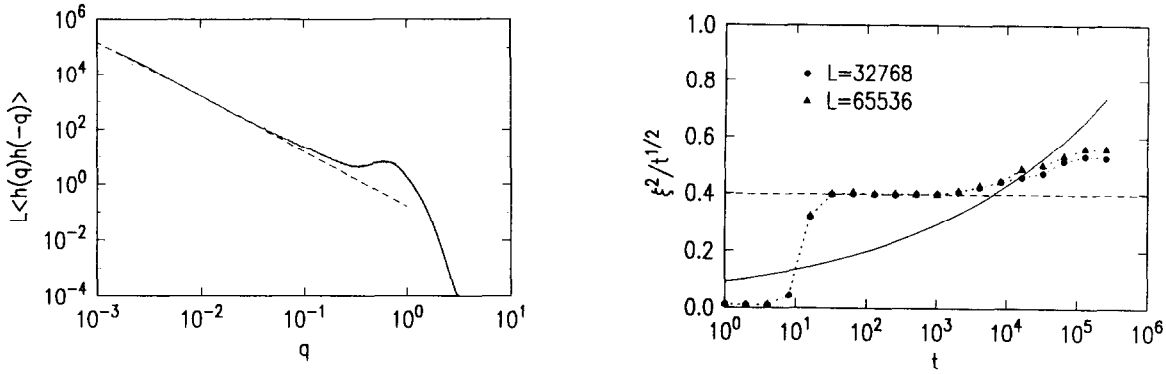

Fig. 3.11. Fourier spectrum of the stationary height fluctuations, as determined in the the brute force integration of the KS equation for system size L=4096 [Sne92]. The dashed line corresponds to the long-wavelength behavior A/q^2 with $A = D/2\nu$=0.158 and the peak at $q_0 = 1/\sqrt{2}$ dictates the scale of the cellular structure characteristic of the KS flame front interface.

Fig. 3.12. Time dependence of the rms width of the KS interface. The data for the larger system size $L = 65536$, follow from an average over 70 independent runs, while the smaller simulation involved 152 runs. The dashed line yields the estimate $D/\sqrt{2\pi\nu} = 0.397$, while the full line shows the asymptotic KPZ behavior $\xi^2(t) = 0.092t^{2/3}$.

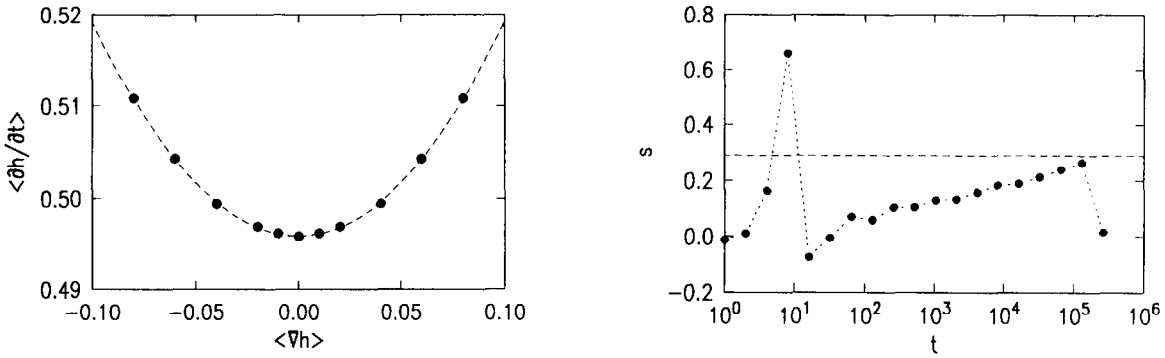

Fig. 3.13. Extraction of the phenomenological KPZ nonlinearity parameter λ appropriate to the KS interface is obtained by studying the tilt-dependence of the asymptotic growth velocity. The data here are for a system size L=1024 and the velocity was averaged over the time interval $4.19 \times 10^5 < t < 1.26 \times 10^6$, see [Sne92].

Fig. 3.14. *Skewness* of the KS interface as a function of time confirms membership in the KPZ universality class. The system size is L=32678, with averaging performed in this case over 40 independent runs. The horizontal dashed line corresponds to the KPZ value $|s| = 0.29$, see [KrMHH92].

(iii) Finally, the coefficient λ is estimated via the expansion $v(\theta) \approx v_0 + (\lambda/2)\theta^2 + \cdots$ of the ensemble averaged growth rate $v = \langle \partial h/\partial t \rangle$ at a fixed macroscopic inclination $\theta = \langle \partial h/\partial x \rangle$; see Fig. 3.13 which yields $\lambda_{KS} = 4.65 \pm 0.15$.

With these values for ν, λ, and D, one obtains, as advertised above, the coupling constant $g \approx 0.60 \pm 0.016$, which indicates that system sizes exceeding $L_c \approx 2500$ are needed to observe asymptotic KPZ behavior with the crossover time roughly $t_c \approx 7000$. Interestingly, this is precisely when deviations from Edwards-Wilkinson behavior, $\beta = \frac{1}{4}$, is noted in the simulations [Sne92], see Fig. 3.12. Observe, furthermore, that the data appear to approach the asymptotic behavior up to $t \approx 10^4$, where it is cutoff and the size dependence of the width manifests itself, indicating the onset

of saturation effects. Additional evidence supporting Yakhot's conjecture that the one-dimensional deterministic KS equation belongs to the universality class of noisy interface models described by the KPZ equation is provided by the *skewness* of the height fluctuations. Recall, see section 3.7.3, that the asymptotic regime is characterized by a universal skewness of magnitude $|s| \approx 0.29$ and a sign equal to the sign of λ [KrMHH92], while the surface fluctuations in the intermediate ($\lambda = 0$) scaling regime are strictly Gaussian with $s = 0$. Fig. 3.14 shows the simulation results for the skewness of the KS equation [Sne92]. The skewness is nonzero and positive, entirely consistent with the observation that $\lambda > 0$, discerned in studies of the tilt-dependent growth velocity, recall Fig. 3.13. After a peak incurred by the initial exponential instability, the skewness increases slowly in time and reaches a maximum value of 0.26, rather close to the prediction. The sharp decrease in the skewness at the latest times is, again, a consequence of saturation effects, which are known to set in early and abruptly for this quantity.

After initial numerical work, people realized that the key question is whether KS and KPZ equations at large scales belong to the same universality class. In 1+1 dimensions, this question appears to have been settled. The Weizmann group [LLPP93] has shown that to all orders in their perturbative expansion KS and KPZ indeed have the same asymptotic behavior. What is important is to realize that the KS equation does not have weak coupling solutions, as opposed to the KPZ counterpart. Are the asymptotics of the KS equation dictated by KPZ for all dimensionalities? In the most interesting case, $d = 2 + 1$, the situation appears particularly subtle [JHP93] – numerical [P92] and analytical [LP92,LLPP93] work suggesting that the large-scale behavior is not that of the KPZ universality class. L'vov and Procaccia [LP92] found that KS in $d = 2 + 1$ has the "trivial" dynamic scaling exponent $z = 2$, this is also supported by numerical work of Jayaprakash, Hayot and Pandit [JHP93]. However, intepretations of the results vary much. What is likely at the origin of the earlier confusion is that even though KS appears to have the trivial scaling in $d = 2 + 1$, but it is a nontrivial strong coupling result, its nature is very different from RG point of view from that of KPZ. In the end we recall KS is a very peculiar system that does not possess a weak coupling region by construction (built-in linear instability).

3.10. Singular interface equation

Another deterministic equation which, nevertheless, gives nontrivial self-affine dynamic scaling is the following [Z92],

$$\frac{\partial h}{\partial t} = \nabla^2 h + \ln|\nabla h|. \tag{3.109}$$

This equation was a by-product in the study of complex directed polymers. Here we are not interested in its origin, but consider the above equation as a prototype of much more complicated systems. Note that (3.109) is unstable, for the interface cannot be flat, thus the most natural starting configuration is denied! In this manner, an amusing contradiction arises: no matter what configuration we start with, the surface tension term strives to flatten the interface, whereas the logarithm opposes such attempts. These two conflicting tendencies drive the interface in perpetual chaotic motion. Before discussing the model any further, let us emphasize a fundamental distinction between lattice and continuum versions. Firstly we examine the continuum description in $d = 1$. Define $v = \partial_x h$ as we did before and (3.109) becomes

$$\dot{v} = \partial_x^2 v + \frac{\partial_x v}{v} \tag{3.110}$$

multiplying both sides by $v/2$ and integrating over x, we obtain

$$\frac{d}{dt}\int v^2 dx = -\int (\partial_x v)^2 dx \tag{3.111}$$

where we have dropped the surface terms. Defining the total energy

$$E = \int v^2 dx \tag{3.112}$$

(this is only true for $d = 1$) we see that E vanishes in the infinite time limit (V. Lebedev is thanked for helpful remarks). The only possible solution is $v = 0$ everywhere or $h(x, t)$ is flat ($h =$ constant), contradicting the singular term. While the above analysis is nominally correct, we note that the stability associated with zero energy is extremely fragile; so much so that any discretization cannot possibly preserve it! As a consequence, Eq. (3.109) realized on a lattice is fundamentally different from its continuous counterpart. Thus, even though we may write down a continuous equation, at the end of the day our attention will be focussed upon the discretized version, which is inherently chaotic and unstable.

It is important to stress that, as soon as we are away from a condition of zero slope, the singular term is quite benign – large pushing forces become tamed once again by the relaxation term. Observe that chaos does not mean no order at all, since experience shows that the simulational data follow well defined scaling behavior. For example, starting from a globally flat configuration (e.g., alternating $\nabla h = \pm c$), we find that the early-time roughness of the interface scales as $w \sim t^{\beta}$, with $\beta \simeq 1/5$. Unfortunately, present day analytical tools are not sufficiently powerful to permit us to discern the exponents in a rational way. In summary, this equation exhibits intriguing scaling behavior – it is deterministic, yet unstable just like the KS equation, but differs from the latter in that it is linearly stable with a nonlinear instability providing effective noise as well as nontrivial interactions.

The above equation is an extreme case of the generalized KPZ equation without external driving noise

$$\dot{h} = \nabla^2 h + \tfrac{1}{2}|\nabla h|^{\alpha} \tag{3.113}$$

where α is a non-negative constant. Krug and Spohn [KS91r] first considered this type of generalization. Typically one starts with a rough initial condition and follow the slow decay of the initial fluctuations. Implicitly one usually assumes that without driving noise the above equation is stable. However, while this is true for $\alpha \geq 1$ (Krug and Spohn examined $\alpha = 1$), there is a hidden instability for $0 \leq \alpha < 1$. Consider an initially flat surface with only infinitesimal ϵ deviations, it is easily shown that (Zhang, unpublished 1992)

$$\dot{\epsilon} = -\epsilon + |\epsilon|^{\alpha} \tag{3.114}$$

leads to uncontrolled growth of such deviations – thus instability. However, unlike in the KS equation where we need an extra term to tame the eventual explosion, here everything is well behaved – surface tension term soon has the upper hand over the nonlinear term. Therefore microscopically fluctuations can only grow to order unity and the Lyaponov's exponent is strictly zero. Yet this non-singular equation (as opposed to $\log|\nabla h|$) perpetually roams in chaotic attractors since no single

configuration is stable, but with well defined self-affine roughening exponents. For related numerical study, see Amar and Family [AF93] (and M. Vicsek and T. Vicsek, unpublished 1994).

4. Nature's kinetic roughening phenomena

4.1. Experimental manifestations

In the preceding chapter, we have presented the KPZ equation and its kin as a relatively smooth story; indeed, theorists were tempted, early on, to put them in the archives in a complete, contradiction-free account, since the analytical and simulational results went essentially hand-in-hand. They did not bother to check experimental situation initially, assuming perhaps that it would follow suit. However, a few years later, a new breed of experimentalists emerged, including many improvising theorists, to spoil such naive dreams. They didn't give a damn at all about the KPZ equation, nor sophisticated renormalization group analyses, but rather went about the business of explicitly observing Nature's own kinetic roughening phenomena by means of various ingenious, desk-top experiments. To the surprise of many theorists, the apparently simple, real interfaces exhibit very different scaling behavior than that of the naive predictions. Eventually, theorists were obliged to rethink the implicit assumptions, a fruitful process that revealed many additional hidden secrets of the KPZ equation, including the lack of continuum limit, growth nonuniversality, and to consider other experiment-motivated models using, most notably, quenched disorder.

This section is devoted to a discussion of a number of intriguing small-scale experiments which have recently caused substantial debate within the community thanks to their apparently conflicting, unanticipated findings. Naively, the first three experimental systems, which concern in turn the interfacial dynamics of fluid flow through porous media, the growth of bacterial colonies, and fire front propagation, might be typecast as potentially ideal physical realizations of interface growth phenomena. Nevertheless, the experimental situation has stubbornly resisted such a quick and simple characterization, resulting in various amendations within the theory, such as the possiblity of non-gaussian power-law noise, correlated noise, quenched disorder, as well as alternative models based on completely different physical ideas, such as the directed percolation and random-field arguments in the case of viscous imbibition and forced fluid flow experiments, respectively. The bottom line is that in each of these experimental contexts, the kinetically roughened interface, though self-affine, behaves *anomalously* in that it is typically described by a saturation width exponent $\chi \approx 0.7$–0.8 that exceeds the naive value $1/2$, assuming uncorrelated Gaussian noise. Surprisingly enough, the fourth experimental system that we discuss explicitly, electrochemical deposition of copper, perhaps the least promising candidate to exhibit the unadulterated scaling behavior, nevertheless possesses a measured self-affine roughness exponent entirely consistent with standard expectations. Here, we briefly cover the various systems, following up with veritable feast of theoretical ideas seeking to reconcile the theory and experiments. We propose, as well, some new experiments, including the acidic erosion of vulcanic rock as a means of exploring the isotropic fractal surface growth mechanism.

4.1.1. Forced fluid flow in porous media [Rubio89,Wong92b]

The displacement of one fluid by another in porous media has, in the course of the last decade, revealed itself to be a startling rich and devilishly subtle experimental system, very strongly dependent

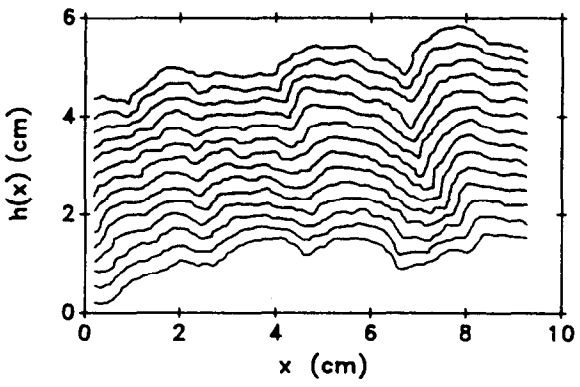

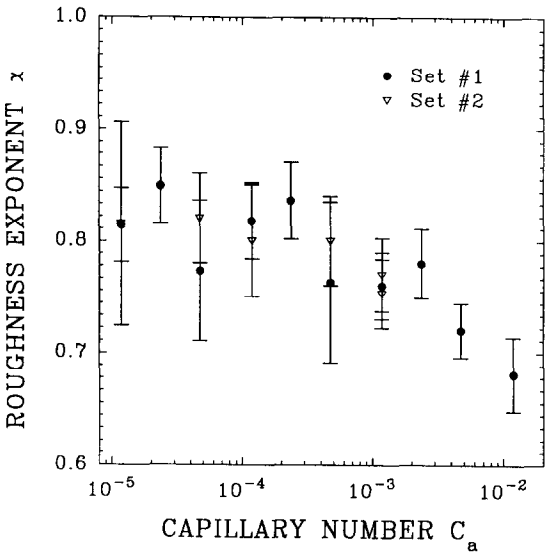

Fig. 4.1. Successive interface profiles – fluid flow through porous media [Rubio89]. The time interval between configurations is 30 s. The capillary number $Ca = 4.93 \times 10^{-3}$.

Fig. 4.2. Anomalous roughness exponent χ as a function of capillary number – fluid flow in porous media [Wong92b].

on a variety of factors such as the relative viscosities of the two fluids, as well as their mutual wettability with respect to the host medium, nevertheless yielding a wonderful array of flat, fractal, and self-affine interfaces [Wong92c]. Here, we concentrate on the very special case of *forced flow*, which refers to the displacement of a nonviscous nonwetting fluid (typically air) by a more viscous wetting fluid (water, glycerol,...) in an essentially two-dimensional random bead pack sandwiched between a pair of rectangular glass plates. In Fig. 4.1, we show a plot which collects a series of interface profiles, captured by video camera, as the water advances. This landmark experiment on the resulting kinetically roughened self-affine interfaces was performed by Rubio, Edwards, Dougherty, and Gollub [Rubio89], who reported an apparently robust roughness exponent $\chi = 0.73 \pm 0.03$, as their control parameter, the modified capillary number $Ca = \eta v a^2/k\gamma$, varied over nearly two decades, between 10^{-3} and 10^{-1}. Here η is the dynamic viscosity of the water, v the average interface velocity, a the average bead size (100, 200 or 350 μm, diameter variation the order of 20%), k the hydraulic permeability, and γ is the air-water interfacial tension; as such, Ca provides a useful measure of the ratio of the average viscous pressure drop across a bead, $\eta v a/k$, to the capillary pressure in a single pore, γ/a. Recall that it is the competition between the global viscous pressure drop, which works to flatten the propagating interface, and the local fluctuations in the capillary pressure due to the random medium, which work mercilessly to roughen it. Rubio, et al. noted, too, that the amplitude of the roughness increased with falling capillary number, according to $A \propto Ca^{-0.47\pm0.06}$. The experimentalists alluded to a variety of theoretical explanations, including a stubborn stochastic PDE with *quenched* noise [BA84,KL85], *correlated* noise [MHKZ89], as well as the hands-on microscopic model of Cieplak and Robbins [CR88]. Subsequent experiments by Horváth, Family and Vicsek [HFV91a,b] suggested different, though still anomalously roughened interfaces, while endorsing entirely new unrelated theoretical viewpoint, advocating *power-law* noise. In the following sections, we address these matters.

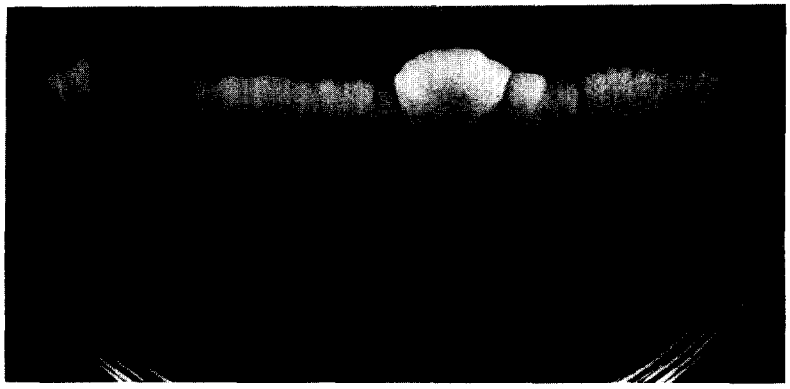

Fig. 4.3. *Aspergillus Oryzae* colonies grown on glucose rich medium [MM92].

The entire experimental situation has been further exacerbated recently by the very careful work of He, Kahanda and Wong [Wong92b], who redid the Rubio experiment on a grander scale using a larger Hele-Shaw cell (26×116 cm) that possessed a smaller gap (just 0.9 mm rather than 1.5 mm, yielding a much better aspect ratio) and covering three decades in capillary number, roughly 10^{-5} to 10^{-2}. They find, see Fig. 4.2, that the effective roughness exponent χ does vary with capillary number! Furthermore, taking their cue from Kessler, Levine and Tu [KLT91], they argue that in the limit $Ca \to 0$, the dynamics are controlled by many metastable, but partially pinned interfacial configurations, yielding the RF Ising model roughness exponent of unity, while in the opposite limit, $Ca \to 1$, the Koplik-Levine equation reduces to KPZ with index $\chi = 1/2$. Unfortunately, such a limit involves a fast-moving interface with a vanishingly small roughness amplitude, which may render fluid flow in porous media a poor testing ground for the theory of kinetic roughening.

4.1.2. Self-affine bacterial colonies [VCH90,MM92]

In one of several resounding successes scored on behalf of the legitimacy of Nature's fractal geometry, Fujikawa and Matsushita [FM89] managed to grow bacterial colonies under near starvation conditions giving rise to stunning DLA type patterns with fractal dimension surprisingly close to the anticipated value $d_f \approx 1.73$. More recently, Vicsek, Cserzo and Horváth [VCH90], Matsuura and Miyazima [MM92], and Diratzouian et al. [DHHT93], motivated by the new interest in kinetic roughening of self-affine surfaces, have considered the opposite limit in which the growth is *reaction*-rather than *diffusion*-limited, very much in the spirit of the original Eden model. By providing the bacteria with a nutrient-rich agar (the food stuff content is typically $10\times$ greater than that yielding DLA-type patterns), and inoculating the medium with a line rather than a point source to insure self-affinity, these experimenters were able to study the role of stochastic roughening in a biological context. The micro-organisms used were *Escherichia coli* [VCH90], *Bacillus subtilis* [VCH90, DHHT93], both fairly mundane bacterial species, and *Aspergillus oryzae* [MM92], a fairly common fungus. In each case the colonies were observed to exhibit self-affine scaling, though the roughening was always anomalous, characterized by an exponent greater than the value $\chi = 1/2$. We show in Fig. 4.3, a typical self-affine fractal growth front of *Aspergillus oryzae* [MM92], which was grown on Czapek synthetic agar medium, containing $NaNO_3$, K_2HPO_4, $MgSO_4 \cdot 7H_2O$, KCl, $FeSO_4 \cdot H_2O$, glucose, and Difco Bact-Agar 1.5wt% in a 9cm diameter Petri dish for several weeks. As is apparent from Fig. 4.3, the fungi consist of multi-branched filaments (called *hyphae*) that

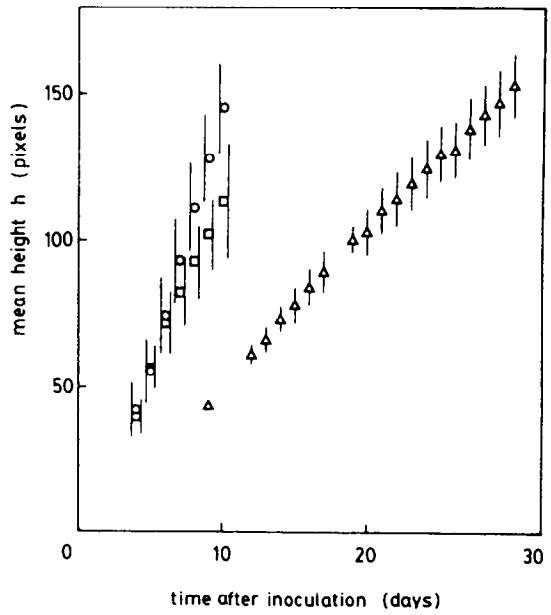

Fig. 4.4. Growth of *Aspergillus Oryzae* colonies on solid media for various concentrations of foodstuffs and at different temperatures. ⊙: 0.1 wt% glucose, 24°C; △: 0.1 wt% glucose, 18°C; □: 0.01 wt% glucose, 24°C [MM92].

evolve at different rates, resulting in the formation of fjord-shaped cleavages, also observed for the bacterial colonies [DHHT93]. The fungal growth proceeds via cytoplasmic flow towards the tips of these filaments, resulting in their stochastic augmentation. Nevertheless, the geometric aspects of the spatial distribution of the filaments depends in a highly nontrival manner on a variety of factors, including the diffusion of nutrient substances, temperature, respiratory conditions, as well as other biological matters of importance, such as autotropism among the growing filaments and the inevitable accumulation of waste products. In Fig. 4.4, we show the average growth rate for this *Aspergillus oryzae* experiment. Note that, in contrast to our experience with standard stochastic growth models, such as Eden and ballistic deposition, the growth rate in an actual biological system is not automatically constant, but can actually decease slightly with time, which Matsuura and Miyazima attribute to the gradual formation of the global fiord structure. This feature naturally causes difficulty defining the early time exponent β and work is presently in progress to investigate this matter further for the bacterial colonies proper [DHHT93], though it should be mentioned that an entirely analogous effect is observed in the viscous fluid imbibition experiments, see previous section. In any case, there is no ambiguity concerning the extraction of the roughness exponent, only the limitations posed by finite-size and boundary effects (painfully apparent in Fig. 4.3). For their fungal colonies, Matsuura and Miyazima show no data, but quote the value $\chi = 0.70 \pm 0.07$ for a sample grown at 18°C. At 24°C, the roughness exponent was a bit lower, leading them to suggest, somewhat generously perhaps, that it was Eden-like. In Fig. 4.5, we show the relevant data of Vicsek, Cserzö and Horváth [VCH90] for their work on *Escherichia coli* grown on nutrient rich LB agar. A least-squares fit in their log-log plot of the length-scale dependent surface width reveals a roughness exponent $\chi = 0.78 \pm 0.07$,which again is well above the standard value. Their work on *Bacillus subtilis* produced similar results, with $\chi \approx 0.74$, which led the authors to suggest that correlations (Section 4.3.1) in the surface

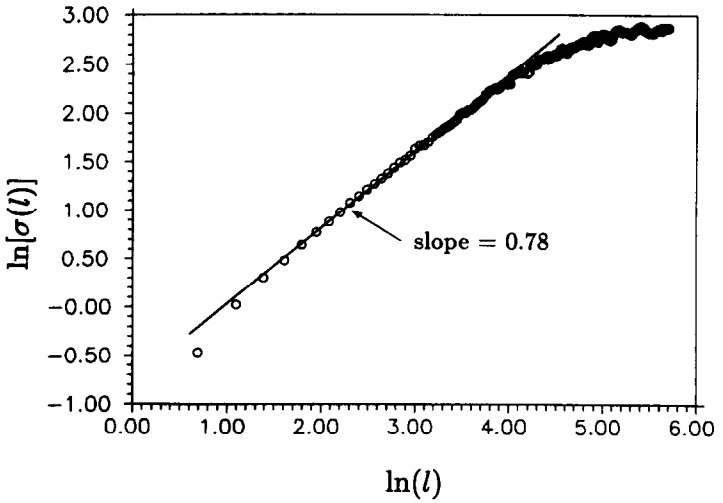

Fig. 4.5. RMS width of a self-affine *E. Coli* bacterial colony interface, as a function of lengthscale [VCH90]. The anomalously high roughness exponent χ is indicated.

growth were responsible for the anomalous roughening. The moral, however, is clear – much more work needs to be done to understand the complexity of bacterial colony formation. Of course, the biology community has come upon these same issues from a vantage point [e.g., Shap87] quite independent, and different from that of kinetic roughening phenomena. Even so, the latter can be a fruitful departure point, indeed; witness the recent phase diagram work of Matsushita and Matsuyama [MM93,OMM92], as well as efforts by Ben-Jacob et al. [EBJ94] to unearth self-organizational aspects of colony growth.

4.1.3. Flameless fire lines

Ecologists and physicists alike have long been interested in understanding the dynamics of forest-fire propagation. Early fire-spread models (see, for example, [GGN83]) were focussed primarily upon the final contours of regions burnt by forest fires started from a solitary point in a random fuel bed, a situation naturally akin to Eden growth in the radial geometry. While Sornette and Zhang [SZ93] are presently analyzing satellite photographs of large-scale forest fires across the globe to ascertain precisely how far this suggestion can be pushed, a group in Copenhagen [ZZAL92] recently performed an idealized paper-burning experiment to examine, first-hand, the kinetic roughening of a propagating fire line. The paper consumed by fire in their experiment, ordinary optical lens cleaning tissue, is noted for its extreme lightness, just 9.1 g/m^2 (or thickness 45 μm) – roughly 1/9 that of standard Xerox paper. The fineness of the lens tissue helps keep heat production by the fire to a minimum, thereby avoiding additional complications due to fire propagation by strong air circulation, as well as associated effects of turbulent smoke. Indeed, by treating their samples (46 cm wide by 110 cm tall) with KNO_3 solution, a common oxidation aid employed in the design of explosives, the experimenters were able to achieve flameless, relatively slow burning for a KNO_3 concentration slightly above a lower threshold value 0.87 g/m^2, yielding a mean fire propagation speed near 5.5 mm/s. Increasing the KNO_3 concentration toward an upper threshold value 1.6 g/m^2 resulted in a faster propagation speed, near 8.2 mm/s, but eventually caused the sample to burst into flame

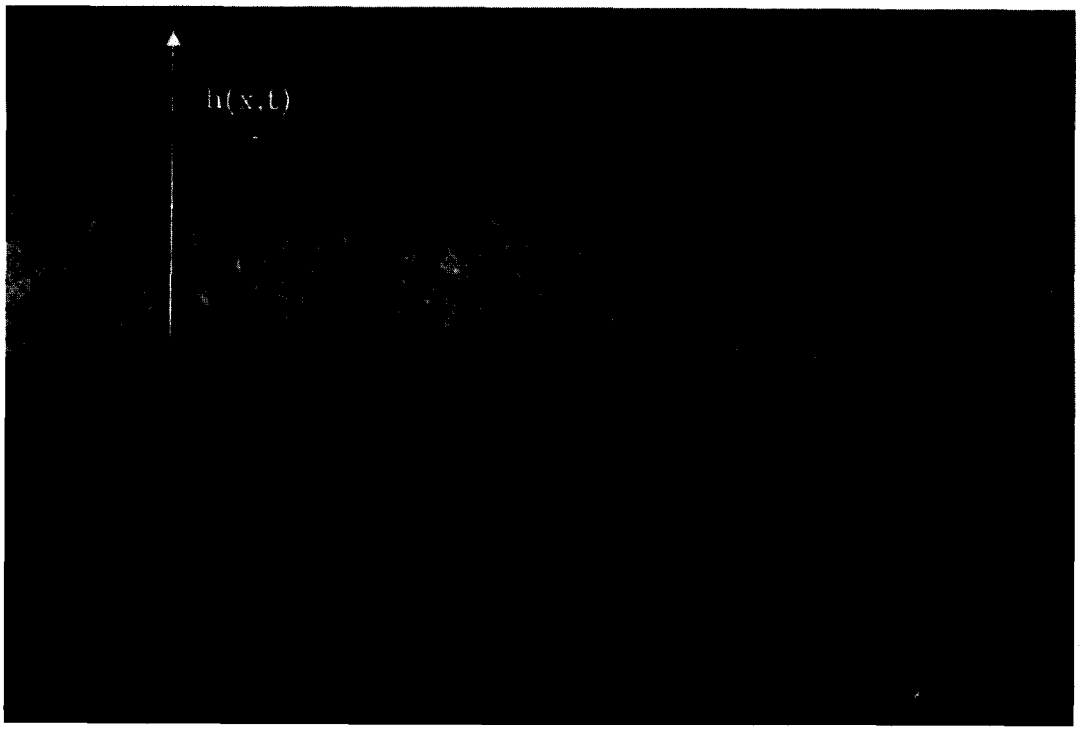

Fig. 4.6. A 8.5 cm segment of the 46 cm wide fire line in paper burning experiment [ZZAL92]. The fire is propagating upwards, with minimal flame and a near absence of turbulent smoke.

in a somewhat undesirable fashion. Paper preparation was a highly nontrivial matter because of the necessity of maintaining a flat sheet as the sample dried following treatment with the KNO_3 solution. The paper was then set in a vertical frame, a slight tension applied to its lateral sides, and finally ignited by a straight electric heating wire attached to the bottom side, which insures the self-affine character of the geometry. The propagating fire front is kinetically roughened by dynamical fluctuations, as an initially straight fire line gradually develops irregular features on ever larger length scales. In Fig. 4.6 is shown a section of the evolving fire line after some 80% of the sample has been consumed, with $h(x,t)$ denoting the height of the interface at time t for transverse coordinate x. Making a digital record of the fire line was a 2-step process that involved first taking high resolution photographs, which were then captured by a video camera into a 512×750 pixel buffer with multi-level grey scale. To extract the roughness exponent χ, the traditional procedure requires finding the length scale dependence of the rms width $w(L)$ of the saturated interface where, in the experiment at hand, $0.05 < L < 18.3$ cm is the length of a fire line segment under examination, large compared to microscopic scales, but still smaller than the paper's width to avoid boundary effects. In contrast to numerical simulations that typically determine χ by mercilessly averaging the full saturation width over many independent runs, the practical constraints of real-world experimention demand a different approach, since there may be, relatively speaking, just a handful of samples. In particular, one averages over all segments obtained from a single fire line by continually shifting the window starting point. Fig. 4.7 reveals the results of such an analysis by [ZZAL92] for a *single* sample with KNO_3 concentration ≈ 0.95 g/m^2, the log-log plot showing surprisingly good scaling

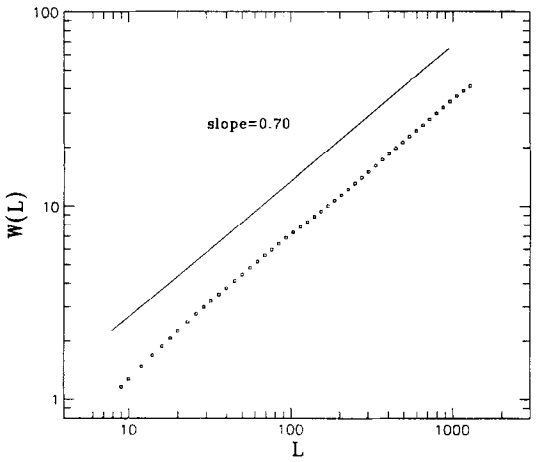

Fig. 4.7. RMS width $W(L)$ of a kinetically roughened fireline as a function of transverse length scale, determined from a single snapshot of the full sample [ZZAL92].

over nearly two decades with an estimated slope $\approx 0.70 \pm 0.03$. Averaging over 15 different samples, burnt under nearly identical conditions, gave a slightly larger value 0.71 ± 0.05, with a somewhat greater uncertainty because of apparently nonuniversal sample to sample variations. Nevertheless, the verdict of anomalous kinetic roughening is inescapable and the self-affinity ($\chi < 1$) of the interface beyond question.

4.1.4. Painfully slow electrochemical deposition [Wong92a]

As stressed earlier in the discussion establishing the KPZ equation as a valid description of Eden clusters, ballistic deposits and the like, the essential assumption was one of locality – the growth at any given point is controlled entirely by (i) surface relaxation $\propto \nabla^2 h$, (ii) lateral coarsening $\propto (\nabla h)^2$, and (iii) the incessant prodding of stochastic noise $\eta(x,t)$. Of course, the first two effects are due strictly to surface geometry. Such a local approach has secured for itself an important niche in the discipline of rough and fractal surfaces, but is in marked contrast to *nonlocal* Laplacian growth models, relevant to diffusion limited aggregation (DLA) and dendritic solidification, where the growth at any given point depends upon the overall interfacial configuration at that instant. Recently, Kahandra, et al. [Wong92a] performed a systematic study of the electrochemical deposition of copper to elicit the crossover between nonlocal and local growth effects and to reveal how the interplay of the two gives rise to interesting patterns. By growing structures at exceedingly slow rates, corresponding to surfaces propagating forward at 0.01–0.2 mm/h, they were able to access the regime where local growth effects, particularly surface relaxation and stochastic noise, could compete with the nonlocal Laplacian phenomena which, at somewhat higher growth velocities ($\geq$ 1 mm/h), ordinarily give rise to DLA fractals. The experimental set-up has a 25 μm thick copper foil, which functions as the cathode, sandwiched between two horizontal acrylic plates 13 × 25 mm, its edge exposed to a nearly saturated 2M $CuSO_4$ solution which fills the thin gap of this quasi-2D rectangular cell, with a copper rod counter electrode at the opposite end and an elaborate feedback circuit present to maintain the desired overpotential. The evolution of the interface profile is recorded by a video microscopy imaging system that provided a field of view 2.35 mm wide, while being operated, typically, at a resolution of 4.9 μm/pixel. The microscope moves upon a horizontal track with vernier positioning

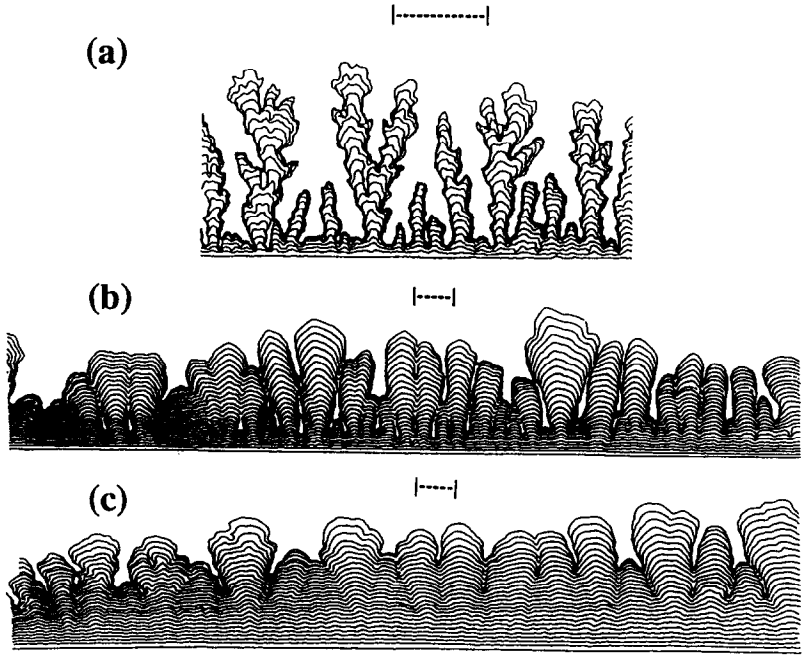

Fig. 4.8. Interfacial profiles – electrochemical deposition done sufficiently slowly to highlight local KPZ-type growth mechanisms [Wong92a]; growth at overpotentials (a) −0.5 V, (b) −0.35 V, and (c) −0.25 V.

to permit access to the full 13 mm width of the cathode, though the outer two video fields were discarded to avoid edge effects, leaving the four inner fields covering a total width of 8.8 mm.

Shown in Fig. 4.8 is the temporal evolution of the interfacial profiles for various values of the driving field. Fig. 4.8a corresponds to an overpotential of −0.5 V, which yields a standard DLA-type pattern with its characteristic branching morphology. As noted, however, by Kahandra et al., thanks to the relatively slow growth rate, the widths of the branches are comparable to the spacings between them, producing an Escherian complementarity between the deposit and void regions near the cathode. By contrast, Figs. 4.8b and c, illustrating the growth for overpotentials −0.35 V and −0.25 V, respectively, reveal patterns dominated on the largest scales by columnar morphology (a manifestation of the Mullins-Sekerka instability [MS63]), with DLA-type sidebranching precluded by the increasing importance of lateral coarsening associated with the standard nonlinearity. Sidebranches, rather than competing and screening, simply fatten and merge with their neighbors, leaving behind narrow closed-off crevices and columns of comparable width with noise induced roughness *on the surface*. To extract the roughness exponent associated with the resulting interfaces, Kahandra et al. construct a single-valued height profile $h(x)$ by taking the highest point for each horizontal position x and calculate its power spectrum $S(k) \equiv \langle |F(k)|^2 \rangle$, where $F(k)$ is the Fourier transform of $h(x)$. Fig. 4.9 shows a double-log plot of $S(k)$ versus k for the interfacial profiles in Fig. 4.8c at different times. The crucial feature is that at late times, $S(k)$ becomes a power-law with exponent $1 + 2\chi$. Because the cell thickness $\delta \approx 25$ microns, and the column width $W_c \approx 500$ μm, the experimenters performed least-squares fits to determine χ over the range $0.01 < k < 0.25$, which corresponds to wavelengths in the range $\delta < \lambda < W_c$. The six fitted lines in the figure give roughening exponents

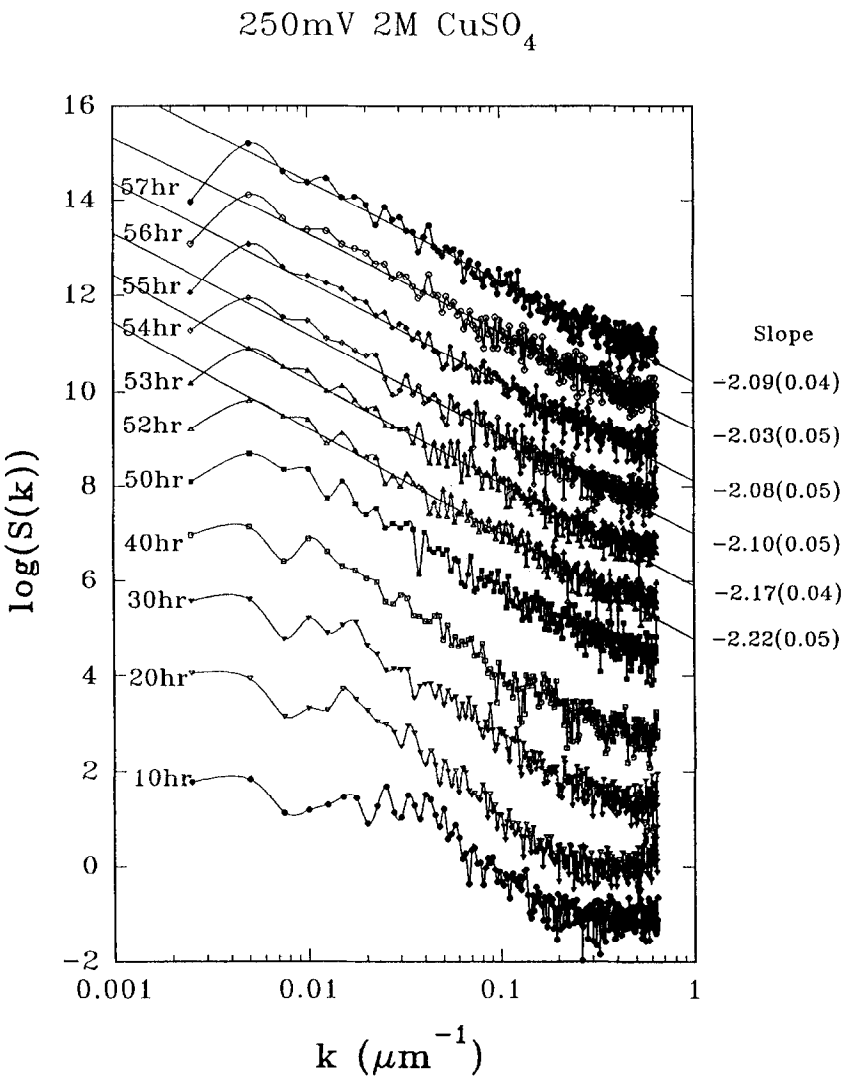

Fig. 4.9. Power spectrum determination of roughness exponent χ for painfully slow electrochemical deposition yields a value, 0.55 ± 0.06, consistent with standard KPZ [Wong92a].

in the range 0.52–0.58, each with statistical errors $\approx \pm 0.03$. Hence, Kahandra et al. report a value $\chi = 0.55 \pm 0.06$, with the standard result just within their error bars. It should be emphasized that this exponent refers only to roughness atop the crowns of the individual columns, whereas the larger scale columnar structure is a consequence of the usual Mullins-Sekerka instability of directional solidification; see, however, [Keb93,Wong93]. Indeed, this experiment was the first to observe a bona-fide KPZ exponent, but also one of the few to explicitly verify the Mullins-Sekerka dispersion relation for the growth of unstable modes, see Fig. 4.10, which predicts $\omega(k) = v_0 k(1 - d_0 l_D k^2)$, where v_0 is the average velocity of the interface, d_0 the capillary length related to the intrinsic surface tension, and $l_D = D/v_0$ the diffusion length. Aside from the impressive quadratic fit, for

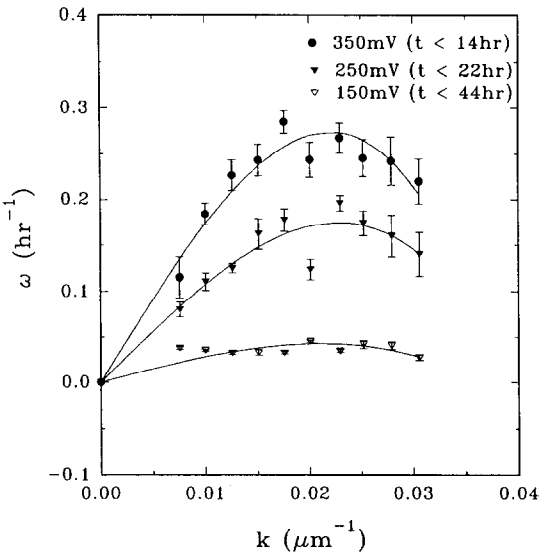

Fig. 4.10. The Mullins-Sekerka instability observed and measured. Evidence for the quadratic dispersion relation in an electrochemical deposition experiment [Wong92a].

overpotentials −0.25 V and −0.35 V, the extracted growth velocities, $v_0 = 3.17$ and 5.15 nm/s, resp., agreed surprisingly well with the directly measured velocities, 6 and 8.6 nm/s. This is surprising because the Mullins-Sekerka analysis is strictly valid only in long-wavelength, low frequency limit. For an overpotential −0.15 V the agreement was less good, but in this case the growth is so slow that local effects dominate, rendering Mullins-Sekerka invalid. In this regard, it is interesting to note that Bales, Redfield and Zangwill [BRZ89] have proposed adding a linear-h term to Eq. (3.1) to mimic the actual Mullins-Sekerka instability.

4.2. *Power-law noise*

4.2.1. *Nonuniversality [Z90a]*

Motivated by the Rubio et al. experiment [Rubio89] on fluid flow in porous media ($\chi_{ff} = 0.73 \pm 0.03$) and the work of Vicsek, Cserzö, and Horváth [VCH90] who studied the self-affine border associated with bacterial colony development on nutrient agar ($\chi_{bact} = 0.78 \pm 0.06$), both of which provided indications of anomalous kinetic roughening, Zhang [Z90a] proposed early on a rather enticing solution to the mystery, backed by the suspicion that universality and continuum limit were not sacrosanct notions in many non-equilibrium systems. Without attempting to model the details of the particular growth experiment, yet trying to accommodate matters within the context of the *local* KPZ equation, he suggested in an entirely phenomenological manner that η, the noise term in the original equation, was an uncorrelated, but *non-gaussian* random variable. In most of statistical physics, such microscopic details are not typically important on large scales; this accumulated wisdom, based upon proven example, goes under the rubric *universality*. However, it turns out a microscopic detail that can, nevertheless, influence large scale behavior in a substantial way, thus violating the naive universality concept and, most propitiously, pushing the roughening exponent χ higher than its standard value 1/2. His starting point was based upon a KPZ prototype, but assumed that the noise

was independently distributed on each site, in accordance with the probability distribution

$$P(\eta) \sim \eta^{-(\mu+1)}, \quad \eta > 1; \quad P(\eta) = 0, \quad \text{otherwise} \tag{4.1}$$

where μ sets the fall-off of the power-law tail. Zhang restricted himself to the case $\mu > 2$, for which the power-law distribution has a well-defined, finite mean and variance. Indeed, it is precisely for such tails that the naive expectation would presumably demand, thanks to the central limit theorem, results identical to that of the gaussian distribution. That is, for most known physical processes, replacing gaussian noise by $\mu > 2$ power-law noise will not make any difference in dynamical properties on large length scales. The philosophy behind the suggestion is that Eq. (3.1) is more sensitive to the nature of the noise than most of traditional systems (e.g., entire equilibrium physics). Thus, rather mildly singular noise (finite variance, divergent higher moments!) can drastically change the large scale behavior. Note, in particular, since the power-law distribution does not have an absolute cut-off, singularly large values of η can appear. Such events, though rare, will control the scaling, as we shall see shortly. To give an indication of the nature of these distributions, we contrast in Fig. 4.11, random samplings of points, scattered in the unit square, whose sizes are dictated by power-laws with $\mu = 2$ and 3, affording the reader a view of the substantial difference between these two cases. In fact, there appears to be much less of a difference between the $\mu = 3$ power-law and the gaussian case, which has been included for convenience. The growth algorithm is based upon a discretized version of Eq. (3.1) with the parallel update prescription,

$$h(i, t+1) = \max[h(i-1, t) + \eta(i-1, t), h(i+1, t) + \eta(i+1, t)] \tag{4.2}$$

where the spatial index i runs over even (odd) integers when the time t is even (odd). Since η is a continuous variable, so is h. The initial condition corresponds to a flat interface, $h = 0$; periodic BC were used in the transverse direction i, whose linear size is L. Fig. 4.12 shows a sequence of successive interface profiles resulting from the choice $\mu = 3$, which yields the anomalously large roughening exponent $\chi = 0.75 \pm 0.01$. The system size was $L = 1000$ and the interface had evolved 50000 time steps, starting from a straight line geometry. The longer time interval between snapshots is 30 time steps, the shorter interval at the top is 5 time steps. Visually, the obvious crucial feature is an occasional, but abnormally large thrust of the growth front. The choice $\mu = 2.5$ produced an anomalous roughness exponent $\chi \approx 0.82$. The results for various $\mu > 2$, see Fig. 4.13, reveals that $\chi = 1$ for the borderline Lévy flight case $\mu = 2$, but the roughening exponent decreases in an apparently monotonic fashion as the power-law tail falls faster and faster, approaching the value 1/2. Note, too, the independent determination of the early-time exponent permitted to verify that, within the error bars, the characteristic exponent equality, $\chi + \chi/\beta = 2$ stood satisfied for power-law, as well as gaussian noise, see inset. Implementing power-law noise for related ballistic deposition processes is simple, see [BHK91] and [CV92], who provide compelling snapshots of the resulting structures, while other traditional stochastic growth rules such as Eden and SS must be recast [RHH91,TKW91] in terms of a waiting-time formulation that dates back, ultimately, to Richardson [R73].

Why should noise in nature obey a power-law distribution? More specifically, how might it arise in the fluid flow experiments? There, the beads have a typical mean diameter of several hundred microns and a variance of 20% or so. Surely, the bead size distribution does not follow a power-law! In the experiments, however, we can easily imagine that during the packing process, beads are broken into smaller pieces. Such fragmentary debris can, interestingly, manifest power-law scaling [Wong85].

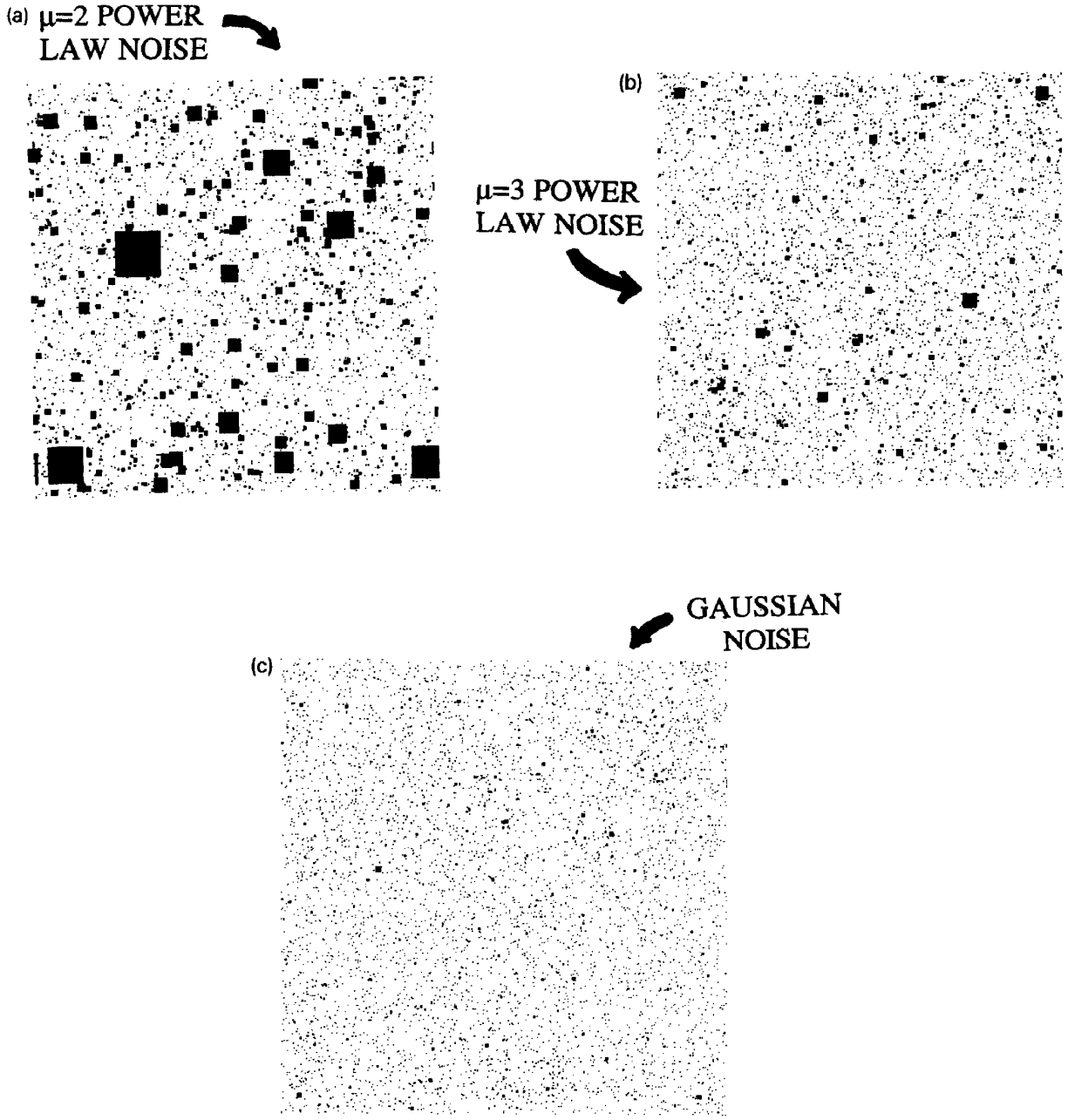

Fig. 4.11. Dots, whose size is dictated by various probability distributions, randomly distributed throught the unit square. The distributions have been constructed to have the same mean.

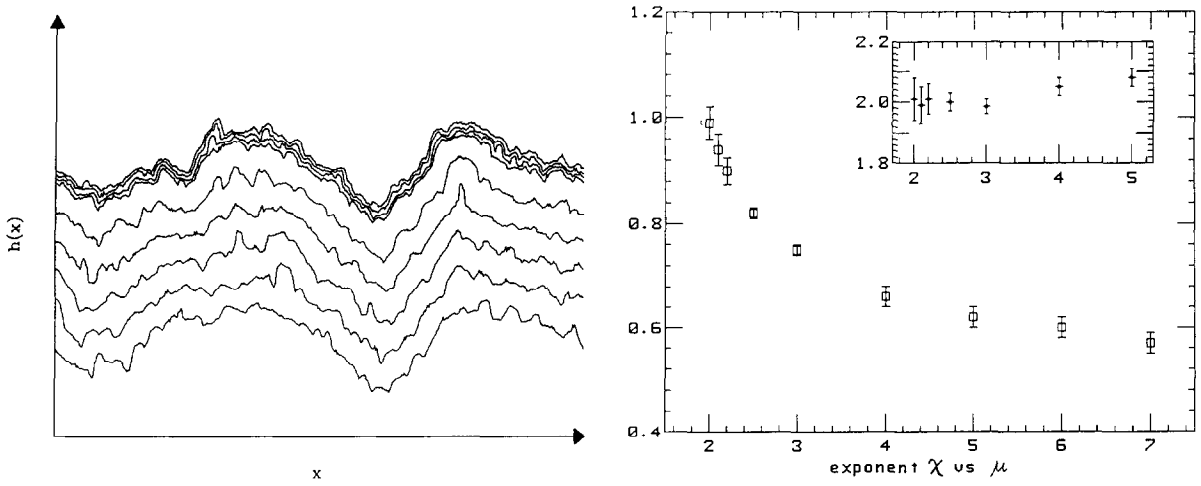

Fig. 4.12. Successive profiles of a KPZ surface grown with power-law noise. [Z90a]

Fig. 4.13. Anomalous saturation width exponent χ as a function of μ for KPZ growth with power-law noise [Z90a]. The inset confirms the characteristic KPZ exponent equality, $\chi + z = 2$, despite the non-gaussian nature of the noise.

Furthermore, the beads do not have perfectly spherical shape, nor are their surfaces equally clean and smooth. Nevertheless, the origin of the noise is necessarily more complex, as made clear by the idealized Cieplak-Robbins model [CR88], see Section 4.2.5, later, which incorporates no such effects, but yields convincing power-laws [NKMR93]. Ultimately, it must be tied to the distribution of pore sizes in the bead pack, a highly nontrivial matter, even for the geometrically regular array assumed by Cieplak and Robbins [CR88]. The pore size distribution determines the distribution of capillary forces, which in turn dictates the kinetic roughening exponents of the fluid interface. Power-laws may arise at any point en route; even so, the important point is that drastic revisions are not required. Take, for example, the case $\mu = 3$, which gives an anomalous roughness exponent $\chi \approx 3/4$. If the average displacement of the interface per unit time is, let us say 1mm, who could be sure there is not an occassional, abnormally large thrust of size 10mm, occurring with probability 1 part in a 1000? Indeed, may very well be the case, given recent experimental and numerical findings [HFV91a,NKMR93].

4.2.2. *Exceptional fluctuations*

Despite evidence to the contrary, it may still seem surprising that the power-law noise, being just a microscopic detail, could so drastically alter the dynamic scaling of KPZ-type growth processes. A clue to an intuitive understanding of this apparent puzzle can be had by emphasizing that while the interface is growing, as shown in Fig. 4.12, it encounters some rare, but very large thrusts with respect to average places. These rare thrusts have much more influence than their small statistical weight might suggest, thanks to the following mechanisms:

(i) *Amplification.* During the lateral growth, a rare large thrust will expand laterally to cover its neighboring area as if there were many simultaneous thrusts.

(ii) *Memory.* A large thrust probably will result in a hill on the interface. This geometry will be remembered for a long time and if during this period there appears another rare thrust, they can have combined effect to roughen the interface.

It should be stressed that, in contrast to matters just discussed, the Edwards-Wilkinson equation subject to power-law, rather than gaussian or flat noise, yields no change, whatsoever, in the traditional exponents, $\chi = (3-d)/2$ and $z = 2$; the feature of lateral growth is absolutely crucial.

Unfortunately, despite the great interest in power-law noise as a possible mechanism to account for anomalous kinetic roughening, there remained two very severe obstacles. Firstly, there seemed little from the materials science point of view to justify embracing power-law over gaussian distributions; then again, the historical bias of the latter over the former was based solely on mathematical expediency, with essentially no physical justification. In fact, power-laws are rampant in nature [S88]; for example, it is known that a great variety of substances (rock, sand, ash, etc.), when obtained by breaking larger objects, have a distribution which is power-law [T86], rather than gaussian. Indeed, this appears to hold down to the atomic scale: the debris of nuclei multifragmentation is found to follow a power-law as well [F82]. Secondly, aside from a simple Flory-type argument due to Krug [Kr91a], Bouchaud and Huse [BH91u], Derrida [unpublished] and Zhang [Z90b], KPZ with power-law noise initially defied all known traditional analytical approaches. The reasoning behind this Flory scaling argument is straightforward enough and is based upon ramifications of the full-fledged dynamic scaling hypothesis (for additional details, see [KrS91r]), which assumes that the typical amplitude $\xi_\perp$ of transverse fluctuations of a roughened interface increases algebraically with distance, $\xi_\perp \sim r^\chi$, only on length scales below the dynamical correlation length $\xi_\parallel(t) \sim t^{1/z}$. Hence, suppose we consider a patch of linear extension r and assume that the roughness is stationary on that scale, so that $r \ll \xi_\parallel(t)$. The number of random events within the patch in a time interval of duration τ is $N = r^d\tau$. If we desire to estimate the size $\eta_{max}(N)$ of the largest of these events, it is clear that

$$\text{Prob}\{\eta_{max}(N) < x\} = (\text{Prob}\{\eta < x\})^N = (1 - x^{-\mu})^N \tag{4.3}$$

which yields, for large N

$$\langle \eta_{max}(N) \rangle \sim N^{1/\mu}. \tag{4.4}$$

Therefore, the waiting time necessary before a transverse fluctuation of amplitude $\xi_\perp$ is created scales as

$$\tau_c \sim \xi_\perp^\mu / r^d \tag{4.5}$$

Of course, once created, such a fluctuation spreads laterally across the patch, driven by the nonlinearity of Eq. (3.1). Balancing this nonlinear term against the time derivative, we obtain the spreading time scale

$$\tau_s \sim r^2/\xi_\perp. \tag{4.6}$$

As Krug informs us, in a stationary situation, the largest fluctuations that contribute to the roughness are precisely those with $\tau_c \sim \tau_s$. Larger fluctuations will occasionally appear, but they spread too rapidly to have significant statistical weight. Hence, the spontaneously created large fluctuations give rise to a transverse roughness $\xi_\perp \sim r^{\chi_F}$, with a μ-dependent Flory exponent,

$$\chi_F(\mu) = \frac{d+2}{\mu+1} \tag{4.7}$$

where d denotes the dimensionality of the interface. That the characteristic identity should survive the inclusion of power-law noise is apparent for the spreading time, which implies $\tau_s \sim r^z$ with $z = 2 - \chi$. Note that for $d = 1$, the Flory formula yields very good agreement with the simulation results for small $\mu > 2$. In particular, the limiting behavior $\chi(\mu \to 2) = 1$, while $\chi_F(\mu = 3) = 3/4$. However, $\chi_F(\mu = 4) = 3/5$ falls a little below the numerical estimate, 0.66 ± 0.02, and the Flory formula erroneously (?) predicts $\mu_c = 5$, beyond which the power-law noise roughness exponent drops to its standard value, $1/2$, in one dimension. Indeed, later work of Bourbonnais, Herrmann, and Vicsek [BHV91] suggested rather strongly $\mu_c \approx 7$. Since the Flory argument completely ignores the cumulative effect of small fluctuations, known to be all important for flat or gaussian noise distributions, it is conceivable that the roughness exponent might be underestimated for larger values of μ, where the exceptional nature of the power-law fluctuations are considerably more muted. Additional simulations by independent investigators in $d = 1$ [AF91,BHK91] and $d = 2$ [BKW91] apparently confirm the notion that (4.7) is merely approximate, though providing a helpful lower-bound. Even so, Lam and Sander [LS92,93b] have subsequently proposed a novel scaling theory for KPZ that claims the Flory exponent to be exact and suspects, as well as explains, why all previous numerical findings, particularly at large μ, are hampered by severe crossover effects. Nevertheless, the precise value of μ_c may be an academic point, since the experimental relevance of power-law noise seems, curiously enough, restricted to the range $\mu \approx 2$–3, precisely where the numerics and theory agree best!

4.2.3. Caveat – continuum limit [Z90b]

It is very striking indeed that, via power-law noise, the macroscopic behavior can depend crucially on the microscopic details at the smallest cutoff scale, thereby violating the sacred universality concept for some interfacial growth processes. This peculiar feature can be traced to the lack of a proper continuum limit for the models under consideration. This mystery has been discussed previously within the directed polymer context [Z90b]. Here, we consider the flip side of the coin, addressing the matter for interfaces. Our starting point is Eq. (3.1) which, given our previous discussions, seems a perfectly legitimate continuous, stochastic PDE to which we can apply traditional analytical approaches, such as the renormalization group. However, as we shall see below, this appearance is deceiving. In fact, a brief moment's reflection reveals that the equation must be accompanied by a discrete regularization of the physical space. Furthermore, its continuum limit is not uniquely defined.

To motivate this proposition, let us consider an (ultimately paradoxical) rescaling of Eq. (3.1), in which the variables x, t, and h are transformed accordingly to,

$$x \to ax, \quad t \to bt, \quad h \to ch \tag{4.8}$$

where $a = \bar{\lambda}^{2/(d-2)}$, $b = \bar{\lambda}^{4/(d-2)}/\nu$, and $c = \nu/\lambda$ are constants, with $\bar{\lambda}^2 = D\lambda^2/\nu^3$. Eq.(3.1) then reads

$$\dot{h} = \nabla^2 h + \frac{1}{2}(\nabla h)^2 + \eta \tag{4.9}$$

with

$$\langle \eta(\boldsymbol{x}, t)\eta(\boldsymbol{x}', t')\rangle = 2\delta^d(\boldsymbol{x} - \boldsymbol{x}')\delta(t - t'). \tag{4.10}$$

What has happened to our original equation? Note that for $d \neq 2$, which corresponds to the marginal dimension, all the physical parameters (ν, λ, D) have disappeared, and we are dealing with a genuinely parameter free equation! All hell breaks loose immediately: what exactly did we mean by the perturbation expansion, which was based upon the existence of a small parameter, and what was the implication when we asserted that $\bar{\lambda}$ was renormalized, approaching a particular fixed point value? Apparently, a simple linear reparametrization at the tree level renders such an analysis meaningless. The paradox is all the more perplexing for $d \geq 3$, where our knowledge of the DPRM, see Section 5.9.4, suggests the existence of both weak and strong coupling regimes, which presupposes that it is physically meaningful to say a coupling constant is large or small. The short answer to this enigma is that Eq. (3.1) is only unambiguously defined when a short distance cut-off length is specified. This act breaks the continuum reparameterization symmetry, since it involves changing $x \rightarrow ax$ uniformly. In other words, in our original equation, we must have an additional parameter hidden behind the reparameterization scheme; thus, the theory is not truly parameter free and there still remains one free handle to play the equation.

To better appreciate this paradox, let us consider a simpler case, the EW equation with quenched noise, but in 0+1 dimensions,

$$\dot{h} = \eta(h) + c \tag{4.11}$$

with $\langle \eta(h) \rangle = 0$ and $\langle \eta(h)\eta(h') \rangle = \delta_{h,h'}$. Interestingly, this seemingly trivial equation shares the same difficulty with the continuum limit, a lattice being implicit in the formulation with h assuming discrete values. Suppose, for an instant, that h is increasing (i.e., as an "interface", being pushed from the left to the right) at a given point h_0, where it finds an $\eta(h_0) < -c$. Then the interface motion implied by the above equation comes to a stop at h_0. Let us consider what happens when a reparameterization is made to the same problem. Define a larger lattice spacing which contains several of the original lattice sites. Without loss of generality, we take η on the new lattice site to simply be the average value within. In so doing, we may have completely changed the original problem! While the motion stops, pinned at h_0 in the first case, it can be unpinned after the above block-spin scheme. This illustrates that the original problem is not invariant under reparameterization, a common feature shared by a host of stochastic PDE's relevant to kinetic roughening phenomena. This is a rather surprising suggestion, since the concept of universality is one of the cornerstones of modern statistical mechanics. We normally expect that the microscopic details of a model should not influence the scaling at large scales. However, the universality principle is only well-tested for equilibrium or near equilibrium phenomena, and in the domain of irreversible dynamical processes, it is far from established. The above examples show just the contrary and that details on the smallest length scales do influence the outcome of the physics on the macroscopic level, thus wreaking havoc upon the naive universality concept.

4.2.4. Experimental evidence? [HFV91b]

Reporting results of their experiment on anomalous kinetic roughening of self-affine interfaces, Horváth et al. [HFV91b] provided the community with rather suggestive evidence as to the possible physical relevance of power-law noise distributions for fluid flow in porous media. Motivated by comments of Zhang [Z90a] concerning Fig. 4.12, these authors carefully monitored the sequence of successive interface profiles to extract the very noise distribution responsible for kinetic roughening.

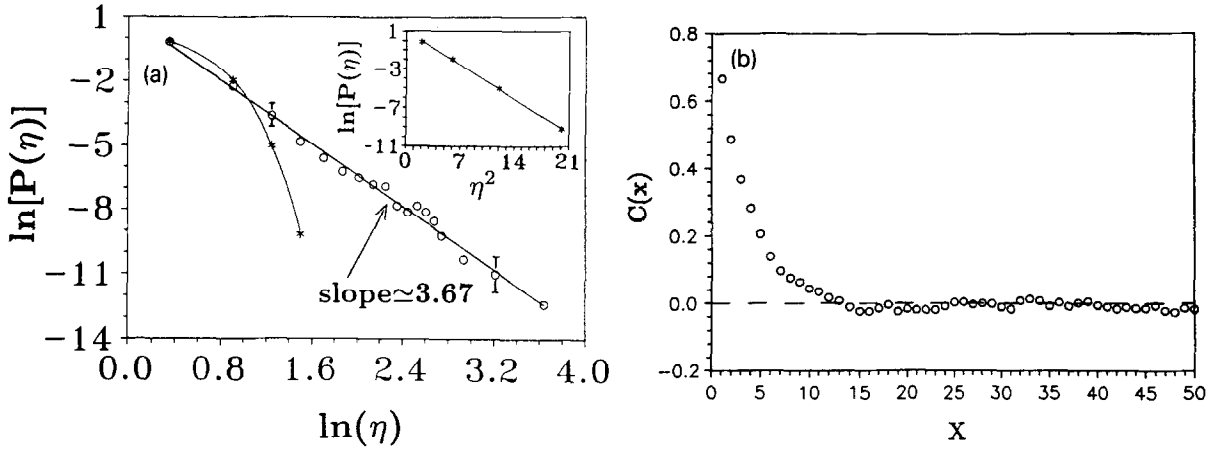

Fig. 4.14. (a) Evidence for power-law noise distribution in a fluid flow through porous media experiment [HFV91b]. Inset shows same procedure yields gaussian noise distribution for the of Kim-Kosterlitz RSOS growth model [KK89], (b) absence of spatial correlations in the same experiment.

Their results, summarized in Fig. 4.14a, indicate a power-law noise distribution with $\mu \approx 2.67$, a value not at all inconsistent with the independently determined roughness exponent $\chi \approx 0.81$ measured by them in a related experiment [HFV91a]. As a check on their method, Horváth et al. applied their indirect noise extraction procedure to a computer simulation of the RSOS model of Kim and Kosterlitz [KK89], confirming the gaussian nature of its renormalized noise distribution – see remainder of Fig. 4.14a, as well as its inset. Finally, Horváth et al. were able to show that the noise in their fluid displacement experiment was extremely short-ranged both spatially, see Fig. 4.14b, and temporally, ruling out the possibility, at least in their own experiment, of correlated noise, which we discuss shortly, see section 4.3, as another possible source of anomalous kinetic roughening.

4.2.5. Cieplak-Robbins model [CR88,MCR91,NKMR93]

In the work of Martys, Cieplak, and Robbins [MCR91], fluid invasion of porous media is investigated as a critical phenomenon, using a numerically intensive realistic microscopic model in which a nonviscous, but wetting (or nonwetting) fluid is injected under an applied pressure P at the edge of a regular triangular lattice of randomly-sized disks, geometric disorder arising from local variations in pore size. The advancing interface consists of arcs connecting pairs of discs and an individual arc is stable if it intersects both discs at the prescribed contact angle θ, while possessing curvature P/γ, where γ is the surface tension. If these conditions cannot be satisfied simultaneously, the arc is judged unstable; at each time step, all such unstable segments of the interface are advanced. It was discovered numerically in this model that for wetting (nonwetting) invasion at the critical driving force f_c, the interface is self-affine (self-similar, reminiscent of percolation), with anomalous roughness exponent $\chi_w \approx 0.81$ ($\chi_{nw} = 1$). Recently, Nolle et al. [NKMR93] returned to the case of wetting invasion in order to study the fluid interface driven beyond threshold, $f > f_c$. They note the existence of a diverging correlation length $\xi \sim (f - f_c)^{-1.3}$ below which the roughness is self-affine, though anomalous as before, while above which there is a clear crossover to the value $\chi = 1/2$. In fact, the same behavior had been noted in the real fluid flow experiment of Horváth, Family, and Vicsek [HFV91a], with nearly the same values for the exponents! Better yet, Nolle and collaborators observe a power-law

distribution for the effective noise amplitude extracted from their model, with a tail given by $\mu \approx 2.7$ which, via the Flory formula above, yields precisely the roughness exponent $\chi \approx 0.8$, obtained via traditional methods involving direct analysis of the interface fluctuations. Moreover, this is the very same power-law tail discussed previously [HFV91a]. Interestingly, their complementary study of driven domain-walls in the random-field Ising model context [NKMR93,JR91-2] reveals strikingly different self-similar structures (akin to the case of nonwetting invasion alluded to above), characterized by an abundance of overhangs, and a measured power-law noise distribution with $\mu \approx 0.7$, entirely consistent with the expectation of Zhang [Z90b] and Krug [Kr91a] that $\chi = 1$ for $\mu < 2$.

4.2.6. Extreme disorder: generalization to isotropic fractal interfaces

Interestingly, there is evidence that sandstones, carbonate rocks and perhaps many other porous materials, including those that are conspicuously so, such as solidified vulcanic lavas, contain pores whose size distributions obey nonuniversal, but approximate power-laws [Wong85]. We can imagine, therefore, the simple experiment in which a strong corrosive acid dissolves a piece on sandstone in a uniform but probabilistic manner, giving rise to a dynamically evolving rough surface. If the corrosion process is sufficiently slow and the acid source amply abundant, the acid does not get neutralized and the corrosive action remains constant. Pore spaces, being empty, conduct the acid faster. The natural expectation would be that the pore size distribution in the bulk, characterized by μ, would give rise to self-affine rough surfaces with the theoretically predicted anomalous exponent χ.

To model such a process on a lattice, we might define three distinct states: rock, pore, and acid. Acid is introduced at the top of the sample, the bottom is unbounded, and the two lateral sides are connected in the simulation by periodic boundary conditions. The stochastic evolution rules are as follows – if an acid site is next to a rock site, the latter can turn into an acid site, with probability $p < 1$. If, however, an acid site is next to a pore site, the algorithm will turn all neighboring pore sites into acid sites, no matter how many are in the connected cluster. As the above process is repeated many times, a kinetically roughened interface is created. Naively, for pore size distributions that are gaussian or truncated, we would expect this model to reproduce an Eden-like surface. If the pore sizes are power-law distributed, let's say with $\mu > 2$ for mass-filling rocks, we anticipate finding a self-affine interface, with a non-universal roughening exponent depending on the precise power-law. What if $\mu = 2$? What happens with a very porous rock, like that from vulcanic lava? How porous can a rock be ? It turns out that one should not extend the distribution to $\mu < 2$, as one might expect. As long as we stick to the power-law distribution of pore space, μ can at most saturate at $\mu = 2$. At this special value the distribution becomes scale invariant – or isotropic fractal as discussed in the celebrated monograph of Mandelbrot [Man82].

With the exponent μ fixed at 2, the distribution is further classified by a "finer" measure – the fractal dimension D of the pore space in a rock. D enters the distribution through the coefficient of the power-law

$$P(l) = 2\rho\frac{1}{l^3}, \quad l > l_c \tag{4.12}$$

where $P(l)$ is the probability per unit volume, which can be derived from Mandelbrot's earlier results, see page 302 of [Man82]. The fractal dimension is related to the constant ρ by

$$D = d - 2\rho. \tag{4.13}$$

Fig. 4.15. Acid-etched rock simulation possessing anisotropic power-law distributed pores, giving rise to a self-similar fractal surface with many overhangs [Zhang, unpublished].

From the simulations [Z90a,BHK91], we learned that as $\mu \to 2$, the roughening exponent approaches unity, whereupon the self-affine interface becomes an isotropic fractal. Here we see, by contrast, that it is natural for isotropic fractal pores to result in a fractal interface.

Fractal interfaces can also arise from nonisotropic pores. As an extreme example, let us consider one dimensional line-like pore spaces with random length and orientations. In Fig. 4.15, we see that in the stationary region, isotropic fractal interface appears while the rock still apears as mass-filling. Cracks as shown should be better described by notions of "cirri" and "succolarity," a là Mandelbrot, rather than fractal dimension itself. For $\mu > 2$, the roughening exponent $\chi < 1$, so the interface growth equation can be regarded still valid. However, for the $\mu = 2$, $\chi = 1$ isotropic interfaces, the growth equation is no longer valid, for in its derivation, a crucial approximation $|\nabla h| \ll 1$ was used and can no longer be justified. We need to generalize Eq. (3.1) to accomodate not only self-affine interfaces but self-similar surfaces as well, resulting from pores that are, themselves, fractal or via anisotropic singular cracks.

Consider the position of interface in 2d $\boldsymbol{x}(t, \sigma)$ as a function of time t and the parameter along the interface σ. Maintaining the spirit of our original derivation of Eq. (3.1), but allowing for a more general kinetically roughened surface, we write down the dynamic evolution equation:

$$\dot{\boldsymbol{x}} = \frac{\partial^2}{\partial \sigma^2}\boldsymbol{x} + \boldsymbol{n} + \boldsymbol{\eta} \tag{4.14}$$

where the first term on the right is the isotropic tension, the second term is the unit vector normal to the interface, which represents the uniform growth and last term is noise, both quenched (e.g., pores) and stochastic. The vector $\boldsymbol{n}$ can be easily expressed

$$\boldsymbol{n} \propto \left(\frac{\partial x_2}{\partial \sigma}, -\frac{\partial x_1}{\partial \sigma}\right) \tag{4.15}$$

this construction is based on the tangent vector

$$\boldsymbol{t} \propto \left(\frac{\partial x_1}{\partial \sigma}, \frac{\partial x_2}{\partial \sigma}\right) = \frac{\partial \boldsymbol{x}}{\partial \sigma}$$

and we have $\boldsymbol{t} \cdot \boldsymbol{n} = 0$. The above equation is invariant under the reparametrization group. To make (4.15) meaningful we have to fix a gauge by requiring, for instance, that the total intrinsic length being a constant.

$$\int \sqrt{1 + \left(\frac{\partial \boldsymbol{x}}{\partial \sigma}\right)^2}\, d\sigma = L. \tag{4.16}$$

Recently, a more refined work on this type of generalized isotropic equation is advanced by Maritan et al. [MTKB92]. We summarize their work in the following.

A fundamental assumption underlying KPZ is that the kinetically roughened surface can be represented by a single-valued function $h(\boldsymbol{x}, t)$, representing the height profile at time t and basal coordinate x. Implicit in this notion is the expectation that on large length scales, the overhangs present in some microscopically defined lattice models such as Eden growth and ballistic deposition, see Section 2.5, are irrelevant in the renormalization group sense. The usual assumption of no overhang condition and $(\nabla h)^2 \ll 1$ can be only justified a posteriori for self-affine surfaces, we need to see a reformulation of Eq. (3.1) without this condition imposed by hand from the beginning. From the analysis below we shall see that a completely isotropic growth equation recovers the standard scaling behavior, provided the overall surface is self-affine with $\chi < 1$. While the reformulation is cosmetic for normal cases ($\chi < 1$), for very rough surfaces ($\chi \geq 1$) we shall be obliged to generalize the anisotropic surface growth equation to the isotropic equation, since the above condition no longer holds microscopically as well as macroscopically.

The starting point in $d = 1$ is a stochastic PDE for the temporal development of the parametric curve $\boldsymbol{r}(s)$ describing the shape of the kinetically roughened edge:

$$\frac{\partial \boldsymbol{r}}{\partial t} = \nu \frac{1}{\sqrt{g}} \frac{\partial}{\partial s} \frac{1}{\sqrt{g}} \frac{\partial}{\partial s} \boldsymbol{r} + \lambda \boldsymbol{n} + \boldsymbol{\eta} \tag{4.17}$$

with noise that is gaussian distributed, possessing zero mean, and variance:

$$\langle \eta^{\alpha}(s,t) \eta^{\beta}(s',t') \rangle = 2D\delta^{\alpha\beta} \frac{\delta(s-s')}{\sqrt{g(s)}} \delta(t-t') \tag{4.18}$$

where D gauges the strength of the noise, as before, and $g = |d\boldsymbol{r}/ds|^2$. Note the form of the noise correlator, which ensures that the above description is *invariant* under reparametrization. This invariance property, not shared by the original Eq. (3.1), thereby accommodates any change in local time scales resulting from an arbitrary nonlinear distortion. Furthermore, and perhaps most importantly, there is no assumption in (4.17) regarding the presence or absence of overhangs. Nevertheless, the physical origin of the first two terms in (4.17) are easily understood from usual considerations. The height diffusion term, involving the phenomenological parameter ν, follows simply from minimization of the elastic perimeter energy associated with the surface (line) tension $A = \nu \int \sqrt{g}\, ds$, and is given by $-(1/\sqrt{g})\delta A/\delta \mathbf{r}$. The second term is just an explicit, literal implementation of the of locally normal growth prescription, with λ the characteristic nonlinearity parameter and $\boldsymbol{n}$ the local normal to the contour.

To bring ourselves a step closer to the original KPZ equation, while maintaining the intent to test the relevance of (4.17), we implement the no overhang approximation by defining $\boldsymbol{r} =$

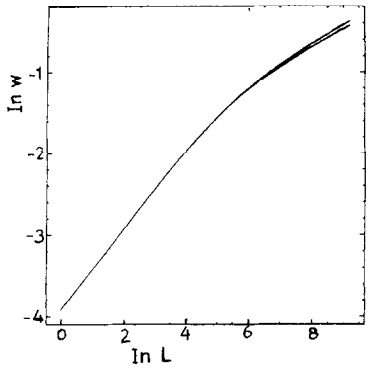

Fig. 4.16. *Early-time roughness* of the interfacial width $w(t)$, following from numerical integration of KPZ (lower) and its modified progenitor (upper), given by Eq. (4.19) indicating an instability in the latter and calling into question the no overhang assumption implicit in KPZ. The phenomenological parameters $(\nu, \lambda, D) = (1, 1, 0.4)$. For details, see [MTKB92].

$(x(s,t), h(s,t)) \equiv (x, h(x,t))$, invert, and obtain the following stochastic PDE for the single-valued function $h(x,t)$:

$$\frac{\partial h}{\partial t} = \frac{\nu}{g}\frac{\partial^2 h}{\partial x^2} + \lambda g^{1/2} + \xi(x,t) g^{1/4} \tag{4.19}$$

where ξ is Gaussian noise having zero mean and variance $\langle \xi(x,t)\xi(x',t')\rangle = 2D\delta(x-x')\delta(t-t')$, while $g = 1 + (\partial h/\partial x)^2$. Of course, KPZ is retrieved by expanding g in the limit $(\partial h/\partial x)^2 \ll 1$, and keeping only the lowest order terms. In any case, from (4.19), we see that the a large local slope, which implies a large g, results in an effective diffusion constant which is reduced, a consequence of the fact that large height differences between neighboring columns require longer relaxational time scales. By contrast, the growth term with λ increases when g becomes bigger because there is a larger section of surface that participates in the growth, a geometric matter already known very early on [KPZ86]; here, however, we keep g as is. Finally, that the last term involves a corrective factor $g^{1/4} = (g^{1/2})^{1/2}$, follows from the random nature of the noise.

We are thus confronted by a crucial question – is there a fundamental distinction between the original Eq. (3.1) and its modified progenitor (4.19)? (If a difference exists already at this level, we admit an even more serious disparity with (4.17)...) On physical grounds, we might expect that differences between the two will be exacerbated in situations of large local slope $\partial h/\partial x$, where diffusional smoothening is minimized, leading to noisier, more persistent growth and a possible breakdown of the no overhang assumption. To test this scenario, Maritan et al. [MTKB92] numerically intergrated the two equations in an effort to discern any important differences, focussing their attention on the early-time width of the kinetically roughened edge. Their data is shown in Fig. 4.16, which is typical their of simulations starting from a nearly flat initial configuration $|\partial h/\partial x| \ll 1$ and a weak (but not overly so) noise amplitude D. The figure reveals that both equations scale identically in the inital, random deposition regime, where the behavior is Poissonian and $w \sim t^{1/2}$, but soon thereafter an instability sets in, yielding rougher surfaces and non-KPZ scaling for (4.19)! For large values of the noise strength D, Maritan and coworkers note the existence of a crossover time scale $t_c \sim 1/D$ beyond which the differences between (3.1) and (4.19) become manifest. They very naturally suggest this instability to be instigated by the breakdown of the no-overhang approximation

and thereby proffer (4.17), the fully reparametrization invariant generalization of Eq. (3.1), as the correct stochastic PDE governing the dynamic scaling behavior of growing interfaces. Nevertheless, they also point out that in situations where the bare noise parameter is weak, the thankless progenitor (4.19) behaves like the KPZ equation for a relatively long time, possibly explaining the apparently healthy agreement between the analytical results and the best Eden and ballistic deposition simulations to-date.

4.3. Correlated noise [MHKZ89]

Perhaps the earliest known and best studied mechanism leading to anomalous kinetic roughening involves spatially or temporally correlated Gaussian noise, a matter which was first investigated systematically by Medina et al. [MHKZ89], who applied the dynamic renormalization group upon KPZ equation to make explicit, though *approximate* predictions concerning the scaling indices. Here we concentrate on the spatially correlated case, enumerating the wealth of different analytical approaches and related numerical efforts that have nearly, but not quite resolved the situation in two dimensions. The final section is reserved for a quick glance at temporal correlations.

4.3.1. Purely spatial correlations [MHKZ89,ALF91,PHSS91]

Our starting point is the standard equation, but with noise $\eta(\boldsymbol{r}, t)$ that is characterized by a variance

$$\langle \eta(\boldsymbol{r}, t), \eta(\boldsymbol{r}', t') \rangle \sim |\boldsymbol{r} - \boldsymbol{r}'|^{2\rho - d'} \delta(t - t') \tag{4.20}$$

indicating algebraic correlations in space, where $d' = d - 1$ is the dimension of the interface. Fourier transformation in the spatial coordinate yields noise correlations of the form

$$\langle \eta(\boldsymbol{k}, \omega), \eta(\boldsymbol{k}', \omega') \rangle \sim k^{-2\rho} \delta(\boldsymbol{k} + \boldsymbol{k}') \delta(\omega + \omega'). \tag{4.21}$$

The analytical efforts, which have sought to pin down the ρ-dependence of β and χ, are as follows:

(i) *Dynamic RG [MHKZ89].* This one-loop perturbative RG treatment, done in Fourier space, yields the prediction in $d = 2$ that,

$$\chi = (1 + 2\rho)/3, \quad \beta = (1 + 2\rho)/(5 - 2\rho) \quad \text{with } 1/4 < \rho < 1 \tag{4.22}$$

while for $0 < \rho < 1/4$ the exponents stick to the values, $\chi = 1/2$ and $\beta = 1/3$, associated with uncorrelated noise. It is a little appreciated fact that even in $d = 2$, the dynamic RG is generally approximate. The only exact results are at the endpoints, where a fluctuation-dissipation theorem [HuHF85] fixes the exponents $\chi = 1/2$ and $\beta = 1/3$ for $\rho = 0$, while the replica scaling theory [Z90d] and an exact RG calculation [Z86b] requires $\chi = \beta = 1$ at $\rho = 1$. For $\rho \neq 0$, there is no fluctuation-dissipation theorem; hence, one-loop results may not be exact!

(ii) *Functional RG – directed polymers [HH89a,90].* Thanks to an explicit mapping between the directed polymers in random media (DPRM) and kinetically roughened surfaces (for details, see [KrMHH92]), the polymer exponents carry hard currency in this section. More specifically, Halpin-Healy [HH89a,90] has applied a functional renormalization group to the DPRM problem finding complete agreement with the predictions of the dynamic RG. This is rather astonishing, given that his functional RG is perturbative about the zero-temperature, strong coupling fixed point, whereas the dynamic RG is an expansion at the opposite extreme, near the weak-coupling

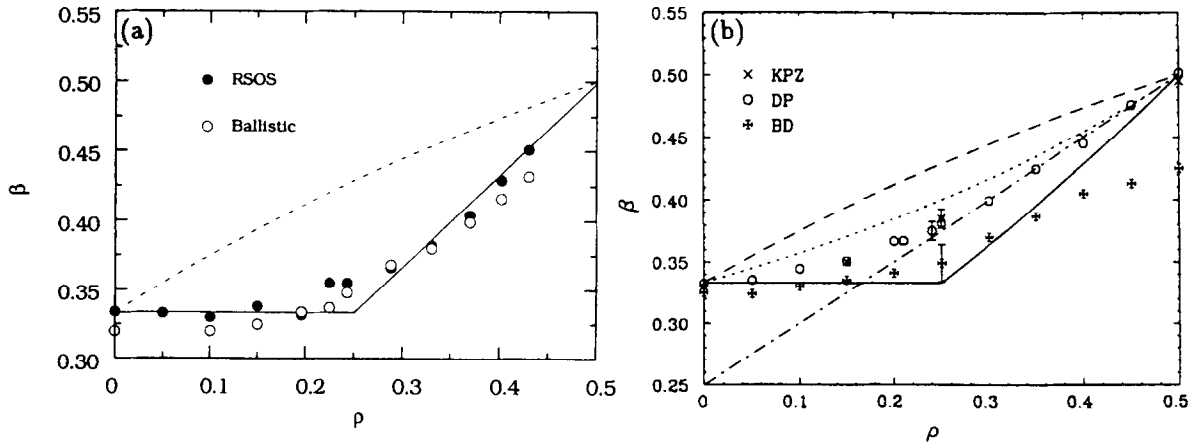

Fig. 4.17. Early-time roughness exponent β for spatially correlated randomness. Simulations done for (a) RSOS and ballistic deposition models [ALF91], (b) KPZ brute force integration, DPRM transfer matrix, where $\beta = \omega$ the energy fluctuation exponent, and, again, ballistic deposition [PHSS91].

EW fixed point. Nevertheless, the functional RG statement is precisely as above, with $\rho_c = 0.25$ indicating departure from the case of delta-correlated noise.

(iii) *Replica-scaling method [Z90d].* Interface growth in correlated noise can also be mapped into the problem of equilibrium domain-wall roughening by quenched, correlated disorder. Zhang [Z90d] has proposed a simple, but physical scaling argument based upon careful considerations of attractive or repulsive energies in the many-body ground-state of the replicated Hamiltonian, see Section 5.4.3. The bottom line is a $\rho_c = 1/2$, beyond which Zhang is in agreement with the functional RG Flory exponent, but elsewhere he finds

$$\beta = \chi/(2-\chi) = (1+2\rho)/(3+2\rho), \quad \text{for} \quad 0 < \rho < 1/2 \tag{4.23}$$

which is quite a different behavior from that predicted by the dynamic and functional renormalization groups – glance ahead to Fig. 4.17.

The first systematic numerical work done on spatially correlated noise is due to Amar, Lam and Family [ALF91], who used large system sizes ($L = 2^{17} = 131072$) to pin down estimates for $\beta(\rho)$ in their simulations of the Kim-Kosterlitz RSOS model and ballistic deposition, see Fig. 4.17a. As stressed by these authors, generation of correlated noise is relatively straightforward in principle, but surprisingly subtle in practice. To construct algebraically correlated noise $\eta(x,t)$, one first generates a representation of random uncorrelated noise $\eta_0(x,t)$ which, upon fast Fourier transformation, becomes $\eta_0(k,t)$. Defining $\eta(k,t) \equiv |k|^{-\rho}\eta_0(k,t)$, the desired noise $\eta(x,t)$ is obtained by Fourier transforming $\eta(k,t)$ back into real space. This procedure is repeated at each time slice and a parallel growth algorithm is employed to assure that the noise was delta-function correlated in time. As a consistency check, Amar et al. calculated explicitly the noise-noise correlation function for each value of ρ, comparing to the expected behavior $r^{2\rho-1}$. They discovered that for small $\rho < 0.20$, things were fine, but for increasingly larger ρ, their measured decay exponent was somewhat smaller than expected (*e.g.*, worst case scenario – when they put in 0.5, they got out $\rho = 0.43$). This subtlety notwithstanding, the data in Fig. 4.17, which plot the *measured* ρ, clearly favor the dynamic and functional RG prediction over that of Zhang's replica scaling argument, though the β values near

$\rho_c = 0.25$ are a little high. Subsequent very careful work by Peng et al. [PHSS91], involving smaller system sizes but covering a variety of complementary models with correlated noise (DPRM, direct numerical integration, ballistic deposition) yield data, see Fig. 4.17b, that is somewhat at odds with earlier numerical work [ALF91]. For example, their simulation of the T=0 DPRM with correlated noise (path length=10^4 steps, with 10^5 realizations of the random energy landscape) gives a wandering exponent $\zeta = 0.688$ for $\rho = 0.24$, which translates into a $\beta = 2\zeta - 1 = 0.376$, for this telling test case. While finding some flaws in previous numerical work, [PHSS91] came to the conclusion that none of the analytical formulas were correct, their data falling smack in between the replica-scaling and renormalization group results, which makes one optimistic that an exact answer may be had eventually. It is interesting to note that both groups report trouble for ballistic deposition subject to correlated noise. [ALF91] attribute this to long crossovers, while [PHSS91] go considerably further, suggesting that for $\rho \neq 0$, ballistic deposition belongs to a different, non-KPZ universality class! Clearly, the jury is still out on these matters, it being likely, however, that the 1-loop dynamic and functional RG calculations all have small corrections for non-zero ρ. Indeed, a very recent simulation [PYHH94] confirms this notion, though ρ_c may be pushed to zero. Results of a 2-loop dynamic RG of correlated KPZ, presently in progress [F95], are eagerly awaited.

Exercise: *It is instructive to see how mathematically correlated noise arises. Suppose* $\omega(x)$ *is white noise and* $\eta(x) = \sum_{x'} G(x - x')\omega(x')$ *is the composite correlated noise dictated by the kernel G. Find the scaling form of G if the required correlation function is* $\langle \eta(x)\eta(x') \rangle = C(x - x')$, *where* $C(x) \sim x^{\alpha}$. *Show that for* $\alpha > 0$, $C(x) = A + Bx^{\alpha}$ *with* $A > 0$ *and* $B < 0$ *no matter what G has been used. For* $\alpha < 0$, *B is necessarily positive. Hint: two simplest choices,* $G_1(x) = 1/|x|^{\alpha}$, $G_2(x) = sgn(x)/|x|^{\alpha}$, *yield* $C_1(x) = 2L^{1-2\alpha} - \alpha B_1|x|^{1-2\alpha}$, $C_2(x) = 2L^{1-2\alpha} - 2B_2|x|^{1-2\alpha}$, *where* $-L < x < L$, B_1, B_2 *are constants.*

4.3.2. *Temporally-correlated noise [MHKZ89,LSW92]*

Given the small controversy that persists for the case of purely spatially correlated noise, it is not at all surprising that considerable difficulties hamper investigators interested in surface growth subject to *temporally* correlated noise. Indeed, aside from the 1-loop dynamic RG calculation of Medina et al. [MHKZ89], there exists little formal work on this matter, where explicit destruction of Galilean invariance preempts the classic index relation, $\chi + \chi/\beta = 2$, and renders the exponents essentially independent quantities. With spatially uncorrelated, temporally correlated noise of the form,

$$\langle \eta(x,t)\eta(x',t') \rangle \sim \delta(x - x')|t - t'|^{2\theta - 1} \tag{4.24}$$

in 1+1 dimensions, [MHKZ89] were forced into a numerical analysis of their dynamic RG, finding that for sufficiently small values of the decay parameter, $\theta < 0.167$, corresponding to short-ranged correlations, the exponents stick to their standard, uncorrelated values, $\chi = 1/2$ and $\beta = 1/3$. By contrast, for $0.167 < \theta < 0.5$, the temporal correlation was relevant, leading to anomalous kinetic roughening exponent numerically fit to the form

$$\chi(\theta) = 1.69\theta + 0.22 \tag{4.25}$$

with their expression for the early time exponent,

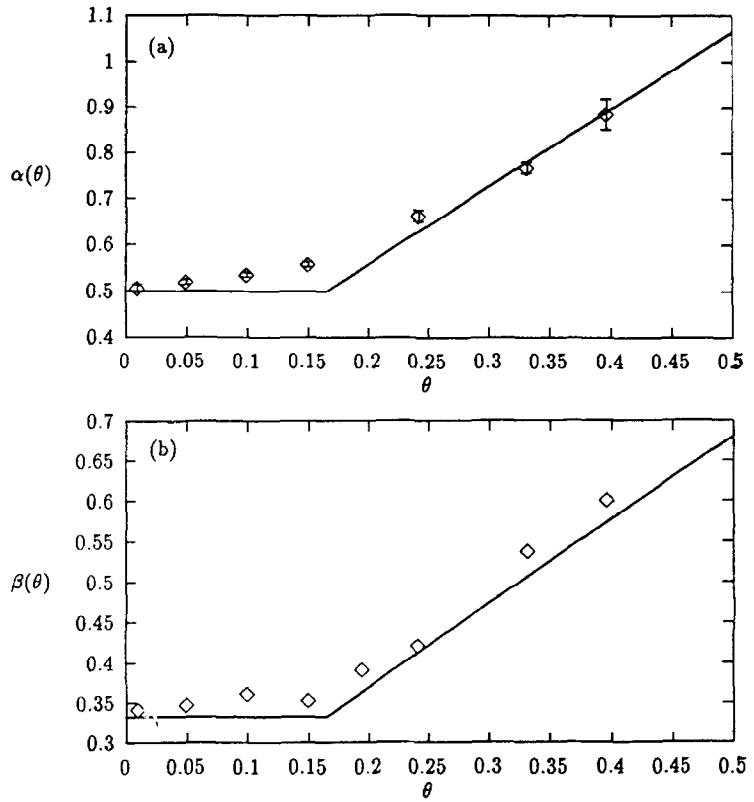

Fig. 4.18. Ballistic deposition subject to temporally correlated noise [LSW92], simulation results for (a) saturation width exponent $\chi = \alpha$, and (b) early-time index β.

$$\beta(\theta) = \frac{(1+2\theta)\chi(\theta)}{2\chi(\theta)+1} \tag{4.26}$$

a consequence of the 1-loop fixed point condition, as well as the unrenormalized nature of the noise correlator. There the situation sat, till Lam, Sander and Wolf [LSW92] put themselves to the task of testing these predictions via simulations of a ballistic deposition model with temporally correlated noise. Using a generalization of Mandelbrot's fast fractional Gaussian noise (FFGN) generator to obtain the desired correlations, with temporally correlated $\eta(x,t)$ dictating the size of the rod dropped ballistically to site x at time t, [LSW92] discovered quite good agreement with the dynamic RG predictions, see Fig. 4.18, there being only modest deviations from theoretical predictions near $\theta_c = 0.167$. Again, this might be the consequence of higher-loop corrections, as is suspected in the spatially correlated case. Their extraction of the roughness exponent χ necessitated extremely long simulations ($t = 400\,000$ time steps), as they varied the system size $30 < L < 1200$. Determination of β required maximal lattice size, $L = 32\,760$, simulating growth up to 5000 and 20 000 time steps for θ smaller or greater than 0.25, respectively. In both cases, they averaged over 10 runs or so to obtain good statistics. A number of numerical nuances, some of potential physical relevance, were uncovered en route:

(i) Reminiscent of the findings of [ALF91] for spatially correlated noise, [LSW92] note an increasing discrepancy between input and measured noise correlations for large values of θ, the latter being smaller than expected (e.g., 0.45 in, 0.40 out).
(ii) The "intrinsic surface width" [KW88] of a ballistic deposit grown with strong temporal correlations in the noise is substantially greater than that in the uncorrelated case.
(iii) The existence of severe model-dependent crossover effects, which were minimized by their use of Mandelbrot's FFGN generator, but were painfully apparent for other choices even in the neighborhood of $\theta = 0$, where they expected to retrieve standard exponents!

Nevertheless, the bottom line here is that the [LSW92] simulation of temporally-correlated ballistic deposition provides strong qualitative support for the dynamic RG calculation.

4.4. *Quenched noise*

A moment's reflection reveals that the physics of the various fluid flow experiments [Rubio89, Wong92b,HFV91a] differs from that embodied in the KPZ equation in at least two fundamental aspects. Firstly, since the irregularities of the bead pack constituting the porous medium are fixed spatially, independent of time, the experimental system actually contains both *quenched* and thermal types of noise. This fact was known to the workers in the field from the very beginning, but they mistakenly assumed that the stochastic noise was *always* dominant. In many cases, thermed noise washes out the effect of quenched noise – which only makes contribution in the so-called transient crossover regions. In the following, we assume conversely that quenched noise only, of the form $\eta(x, h(x,t))$, being a function of the fluid interface position $h(x,t)$, is responsible for the kinetic roughening phenomena exhibited in these experiments. This, of course, is in sharp contrast to the uncorrelated, explicitly time-dependent noise $\eta(x,t)$ typically associated with the standard equation. As stressed by Kessler, Levine and Tu [KLT91], the major effect of quenched vs explicitly time-dependent noise would be to broaden the interface substantially. The reason is manifest – if the interface encounters a point where it becomes temporarily pinned, it will tend to experience that particular condition for a relatively long time, until it becomes depinned, instead of being subject to entirely independent noise the next moment. Indeed, in numerical studies investigating kinetic interfaces subject to quenched noise, Parisi [Pa92] noted specifically such effects, with segments of the interface remaining pinned for extended periods. The second substantive difference in the fluid flow experiments, vis-a-vis the naive applicability of standard theory, concerns the nonlocal nature of the flow field, a point which has emphasized by numerous physicists [KLT91,Wong92bc], but would lead, unfortunately, to an increased stability of the interface. Recently the Budapest group, led by T. Vicsek, has found convincing evidence that the *power law* noise can arise naturally with certain class of *quenched* noise models [CHSVV93]!

Since the inclusion of nonlocal effects normally (but not always! [KrM91]) renders matters analytically intractable while, more importantly, the experiments clearly indicated anomalous kinetic roughening exceeding standard expectations, attention has focussed, recently, on manifestations of quenched noise in the EW and KPZ context, as well as the behavior of relevant growth models. Following some initial confusion about the scaling of quenched models, a clear, aesthetically appealing understanding has been achieved using a self-organized depinning model, proposed independently by the Boston group [BU91], Sneppen [Snp92] and Zaitsev [Zt92]. Early on, Tang and Leschhorn [TL93] realized that this model "almost" mapped onto the well known Directed Percolation problem

(it haunts us again!). The Weizmann group [OPZ94] then systematically developed a scaling theory using the concepts of hierachical clusters (see also independently [LT94]). They were able to obtain virtually all exponents from just one, the roughening exponent χ. Thus all dynamic aspects as well as multi-fractal features can be understood. This is quite contrary to what we would expect from a highly nonlinear, nonlocal model. The reader is urged to study their original work for other exciting aspects of the quenched models. At the time of this writing, waves of preprints from the Boston and Weizmann groups were still pouring out in this direction.

4.4.1. Rubio's roughness exponent, $\chi \approx 3/4$? [KLT91]

Motivated by earlier, very important work of Bruinsma and Aeppli [BA84] and Villain [V84] concerning metastability, dynamics, and the pinning of domain-walls in random-field Ising magnets, in addition to the later, related efforts of Koplik and Levine [KL85] on interfacial pinning arising in segregating fluids in porous media, for whom the common denominator was, in retrospect, the EW equation subject to quenched noise,

$$\partial_t h = \nu \nabla^2 h + \eta(\boldsymbol{x}, h) + F \tag{4.27}$$

with

$$\langle \eta(\boldsymbol{x}, h)\eta(\boldsymbol{x}', h')\rangle = \delta(\boldsymbol{x} - \boldsymbol{x}')\delta(h - h'). \tag{4.28}$$

Kessler, Levine and Tu [KLT91] initiated a renaissance in this equation, as they sought to explain the Rubio forced fluid-flow experiment; recall Section 4.1.1. Here, of course, $h(\boldsymbol{x}, t)$ is the interfacial profile as a function of transverse coordinate $\boldsymbol{x}$ and time t, while F is the driving force and ν the relaxation coefficient. The quenched noise is assumed to have zero mean, with delta function correlation in its arguments. Because the noise is quenched (i.e., a nonlinear function of the interface position), the renormalization group obviously (?) generates the characteristic KPZ nonlinearity for the unpinned phase, supplementing the terms already present in the above equation. This is easily motivated physically – suppose an advancing interface encounters an obstacle so that it becomes temporarily pinned at a particular site. In the same time, nearby opposing segments of the interface continue advancing, but begin to pinch off the guilty pin, effectively generating the lateral growth mechanism associated with the $(\nabla h)^2$ term. Since we are in the macroscopically unpinned regime, however, the obstacle is eventually overcome and the ordinary EW translation mechanism prevails until the next serious pinning event. The behavior of this model is clear in the extreme limits:

(i) *Strong pushing regime – moving interface* $F \gg \langle \eta^2 \rangle^{1/2}$. Here, we can write $h = Ft + \tilde{h}$, so that the above becomes $\partial_t \tilde{h} = \nu \nabla^2 \tilde{h} + \eta(\boldsymbol{x}, Ft)$. In this regime the interface is being driven through the random medium so quickly that there are no severe pinning events and the quenched noise is transformed into one which is explicitly time-dependent. The model reduces to the usual EW scenario with uncorrelated noise, possessing solution $\tilde{h}(\boldsymbol{k}, \omega) = G(\boldsymbol{k}, \omega)\eta(\boldsymbol{k}, \omega)/\sqrt{F}$, with diffusion propagator $G(\boldsymbol{k}, \omega) = (i\omega - \nu k^2)^{-1}$. Given the correlation in the noise, it is apparent that $\langle \tilde{h}(\boldsymbol{x}, t)\tilde{h}(\boldsymbol{x}', t)\rangle \sim (g^2/\nu F)|\boldsymbol{x} - \boldsymbol{x}'|^{(2-d)}$ so that in $d = 1$, the length-scale dependent roughness satisfies $w(L) \sim \sqrt{g^2/\nu F}L^{1/2}$, with the standard EW (or KPZ) saturation width exponent $\chi = 1/2 < \chi_{Rubio} = 0.73 \pm 0.03$, but with an amplitude that, somewhat propitiously, scales with the driving force in a manner entirely consistent with the Rubio experiment.

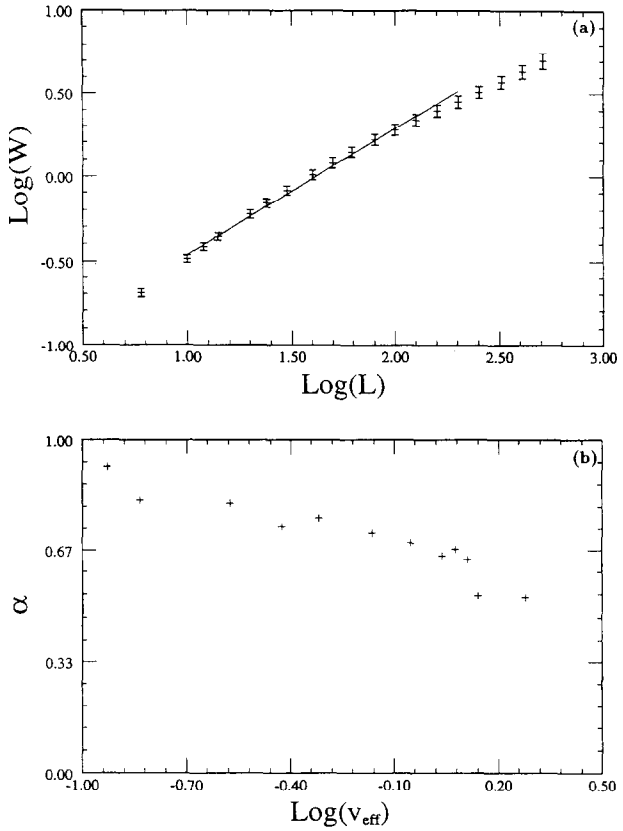

Fig. 4.19. Numerical integration of the EW equation subject to quenched disorder [KLT91]. (a) Saturation width as a function of length scale. Note the effective value $\chi \approx 3/4$. (b) Effective value of the saturation width exponent as a function of the growth velocity.

(ii) *Static regime – pinned interface, $F < F_c$.* Here Grinstein-Ma type arguments, developed in the context of domain-wall roughening in random-field Ising magnets, require that in $d = 1$ that the roughness exponent be unity, χ=1, since $w \sim L$; see [HH90], diverse manifolds in random media.

It is interesting to note that between these two extremes for the driving force, the roughness exponent varies only between 1/2 and 1, a feature which has been stressed by [Wong92b], who emphasizes that his own experiments at very small capillary number successfully hint at the regime where RF ideas are germane and control the dynamics.

With the intent of elucidating the complex scaling behavior expected in the broad intermediate regime commencing just beyond the depinning transition, [KLT91] numerically integrated the EW equation with quenched noise and measured the lengthscale dependent roughness, $w(L)$, precisely as in the Rubio experiment. With a system size 900×4000, horizontal by vertical, pinning sites occupying just 10% of the lattice, with strengths gaussian distributed, and averaging over ten different runs, they discovered an intriguing fact. Although the data could be well fit over more than a decade by an exponent χ=0.75±0.02, see Fig. 4.19a, at the largest length scales, corresponding to the cm-sized parabolic features apparent in Rubio's interfacial profiles, recall Fig. 4.1, the effective exponent, given

by the local slope in the double log plot, began to decrease noticeably. A systematic investigation of this phenomenon led them to study the dependence of χ upon the asymptotic growth velocity $v_{eff} = \lim_{t\to\infty} \langle h(t)\rangle/t$, known to be a monotonically increasing function of F. Their results, summarized in Fig. 4.19b, reveal that despite a noticeable plateau region where the roughness exponent $\chi \approx 3/4$, at large velocities it dropped down towards the standard value $1/2$, while close to, but above, the depinning transition, where the interface is moving slowly, the exponent creeps upwards towards unity – a stunning corroboration of Wong's assertion [Wong92bc] that the experimental results are very much dependent upon the capillary number *Ca*. Nonetheless, in the plateau region where the exponent $\chi \approx 3/4$, the EW equation with quenched noise did yield an amplitude that scaled as $v_{eff}^{-0.47\pm0.03}$, entirely consistent with Rubio's findings in that regime, assuming, as is natural, that $Ca \propto v_{eff}$.

4.4.2. Early simulation of Parisi [Pa92]

Independently of Kessler, Levine and Tu [KLT91], who had concentrated on the static roughening exponent χ, Parisi [Pa92] commenced his own program of research on the EW equation with quenched noise, concerned primarily with determining the early-time exponent β for systems driven just above the depinning threshold. His considerations were motivated by the fluid flow experiment of Horváth, Family and Vicsek [HFV91a], discussed further in the next section, who were the first group to investigate the dynamic properties of moving fluid interfaces in porous media, finding that the rms width increased as a power-law with the anomalously large exponent $\beta \approx 0.65$, nearly twice the standard value! Parisi's approach was based upon simulation of a simple stochastic growth model (which he assumed to be within the new quenched KPZ universality class), straightforward numerical integration of the EW equation with quenched noise, and finally a plausible, "back of the envelope" argument, using his earlier work with Pietronero [Pa91] on charge density waves, that produces the exponent $\beta_c = 3/4$ to characterize the divergence of both the mean interface position $h(t)$ and the rms width $w(t)$ at the pinning-depinning transition.

Parisi's simple stochastic model of surface growth in random media is defined on a square lattice, with the integer-valued interface height $h(i,t)$ being a function of the transverse coordinate i. At each point on the lattice is placed a quenched random variable $\eta(i,h)$, uncorrelated from point to point, uniformly drawn from the interval $(-1,1)$, which represents the strength of the pinning site experienced by the surface at the point (i,h). The evolution algorithm for the surface involves comparing the pinning strength at a given site, $\eta(i,h(i,t))$, to

$$F(i,t) \equiv v(\max[h(i+1,t), h(i-1,t)] + 1 - h(i,t)) \tag{4.29}$$

which is meant to mimic a driving force in the actual experiment. Here, v is a control parameter, allowing us to tweak up the force which pushes the interface through quenched random medium. If F exceeds η at a given site the driving force overcomes the local pin, the interface grows and we set

$$h(i,t+1) = \max[h(i+1,t), h(i-1,t)] + 1 \tag{4.30}$$

otherwise the surface remains hung up at the pin until the next try. Shown in Fig. 4.20a is a typical interfacial configuration for $v = 0.14$, slightly above the critical depinning threshold $v_c \approx 0.1$, found by Parisi. The above discrete equation is believed to be in the same universality class of the EW equation in quenched noise. Conspicuously, Parisi did not include the KPZ nonlinear term arguing that, near the critical depinning point, *both* with and without the nonlinear term the critical scaling

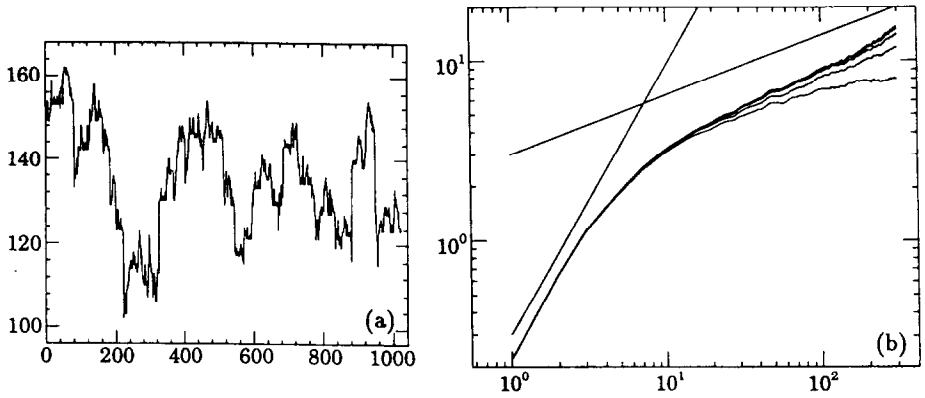

Fig. 4.20. Parisi's model of kinetic roughening by quenched disorder [Pa92]. (a) Interfacial profile for driving just beyond the depinning threshold, and (b) early-time interfacial roughness, illustrating crossover to standard KPZ exponent. Curves bottom to top: increasing system size.

behavior would be the same. Later we shall see, with the help of the SOC trick of sitting-on critical point, this assumption is wrong- the nonlinear term makes a big difference at criticality. The characteristic features are due mainly to the presence of several very strong pinning sites, giving the profile its severe jagged appearance. An examination of the early-time interfacial width for this value of v reveals, see Fig. 4.20b, an apparently non-KPZ exponent $\beta_c = 3/4$, though further from the depinning transition ($v = 0.24$), where the interface is driven harder, there is a clear crossover to the standard index $1/3$. From the numerics it is apparent that the crossover timescale t^* depends very sensitively on the relative proximity of the pinning-depinning transition. In fact, within the Parisi-Pietronero model, which has slightly different asymptotics, t^* scales as $(v - v_c)^{-4/(d-1)}$. When Parisi numerically integrates the $d = 2$ EW equation with quenched noise according to the prescription,

$$h(i, t+\epsilon) = h(i,t) + \epsilon(v + \Delta h(i,t) + \lambda\eta(i, h(i,t))) \tag{4.31}$$

with λ a parameter and Δ the lattice Laplacian, he discovers this same characteristic exponent $\beta_c \approx 3/4$ at the depinning threshold. The essence of the Parisi-Pietronero model is a noise term, $\eta(x)$, that is strictly *time-independent* with neither dependence upon the time t, nor the interface position h! Parisi argues that, as one approaches the depinning transition from above, the statistical weight of pinned interfacial segments becomes increasingly important. Indeed, it is precisely because the average velocity of the interface vanishes at v_c that one can ignore the height dependence of the noise. After all, if much of the interface is stuck in place, the noise term has neither an explicit nor implicit time dependence! As justly pointed out by Parisi, himself, such an argument seems a bit "fishy" since it is clear that $h(t)$ goes to infinity at the transition. However, the thing to keep in mind is that $\partial h/\partial t$ vanishes at the same time. What saves the day is the presence of pinned regions where h is practically time-independent. For more details concerning Parisi-Pietronero argument, the reader is referred to the original papers [Pa91,92].

4.4.3. Functional RG treatments [NSTL92,NF92]

Because of its relevance to a variety of physical contexts, including the dynamics of vortex lines in dirty superconductors, the behavior of sliding charge density waves, as well as its connection to the forced-fluid flow experiment, the problem of kinetic roughening via quenched disorder has received

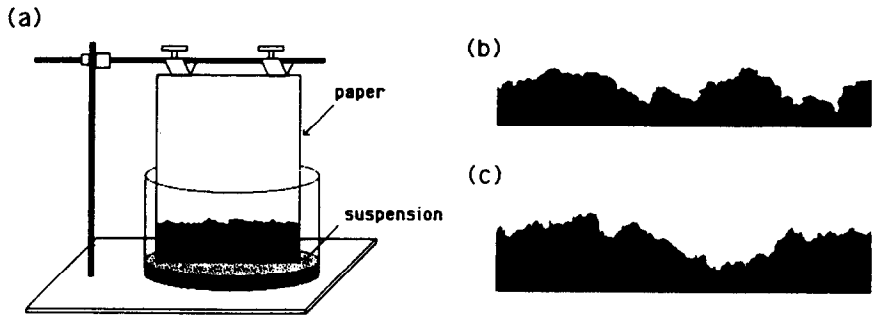

Fig. 4.21. (a) Viscous imbibition experimental set-up [Boston92]. (b) Digitized interface of actual 20 cm wide sample. (c) Typical result of related directed percolation model with $L = 400$ and $p = p_c \approx 0.47$.

much due attention. In particular, following the numerics of Kessler, Levine and Tu [KLT91] and the work of Parisi [Pa92], Nattermann, Stepanow, Tang and Leschhorn [NSTL92] performed a functional renormalization group calculation of the quenched EW equation, in an effort to extract the critical exponents associated with the near-threshold, depinning dynamics of a driven interface in a random medium. Their analysis, accurate to first-order in $\epsilon = 4 - D$, where D is the interface dimension, reveals the dynamics to be superdiffusive at the depinning transition, characterized by a dynamic exponent $z \approx 2 - 2\epsilon/9$, while the steady-state roughness is given by $\chi \approx \epsilon/3$. The average velocity of the moving interface vanishes as $(F - F_c)^\theta$, with $\theta \approx 1 - \epsilon/9$, as the driving force approaches its critical value from above. Equivalent results were obtained, independently, by Narayan and Fisher [NF92]. Interestingly, for $D = 1$, this suggests $\beta = \chi/z \approx 3/4$, in agreement with Parisi's value. Of course, this must be taken with a grain of salt, given (i) the usual caveats concerning extrapolations far from the UCD, and (ii) the fact that the Parisi-Pietronero prediction, $\beta_c = (4 - D)/4$ differs from the RG calculation in higher dimensions. Subsequently, Leschhorn [L93] reported a somewhat high value, $\beta_c = 0.88 \pm 0.02$, but finds 0.475 ± 0.015 for $D = 2$ and argues that his results support the RG calculation because the deviations decrease with increasing ϵ.

4.5. Viscous imbibition: pinning via directed percolation [Boston92,TL92]

In sharp contrast to the difficult experimental situation associated with *moving* fluid interfaces in porous media, there have been, recently, several rather intriguing experiments involving *viscous imbibition* [Boston92,FCA92], in which a dark staining fluid (such as ink, coffee, food coloring, etc.) is soaked up by a properly suspended sheet of highly absorptive paper, being kinetically roughened in the process. Because the fluid is being drawn passively into the sheet, rather than being pushed through at a strictly controlled constant rate as in the bead pack experiments [Rubio89,Wong92b], the capillary number is variable and the mean position of the interface is not a simple linear function of time. Nevertheless, very definitive conclusions have been reached in these experiments regarding the roughness of the final, pinned interfacial configuration. In Fig. 4.21 is shown a schematic of the experimental set-up of the Boston group, as well as comparative interface profiles from the experiment itself and their directed percolation model (discussed below), which forms the basis of our present understanding of the pinned phase in this viscous imbibition process. The essence of the [Boston92] model is straightforward enough – one considers, see Fig. 4.22, a square lattice of size

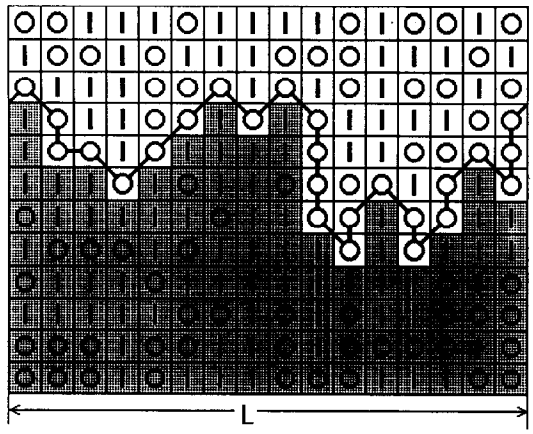

Fig. 4.22. Essence of the directed percolation model for viscous imbibition [Boston92]. The bold line illustrates the *spanning* path formed by connected nn and nnn blocked cells that pin the interface.

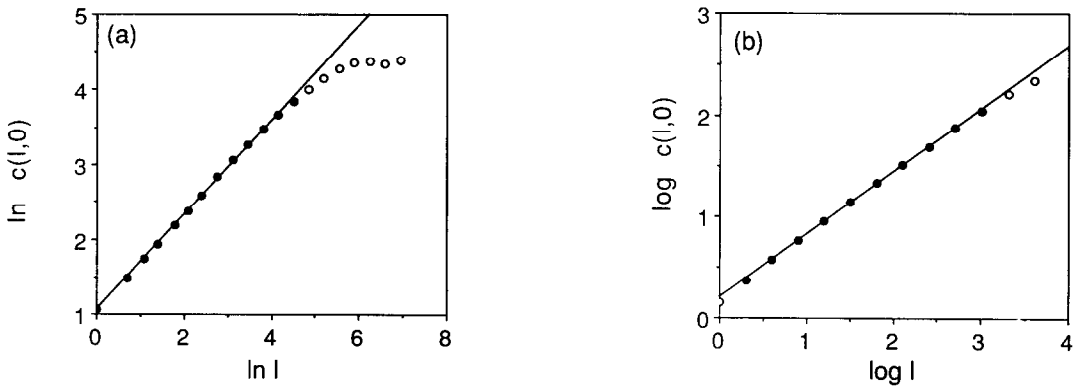

Fig. 4.23. Double log plots of the static height-height correlation function $c(l,0)$ as a function of length scale l for (a) experimental imbibition lines, and (b) directed percolation model [Boston92].

L with periodic boundary conditions, in which a finite fraction p of the cells are blocked (marked by the letter O), the remainder being susceptible to invasion (denoted I). The baseline row is filled with fluid (shaded), the imbibition process proceeding by randomly choosing, with equal probability, one of the neighboring I-cells that is dry. That cell becomes wet; in addition, any dry cell (regardless of type!) below it in the same column also gets shaded. In this manner, the erosion of overhangs is explicitly encoded into the iterative prescription that governs the evolution of the interface, ensuring an SOS condition at all times. For values p below a critical threshold $p_c(L)$, the interface propagates without stopping, while if the density of blocking cells is sufficient, $p > p_c(L)$, the interface will eventually get pinned across its entire length when it meets a directed, percolating string of O-cells that run West to East across the lattice, see Fig. 4.22. Note that the string must be directed, since the erosion process renders passable any string with a segment that doubles back.

In Fig. 4.23a, is shown the length-scale dependent width of the pinned interface in the viscous imbibition experiment of Buldyrev et al. [Boston92], which yields a roughness exponent $\chi = 0.63 \pm 0.04$, the result reflecting an average done over 15 different experiments. Fig. 4.23b shows the analogous quantity for their simulations of the invasion/erosion model, using 1000 realizations for

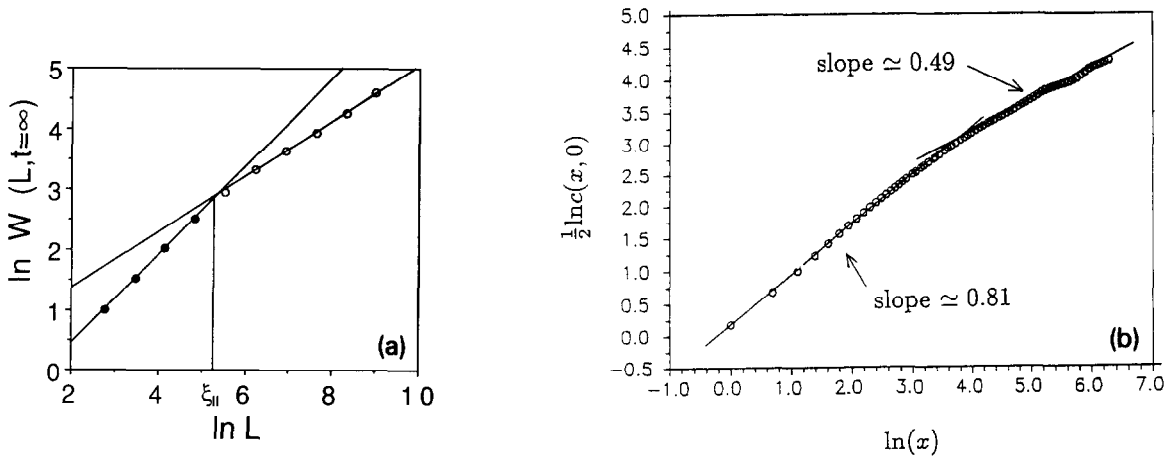

Fig. 4.24. Crossover effect in size-dependent global interface width, thanks to finite correlation length. (a) Directed percolation model [Boston92], and (b) fluid-flow experiment [HFV91a].

system size $L = 16384$, fine tuned very close to the percolation threshold $p_c \approx 0.469$, which gave a characteristic exponent 0.63 ± 0.02 for the roughness of the directed, percolating string. Indeed, much is known about the directed percolation in two dimensions – recent series expansions for this anisotropic problem estimate

$$\nu_\perp = 1.097 \pm 0.001, \quad \nu_\parallel = 1.733 \pm 0.001, \tag{4.32}$$

for the perpendicular and parallel correlation length exponents, respectively [Ess88]. Since these two diverging correlation lengths are related via $\xi_\perp \sim \xi_\parallel^{\nu_\perp/\nu_\parallel}$, while it is natural to identify $w(L) \sim \xi_\perp$ and $l \sim \xi_\parallel$, it should be no surprise that the simulations produced $\chi = \nu_\perp/\nu_\parallel \approx 0.63$. Thus, the *static* properties of the pinned interface in viscous imbibition appear very well described by directed percolation ideas. Independent, but related work involving a microscopic model slightly different from the Boston group was proposed simultaneously by Tang and Leschhorn [TL92].

Although the viscous imbibition experiment of the Boston group concentrated on the geometric properties of the final configuration of the pinned interface and ignored the dynamics enroute, it is natural to ask precisely what the invasion/erosion model has to say concerning these aspects. Interestingly enough, the model may shed some light on the small length scale pinning processes crucial to the fluid flow experiments discussed earlier. More specifically, an examination of the global width of the interface as a function of system size L below the percolation threshold reveals a rather distinctive *crossover* phenomenon, see Fig. 4.24a, that had been noted in a previous forced fluid flow experiment by Horváth, Family, and Vicsek [HFV91a]. If the system size is less than the finite value of the correlation length, $L < \xi_\parallel$, the moving interface will eventually be pinned by a directed pecolation path but until then the roughening is anomalous, typically larger and somewhat more stubborn to pin down (0.66-0.73) than for the stopped line. By contrast, for $L > \xi_\parallel$, the moving interface has a roughness entirely characteristic of standard value, $\chi = 1/2$. In the Horváth et al. experiment, the short lengthscale roughness was anomalous, $\chi \approx 0.81$, whereas the large lengthscale roughness was very nearly KPZ-like, with an estimated exponent 0.49, see Fig. 4.24b. In addition, the Horváth et al. measured temporal correlations in their moving interface, extracting an early-time exponent $\beta \approx 0.65$, in rather extraordinary agreement with the invasion/erosion model of the Boston

group, who find a value ≈ 0.68 at the percolation threshold, as well as Tang and Leschhorn [TL92], who quote $\beta \approx 0.63$. Indeed, the latter group has worked hard to explain the effects of pinning above and below the percolation threshold, observing that later the time-dependent width saturates, of course, for the pinned phase ($p > p_c$), but eventually scales as $t^{1/3}$, à la standard KPZ! All of which reveals the importance of small length scale pinning events, with short segments of the interface being momentarily tied up, on the short time dynamics and microscale roughness. See [TL92] for details, including corroboration of the stubbornly variable χ for the moving interface.

The above work manifestly refers to the directed percolation problem since we put explicitly two different cells and adjust, by hand, the relative concentration – the behavior exhibited by the model depending sensitively on the proximity to ρ_c. We shall see below that a modified version, the so-called "self-organized depinning" model gives rise in a very natural way directed percolation clusters.

4.6. The self-organized depinning model

Intrigued by the fundamental distinction between *non-local* growth mechanisms, such as DLA and invasion percolation [F88r], which give rise to self-similar geometric structures, and intrinsically *local* models, exemplified by the RSOS model of Kim and Kosterlitz [KK89], that lead to purely self-affine surfaces, Sneppen [Snp92] analyzed an interesting growth model suggesting a dynamical mechanism for the fine tuning assumed in the directed percolation explanation [Boston92,TL92] of the viscous imbibition experiments [Wong92b].

Immediately following publication, Sneppen's paper received much attention, directly inspiring important later work [TL93,SJ93,LT94,OPZ94] on self-organized processes in the kinetic roughening context. Interestingly, with much of the history now behind us, it has become apparent that both Stanley's group in Boston [BU91] and Zaitsev [Zt92], with his "Robin Hood" model, had independently proposed similar ideas. As the paternity of this model became contentious, we are told that the belligerent parties have reached a cease-fire agreement, to share the credits, call the model "Self-Organized Depinning" (SOD), and quote all three references [BU91,Snp92,Zt92].

There are three essential building blocks in the SOD model:

(i) global equilibration of external driving force – growth occurs at sites where the local pinning energy is minimal, reminiscent of invasion percolation [WW83],

(ii) local pins are represented by quenched, random variables [KLT91,Pa92], and, finally, to ensure self-affinity, supplement the above by

(iii) Kim-Kosterlitz [KK89] constraint of small local slopes.

In Version A (B) of Sneppen's SOD growth algorithm, one insists upon the small slope constraint before (after) permitting global equilibration of the interface. Somewhat surprisingly, despite (iii), Version A results in a marginally self-similar geometry characterized by the exponent $\chi = 1$, identical to that of quenched noise in the pinned regime [KLT91], where RF Ising model ideas are relevant, and suggested by the fluid flow experiments at vanishingly small capillary number [Wong92b]. By contrast, Version B yields a self-affine interface with roughness exponent $\chi \approx 0.63$, very close to that of the directed percolation model. Here we concentrate on Model B, in which an interface $h(x)$, defined on a discrete chain $x = 1, 2, \ldots, L$, is moved by finding the site along the interface with the smallest pinning force $\eta(x, h)$, a quenched uncorrelated gaussian random variable. On this site the interfacial height h is augmented by unity, then *neighboring sites are adjusted upwards* ($h \to h + 1$) until all slopes satisfy the RSOS condition $|h(y) - h(y-1)| \leq 1$, whereupon new random noise

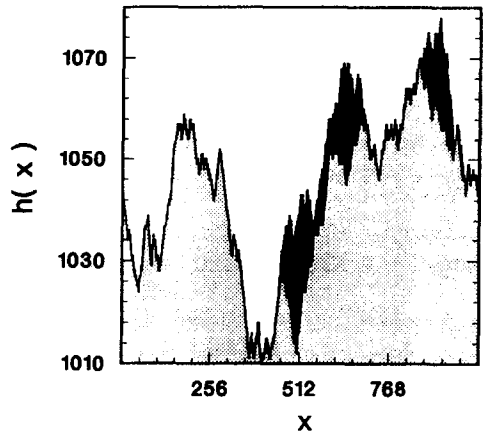

Fig. 4.25. SOD Interface Model B: Typical interfacial configuration, indicating sites of latest activity and self-organized nature of the Sneppen algorithm.

$\eta \in [0, 1]$ is assigned to all adjusted sites. Typical saturated interfacial configurations of Model B are illustrated in Fig. 4.25, with black indicating the regions of latest activity, apparently, though not surprisingly, a highly nonhomogeneous, localized affair. Interestingly, thanks to the evolution algorithm defining Model B, which raises the interface much as a pole does a tent, there are, potentially, a variable number of neighboring sites that participate in the update. Sneppen noted that the distribution of such time-reversed "avalanches" have a characteristic size of about 4 or so, with exponentially small probability for bigger events. As mentioned above, when Sneppen examined the dependence of the saturation width $w(L)$ as a function of finite system size L, he discovered a roughness exponent familiar from the directed percolation context, extracting the value $\chi = 0.63 \pm 0.02$. Hence, SOD Model B demonstrates that global equilibration of pinning forces can give rise to interfaces that are self-affine rather than self-similar and, furthermore, its underlying dynamical mechanism results in self-organized, kinetically roughened surfaces that automatically assume a critical state without any external fine tuning. In addition, the importance of nonlocality in generating anomalous roughening cannot be overemphasized, for localized versions of SOD Model B in which, for example, sites are randomly picked (or even chosen with a chance proportional to a local $\eta(x, h) \in [0, 1]$) for a forced move $h \rightarrow h+1$, with neighbors adjusted upwards in compliance with the RSOS constraint) all result in the standard exponents, $\beta = 1/3$ and $\chi = 1/2$. Finally, it is intriguing that interfacial roughness in the saturation regime can be, compare SOD Models A and B, so very sensitive to whether the constraint upon local slopes acts before or after the motion takes place. Indeed, nearly all experiments indicating anomalous kinetic roughening have measured χ's in between the values predicted by these two models.

4.6.1. Directed percolation and scaling theory [OPZ94,LT94]

Following its introduction, the SOD model came under intense scrutiny by virtue of its nontrivial scaling index and tuned, self-organized criticality [BTW87]. Early work mainly explored numerical consequences. However, two groups [OPZ94,LT94] were able to break through the analytical front by relating the SOD to the directed percolation model, and by using the concepts of blocking surfaces and associated processes. A nearly thorough understanding has recently been had. It started first with Tang and Leschhorn, who proposed [TL93, see also SJ93] and later showed instructively [LT94]

that SOD is essentially a dynamical version of directed percolation, just at critical p_c. Soon after Olami, Procaccia and Zeitak [OPZ94] were able to construct a systematic scaling theory which rationalizes all the critical behavior of the model, based on the above mentioned two concepts. Similar conclusions were also obtained independently by Leschhorn and Tang [LT94]. Together, they suggest the model to be "almost completely solvable" in the sense that the whole family of exponents (dynamic, distribution, multifractal, etc.) can be found by a relatively simple, though novel scaling theory. In fact, they believe that most, if not all of the exponents can be related to those of directed percolation, $\nu_\parallel \approx 1.733$ and $\nu_\perp \approx 1.097$. Here, we quickly cut to the chase, revealing the magic trick which makes directed percolation appear from such an innocent growth model, even more so that an invisible hand always takes care to tune the model to be just critical. The key point is that many critical percolating strings lie ahead of the SOD model interface, awaiting its arrival; each acts briefly as a fence, detaining interfacial segments and insisting upon complete overlap before permitting any advance beyond, thereby dictating the steady-state roughness exponent $\chi = \nu_\parallel/\nu_\perp \approx 0.63$. The latest analysis shows however, this mapping is not exact, i.e. the SOD model's $\chi \approx 0.61$, smaller than the generally believed value, and cannot be exactly expressed by $\chi = \nu_\parallel/\nu_\perp$ (Procaccia, private communication). This is because statistically a SOD interface should be viewed as a random walk on the directed percolation clusters. This readjustment of χ does not influence the qualitative conclusions of the above mentioned scaling theory, all the relations to χ hold except that χ's value is slightly shifted downwards.

Furthermore, an examination [SJ93,LT94] of the the entire distribution of pins, as well as that of the minimal pin η_{min}, along the SOD interface satisfies the inequality [TL93] $\eta_{min} < 1 - p_c$, with $p_c = 0.5385$ for 2d directed percolation, confirming the notion that the model develops saturated configurations intimately related to directed percolating strings. Even so, the SOD model enjoys a nontrivial dynamics, involving an interplay of local and global growth rules that necessitates modification of standard ideas of dynamical scaling. It is possible, however, to isolate the local contribution by defining a sequence of causal growth events, or "avalanche," with dynamical exponent $z_{loc} = 1 + \chi \approx 1.63$ relating characteristic time and length scales; for details, see [OPZ94]. In fact, the full multifractality of the SOD model, encoded in the family of exponents necessary for describing the moments of the height-height correlation function

$$C_q(t) = \langle \overline{|\Delta h - \overline{\Delta h}|^q}^{1/q} \rangle \sim t^{\beta_q} \tag{4.33}$$

appears tractable within the new approach, which yields $\beta_q = 1 + (1 - q)/qz_{loc}$, in nice agreement with the numerical results $\beta_2 = 0.69 \pm 0.02$ [SJ93] and $\beta_\infty = 0.40 \pm 0.01$ [OPZ94,LT94], the latter being just $\beta_{loc} = \chi/z_{loc}$. Finally, the spatial-temporal correlations between successive growth events can be well-understood via a scaled probability distribution which predicts the spatial distribution function of distances x between the two minimal η values along the SOD interface to fall as $x^{-\gamma}$, with $\gamma = 1 + (2/\nu_\parallel) \approx 2.16$, very close to the numerical estimate $\gamma = 2.20 \pm 0.05$ [OPZ94,LT94]. Subsequently, a refined scaling theory due to Maslov and Paczuski [MP94], which predicts $\gamma = 1 + (1 + \nu_\perp)/\nu_\parallel \approx 2.21$, has led to even better agreement. For very recent exciting work connecting self-organized depinning, direct percolation, and the Bak-Sneppen model [BS93] of punctuated evolution, see [MPB94].

4.6.2. EW and KPZ equations in quenched disorder

The crucial ingredient of the SOD model (similarly Zaitsev's related "Robin Hood model" [Zt92]) is the quasi-static driving condition which makes sure each time there is only one site that moves, no matter how large the system size is. It is clear this condition can be applied also to the EW and KPZ equations with quenched disorder. Traditionally held wisdom [Pa92] argues that at criticality both equations scale the same way. However, we shall see that the criticality here is an ill-defined notion. Without the SOD trick we need to finely tune the global driving force F – we shall argue below that such a constant F_c does not exist, no matter how precisely we tune F.

Let us reconsider both equations, with the new input of the quasi-static driving condition

$$\dot{h} = \nabla^2 h + \lambda(\nabla h)^2 - \eta(x, h) + F \tag{4.34}$$

the EW equation obtains when $\lambda = 0$. For the moment we assume F constant. We shall return later to discuss its precise role and definition. Sneppen's idea is readily generalized here. Consider the above equation in a lattice version. We concentrate on the quantity

$$\nabla^2 h + \lambda(\nabla h)^2 - \eta(x, h) + F. \tag{4.35}$$

The quasistatic condition requires that in the whole range of $1 \leq x \leq L$, we choose the site x_0 whose value is the maximum of equation (4.35). This can be achieved by choosing a suitable F so that everywhere else the value is negative, except at x_0 positive. With the additional condition of no-backwards-return of the h variable, we see that only one site x_0 can move. Once the h variable on site x_0 has moved forward a new η is seen and this site has further chance to move without subjecting to RSOS. However, after a move at x_0, the neighboring sites $(x_0 \pm 1)$ have also better chance to move, since both $\nabla^2 h$ and $(\nabla h)^2$ get updated in their favor. It is natural to expect the above realizations would reproduce the SOD universality class, or the directed percolation exponents. Olami, Procaccia and Zeitak [OPZ94p] and, independently, Galluccio and Zhang [GZ94] have performed numerical simulations finding, for $\lambda \neq 0$, the roughening exponent $\chi \simeq 0.63$, trademark of directed percolation. The surprise comes, however, when the nonlinearity is turned off. The exponent $\chi \simeq 1.20 > 0$. Besides the above two groups, this was reported early by Roux and Hansen [RH94] for $\lambda = 0$ case. A careful examination of these super-rough surfaces reveals that, for a fixed system size L, the profiles are still self-affine, though with a smaller exponent $\chi_1 \simeq 0.85$ [RH93,GZ94]:

$$w(l, L) \sim l^{\chi_1} L^{\chi_2} \tag{4.36}$$

where l is the measurement lengthscale (window-size) of the width w, L the constant system size, and $\chi_2 \simeq 0.35$. The description of a self-affine surface by two exponents is new. This can only happen when the global exponent $\chi > 1$. From (4.36), it is clear that when the window is taken to be of the system size L, we recover $w \sim L^{\chi}$, with $\chi \simeq 1.20$.

The short explanation for this bizarre behavior can be traced to the EW equation, which has one symmetry too many in comparison to KPZ, i.e., $h \to h + cx$, while the Galilean invariance satisfied by KPZ is much more restricive. Numerically, it is manifest that as soon as we add a term to break this unsolicited symmetry (using say, $|\nabla h|^{\alpha}, \alpha \geq 1$), the directed percolation universality class is recovered. In the absence of a brute force RSOS condition, this extra symmetry permits the difference of the neighboring h's (or the derivatives) arbitrarily large. As a matter of fact, the scaling relation with double exponents is a manifestation of diverging derivatives and the edge can be modeled by

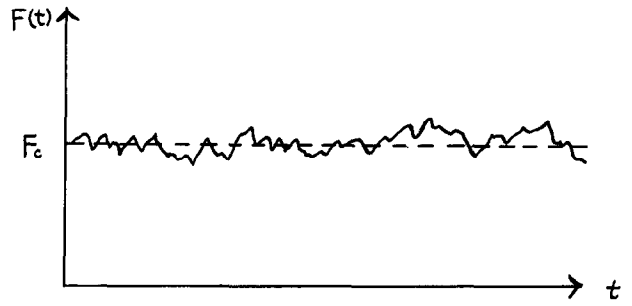

Fig. 4.26. The instantaneous critical depinning force $F(t)$, contrasted [Z94u] with a conventional constant F_c.

a correlated Lévy flight. This is in contrast to an ordinary kinetically roughened edge, for which we associate a correlated random walk.

Let us return to our driving force F. We said that with a suitably chosen F only one site moves. However, for the next move, we need to find an appropriate F again – this is automatically done in the SOD prescription by requiring the maximum in each step. If we plot all the F as a function of time, we would see that F fluctuates around a constant value, call it F_c, the critical depinning force. But which is more natural in reality: a fluctuating F or a constant F? Consider the Rubio experiment at the microscopic level – the applied pressure field furnishes the driving force. Imagine that pressure slowly builds up and suddenly the interface at one site breaks forward. This will result in a temporary reduction in pressure, however small it may be. Since the water is still being pumped in, pressure builds up again until the next event happens. This is depicted in Fig. 4.26. It is clear that the larger the system size, the smaller the fluctuations around F_c. As a matter of fact, such fluctuations can be readily estimated [Z94u],

$$\Delta F \sim L^{-1/\xi_{\parallel}} \tag{4.37}$$

We see the fluctuations approach zero rather slowly as $L \to \infty$. Now we are in a position to understand why the surface growth equations with the quasistatic condition significantly differ from those with constant driving force. Suppose the very same system is been driven by a presumed critical F_c. The sites which require a slightly larger F would pin the interface completely. To remedy this disaster we may want to raise F by defining F_c to be just above the upper bound of the fluctuating F in the figure. A moment's reflection reveals that this does not work either since, by definition, we are in the unpinned region; hence, no site can stop the advancing interface. We are off nominal criticality by at least the amount ΔF, see (4.37). It is clear that the concept of a critical constant value of driving force is at fault. The precise meaning of F_c is only the average value of $F(t)$ but cannot be used to drive an interface! To probe the criticality we need a fluctuating $F(t)$, no cleverly chosen F_c constant can really approach the depinning transition. This idea may have unexpected implications for similar models as well, notable for the charge density waves.

In a recent preprint, Olami, Procaccia and Zeitak [OPZ94p] have extended their scaling theory of the SOD model to both continuous EW and KPZ equations in quenched disorder. Besides the numerical results mentioned above used to support their analytical conclusions, they derived the universal scaling relations that treat EW, KPZ and SOD models in a coherent way. In particular, as a corollary they show that the discrete SOD and the continuous KPZ are equivalent. Their approach has the merit of giving the seemingly complicated models in quenched disorder a much simpler

understanding. The reader is urged to consult the latest literature to get informed of this rapidly developing field.

4.7. *Facing additional realities – kinetically roughened surfaces*

In previous sections, we discussed the wealth of experimental data indicating anomalous scaling of Nature's kinetically roughened *edges*. Here, we consider full-fledged *surfaces*, calling to task surface diffusion models in the context of thin film growth via molecular beam epitaxy (MBE). We close by examining some intriguing erosion experiments involving i) sputter-etched graphite and ii) geomorphological evolution of micromountains.

4.7.1. *Towards a working theory of MBE: surface diffusion models [V91,LDS91,KrPS93]*

Following the explication of kinetic roughening for Eden clusters, ballistic deposits and single-step surfaces, there has been, recently, a concerted effort to tailor stochastic differential equations to describe actual film growth via molecular beam epitaxy, particularly in circumstances where surface diffusion of adatoms to highly coordinated sites is assumed the dominant relaxational process. In such "ideal MBE" surface diffusion models, vacancies, overhangs and particle desorption are strictly forbidden, apparently insuring dynamic scaling behavior outside the KPZ universality class. The defining equation for this new class of surface diffusion models reads

$$\partial_t h = -\nabla \cdot \boldsymbol{j} + \eta \tag{4.38}$$

where $\boldsymbol{j}$ is the particle current density along the surface. Because of its characteristic nonlinearity, the KPZ equation is fundamentally incompatible with such a continuity equation. The obviously difficult task is to prescribe the form of the surface diffusion current appropriate to a given microscopic scenario. Under the admittedly questionable assumption of quasi-equilibrium, the Mullins theory of surface diffusion [M59] has been invoked, suggesting $\boldsymbol{j}$ proportional to $\nabla\mu$, with μ the local chemical potential. Since the chemical potential is a scalar quantity, it depends only upon properly formed rotationally invariants, the lowest-order being the surface curvature, so that $\mu \propto \nabla^2 h$, leading to,

$$\partial_t h = \nabla^4 h + \eta \tag{4.39}$$

a partial differential equation first proffered to the kinetic roughening community by Wolf and Villain [WV90]. Being linear, the Mullins equation (4.39) is quickly solved by Fourier methods, yielding $z = 4$, $\chi = (5-d)/2$, and $\beta = \chi/z = (5-d)/8$ for the dynamic, steady-state, and early-time roughness exponents, respectively. Interestingly, these exponents satisfy the identity,

$$2\chi = z - d + 1 \tag{4.40}$$

an all-important hyperscaling relation characteristic of surface diffusion models as a class, which follows, ultimately, from the fact that the noise suffers no renormalization – see the papers of Tang and Nattermann [TN91], as well as Lai and Das Sarma [LDS91]. An independent derivation has been supplied by Krug [Kr91b, final paragraph], with a heuristic explanation originally advanced by Wolf and Villain, themselves [WV90]. For the surface diffusion models, (4.40) stands as a superuniversal feature, the analog of the fundamental exponent identity.

In the context of the Mullins equation, Wolf and Villain [WV90] and Das Sarma and Tamborenea [DST91] proposed candidate microscopic models thought to be within the new universality class. Unlike the Edwards-Wilkinson growth algorithm, however, which demands deposited particles to move to the nearest local minimum, the [WV90,DST91] rules permitted atoms to maximize the number of neighbors, in keeping with MBE objectives. Wolf and Villain obtained the numerical estimates $\beta_{eff} = 0.365 \pm 0.015$ and $\chi_{eff} = 1.4 \pm 0.1$, alluding to the slow dynamics induced by the large value $z = 4$ and warning of delayed crossovers associated with relevant non-KPZ nonlinear terms; Das Sarma and Tamborenea quote $\beta = 0.375 \pm 0.005$, while estimating $\chi \approx 1.5$. Of course, all this was suggestively close to the naive exponents predicted by the Mullins equation for this dimensionality. Even so, history has revealed these early results to have been merely fortuitous. In particular, recent work by the Vancouver-Duisburg connection [PSW93,SWP93, see also Kr94], which relies upon numerical studies of the height-height correlation function and structure factor, rather than just the interfacial width [WV90,DST91], has shown the behavior of these microscopic models to be rather unconventional, requiring a modified dynamic scaling ansatz that incorporates a time-dependent average step-size, introducing a new exponent into the problem. Furthermore, an appreciation of the surface current properties [KrPS93] of these models has revealed, rather surprisingly, that the microscopic models proposed in [WV90,DST91] actually belong to different universality classes, despite their apparent similarities.

There were, however, suspicions from the start. As pointed out by Wolf and Villain [WV90], and discussed further by Villain [V91], the Mullins equation could only hold if the surface does not develop arbitrarily large steps. Paradoxically, this was clearly not the case for their microscopic model, since it possessed very high steep "cliffs", a fact betrayed explicitly by a roughness exponent $\chi > 1$. Consequently, they stressed the importance of nonlinear perturbations, suggesting the relevance of a growth-generated nonequilibrium contribution, $\mu_{NE} \sim (\nabla h)^2$, to the "chemical potential", leading to the stochastic PDE,

$$\partial_t h = \nabla^4 h + \nabla^2 (\nabla h)^2 + \eta \tag{4.41}$$

In the literature it is referred to as the Villain-Das Sarma (VDS) equation, but the reader should realize it is just a rederivation of the SGG equation (3.21) without the noise conservation constraint. A renormalization group analysis by Lai and Das Sarma [LDS91] revealed an upper critical dimension $d_c = 5$, with exponents $z = (7 + d)/3$, $\chi = (5 - d)/3$, and $\beta = \chi/z = (5 - d)/(7 + d)$, fixed by the requirements of the characteristic surface diffusion hyperscaling relation mentioned above, $2\chi = z - d + 1$, and the index equality, $\chi + z = 4$, familiar from Sun, Guo and Grant [SGG89], see Section 3.3. Lai and Das Sarma proposed a physical interpretation for this nonlinear term – it follows from a tendency of particles landing at high steps (large derivatives) relaxing to lower steps (smaller derivatives), corresponding, perhaps, to a high-temperature MBE regime in which surface atoms at kink sites can break bonds and hop with larger probability to steps with smaller height. Indeed, for an appropriately defined growth algorithm incorporating such effects, Lai and Das Sarma obtained the numerical values $\chi = 1.05 \pm 0.10$ and $\beta = 0.340 \pm 0.015$ in $d = 1 + 1$ dimensions, in good agreement with theoretical predictions. Later work by Wilby, Vvedensky, and Zangwill [WVZ92] confirmed the matter. Interestingly, for the physically relevant case, $d = 2 + 1$, the VDS equation yields a steady-state roughness exponent, $\chi = 2/3$, considerably larger than the KPZ value ($\approx 2/5$) and may provide a partial explanation for elevated estimates extracted from some high temperature

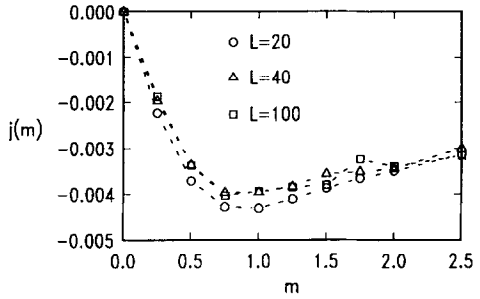

Fig. 4.27. Surface diffusion current for WV model in 2 + 1 dimensions [KrPS93]. The downhill current ($j < 0$) gives rise, for small m, to stable ($\partial j/\partial m < 0$) EW-type growth, at least asymptotically. If the very same model is simulated at sufficiently large miscut, however, the growth is unstable ($\partial j/\partial m > 0$).

MBE experiments [He92], where surface diffusion processes and the absence of bulk vacancies and overhangs may control the surface roughness.

Nonetheless, subsequent work by Krug, Plischke and Siegert [KrPS93] has furnished the kinetic roughening community with an unexpected, but effective take on these surface diffusion models. In particular, it has been suggested by these authors that the nonequilibrium conditions of MBE growth generate surface diffusion processes *unaccountable* by means of a generalized chemical potential. Rather, they consider a gradient expansion of the surface diffusion current, much as was done for the growth velocity in the interface growth context [see, e.g., KrS91r], and suggest within their unifying picture a tilt-dependent mass current $j(m)$ to be the dominating feature of these surface diffusion models. More specifically, if the surface diffusion current is a decreasing function of the inclination, $\partial j/\partial m < 0$, it stabilizes the surface, leading generically, but somewhat surprisingly, to dynamic scaling characteristic of the Edwards-Wilkinson universality class [EW82]. By contrast, a current that increases with inclination, $\partial j/\partial m > 0$, incurs a growth instability, resulting in a grooved state, as observed previously in a special case by Siegert and Plischke [SP92]; see also, Racz, et al. [RSLP91]. In fact, both types of behavior can be seen within a single model, following from a nontrivial $j(m)$; see, for example, Fig. 4.27, which shows the tilt-dependence of the surface diffusion current for the Wolf-Villain microscopic model [WV90] in 2+1 dimensions, revealing the non-vicinal surface to be stable and EW-like, at least asymptotically [KrPS93], though the intermediate scaling gives $\beta \approx 0.2$, not far from the VDS value 1/5; see also [KL92]. (By contrast the microscopic model proposed by Das-Sarma and Tamborenea [DST91] possesses a symmetry that precludes such downhill currents explicitly, resulting in asymptotic behavior that cannot be EW, but most likely will be VDS.) Interestingly, [KrPS93] suggest a prescription for extracting the coefficient multiplying the EW laplacian term; it follows from an analysis of the inclination-dependent surface current and is simply $-j'(0)$. Moreover, knowledge of this coefficient permits determination of the crossover timescale to EW behavior [KrPS93,SK94]. Krug, Plischke and Siegert examine such matters for a variety of surface-diffusion models, and conclude finally that, on account of the generic occurrence of current-induced instabilities, the draconian SOS assumption of ideal MBE models is physically unreasonable, leading inevitably to amorphous, non-epitaxial growth within the KPZ universality class. In fact, suggestions to this effect were made earlier by Yan [Y92], as well as Kessler, Levine and Sander [KLS92], who, troubled by a number of "weak points" in the VDS equation, investigated physically correct ballistic deposition models, incorporating realistic surface diffusion effects, and observed a carefully documented crossover to the standard exponents. By contrast, an insistance upon

true epitaxial growth may result in the Edwards-Wilkinson equation being, in the words of Krug, Plischke and Siegert, the "only consistent large-scale description for MBE." As such, it predicts essentially flat epitaxially-grown surfaces, for which there are some experimental indications, see [Sud92].

4.7.2. Experiment: homoepitaxial systems [Chev91,Her92]

Only recently has the very active crystal growth community sought to interpret matters from the perspective of the dynamic scaling hypothesis, using the language of kinetic roughening. With powerful direct visualization techniques such as scanning tunneling microscopy (STM) and atomic-force microscopy (AFM), as well as the refinement of traditional, but indirect methods including reflection high-energy electron diffraction (RHEED), x-ray reflectivity, and helium scattering, it is becoming possible, however, to extract increasingly reliable estimates for the early-time and steady-state roughness exponents of kinetically roughened surfaces grown via molecular beam epitaxy or vapor deposition. Nevertheless, the experimental situation remains rather stubborn, refusing simple characterizations within specific surface diffusion universality classes. Even so, there is much cause for optimism since the theoretical framework based upon dynamically scaling self-affine surfaces appears to be the correct one. With an actual experiment given to a profusion of physically relevant parameters, such as temperature, diffusion scales, Schwoebel barriers, vicinal miscuts, chemical bond strengths, finite system size, etc., it may be a bit presumptuous, perhaps, to expect a complete description in terms of any one stochastic PDE. Furthermore, while there may be suggestions of, let us say, KPZ, EW or VDS scaling, it is likely these will be compromised by crossover effects [TN91], either in the approach to asymptopia or between the universality classes themselves! With these caveats in mind, we discuss briefly below some important preliminary experiments, but urge the interested reader to keep abreast of this rapidly developing field.

A well-defined class of kinetic roughening experiments concerns the growth of thin metal films via vapor deposition or MBE. The baptismal effort, here, was the RHEED study of Chevrier et al. [Chev91], who investigated the epitaxial growth of thin (< 800 Å) iron films upon a silicon (111) surface at temperatures ($\approx 50^{o}$C) low enough to prevent long-range atomic diffusion and to permit the formation of KPZ-relevant overhangs. Their measurement of the early-time roughness exponent was consistent with values in the range $\beta_{IRON} \approx 0.22$–$0.3$, though they chose to fit their data for the surface width versus film thickness with the value $\beta_{2+1} = 1/4$, see Fig. 4.28a. Shortly thereafter, Herrasti et al. [Her92], reported results from an STM analysis of room-temperature vapor deposited gold films (average thickness running from 300–10000 Å), in which they presented some extraordinary snapshots, see Fig. 4.29, capturing the evolution of the kinetically roughened surface and explicitly verified the exponential distribution of columnar heights characteristic of the ballistic deposition [MRSB86], thus establishing the notion of a self-affine fractal surface and suggesting the possible validity of KPZ universality. From a digital analysis of their STM images, Herrasti et al. extracted the steady-state roughness exponent $\chi_{GOLD} = 0.34 \pm 0.035$, a bit lower than but not entirely inconsistent with the estimate $\chi_{2+1} \approx 0.38$ [FT90]. In a separate, subsequent publication [Salv92], this group discussed how the steady-state roughness depends on the scan length L, finding $w \sim L^{\chi}$, with $\chi = 0.35 \pm 0.05$ for $L > d_s$, where d_s is the columnar size, and $\chi = 0.89 \pm 0.05$ for $L < d_s$. That the effective steady-state roughness exponent is large on small scales is noteworthy. In a variation upon the Chevrier et al. experiment, He, Yang, Lu, and Wang [He92] measured both

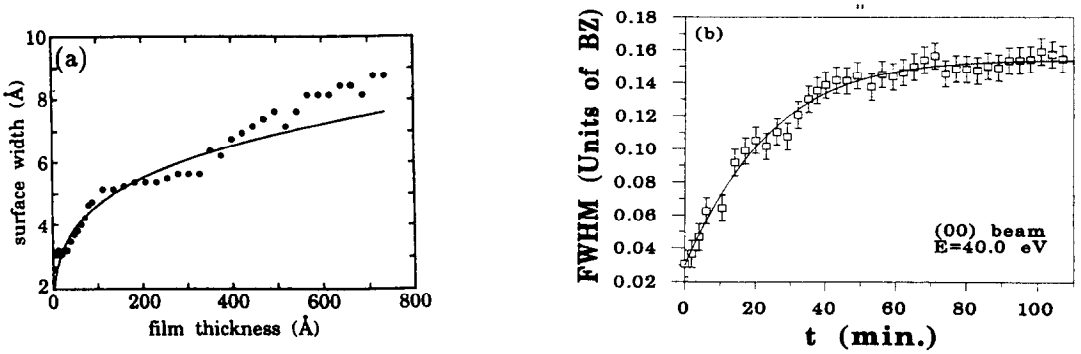

Fig. 4.28. Early-time roughness for thin film growth of iron. (a) [Chev91], Fe on Si(111): the data plots surface roughness vs. film thickness, directly. The drawn curve corresponds to the KPZ value $\beta = 1/4$, (b) [He92], Fe on Fe(001): FWHM of angular profiles of scattered beam intensity as a function of growth time. Best fit to the data, indicated, yields the estimate $\beta = 0.22 \pm 0.02$.

the early-time and steady-state roughness exponents for epitaxial growth of Fe on Fe(001), reporting $\beta_{IRON} = 0.22 \pm 0.02$, see Fig. 4.28b, and $\chi = 0.79 \pm 0.05$, referring to the latter as characterizing the time-invariant, self-affine roughness on short lengthscales. It is interesting (and very encouraging!) that both iron film experiments employing electron diffraction methods yield consistent early-time exponents, not too distant from the KPZ value. Even so, He et al. argue that their exponents are those of VDS, $\beta = \frac{1}{5}$ and $\chi = \frac{2}{3}$, and that iron film growth is best understood via this nonlinear, conserved surface diffusion equation. Indeed, the measured exponents [He92] conform, more or less, with the surface diffusion hyperscaling relation, Eq. (4.40). Helpful real-space, rather than k-space, views of homoepitaxial growth of Fe on Fe(001), as well as an informative critique of RHEED data interpretation, have been provided by Stroscio, Pierce and Dragoset [SPD93]. Recently, You, Chiarello, Kim and Vandervoort [You93] re-examined the kinetic roughening of sputter-deposited gold films using X-ray reflectivity and STM techniques, finding $\chi_{GOLD} = 0.42 \pm 0.03$, in rather good agreement with previous work [Her92, Salv92], though now just slightly above the standard value! Unfortunately, however, their estimates for the early-time roughness exponent, 0.42 (0.40) at 220 K (300 K), are inexplicably large, well outside the range permitted by KPZ or surface diffusion equations. Despite the myriad of experimental exponents, this result appears anomalous; for example, an interesting study by Miller et al. [Mill92] on sputter-deposited NbN films uses a novel multilayer decoration technique to reveal many features characteristic of KPZ dynamics (particularly the idea of locally normal growth) and, furthermore, finds $\beta \approx 0.27$. Likewise, Palasantzas and Krim [PK94] observe $\beta = 0.29 \pm 0.06$ for silver films. Even heteroepitaxial, metalorganic MBE of semiconductor InP films seems, at least for early-times, to be characterized by a $\beta \sim 0.2$ [Cot93]. That kinetic roughening ideas remain valid for heteroepitaxy, as well, received strong support in studies of CuCl growth on $CaF_2(111)$ [TW94].

4.7.3. Schwoebel instabilities observed [John94,Ern94]

Following the theoretical work of Krug, Plischke and Siegert [KrPS93] concerning tilt-dependent surface currents, two experimental teams [John94, Ern94] quickly jumped into the fray, reporting current-induced growth instabilities. In fact, the observed instabilities [for earlier indications, see AFG93, S93, EG92] appear to be instigated by the Schwoebel phenomenon [SS66], which follows

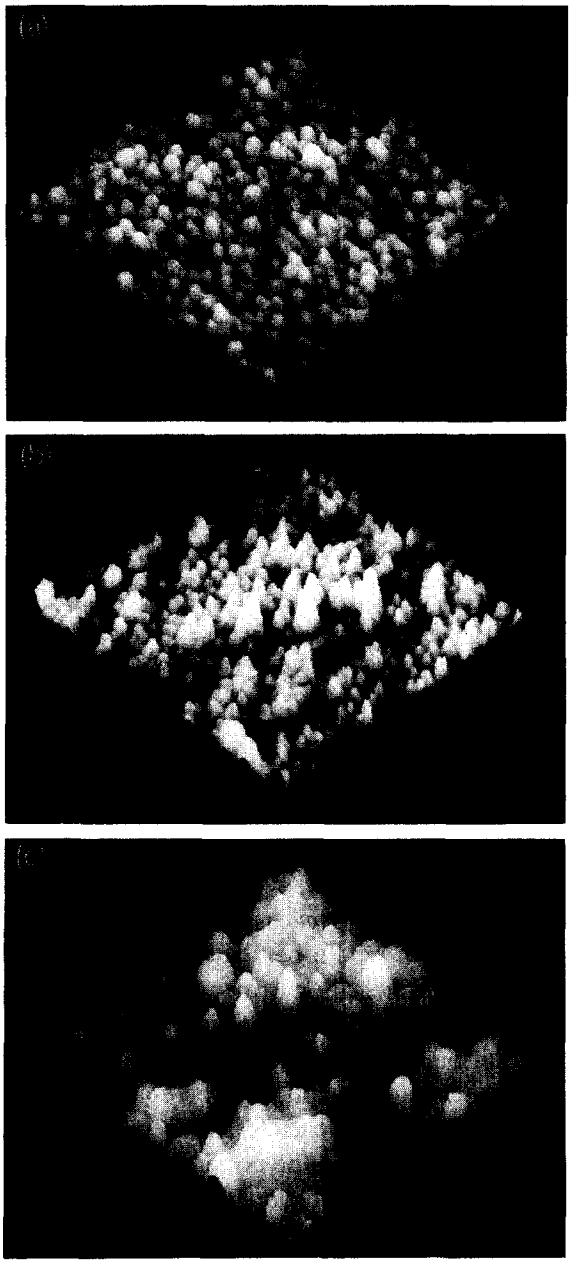

Fig. 4.29. Snapshots of a kinetically roughened gold film, grown via vapor deposition [Her92]. The STM images capture increasing later stages of growth, with mean film thicknesses (a) $\bar{h} = 30$ nm, (b) $\bar{h} = 160$ nm, and (c) $\bar{h} = 850$ nm. The basal areas are of order 600×600 nm^2.

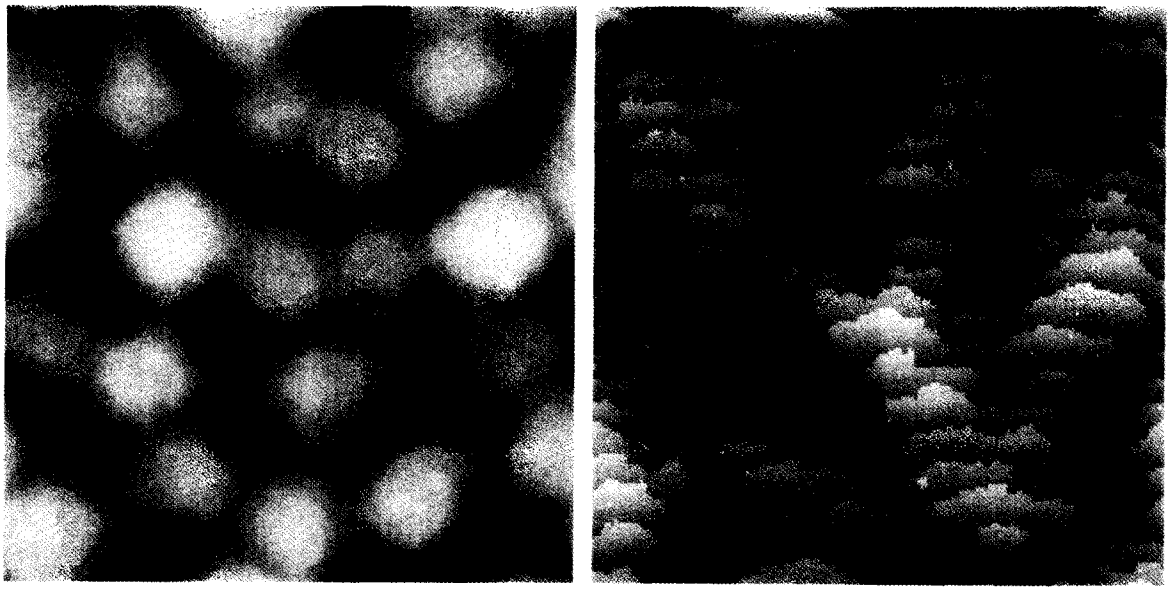

Fig. 4.30. Surfaces generated by Monte Carlo activated hopping model with Schwobel barriers, following 50 deposited layers [John94]. (a) Singular surface exhibiting large mounds, obtained with $S_c = 0.40$ and $\sigma = 16$; (b) vicinal surface with slope 0.1, showing stable terraces. In this case, the model parameters were $S_c = 0.40$ and $\sigma = 8$.

from a tendency of diffusing adatoms to be incorporated at the ascending step bordering a terrace, rather than a descending step, since the latter would necessitate traversing a potential barrier [EH66]. For a large vicinal slope m, where terraces are small and nucleation of islands negligible, the Schwoebel barrier generates an *uphill* surface current $j(m) \approx F/m$, where F is the incident particle flux. Although $j' < 0$, thereby suggesting stability, symmetry requirements demand $j(0) = 0$, leading to unstable growth, $j' > 0$, for small enough m, as pointed out by Villain [V91]. Thus, it was Villain's suggestion that step flow growth would be stable for a sufficiently miscut, vicinal surface, but unstable for singular one, where the nucleation of new islands would lead to a pyramidal surface profile, composed of terraces of uniform width.

In the AFM/STM study of Johnson et al. [John94], these two distinct growth modes, separated by a critical miscut angle. have been noted explicitly for epitaxial GaAs films. Aside from very small statistical roughening, their highly miscut vicinal surface appears essentially smooth to the eye suggesting, perhaps, $\beta \approx 0$, à la EW. By contrast, the nominally singular GaAs(001) surface develops "large-scale mounds," with sloped sides lying in the stable regime. Using a complementary numerical model that incorporates a Schwoebel parameter, as well as relevant geometric effects associated with mean terrace size and island separation, Johnson et al. obtain qualitative results highly reminiscent of experiment – see Fig. 4.30, which illustrates the distinctive growth morphologies for singular and vicinal surfaces. Furthermore, an exploration of parameter space leads them to suggest a novel scaling form for the tilt-dependent surface current, nicely confirmed by the collapse of their numerical data. Motivated by these findings, they propose a new continuum surface diffusion equation based upon the current $j = FS_c\sigma^2\nabla h/[1 + (\sigma m)^2]$, where S_c is the size of the Schwoebel barrier and σ the nucleation distance, i.e., the average separation between islands on the terrace. Numerical integration of this equation produces large scale features characteristic of the experimentally observed instability.

In related experimental work, Ernst, Fabre, Folkerts, and Lapujoulade [Ern94] investigate the low-temperature MBE growth of Cu(100), using helium atomic beam scattering, a technique which permits them to monitor the deposition process in real-time and also to distinguish between the geometric features of steps and terraces. At 160 K, they observe a singular (001) surface evolve into a state characterized by "pyramidlike" structures whose sides correspond to the Cu(113) vicinal surface, whereas at 200 K, the mounds are sloped in accordance with a (115) surface, the different growth morphologies apparently evidence of a temperature controlled Schwoebel instability. Interestingly, Ernst et al. report a low-temperature, early-time roughness exponent $\beta \approx \frac{1}{4}$, which is common to nearly all previous MBE experiments, but a high-temperature value close to $\frac{1}{2}$, suggesting perhaps a Schwoebel-related explanation for the anomalously large β exponent reported previously [You93]. Indeed, both experimental groups emphasize the generic nature of Schwoebel-induced growth instablities for singular MBE surfaces. Subsequent theoretical work on the temporal evolution of these instabilities has concentrated on pattern formation and "coarsening" aspects; e.g., Siegert and Plischke [SP94], who also offer an upgrade to the slope-dependent surface-diffusion current of [John94].

4.7.4. Sputter-etched graphite [Ekl91,KHHB93]

In contrast to thin film growth via molecular beam epitaxy, where the surface roughness builds up as more and more material is deposited, we can consider the kinetic roughening associated with explicitly erosive processes, such as particle irradiation of solid surfaces. Work along these lines was begun by Eklund et al. [Ekl91], who investigated the submicron topography of sputter-etched graphite, with a view to test the relevance of the dynamic scaling hypothesis. Surprisingly, they discovered the development of large-scale, KPZ-like correlated structures, see Fig. 4.31, which shows the state of the surface at three distinct points in its evolution. Theoretical aspects of the relationship between the Sputtering processes and the KPZ equation have also been thoroughly examined by Liang and Tang [LT93]. A direct calculation of the height-height correlation function from these STM topographs, whence Fourier transformed, see Fig. 4.32, confirms the notion of a temporally-diverging correlation $\xi(t)$, below which the surface roughness has reached steady-state, with $\langle |h(\boldsymbol{q} > \xi^{-1})|^2 \rangle$ scaling as $q^{-2-2\chi}$. Interestingly, the data suggests $\chi \approx 0.35$, not too far from the standard value. (Work at higher temperatures on sputter-etched gold [KHHB93], however, reveals a steady-state roughness exponent $\chi = 0.53 \pm 0.02$, indicating the importance, perhaps, of surface diffusion processes in this experiment.) In any case, the behavior of the height-height correlation function appears qualitatively consistent with the dynamic scaling hypothesis; moreover, it flatly rules out the alternative, seemingly appropriate linear-response theory advanced by the authors [B90]. That sputter-etching can produce highly correlated kinetic roughening is altogether unanticipated; after all, bombarding a surface with ions should likely flatten it, rather than roughen it in a peculiarly spatio-temporal fashion. Nevertheless, we know well enough from the growth scenario that the generation of such structures via stochastic processes is entirely the norm.

4.7.5. Micro-mountain geomorphology [CSV93]

Motivated by the compelling fractal nature of mountainous landscapes, though daunted somewhat by the requisite physical timescales Czirók, Somfai, Vicsek [CSV93] have recently investigated erosion as the primary kinetic roughening mechanism in a hand's-on micromodel of geomorphological evolution. With an essentially equal mixture of silica sand and earthy soil, they molded a flat

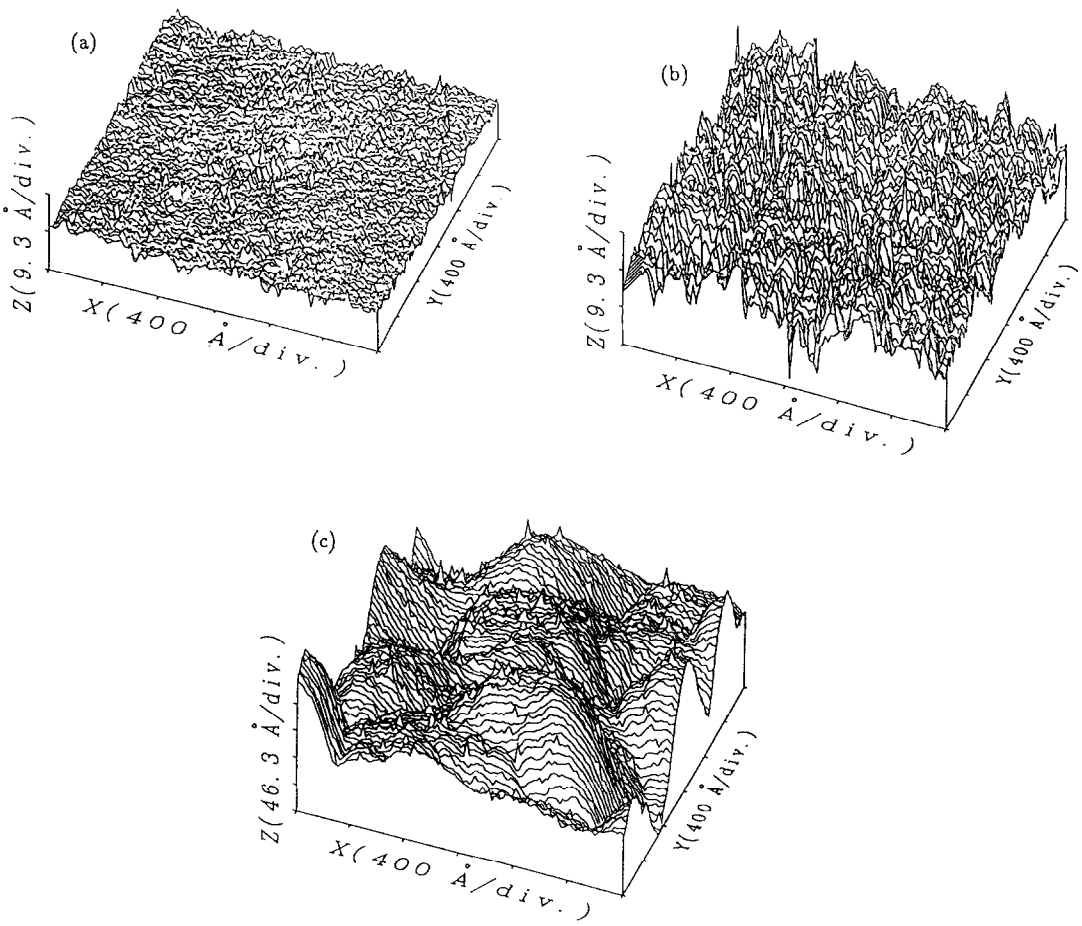

Fig. 4.31. STM topographs of sputter-etched graphite, subject to a beam flux 6.9×10^{13} ions/cm^2 s and ion fluences (a) 10^{16}, (b) 10^{17}, and (c) 10^{18} ions/cm^2, respectively [Ekl91].

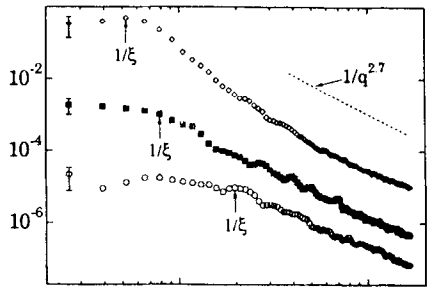

Fig. 4.32. Fourier-transformed height correlation functions, $\langle |h(q)|^2 \rangle$, for the surface profiles of the previous figure, corresponding to fluences 10^{16} (○), 10^{17} (●), and 10^{18} (◇) ions/cm^2 [Ekl91]. The saturated roughness at small scales ($q > 1/\xi$) falling as $q^{-2.7}$ suggests a $\chi \approx 0.35$. Note that ξ, which marks where the correlation function plateaus, increases steadily with ion fluence (time).

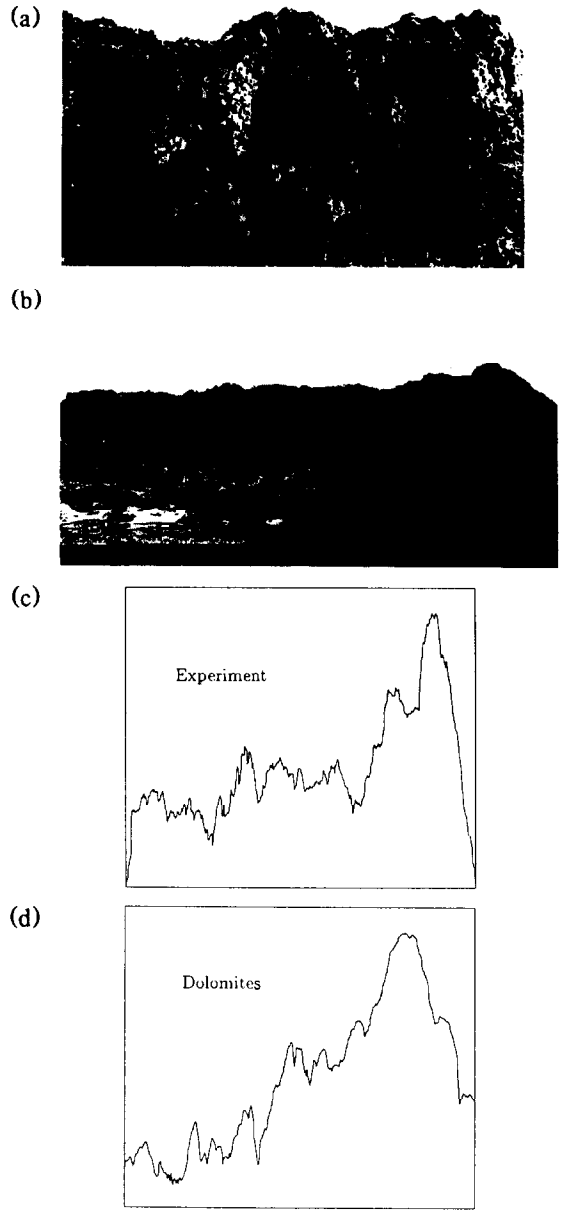

Fig. 4.33. Typical micro-mountain morphologies resulting from the erosive effects of rain for, resp., (a) 20 minutes, (b) 10 minutes. The digitized profile corresponding to the latter is shown in (c). Finally, (d) a representative digitized profile from a region of the Italian Dolomites [CSV93].

rectangular mountain ridge (roughly 60 cm long, 4 cm wide and 18 cm tall), which was then subjected to a continuous spray (1500–3000 cc/min) of water. The initially flat surface was gradually roughened as sections of the ridge were taken away by the effect of *landslides*, as well as the *flow* of fine grain suspensions. Shown in Figs. 4.33a,b are typical miniature mountain ranges resulting from exposure to such erosion for 20 and 10 minutes, respectively. Fig. 4.33c illustrates the digitized

profile following from the high-resolution scanned image of the 20 minute sample, with horizontal axis rescaled by a factor of four. For comparison, a digitized profile of a region in the Italian Dolomites is provided in Fig. 4.33d, which reveals a roughness rather reminiscent, statistically speaking, of their artificially created mountain, Fig. 4.33c.

This notion of similarity is corroborated by a quantitative measurement of the rms surface width for the natural and artificial profiles, which yields, a roughness exponent $\chi = 0.79$ for this particular Dolomite range and ≈ 0.81 for the experimental sample addressed in Figs. 4.33b,c. Note that the experimental data scales convincing over nearly two decades. Averaging over their results for five different eroded mini-mountain ranges, [CSV93] quote a roughness exponent $\chi_{geo} = 0.78 \pm 0.05$, which agrees well with the value extracted for the Italian Dolomites, at least for lengthscales below a few miles. (For scales 10–100 miles, where different physical processes are operative, the effective roughness exponent is smaller; e.g., for the Swiss Alps on these scales, Deitler and Zhang [DZ92] obtain $\chi_{Alps} \approx 0.57$.) Interestingly, the experimental results appear robust provided the sand-soil ratio is reasonably near unity. Changing the ratio dramatically, however, or using a rather different material such as clay produced very different morphological evolution. For example, pure sand simply washed away. By contrast, clay did not let the water penetrate, so there were no landslides, but rather a river network pattern developed on the surface, giving rise to altogether distinct issues of geometric complexity, discussed recently, by various groups in the geophyics, earth science, and nonlinear systems communities [RRR93,TI92,KMr92]. At the end of the day, therefore, [CSV93] conclude the self-affine kinetic roughening exhibited by their eroded mini-mountain ranges requires, beyond the transport of suspended and deposited materials by the flow of water, the existence of landslides which incur abrupt profile changes over short time intervals and widely varying lengthscales.

5. Directed polymers in random media

Overview

The subject of directed polymers in random media is very close to traditional equilibrium physics, where a well-defined Hamiltonian and Boltzmann factor exists. Nevertheless, as is easily seen, this topic is simply the flip-side of the coin of the non-equilibrium growth problem that we have been discussing up to now, since Eq. (3.1), via (3.12), is just a rewriting of the same problem. But in the new form, the whole interpretation is different and we explain here the its significance within the directed polymer context.

An in depth analytical study of the KPZ equation needs insight gained in the DP context. We shall see many methods used and results obtained below are nonperturbative in nature, thus complementing the previous perturbative RG method. Some subtle questions addressed for directed polymers might seem to be of purely academic interest, but when translated back to the interface context, may have strong measurable consequences. Below we shall treat the directed polymer as an independent model, leaving to the reader translation into the language of kinetic roughening.

Within the province of condensed matter physics, there exist a variety of interesting physical situations where we are concerned with the statistical fluctuations exhibited by an essentially linear elastic object, such as longitudinally stretched polymers in a gel matrix, vortex lines in ceramic superconductors, and dislocation lines in disordered solids. Hereafter, for ease of language, we will

simply refer to all such systems as directed polymers and our main emphasis will focus on the behavior of such entities in random media. Cast in a continuum formulation, the directed polymer in a random medium (DPRM) is conveniently described by a vector field $x(t)$, with t denoting the longitudinal direction of anisotropy, its statistical mechanical properties dictated by the restricted partition function (3.14),

$$Z(x,t) = \int_{(0,0)}^{(x,t)} \mathcal{D}x \exp\left(-\int_0^t ds \left[\frac{1}{4\Gamma}\left(\frac{dx(s)}{ds}\right)^2 - \mathcal{V}(x,s)\right]\right), \tag{5.1a}$$

or in the familiar differential form

$$\dot{Z}(x,t) = (\Gamma\nabla^2 + \mathcal{V})Z(x,t), \tag{5.1b}$$

where Γ is the thermal diffusion constant or inverse line tension, and $\mathcal{V}(x,t)$ a position-dependent function meant to mimic the role of local pinning impurities in the medium. In the simplest scenario, and most tractable one analytically, the disorder is assumed to be gaussian with zero mean, and variance

$$\langle \mathcal{V}(x,t)\mathcal{V}(x',t')\rangle = V^2\delta(x-x')\delta(t-t') \tag{5.1c}$$

where V gauges the strength of the disorder. Physically, this corresponds to impurities that are uncorrelated in longitudinal and transverse dimensions, but with individual binding energies that are gaussian distributed. Keep in mind that, in the spirit of the enterprise, the above represents a coarse-grained description of the DPRM that ignores many (hopefully irrelevant) microscopic details, with the intent of capturing the physics (i.e., scaling properties) of the system on large length scales. Since it is but a rewriting of the KPZ equation, all warnings regarding the lack of a continuum limit, recall Section 4.2.3, apply here as well. The above continuum notation serves merely book-keeping purposes. Only a lattice version is unambiguously defined. A proper treatment of this ill-condensed matter system will necessitate not only the traditional configurational average of the Boltzmann weight that constitutes the ordinary partition function of the directed polymer, but also an entirely separate, disorder average over realizations of the random energy landscape due to the local pinning impurities. The physical quantity of immediate interest is the wandering exponent ζ which, defined via the relation $|x| \sim t^{\zeta}$ describes, in geometric terms, the roughening of the DPRM resulting from a competition between the line tension, which discourages deviations from linearity, and the pinning potential, which causes the directed polymer to wander in an ever-increasing fashion from the central symmetry axis, in search of optimal energy configurations. Since the disorder average of the mean transverse position of the DPRM vanishes, it is clear that information regarding the geometric fluctuations of the DPRM are encoded in the wandering exponent. Similarly, thanks to the disorder average, the free energy of the DPRM is no longer fixed, but is, itself, a statistical quanitity whose fluctuations grow as a power-law, characterized by the index ω. These two exponents, ζ and ω, describing the scaling properties of the transverse geometric and free energy fluctuations, lie at the very heart of the DPRM.

The structure of this chapter is as follows – after a brief, warm-up style review, Section 5.1, of the salient features and some needed probabilistic concepts of random walk theory relevant for the discussion of thermal roughening of directed polymers in the absence of pinning impurities,

we introduce, in Section 5.2, a discrete lattice verson of the DPRM for which numerical transfer matrix studies, both at zero and finite temperature, have managed to determine the geometric and wandering exponents precisely. We shall see also that, as a natural generalization of the above DPRM model, traditional directed percolation clusters unexpectedly appear. In this special case, the directed percolation threshold P_c is precisely the ground state energy at zero temperature! It should be stressed that at $T = 0$, the DPRM becomes a matter of global optimization – an amusing variant of the traveling salesman problem in which, most appropriately, maximization of commission rather than minimization of path length can be the goal at hand! Indeed, the DPRM also shares much in common with spin-glasses, a classic, technically difficult, nearly intractable problem of ill-condensed matter. However, because of its directed nature, the DPRM can be viewed as a simplified baby-version of the latter which, despite the hazards of what appears to be a weakly broken replica symmetry, seems much more amenable to various analytical approaches. As such it has drawn great interest from combatants on both sides of the spin-glass divide. Despite these enticing theoretical issues and noting an obligation to our practical-minded readers, we discuss in Section 5.3 the experimental realizations of the DPRM, which in addition to those alluded to above, include the edge statistics of torn paper sheets, domain walls in disordered 2d magnets, and blown fuse networks. Section 5.4 starts with in Kardar's original Bethe ansatz calculation (no more difficult than solving the quantum mechanics of attractive delta function well!). We then discuss all analytical aspects of the $1 + 1$ DP problem. The knowledge accumulated over the past few years allows us to present a coherent, simple, physical picture in a compact format. Virtually all analytical results, including subtle questions related to replica breaking can be understood in simple terms. The physical results are complemented by more careful and mathematical formalism. Sections 5.5 and 5.6 consider the effects of varying the disorder distribution, from the simplest case of uncorrelated, gaussian noise that we have been considering to somewhat more exotic forms, such as (i) correlated disorder in the transverse directions – analytically quite tractable via Flory type arguments and relevant, perhaps, to 2d random field Ising magnets, (ii) uncorrelated, power-law noise distributions, which may be of great importance in explaining anomalous kinetic roughening of self-affine rough edges in fluid flow through porous media, growing bacterial colonies and propagating fire fronts, and (iii) time-independent noise, familiar from electron localization (diffusion with trapping) contexts. We next consider, in Section 5.7, the investigations of ground-state instabilities inherent in the 1+1 DPRM, which raises rather general issues concerning robust solutions to optimization problems plagued by finite tolerances; Shapir's linear response theory of directed polymers subject to random external perturbations is discussed too, permitting the reader access to simple back of the envelope calculations of the instability effects. Section 5.8 is highly visual and concerns the geometric properties exhibited by the ensemble of locally optimal paths in the zero temperature 1+1 DPRM. These patterns, which bear a striking resemblance to river basin deltas formed by Nature herself, are discussed in a quantitative fashion in terms of their ultrametric properties, ancestry and progeny of the network, as well as the branching probability and cross-section of the globally optimal path. Up till this point, the discussion has focussed almost entirely on the 1+1 DPRM, but in Section 5.9, we move onto higher dimensionalities, considering its effect on the strong-coupling, zero temperature exponents, renormalization-group flows and resulting phase diagrams. We note the treacherously slow crossovers expected of the 2+1 DPRM, as well as the finite-temperature phase transition exhibited by the 3+1 DPRM, separating disorder-dominated from thermally-induced wandering of the directed polymer. Numerical transfer matrix studies of the DPRM specific heat by Derrida and Golinelli confirm the existence of this phase transition, as does a related

ballistic deposition simulation by Pellegrini and Jullien. We also discuss in passing, a real-space renormalization group method for calculating the energy fluctuation exponent, as well as the exact travelling wave solution of Derrida and Spohn for the infinite dimensional DPRM on a Cayley tree.

5.1. *Mini-review: coin-flipping random walker [F63]*

Here we remind the reader of some basic results from the classic statistical mechanics problem of the coin-flipping random walker. Consider for simplicity the 1d case where a fellow flips a coin, moving one step to the right if it comes up heads, one step to the left for tails, repeating the procedure once per second. Averaging over many trajectories, we discover that his mean position coincides with the origin, but his rms displacement scales as $\sqrt{t}$. Were we to examine his trajectories in a space-time diagram they would be entirely analogous to a directed polymer roughened by thermal fluctuations with wandering exponent $\zeta_{TH} = 1/2$. Indeed, this *entropic* wandering exponent is known from random walk ideas to have this value regardless of the number of transverse dimensions; afterall, the rms displacement of a random walker always scales as the square-root of the number of steps! More to the point, in the absence of disorder, the DPRM partition function introduced above is entirely tractable since the only piece in the exponent is the entropically-generated elasticity [see de Gennes' book on polymer physics], leading to the well-known *gaussian* result $Z(x,t) = e^{-x^2/2\Gamma t}/\sqrt{4\pi\Gamma t}$. For our purposes, this positional probability distribution is trivial in that, like any symmetric gaussian distribution it is fixed completely by its second moment. All odd moments vanish, while the higher even moments are determined by the second: $\langle x^{2n}\rangle = \Gamma(n+\frac{1}{2})/\sqrt{\pi}\langle x^2\rangle^n$. In fact, defining the ith cumulant $c_i(x)$ of the distribution via the implicit relation $\langle x^n\rangle = \exp[\sum_j n^j c_j(x)/j!]$, it is the characteristic feature of a gaussian distribution that the only nonvanishing cumulant is c_2. As a difficult, but nonetheless accessible problem of ill-condensed matter, the DPRM is a considerably richer in statistical mechanical subtleties than the simple coin-flipping random walker. We'll discover a DPRM positional probability distribution that is symmetric, but non-gaussian and a free energy distribution that is skewed with nonzero c_3. Moments, cumulants, and probability distributions will constitute the core the DPRM lingua franca.

Exercise: *For a random variable with zero mean, show that the fourth cumulant* $c_4(x) = \langle x^4\rangle - 3\langle x^2\rangle^2$. *Observe that this quantity vanishes for a gaussian variable.*

5.2. *Definition of the discrete model*

5.2.1. *Lattice formulation*

The continuum notion assumed above is not, in fact, strictly defined as we already learned in the surface growth context. A lattice realization renders the model concrete and Eq. (5.1) becomes

$$Z(x,t) = \sum_{P\in\Gamma} \exp -\frac{1}{T} H_P, \tag{5.2}$$

$$H_P = \sum_{i\in P} \varepsilon_i \tag{5.3}$$

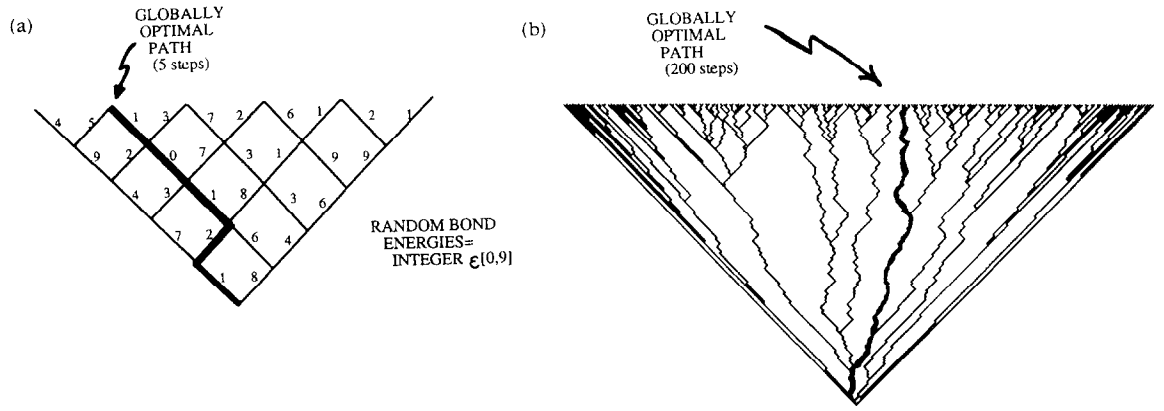

Fig. 5.1. (a) The wedge geometry for the 1+1 DPRM. The globally optimal path up to the fifth time slice is indicated. Its energy is minimal compared to the 32 other paths to the same time slice. (b) Ensemble of locally optimal paths to the time slice t=200, for the same realization of randomness.

where Γ denotes the ensemble of all the directed paths with fixed ends (the origin $(0,0)$ and (x,t)); the sum is over these paths. On the lattice a random energy ε_i is assigned to each bond (site). The Hamiltonian H_P is defined for each path and it is the sum of the random energies along the path P. A parameter called temperature is conveniently introduced. The missing kinetic term $\dot{x}^2$ is simply taken into account by the requirement that within the directed path each step in the forward direction moves only one step in transverse directions. The distribution density for the endpoint x of the DPRM is thus

$$p(x,t) = Z(x,t) / \int_{-\infty}^{\infty} Z(x',t)\,dx', \tag{5.4}$$

from which we can calculate the transverse fluctuation

$$\langle x \rangle = \int x p(x,t)\,dx. \tag{5.5}$$

An alternative possibility is to consider $\langle x^2 \rangle$. The above $\langle x \rangle$ is only thermal average (i.e., probabilistic) and still depends on the particular random sample. We have to take the sample average

$$x_c = \overline{|\langle x \rangle|}. \tag{5.6}$$

Note that without the absolute value $|\ldots|$, the sample average would vanish. Much information can be gleaned about the DPRM from transfer matrix studies, and indeed, although the directed polymer problem is relatively amenable to analytical techniques (compared to NP-complete problems such as spin glasses, traveling salesman, etc.), much of the early information obtained about its scaling properties were first gained via numerical methods. Consequently, we will also pause from time to time in this chapter to depart from the review's stated intent to concentrate on purely analytical approaches in order to discuss these crucial contributions made via small-scale numerical computations. We initiate things presently with a discussion of the zero-temperature 1+1 DPRM. One considers, see Fig. 5.1a, a directed walker who starting at the origin of a square lattice, has the option of making an

immediate step diagonally left or right to (x,t)=(±1,1). These and succeeding diagonal bonds have, in the simplest scenario, random energies drawn from uniform or gaussian distributions of variance σ^2, neighboring bonds being uncorrelated. At the time slice t there are $t+1$ possible endpoints to the 2^t paths emanating from $(0,0)$. For $T=0$, the DPRM becomes a matter of global optimization in which, for a given realization of the random energy landscape, one seeks the path of overall least energy – the total energy of a path being given by the sum of the random bonds visited along the way, recall (5.3). It is clear that the globally optimal path is a member of the ensemble of $t+1$ locally optimal paths that have their endpoints specified across the time slice t, see Fig. 5.1b. The saving grace of DPRM is the fact that it is an optimization problem that can be solved in polynomial time thanks to the transfer matrix method. One merely needs to update the ensemble of locally optimal paths from one time slice to the next; by construction, the globally optimal path at one level must be among the progeny of a locally optimal path at the previous level. As a measure of transverse geometric fluctuations, the mean square position of the globally optimal polymer is recorded after each step; likewise, its energy, and square. To get a meaningful description of the scaling of these fluctuations, it is necessary to disorder average over many realizations of the random energy landscape, as well as to consider paths of sufficient length. Despite these demands, the DPRM transfer matrix is a technique that really earns its pay – because of its directed nature, it renders entirely moot the devastating problems of metastability that typically plague Monte Carlo simulations of disordered systems.

5.2.2. Transfer matrix studies. I. Exponents [HuH85,Kard85b]

From the above definition of the lattice DPRM it is clear that the low temperature limit is of particular interest. The limit $T=0$ can be also investigated, in the sum (5.2) there is only one path which survives; let's call it globally optimal – its hamiltonian is a minimum. Contributions from all other paths can be thus ignored. Similar problems are often posed for other disordered systems, such like spin glasses.

Unlike for spin glasses, the optimal path can be easily found via the transfer matrix method. Transfer matrix methods are in general particularly apt for directed configurations. Such applications date back to Derrida and Vannimenus [DV83] and were used later by Huse and Henley in their early DPRM calculation [HuH85]. Denote $E(x,t)$ as the energy of the optimal path starting from the origin and ending at x, we have the following iterative relation:

$$E(x,t+1) = \min\left(E(x+1,t)+\varepsilon(x+1,t), E(x-1,t)+\varepsilon(x-1,t)\right) \tag{5.7}$$

for a square lattice. Generalizations to higher dimensions and other lattices are straightforward. This relation is extremely simple to implement on a computer. The globally minimal energy (no end point restriction!) can be formed by

$$E(t) = \min_{\{x\}}\left(E(x,t)\right). \tag{5.8}$$

The optimal DP's position can be also inferred, this permits us to calculate the fluctuation by average over samples.

The first transfer matrix calculations for the zero-temperature 1+1 DPRM subject to uncorrelated, gaussian noise were due to Huse and Henley [HuH85], who were interested in the phenomenon of disorder-induced domain-wall roughening in random-bond (RB) Ising models; see later, Section 5.3.2. Their results, with an uncertainty of a few percent, suggested unambiguously a geometric wandering

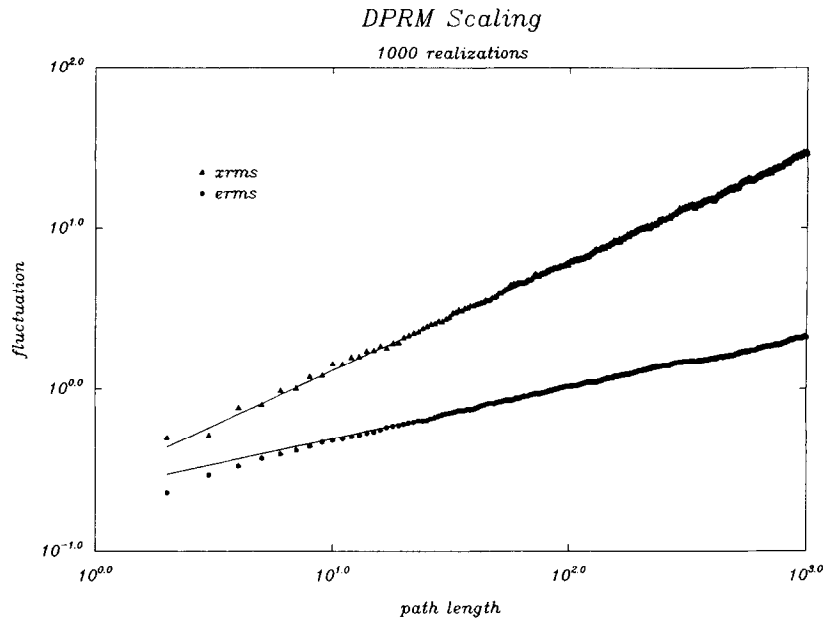

Fig. 5.2. Positional and energy fluctuations of the zero temperature (1+1)-dimensional directed polymer in a random medium. The random bond energies were drawn uniformly from the unit interval [0,1]. Disorder averaging was performed over 10^3 realizations of the random energy landscape. A least-squares fit to the data, dropping the first 50 steps, yields the scaling indices $\omega = 0.33 \pm 0.01$ and $\zeta = 0.66 \pm 0.02$, in complete accord with the anticipated values and the index relation $\omega = 2\zeta - 1$. The simulation took 55 minutes on a 51 MIP SparcClassic [HH93].

exponent $\zeta = 2/3$ as well as an energy fluctuation index $\omega = 1/3$. Soon thereafter, Kardar [Kard85b] confirmed these values at finite temperature. Shown in Fig. 5.2 are the data from a typical, but more recent simulation investigating these matters [HH93], done on a modest workstation requiring small cpu time commitments. For more on the full disorder-averaged probability distributions that govern the geometric and free energy fluctuations of the DPRM, see Section 5.4.4.

5.2.3. *Relation to directed percolation*

We have already met directed percolation in the surface growth context where the SOD model gave rise to directed percolation configurations in an unsuspected, spectacular way. Here, we shall see that directed percolation and directed polymers are close relatives as well, though in completely different fashion. In the lattice definition of the DPRM model, let the hamiltonian H_P be the maximum of all the ε_i's along this path P, rather than the sum of the ε_i's. For this special version of the directed polymer, we have, as before,

$$Z(x,t) = \sum_{P\in\Gamma} \exp\left[-\frac{1}{T}H_p\right], \tag{5.9}$$

but in place of Eq. (5.3) we have

$$H_P = \max_i (\varepsilon_i). \tag{5.10}$$

Each path has its own energy; by taking the $T \to 0$ limit, we search for the trajectory (degeneracies inevitable!) whose Hamiltonian is the *lowest* among all the possible paths. This seems to be a very bizzare version of the directed polymer model, but a careful scrutiny reveals that the optimal paths are nothing but the directed percolation clusters at *criticality!* If the random variable ε_i is uniformly distributed in (0,1), the ground state (i.e. $T = 0$) value of H_P is exactly $P_c \simeq 0.6445$, the directed percolation threshold. We leave the demonstration to the diligent reader, or check reference [HR87, Roux and Zhang unpublished]. The transfer matrix method for the DP problem equation (5.7) generalizes readily for this special case in a strikingly similar form

$$E(x, t+1) = \min\left[\max\left(E(x+1,t), \varepsilon(x+1,t)\right), \max\left(E(x-1,t), \varepsilon(x-1,t)\right)\right]. \quad (5.11)$$

Remark: *It can be shown that starting with an arbitrary initial condition say* $E(x,0) = 0$, *using the flat distribution in the range* $(0,1)$, *Eq. (5.11) quickly converges to the directed percolation* P_c. *Traditionally* P_c *is obtained by much more painful numerical methods in the directed percolation community (see [BH93] for a review). The typical lattice size is* 10×10. *The above method, relying upon (5.11), is an extremely efficient alternative, since it involves only one logic operation (exclusive-OR) and fits well the computer architecture. On a modern machine, lattice sizes of the order* $10^6 \times 10^6$ *can be implemented and one easily beats the best* P_c *evaluation. As a matter of fact, a few hours run on a VAX shows that the believed correct 4th digit is in fact too low, thus supporting a recent analytical result by Ben-Avrahm et al. [BBS91] challenging the widely accepted* P_c *value.*

Exercises:

1. *Turn on your portable computer and use Eq. (5.11) to evaluate* P_c *to* 1% *precision.*

2. *Consider the following definition of yet another DPRM variant: seek out a trajectory for which the sum of the differences is a minimum, rather than the sum of random values themselves; i.e., instead of (5.3),* $H_P = \sum_{i \in P} |\varepsilon_{i+1} - \varepsilon_i|$, *where* ε_{i+1} *and* ε_i *are random values on two successive bonds of a DP. This definition singles out the flattest DP in the random landscape. One tries to stay at the same altitude as much as possible, rather than searching for the deepest valley. Use a transfer matrix method to determine the scaling behavior and compare. To which known universality class does it belong?*

5.2.4. A simple DP model

The DP problem has many surprising consequences, sometimes counterintuitive at the first glance. One simple example helps us to appreciate more the implications of the model. Consider the $1+1$ DPRM problem, (5.1), with the random potential chosen to be concentrated on a line in the t-direction, that is

$$V(x,t) = \eta(t)\delta(x) \quad (5.12)$$

in Eq. (5.1). If the mean value of η (corresponding to negative energy) (over t) is positive $\langle \eta \rangle > 0$, there is an effective potential well, situated at the origin where we would expect an overall bound state.

This is to say, the wavefunction is concentrated around the origin at large times even though it fluctuates in time. What is less trivial is that, even when $\langle \eta \rangle = 0$ it can be shown that the bound state always exists in the unrestricted space (n.b., the case of a half-plane would be different). What

is astonishing is that, the bound state may persist even when $\langle\eta\rangle < 1$; i.e., on average there is rather a potential hill than a well, nevertheless the wave function is attracted by it! Here one should pay attention to the choice of parameters, such as lattice spacing, coupling constants, etc. When $\langle\eta\rangle$ further decreases, suddenly the bound state disappears, the effective mass gap vanishes at the transition point (hence a second order phase transition) and the potential becomes repulsive to the wave function. A fuller account is recorded elsewhere [NZ94]. Even though the above is at odds with our common sense, the physical origin can be easily traced and the proposition is extremely easy to verify numerically. To understand the qualitative physics let us consider an even simpler version: a periodic function

$$V(x,t) = \delta(x)\cos t. \tag{5.13}$$

Its temporal average is zero and a bound state exists even in the continuum. On a lattice let us consider the periodic potential

$$V(x,t) = \delta_{x,0}\eta(t), \quad \eta(t) = \begin{cases} a & t \text{ even} \\ b & t \text{ odd} \end{cases} \tag{5.14}$$

where t and x are discrete. The average $\langle\eta\rangle = (a+b)/2$, is assumed to be negative, in order to "fake" a potential hill. To pin down the mechanism we may choose a to be positive and $b = -\infty$. If a is not too small, the bound state can still arise! The trick is, that on the forbidden bonds with $b = -\infty$, in the sum (5.2), all the paths passing through the b-bonds are eliminated. A DP carefully zigzags the slalom to just pick up the right a-value bonds and avoids the prohibitive b-bonds. Thus a DP path can benefit from the finite gain (a-value) and not paying the forbidden price (b-value). There is, however, a price to pay: the zigzagging costs kinetic energy and avoiding b-bonds makes the space restrictive – thus loss in entropy. Consequently, when all these costs added up to the bill, it may exceed the finite gain and a depinning phase transition may result.

5.3. Physical realizations of the DPRM

5.3.1. Statistics of rough-edged, torn paper sheets [Ktsz92,93]

The essence of the zero-temperature DPRM is the global optimization of trajectories through a random energy landscape. Kertesz and coworkers [Ktsz92,93] have just suggested a wonderfully simple realization of this notion, based upon the examination of the morphology and statistical properties of self-affine fractal tear lines in paper, see Fig. 5.3a. Their efforts were motivated by two points, furnished by the paper science community:

(i) fracture in paper is apparently governed by the random geometry of its fiber network [Mark84], and

(ii) in accordance with the Tydeman-Hiron model [TH64], the rupture line in a torn sheet is highly correlated with the "weakest" paths across the paper, discerned via microdensiometry with light transmission employed to determine the lowest density (i.e., flawed) regions of the page.

The basic idea is that the Tydeman-Hiron model is equivalent to the $T = 0$ $1+1$ DPRM; that is, the fractal tear line passes through the weakest bonds in the sheet. While it is generally appreciated that hydrogen bonding plays a crucial role in holding together the organic materials that constitute the paper, it is unclear whether it is the breaking of interfibrous bonds or the rupture of fibers themselves that dominate the process. Using a variety of papers furnished by the Hungarian Paper Institute,

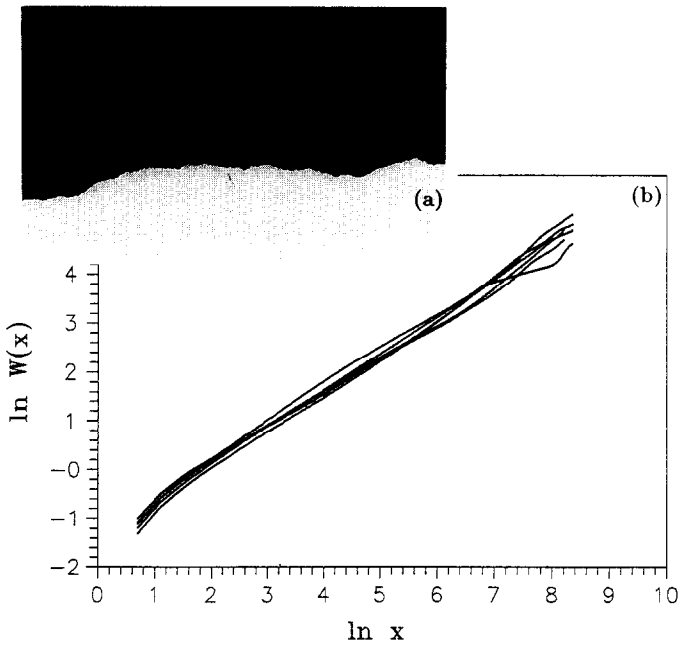

Fig. 5.3. (a) Photograph of the self-affine edge of a torn sheet, and (b) double log plot of the roughness as a function of length scale indicates that the edges of torn sheets do not follow random trajectories, but instead are characterized by a wandering exponent 0.67 ± 0.05 very close to the DPRM value 2/3 [Ktsz93].

Kertesz et al. used a tensile testing machine to apply a strain increasing at the rate 2 mm/minute to sheets 30 cm tall by 45 cm wide, in which a small 1 cm notch had been placed midway to initiate the tear. Averaging over some 30 runs on 5 distinct samples, they arrived at an estimate $\zeta_{pr} = 0.67 \pm 0.05$ for the lengthscale dependent roughness exponent, in extraordinary agreement with the wandering exponent of the 1+1 DPRM. Some representative data is indicated in Fig. 5.3b, which reveals that the scaling holds over more than two decades; despite the extreme variability in physical properties of the samples employed (factors of two or three in paper strength, density, thickness, etc.), all measured exponents fell in the range 0.63–0.72, evidence of the strong universality of the mechanism.

5.3.2. Domain walls in dirty 2d magnets [HuH85]

Consider the following 2d Ising model hamiltonian,

$$H = \sum_{\langle ij \rangle} J_{ij} S_i S_j, \tag{5.15}$$

where $\langle ij \rangle$ are only over nearest neighbors and J_{ij} is made random for each bond. Unlike spin glasses J_{ij} is restricted to be ferromagnetic $J_{ij} < 0$. Imagine we have the following system in which the spins on the top are fixed to be up, and those in the bottom opposite. At the zero temperature, spins like to be all aligned, but there must be a domain wall in between. We may ask where this domain wall would lie. The answer is the domain wall (a line) is precisely an optimal directed polymer.

As noted by Huse and Henley [HuH85], the kinetics of ordering in Ising ferromagnets will be drastically affected by the presence of randomly placed impurities that alter the local exchange couplings between neighboring spins. In these so-called random-bond (RB) Ising models, the disorder

breaks translational symmetry and will tend to pin domain walls in particularly favorable locations where the energy costs are weaker than average, being ameliorated by dilution or even substitution of negative couplings. Evidently, the globally optimal path of the $1+1$ DPRM is nothing but the best configuration of an interface in a 2d RB Ising magnet. For that problem, the key questions concern the geometric roughness of the domain walls and the size of the energy barriers preventing interfacial motion necessary for domain growth to initiate the kinetics of ordering. As is well known, in a ferromagnetic system dropped below its Curie temperature, large ordered domains grow in size at the expense of smaller regions, via coalescence made possible by the macroscopic motion of domain-wall segments. In pure systems, without disorder, this process is purely diffusive in nature and the average linear domain size grows as $R(t) \sim \sqrt{t}$, an old result due to Lifshitz [L62], which has been confirmed numerically [HB91] and experimentally [AC79]. For impurity-stricken 2d RB magnets, however, domain wall motion becomes Arrhenius activated, resulting in much slower growth scaling as $R(t) \sim (\ln t)^{\phi}$, where an argument of Villain [V84, see also N85] allows one to relate the exponent ϕ, which characterizes how the energy barrier for annealing out a domain scales with its size, to the DPRM indices via the relation $\phi = (2-\zeta)/\omega$. For 2d RB magnets, this argument would yield $\phi = 4$. Such logarithmic domain growth was hinted at in the early work of Grest and Srolovitz [GS85], though recently confirmed by Bray and Humayun [BH91]. For related numerical efforts on 2d RF Ising models, see [GKGG84,A87].

5.3.3. *Blown fuse networks [Han91]*

The statistical physics community, bolstered by its successes with fractal geometry in the realm of disordered materials, has recently taken on the very complex matter of fracture mechanics; see, e.g., [HR90r]. In particular, it has been suggested that notions of scaling might be applicable to the final stages of the breakdown process, where the stress field associated with the development of the evolving crack network may exhibit critical behavior [AHHR89]. Specific to our interest here is a fuse model for brittle fracture, introduced by [ARH85], but subsequently proposed by [RHG87] as a realization of the $1+1$ DPRM, with the implication that the response of an elastic-perfect plastic medium under strain is governed, asymptotically, by the KPZ equation. Hansen, Hinrichson and Roux [Han91] have just tested this hypothesis – their findings nodding in the affirmative, as the roughness of the fuse model crack interface scales with an exponent 0.7 ± 0.07, suggesting agreement with the $1+1$ DPRM wandering exponent $2/3$. In an interesting complementary experimental study, Lely and Roux [LR91], reveal strong correlation between the main crack and the minimal energy path crossing fractured plexiglass sheets, supporting a brittle fracture analog of the Tydeman-Hiron conjecture from the context of torn sheets.

The essence of the model is, see Fig. 5.4a, a collection of resistive fuses, placed upon the bonds of a square lattice that is canted and bordered by bus bars. The fuses behave ohmically provided the applied voltage does not exceed a threshold value t_i, beyond which they turn irreversibly into insulators. The threshold voltages are random, drawn from a specified probability distribution. In the related elastic perfect-plastic model, which lies within the fuse universality class, the response is identical up to threshold, at which point the circuit elements carry *constant* rather than zero current; i.e., the deformation of a perfectly plastic material continues, without any additional force necessary, once the critical stress has been applied. A voltage difference is applied across the network. Until the first fuse has "blown," each bond carries the same current, so that the first to go is the one

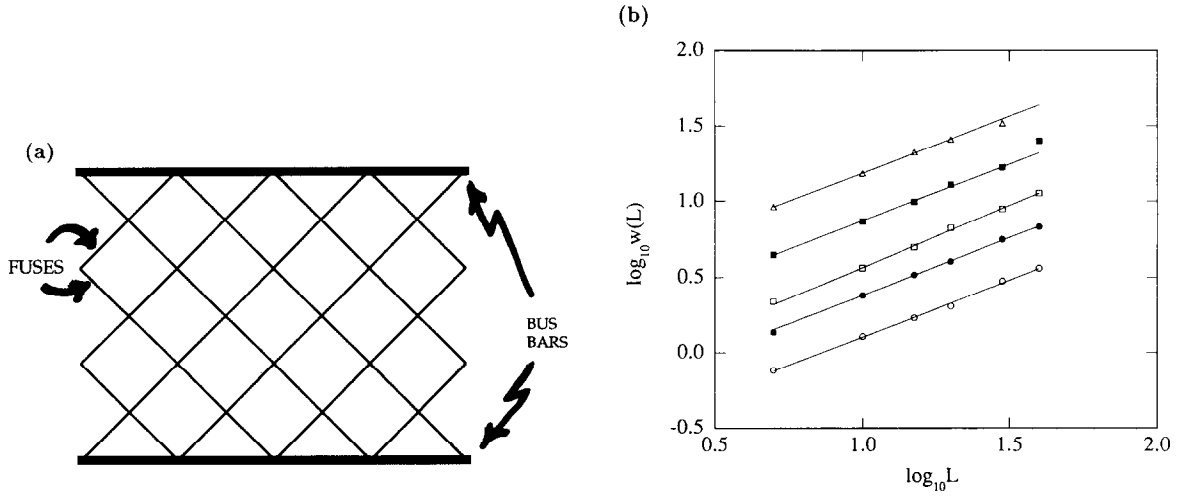

Fig. 5.4. (a) Fuse network [Han91]. Each fuse possesses a random threshold voltage beyond which it is converted irreversibly into an insulator. The voltage between the bus bars is raised until a filamentary path of minimal threshold fuses severs the network in two. (b) Width of this filamentary "crack" as a function of system size for various threshold distributions. All correspond to bounded or short-ranged distributions, save for the middle one, which results from a power-law distribution. See Section 5.5.3 for a possible explanation for this anomalously large wandering exponent.

with minimal threshold value. As the voltage is augmented, fuse after fuse blows, as their individual thresholds are crossed. Each time a fuse dies, the currents throughout the network rearrange themselves so that at any stage of the breakdown process, the next fuse to blow will be the one that minimizes the ratio t_i/v_i, where v_i is the voltage difference across bond i for unit voltage difference across the network. Consequently, the breakdown of the network proceeds in a highly correlated manner, involving a subtle interaction between the quenched threshold and evolving current distributions. In the end, the loss of conductivity between the bus bars is signaled by a filamentary crack that propagates vertically, splitting the network in two. Hansen et al. argue that in the final stages, the crack evolves so as to minimize the number of fuses blown, passing through the spatially uncorrelated, but very low threshold fuses lost early on. In Fig. 5.4b is shown their data for the system size dependence of the total width of the crack *backbone,* branchings ignored, using different threshold probability distributions. Note, in particular, the strong evidence of universality for the bounded and short-ranged distributions, while the central line, with larger slope, arises from a long-ranged power law tail. The backbone forms the visible surface of the crack separating the two pieces of material, rendering it experimentally accessible. (For a discussion of actual fracture experiments on brittle materials, giving rise to possibly optimal 2d RB surfaces, see the wonderful papers of Bouchaud, Lapasset and Planès [BLP90] and Maloy, Hansen, Hinrichsen, and Roux [Mål92]). Measurements of the fluctuations associated with the largest crack (branches included!) throughout the entire fracture process led to slightly smaller values of the wandering exponent. In summary, [Han91] quote $\zeta_{fuse} \approx 0.7$, good to 10% for their numerical simulations on an electrical analog of brittle fracture.

5.3.4. Localization of deformation – Schneebeli models [Poi92]

In a very curious experiment, Poirier, Ammi, Bideau and Troadec [Poi92], studied the deformation process in a simple, entirely regular 2d packing ("Schneebeli") model consisting of equal parallel

cylinders (drinking straws!) subject to a uniaxial compression. The mechanical response of such a system is initially elastic, as the walls of the cylinders are deformed by bending, but under increasing stress the deformation becomes highly localized as buckling precipitates a geometrically complex band cutting through the sample. As stressed by Poirier et al., this *localization of deformation* is tied directly to heterogeneities in the solid arising from *quenched* contact, geometric or compositional disorder, which incur a "softening" in both the local and bulk nonlinear stress-strain characteristics. The actual experimental sample consisted of 58 horizontal rows of 55 cylinders, 3 cm long and 3 mm in diameter, set in a rigid U-shaped frame with vertical compressional displacements imposed from above at very slow speeds, roughly 0.2 mm/minute. Great care was taken to minimize possible edge effects by coating the glass walls of the container and upper piston with Teflon, in addition to maintaining 6-fold symmetry at the boundaries by putting several buffer layers of Teflon cylinders with identical geometric properties as the straws. As the experiment proceeds, photographic records of the sample are made in order to permit a geometric analysis of the strain field. In Fig. 5.5a is summarized the nonlinear elasticity of this bulk 2d cellular solid, as well as the two-straw contact, both indicating a local maximum in the stress, followed by a softening zone where the slope goes negative. In the bulk medium, the force-deformation curve essentially plateaus as the response becomes plastic. This behavior ought to be compared to the fuse model of fracture that we just discussed, which assumes ideal Hookian response, followed by perfect plasticity! Consider a compressional stress applied to the sample – at first, small clusters of crushed straws begin to appear. The number and size of such clusters continue to grow as the strain increases within the sample. Eventually, see Fig. 5.5b, these clusters coalesce in a rather tortuous band that extends across the sample. The *backbone* of this band is strictly localized – as the displacement is further increased, more and more straws join the ranks, but leave unaltered the essential geometric character of this particular band. The process is entirely reversible provided one has not gone too far out on the plateau; upon reintroduction of the stress, the very same complex geometry of the localization band is restored, identical as before at the front and back of the sample. The band's geometrical complexity is all the more striking, given the extremely ordered array from which it arose. Evidently, the *contact disorder* – due, ultimately, to the fact that the straws are not rigorously the same nor is the original array without defects – incurs fluctuations on the microscopic scale that conspire to produce a nontrivial bulk elasticity characteristic of many nonlinear, granular materials. Poirier et al. employed Moire techniques to make comparative studies of the evolving sample geometry whilst on the plateau. In addition, and most importantly for us, they focussed their attention on the growing clusters associated with the incipient localization band, plotting the transverse width as a function of length, see Fig. 5.6. Averaging over five smaller samples, as above, they obtained a wandering exponent $\zeta_{\mathrm{Snb}} = 0.73 \pm 0.07$, not too different from the fuse model estimate of Hansen et al. for the roughness of one-dimensional crack interfaces, both in the right ballpark of the $1 + 1$ DPRM. A bigger sample, consisting of 140 rows of 125 cylinders, produced a slightly larger estimate of 0.75. Granted, the statistics are poor; nevertheless, the results are suggestive.

5.3.5. Vortices in ceramic superconductors [KZ87,NL88,Milne94r]

With the recent discovery of high-temperature superconducting ceramic materials, there has been a renaissance of interest in the physics and phenomenology of the Abrikosov flux-line lattice (FLL); for a comprehensive review covering all aspects, see the Wagnerian epic of Blatter, Feigel'man,

(a)

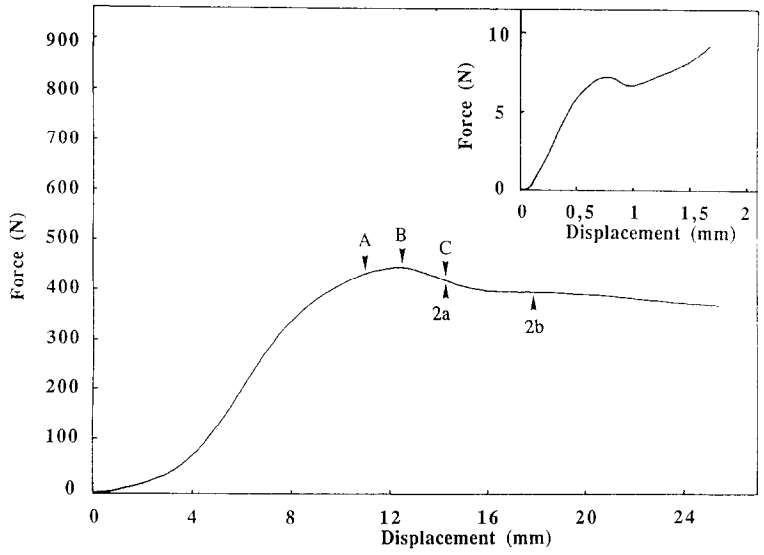

(b)

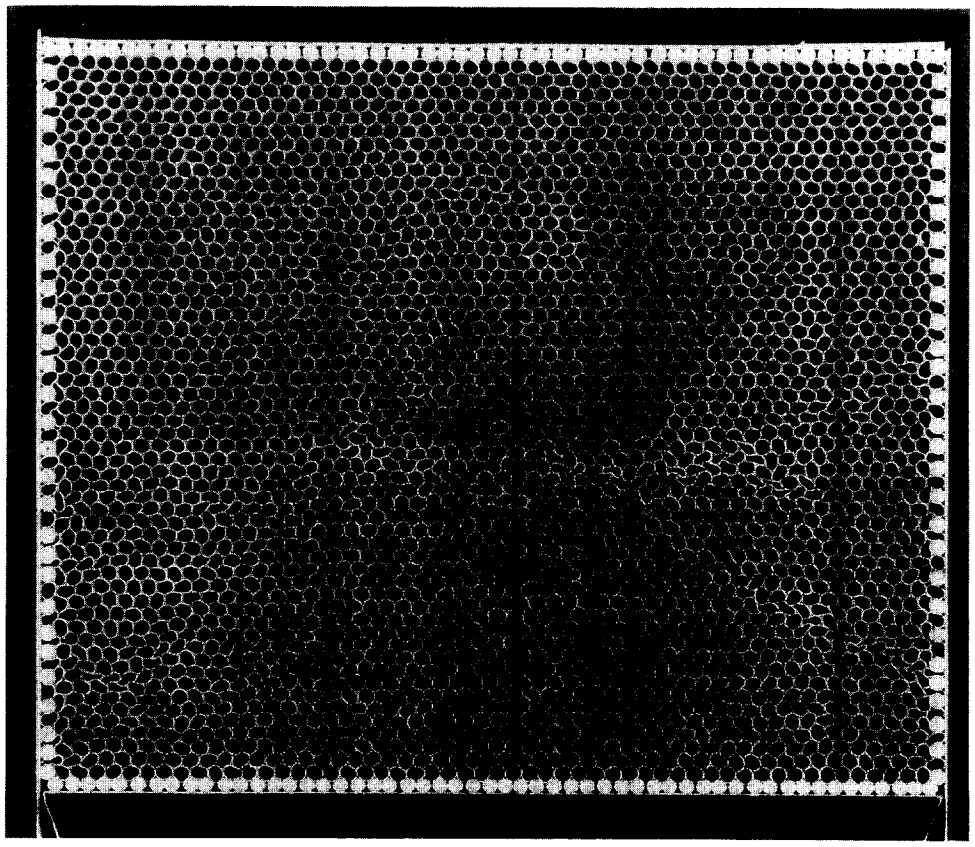

Fig. 5.5. (a) Force-deformation curve of the 2d Schneebeli solid of hollow cylinders [Poi92]. Inset: The local characteristic for two individual straws in contact. (b) A snapshot, illustrating the rough, localized band of deformation (i.e., crushed straws) wandering across the sample.

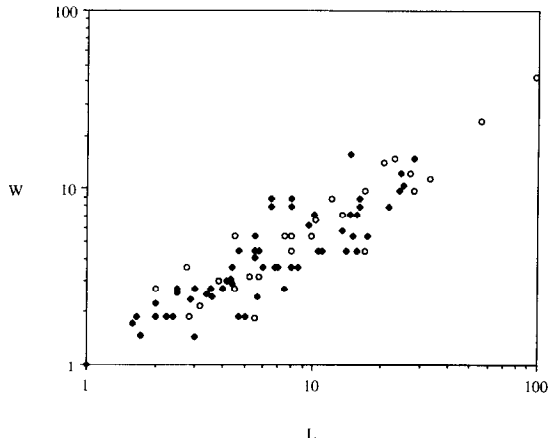

Fig. 5.6. Double log plot of the width W of the deformation band as a function of observation lengthscale L. The data are for (•) five small samples and (○) one large sample, the former yielding a wandering exponent 0.73 ± 0.07.

Fig. 5.7. Electron micrograph [Civ91] of a nearly vertical slice ($\perp$ oxide planes) of $YBa_2Cu_3O_7$ ceramic superconductor that has been irradiated by high energy ion bombardment, producing a dense array of columnar defects, each 50A in diameter but many microns long, which compete with various forms of point disorder to roughen vortex lines. The contributing effects of point and columnar defects on DPRM wandering is discussed in Section 5.5.4.

Geshkenbein, Larkin and Vinokur [Milne94r]. Initially, much attention was paid to the importance of thermal fluctuations – Nelson [Nel88] pointed out that enhanced flux-line wandering would, at fields slightly above H_{c1}, lead to an entangled flux-line liquid, and furthermore would cause the vortex line density to vanish as $n \sim (H - H_{c1})^{\bar{\beta}}$, with $\bar{\beta} = 1$ as one approached the Meissner phase. This critical index is easily understood via a Fisher-type argument, see [MF86r]. Within a FLL of areal line density n, the largest typical transverse fluctuation of a single vortex line is of the order $\xi_\perp \simeq 1/\sqrt{n}$ and occurs over a longitudinal lengthscale $\xi_\parallel \sim n^{-1/2\zeta}$, fixed by the wandering exponent ζ. Consequently, the excess free energy per unit volume associated with the elastic energy costs of vortex line roughening scales as $n(\xi_\perp/\xi_\parallel)^2 \sim n^{1/\zeta}$, assuming unit line tension. For magnetic fields

just above H_{c1},where the flux lattice is sparse, this entropic repulsion between neighboring lines must be balanced against the chemical potential gain, $n(1 - H/H_{c1})$, favoring their creation. Minimizing the Gibbs free energy that incorporates these competing effects yields $\bar{\beta} = \zeta/(1 - \zeta)$ which, for the thermal wandering exponent $\zeta_{TH} = 1/2$, produces $\bar{\beta} = 1$. Nattermann and Lipowsky [NL88], in an interesting comment upon the Nelson paper, extended the analysis to include effects associated with the disorder-induced roughening of vortex lines in the presence of *quenched randomness*. Aware of contemporary efforts of Kardar and Zhang [KZ87] within the KPZ context, they realized immediately that the many-dimensional DPRM could serve well as a streamlined model of vortex line roughening incurred by point defects. Using the knowledge that DPRM wandering is *superdiffusive*, Nattermann and Lipowsky concluded that Nelson's essential conclusions remained intact, including the possiblity of a low-temperature entangled FLL phase, but the vortex line density would, as a consequence, vanish more rapidly as one entered the Meissner phase. In fact, with $\zeta_{2+1} \approx 5/8$, we would have the more severe value $\bar{\beta} \approx 5/3$.

Following the Nattermann-Lipowsky Comment [NL88], we find a veritable explosion of interest in the subject of Abrikosov FLLs roughened by quenched impurities. Subsequent work by Fisher [MPAF89] and collaborators [FFH91], drawing upon a reformulation of collective pinning theory in the language of disorder-induced roughening [FGLV89,HH90], addressed more carefully the difficult issue of vortex line assemblies in the presence of point disorder and predicted a novel *vortex glass* phase. Their theoretical efforts were motivated in part by a series of provocative experiments, [Ko89,Gam91] devoted to transport measurements, which pointed to the existence of an actual phase transition identified with the "irreversibility line" discovered by Malozemoff et al. [Mal88] in these high T_c materials. An alternative theoretical analysis, appropriate to situations of strongly correlated disorder (i.e., where *columnar* defects resulting from twin boundaries or, perhaps, forests of screw dislocations provide the dominant pinning mechanism), was proposed by Nelson and Vinokur [NV92] and has since been referred to as the *Bose glass* model thanks to its origins in Anderson localization effects exhibited by bosons subject to disorder in two dimensions [FWGF89]. An extraordinary experiment by Civale et al. [Civ91] investigated related vortex confinement effects due to an artificially created columnar microstructure which resulted when they bombarded their superconducting sample with a dense beam of high energy ions. For related experiments, see [Kon91,Bud92]. It is interesting to observe, as Nelson and Vinokur have stressed when pointing out the essential differences between the competing vortex and Bose glass models, that point disorder promotes flux line wandering and entanglement, while correlated disorder inhibits wandering and promotes localization. Since the vortex and Bose glass models, as initially proposed, entertained rather different limiting cases, it is natural to consider the competing effects of point and columnar defects. Ideally, within a single model, we would like to determine the consequences of this competition, both on the phase diagram of the Abrikosov FLL, as well as on the disorder-induced roughening of individual vortex lines. Hwa, Nelson and Vinokur [HNV93] have recently tended to the former, extending the nominal Bose glass theory to include point disorder. In Section 5.5.4, we shall do the latter, working within the context of the DPRM, where columnar defects are the result of time-independent noise, a matter which was examined as such by Zhang [Z86a] a few years back using techniques of Mott-variable range hopping. Building on Zhang's efforts and apparently unrelated work [EE84] on *punctuated evolution*, Krug and Halpin-Healy [KrHH93] have performed an exhaustive numerical study of the *purely columnar* DPRM, examining issues of universality at zero and finite temperature. Finally, the competing effects of point versus columnar defects on the disorder-induced wandering of directed

polymers is addressed in the recent work of Arsenin, Halpin-Healy and Krug [AHHK94] on the p/c DPRM.

5.4. Analytical efforts. 1 + 1 DPRM

5.4.1. Bethe ansatz solution

Systems with quenched disorder are notoriously hard to study analytically. In the spin glass community [MPV87r], a conventional weapon known as "replica trick" was designed to bypass the difficulties. Kardar [Kard87a], working within the continuum formulation of the 1 + 1 DPRM, was the first to have successfully applied the replica trick in the DPRM context. The replica trick is based upon a rather innocuous looking identity, $\langle \ln Z \rangle = \lim_{n\to 0}(\langle Z^n \rangle - 1)/n$, motivated by a simple practicality – one cannot directly compute the disorder-averaged free energy, but calculating arbitrary moments of the partition function is a relatively straightforward matter. As is well known from the spin-glass problem, the replica method can be a veritable Pandora's box of sorts, possessing deep conceptual subtleties and pitfalls thanks to an implicit switch of diverging thermodynamic and vanishing replica limits. Nevertheless, with historical hindsight, we can confidently stress that the replica approach to the 1 + 1 DPRM captures most of the essential physics, providing the reader with a quick understanding of the wandering and free energy fluctuation exponents. In replicating the partition function and performing the gaussian functional integral over the quenched, uncorrelated disorder, we arrive at the problem of n bosons in one spatial dimension interacting via an attractive delta function potential, with the many-body Hamiltonian,

$$\mathcal{H}_n = -\Gamma \sum_{\alpha} \frac{\partial^2}{\partial x_\alpha^2} - V^2 \sum_{\beta>\alpha} \delta(x_\alpha - x_\beta), \tag{5.16}$$

$$\mathcal{H}_n \psi = E\psi \tag{5.17}$$

where we recall that Γ represents the inverse line tension in the DPRM problem and V the strength of the quenched disorder. In essence, the replica trick allows us to trade in an apparently intractable single-body problem in the statistical mechanics of random media for a pure, but interacting many-body system. As noted by Kardar, the origin of the statistical interaction between the replicas is easily understood in the context of the lattice model – if m polymers cross at the random bond $\mathcal{V}(x,t)$, the disorder average

$$\langle e^{-m\mathcal{V}} \rangle = \exp\left[-m\left(\bar{\mu} - \frac{V^2}{2} \right) + \frac{m(m-1)}{2} V^2 \right] \tag{5.18}$$

renormalizes the bulk bond energy to $\bar{\mu} - V^2/2$, where $\bar{\mu}$ and V^2 are the first and second moments of gaussian random bond energy distribution, thereby introducing a pairwise attraction between the replicas. Fortunately, the 1d n-boson problem with a delta function attractive potential is solvable via the Bethe ansatz, with groundstate wave function

$$\psi(x_1, \ldots, x_n) = \exp -\kappa \sum_{\beta>\alpha} |x_\alpha - x_\beta| \tag{5.19}$$

where $\kappa = \sigma^2/4\Gamma$ ensures the proper discontinuity in the wave function derivative as two bosons cross. At this level, the 1 + 1 DPRM is no more difficult than elementary quantum mechanics! To

determine the disorder-averaged fluctuations of the free energy, Kardar pointed out that much of the necessary information can be gleaned from the replicated partition function, since it is the generating function for the cumulants $c_j(f)$ of the quenched free energy f,

$$\langle Z_n \rangle = \exp \langle nf \rangle = e^{-\sum_j n^j c_j(f)/j!}. \tag{5.20}$$

In the thermodynamic limit, where the path length of the direct polymer asymptotically approaches infinity, $\langle Z^n \rangle$ is dominated by the ground state energy of the n-boson system, $\langle Z^n \rangle \sim \exp(-tE_0(n))$. Both the ground state wave function and ground state energy can be found exactly. The 1d n-body Hamiltonian with attractive δ potentials is a classical text book example in the Bethe ansatz community. Its solution is well known [NO89,Tha83]. Kardar first noticed its application in the DPRM context.

The above method is exact except the following paradox: in deriving Eq. (5.16) it is necessary to invoke discrete lattice version (remember DP can be only uniquely defined on a lattice), as we have done in Eq. (5.18). On the other hand, the lattice version of (5.16) does not admit any analytical solution! We must strictly stick to the continuum notation even if the model is defined on a lattice. The mathematical problem is the following: on a lattice there is inevitably multiple occupancy for a single site, and any multiple occupancy spoils the solvability of (5.16). Note that this problem automatically disappears for fermions, thanks to Pauli exclusion principle. For bosons this is a unresolved dilemma. In proceeding further, we should bear in mind this pitfall in our formulation. Its consequences to such subtle questions as replica breaking are not yet fully clear.

Below we outline briefly the basic steps of the Bethe ansatz method. Oddly enough, because of the above, it is the n-dependence of E_0 that provides the crucial piece of information. At a typical time slice in the space-time diagram of the n-boson stystem, the bosons are essentially free, possessing a particular spatial arrangement, $x_1 < x_2 < \ldots < x_n$ (note only possible in the continuum where $\leq$ can be avoided), that we can use to label the particles. The net result is a spatial wave function at this time slice of the form,

$$\Psi(x_1, \ldots, x_n) = \exp - \sum_i k_i x_i, \quad \text{where } k_i = 2(i-1)\kappa \tag{5.21}$$

with associated ground state energy $E_0(n) = \sum_i k_i^2 = n(n^2-1)\kappa^2/3$. The absence of a quadratic term in the energy is the noteworthy feature, implying that $c_3(\Delta f) \sim t$ and the free energy fluctuations of the gaussian, uncorrelated 1+1 DPRM scale with an exponent $\omega = 1/3$. The wandering exponent comes in through the back door, via the scaling relation

$$\zeta = (\omega + 1)/2 = 2/3. \tag{5.22}$$

This relation is one of the cornerstones of the DPRM – apparently independent scaling exponents are reduced to just a solitary one thanks, ultimately, to the Galilean invariance, recall (3.8). Relations to the pair (χ, z) are through $\zeta = 1/z$, and $\omega = \chi\zeta$. However, in the DPRM context, (5.22) can be independently derived [HuH85] by quite a few alternative methods, depending personal taste. The relation is expected to hold for all DP models, with the notable exception of time-correlated disorder and complex DP problem.

For those who prefer a direct understanding over the fancy mathematical tricks we show the above Bethe Ansatz solution can be just as well treated by ordinary methods, thus relieving them, perhaps, of some unnecessary burden and mystification. For the n-body Schrödinger equation (5.17)

$$\left\{-\sum_{\alpha}\partial_{\alpha}^{2}-\sum_{\beta>\alpha}\delta(x_{\alpha}-x_{\beta})\right\}\psi(x_{1},\ldots,x_{n})=E\psi(x_{1},\ldots,x_{n}) \tag{5.23}$$

we would like to find the ground state. Consider the simplest case of two particles $n=2$, we define $x=x_1-x_2$, $y=x_1+x_2$, the latter represents the motion of the center of mass, it drops out from our consideration. Eq. (5.23) becomes

$$\{-\partial^{2}-\delta(x)\}\psi(x)=E\psi(x). \tag{5.24}$$

It is straightforward to see that the ground state (which should be symmetric, possess only one node, and match the singularity at the origin) is

$$\psi=e^{-|x|}. \tag{5.25}$$

Generalizing the above solution for arbitrary n just requires educated guesswork. For example, if $n=3$, we can readily check that

$$\psi(x_{1},x_{2},x_{3})=e^{-|x_{1}-x_{2}|-|x_{2}-x_{3}|-|x_{3}-x_{1}|} \tag{5.26}$$

is, indeed, the right solution. It is easily seen that, more generally, (5.19) does the trick.

Exercise: *Consider disorder with arbitrary correlations in the transverse direction, so that* $\langle\mathcal{V}(x,t)\mathcal{V}(0,0)\rangle=R(x)\delta(t)$*; note that the uncorrelated case considered above corresponds to* $R(x)=V^{2}\delta(x)$*. Replicate the DPRM partition function, perform the functional integral over the disorder, and discover that the attractive interaction between the polymers is now* $R(x)$*! In other words, the correlator of the disorder fixes the replica interaction.*

Remark: *Later we shall see that if* $R(x)=\delta(x)$ *is replaced by* $R(x)=x^{2}$*, the ground state w-function will be* $\psi=\exp-\sum(x_{\alpha}-x_{\beta})^{2}$*; if* $R(x)=|x|$*, i.e. the d=2 random field domain problem,* $\psi\simeq\exp-\sum|x_{\alpha}-x_{\beta}|^{3/2}$.

5.4.2. Physical implications of the analytical results

The ground state wave function ψ and ground state $E_0(n)$ contain much more information than determining the scaling exponent ζ. Many hidden implications of ψ as well as the full physical picture of $1+1$ DPRM only emerged rather recently.

• *Real replicas:* Let us forget for the moment that the replicas were introduced as mathematical ghosts to bypass technical difficulties. Consider that n real DP's embedded in the same disordered system. The mathematical expression is the same – the n DP partition function $\langle Z^{n}\rangle$ should be replaced by [Pa90]

$$\langle Z(x_{1})Z(x_{2})\cdots Z(x_{n})\rangle=G(x_{1},x_{2},\ldots,x_{n};t) \tag{5.27}$$

if the n objects are allowed to be at different positions, they all have one endpoint fixed at the origin. It is easy to show that G satisfies the Schrödinger equation (5.23). Therefore for the ground state we have

$$G(x_1, x_2, \ldots, x_n; t) \propto \psi_0 = \exp - \sum_{\alpha>\beta} |x_\alpha - x_\beta|. \tag{5.28}$$

The t-dependent factor concerns only the motion of the center of mass, to which we will return later.

We can interpret that the n DP's embedded in the disordered system will experience a mutual attraction. This is because ψ_0 is related to the probability of finding the free ends of the n DP's. The bound state (5.28) implies that if we put n such objects in the same random environment, they probably will overlap on top of each other, with occasional splittings from each other. Thus these n objects will occupy a localized zone in x-space. We may not wish to distinguish the n objects (the ends of the n DP's), but just want to know what is the physical size of this n-body bound state and what is the density distribution inside.

This bound state problem is interesting per se and we should forget for the moment our original DP problem. We may like to know what is the typical size occupied by the particles. Intuitively we expect this size decreases rapidly when n increases, representing the collapse. This is however, not readily read off from the exact wave function. Using the wave function (5.28), let us define the density

$$\rho_n(x) = \int_{-\infty}^{\infty} dx_1 \cdots dx_n \delta(x_{cm}) \delta(x_1 - x) |\psi_0|^2 \tag{5.29}$$

where x_{cm} denotes the center of mass position. The above integration is not simple to carry out, since ψ_0 contains many singularities and each integral (say x_1) is constrained by the others.

In a completely different context, Calogero and Degasperis [CD75] first accomplished such a deed. By carefully arranging the orders of integrations, which has much to do with the original Bethe Ansatz momenta-matching method, they obtained $\rho_n(x)$ in a closed form

$$\rho_n(x) = \sum_{k=1}^{n-1} (-1)^{k+1} \frac{k(n!)^2 e^{-2kn|x|}}{(n+k-1)!(n-k-1)!}. \tag{5.30}$$

For asymptotically large n, we have the following simpler form, up to a normalization constant,

$$\rho_n(x) \simeq 2n^2 [\cosh^{-2}(nx)] \sim e^{-2n|x|}. \tag{5.31}$$

From this we can read off easily the size of the bound-state: denote it by x_0, we see $x_0 \sim 1/n$. This implies as n increases, the bound state size decreases i.e. more particles occupy less space, what a collapse! Remember our warning regarding continuum limit. If the bound state is on a lattice, multiple occupancy is inevitable for such ill-condensed matter. Thus this solution is no longer valid.

In the above discussions, we have ignored the motion of the center of mass. This motion becomes relevant if we specify an initial condition, say, all the $x_\alpha = 0$ at $t = 0$. There are different ways to take into account the center of mass motion. Bouchaud and Orland [BO90] first considered this aspect systematically. Recall the previous wave function (5.28), Bouchaud and Orland considered the modified wave function

$$\exp\left\{-\sum_{\alpha>\beta}|x_\alpha - x_\beta| - \frac{1}{4n\Gamma t}\left(\sum_{\alpha=1}^{n} x_\alpha\right)^2\right\} \tag{5.32}$$

where we recognize in the last term diffusive motion by the center of mass. Mezard and Parisi considered a slightly different version,

$$\exp\left\{-\sum_{\alpha,\beta}|x_\alpha - x_\beta| - \frac{1}{t}\sum_{\alpha=1}^{n} x_\alpha^2\right\}. \tag{5.33}$$

Physically, the latter may be more natural since it corresponds to the aforementioned initial condition. Even so, the two are essentially equivalent, as long as we are only interested in the leading scaling exponents.

What are the implications of the above discussion, e.g. the wave function (5.33)? Let us digress a little in order to fully appreciate the physics implied in (5.33). In an earlier transfer matrix calculation, Zhang [Z87] considered not only just the globally optimal path through the random energy landscape, but also the second best, third best, and so on. He finds that the differences between the endpoints of these optimal paths scale with path length as $t^{1/3}$.

The gaps of these excited states are found to approach constants. Later it has been shown that the constant gaps go to zero upon letting the lattice spacing a go to zero. Therefore for a single DP in continuum there are degeneracies in the ground state, n real DP's will find themselves probably in distinct degenerate ground states. The existence of the degenerate ground states contributes to the "weakly" broken replica symmetry [Pa90], see below.

In Eq. (5.33), the term $\sum_{\alpha=1}^{n} x_\alpha^2/t$ is just the kinetic energy. We know that the DP transverse deviation must scale as $x \sim t^{2/3}$, both terms in Eq. (5.33) should be of the same order of magnitude. We obtain

$$\sum_{\alpha=1}^{n} x_\alpha^2/t \sim t^{1/3}, \tag{5.34}$$

which in turn implies that the relative distances among the DPs must also scale as

$$|x_\alpha - x_\beta| \sim t^{1/3}. \tag{5.35}$$

Therefore the earlier prediction of [Z87] is confirmed here. Note that this important piece of information is already encoded in the wave function, but unfortunately hitherto overlooked in the literature.

From earlier discussion we may have got the impression that the bound state is very tight since the size is proportional to $x_0 \sim 1/n \ll 1$. However, when the t-dependence is made explicit we see that the very same bound state size is an increasing function of t (typical size $\sim |x_\alpha - x_\beta| \sim t^{1/3} \gg 1$). Does this lead to contradiction? No. The reason is that the DP's experience only a moderate splitting $t^{1/3}$ near their free ends. The most of their trunk parts do come close to each other very often to form a tight bound state.

The lesson to be learned, perhaps, is the following. For n real DPs in the same random environment, they prefer to make relatively large deviations, $x \sim t^{2/3}$, together as a group, since the whole group of degenerate ground states is spread over a narrower region, $|x_\alpha - x_\beta| \sim t^{1/3}$. The implications for

a single DP on a lattice is also interesting: at low temperatures, a DP not only samples the globally optimal configuration, but also jumps to low-lying excited states, thanks to thermal fluctuations. Nevertheless, since these low-lying excited states are all relatively close to the ground state (in position space), thermal noise does not change the overall scaling behavior. This provides us with an intuitive explanation as to why at finite temperature, the wandering exponent $\zeta = 2/3$ remains invariant.

The above ground state wave function in continuum is symmetrical in the index of the objects. Parisi [Pa90] investigated whether the replica symmetry is broken, like his well-known solution for spin glasses. What he found is a weak breaking of the replica symmetry. In layman's words, it is a breaking without scaling consequences. Here we want to explain the physical meaning of the above statement, to help the reader appreciate the physics without getting trapped in the mathematical jungle.

Consider $n = 2$ real DP's and introduce an additional repulsive interaction between the two, the infinitesimal strength being ε. Repeating the calculation for generic n, we find that the two objects form a bound state. However the bound state size is an increasing function of t, i.e. the two ends scale as

$$|x_1 - x_2| \sim t^{1/3}. \tag{5.36}$$

Since x_1 and x_2 are two degenerate states (the energy gap being zero in continuum, see also Mezard's simulation on a lattice [Mez90]) the infinitesimal repulsive interaction makes sure that two DP's occupy distinct states. Even after sending $\varepsilon \to 0$, the two DP's would stay where they are since there is no energy incentive for the two to join. This is in contrast to the situation when there is a unique ground state (the replica symmetry is not even weakly broken), when $\varepsilon \to 0$, there is always a restoration force for the two to join. However, the weakly broken replica symmetry causes only a uncertainty $t^{1/3}$, insignificant compared to the quantity proportional to $t^{2/3}$. Thus this breaking does not make any difference in the scaling behavior of the DP problem.

• *Physical DP's:* Recently Tang [T94] has considered putting two physical DP's in the same disordered system. Physical DP's differ from the DP's that we have discussed so far in that that they cannot overlap; i.e., there is an excluded volume effect. The above considerations do not apply since all the degenerate states have significant portions in overlap, i.e. they belong to a same family (see later discussion of the ultrametric tree structure). In Tang's simulation two DP's are forbidden to share any link, thus the two should never overlap and should belong to two distinct families. We can consider the two physical DP's statistically independent since no link is shared. Statistical independence is a valuable thing. Independent DP's each scale as $x_{1,2} \sim t^{2/3}$, so their difference should be of the same order of magnitude $|x_1 - x_2| \sim t^{2/3}$. This is confirmed by Tang's simulation.

• *Positional probability density:* The scaling law $x \sim t^{\zeta}$ only tells us the most probable location, with no knowledge of the spread. Let us consider Eq. (5.4) after the sample average $\langle \cdot \rangle$,

$$P(x,t) = \langle P_\eta(x,t) \rangle = \langle Z(x,t) / \int dx' Z(x',t) \rangle. \tag{5.37}$$

The free energy distribution $P(F)$, advertised in (3.37), and to be derived in eqs.(5.70)–(5.71), is of much help here,

$$P(F) \simeq \exp - \left(\frac{F - F_0}{t^{1/3}} \right)^{\eta_+} \quad \text{for } F > F_0, \tag{5.38}$$

where $\eta_+ = 3/2$. It is clear, the dominant contribution of $P(x,t)$ comes from the dominant part of $Z(x,t)$ in (5.37), hence the $F - F_0 > 0$ part. That is why the "forward" part (peaks in $F = \ln Z$ landscape, remember $F = h$ is the surface variable in the stochastic growth context) is relevant in our consideration; i.e., it is the peaks of $F = \ln Z$ that make the DP deviate. On the other hand, the (forward) free energy fluctuation is related to the deviation in the following manner [HuH85],

$$x^2/t \simeq F - F_0 > 0. \tag{5.39}$$

Substituting the above into (5.38) permits us readily to obtain (unpublished, Zhang)

$$P(x,t) \simeq P(F) \simeq \exp -x^3/t^2. \tag{5.40}$$

This result reproduces the scaling relation $x \sim t^{2/3}$ and extends it to the complete distribution function, in the same spirit that the Family-Vicsek scaling relation being replaced by the distribution functions in (3.39), (3.40). Warning should be kept in mind however, the above reasoning is only valid where the "peak-dominance" assumption holds. Indeed, recent numerical simulations [GB93] point out non-negligible deviations from the $P(x,t) \sim \exp -x^3/t^2$ law, they can be attributed to the regions where $F \sim F_0$. Recently a direct numerical simulation by Klafter and Zumofen (private communication) also supports the above law. This law can also be obtained by other more sophisticated methods, see the example below. The above is probably the simplest physical derivation.

• *Functional approach:* The foregoing physical picture can be treated more formally and systematically. Bouchaud and Orland [BO90] undertook a functional approach, generalizing a bit further an earlier treatment by Parisi. It has the merits to putting the physics on a more sound basis, as well as providing additional insight into the mathematical structures of the problem. Let us list some of these:

(i) determine that $\zeta = 2/3$ directly,
(ii) confirm independently the scaling relation $\omega = 2\zeta - 1$,
(iii) calculate the amplitude prefactors of the positional moments and free energy cumulants,
(iv) find the finite-size corrections to the disorder-averaged free energy,
(v) confirm specific predictions regarding the tails of positional and free energy probability distributions.

The starting point in the Bouchaud-Orland analysis involves amending Kardar's ground-state wave function to permit the CM to have nonzero momentum,

$$|\Psi_k\rangle \sim \exp\left(ik\sum_\alpha x_\alpha\right)\exp\left(-\kappa\sum_{\beta>\alpha}|x_\alpha - x_\beta|\right) \tag{5.41}$$

with these low-lying excitations possessing energy $E_k = E_0 + n\Gamma k^2$; the first term being familiar, while the second results from the free diffusion contribution of the CM. In the thermodynamic limit ($t \to \infty$), the n-body transfer matrix can be approximated by

$$e^{-t\mathcal{H}_n} = e^{-tE_0}\int dk\sqrt{nt\Gamma/\pi}e^{-nt\Gamma k^2}|\Psi_k\rangle\langle\Psi_k| \tag{5.42}$$

where we have restricted ourselves to the subspace spanned by these $|\Psi_k\rangle$. Using Parisi's gaussian representation [Pa90]

$$\exp\left(-\kappa\sum_{\beta>\alpha}|x_\alpha - x_\beta|\right)$$
$$\equiv \int D\varphi \exp\left[-(1/4\kappa)\int dx(\partial\varphi/\partial x)^2 + \sum_\alpha \varphi(x_\alpha)\right] \tag{5.43}$$

and performing the integral over k-space, we arrive at the expression

$$\langle Z^n\rangle = \int dx_1\cdots dx_n \langle x_1\cdots x_n|e^{-t\mathcal{H}_n}|0\cdots 0\rangle$$
$$\sim \int D\varphi e^{-tE_0}\prod dx_\alpha \exp\left(-\frac{1}{4n\Gamma t}\left(\sum_\alpha x_\alpha\right)^2 + \sum_\alpha \phi(x_\alpha)\right). \tag{5.44}$$

It is here that some basic results shake loose. To isolate the scaling behavior we define rescaled variables, $x = t^\zeta y$ and $\varphi(x) = t^\omega\psi(y)$. To leave unaltered the gaussian φ measure, $\sim \exp[-\int dx\times(\partial\varphi/\partial x)^2]$, we require $\zeta = 2\omega$. Furthermore, if we demand that the two terms in the above equation scale with t in the same manner, we find the famed exponent relation $\omega = 2\zeta - 1$. Taken together, they yield the anticipated wandering and free energy fluctuation exponents. Thus rescaled, our last lengthy equation becomes

$$\int\prod dy_\alpha \exp\left\{-t^{1/3}\left[\frac{1}{4n\Gamma}\left(\sum_\alpha y_\alpha\right)^2 + \sum_\alpha \psi(y_\alpha)\right]\right\} \tag{5.45}$$

which under the assumption of replica symmetry, $y_\alpha = \xi$ for all α, gives

$$\langle Z^n\rangle = \int D\psi \exp\left(-(1/4\kappa)\int dx(\partial\psi/\partial x)^2\right) e^{-nt^{1/3}E_{min}(\psi)} \tag{5.46}$$

where E_{min} is the energy that dominates our saddle point integration in the large t limit. It is determined by the value ξ which minimizes the one-body energy,

$$E(\psi) = \xi^2/4\Gamma + \psi(\xi). \tag{5.47}$$

We have come a long way indeed – having reduced the full-blown DPRM to the consideration of curious little statistical mechanics problem of a point particle attached to the origin with a Hookian spring (of spring constant $1/2\Gamma$), and subject to a potential ψ, the slope of which is a gaussian random variable of variance 2κ; recall the measure and Parisi's sly trick. In fact, this little "toy model" is a veteran performer in the subject of disordered systems, see [SVBO88].

Note that we have already unearthed the finite-size correction to the disorder averaged free energy. From (5.46), we see that

$$\langle f\rangle = -\langle \ln Z\rangle = t\kappa^2\Gamma/3 + t^{1/3}\langle E_{toy}\rangle \tag{5.48}$$

which implies that the corrections to the free energy per unit length vanish as $t^{-2/3}$, a prediction also known from the kinetic roughening context [KrM90], and recently confirmed via transfer matrix simulations of the DPRM [HH91]; see Section 5.4.4. Furthermore, inclusion of CM motion has generated proper behavior for all the DPRM free energy cumulants,

$$[c_n(f)]^{1/n} = t^{1/3}[c_n(E_{toy})]^{1/n} \quad \text{for all } n \tag{5.49}$$

whereas Kardar's ground-state wave function produced only a nontrivial, but correct third cumulant, said nothing explicit regarding c_2, and predicted that fourth and higher order cumulants of the free energy vanished identically. It should be stressed that while the introduction, by Parisi's trick, of φ into the problem as a dummy functional integration variable seemed innocent enough, its role in the subsequent solution was crucial. Moreover, the random variable φ possesses an immediate physical interpretation in the context of the original DPRM problem – that of an effective potential acting on the head of the polymer. Its great advantage arises from the fact that, while the true pinning impurities $\mathcal{V}(x,t)$ of the original DPRM are uncorrelated, the effective potential φ has long-range correlations:

$$\langle(\varphi(x) - \varphi(y))^2\rangle \sim |x - y|. \tag{5.50}$$

Consequently, if one is interested in determining the probability distribution to find the "head" of the polymer at site x after time t, it is possible, using the properties of $\varphi(x)$, to show that [Pa90,FH91]

$$\langle \ln P(x,t)\rangle = -x^2/4\Gamma t \tag{5.51}$$

a result that has been confirmed in the numerical transfer matrix studies by Mezard [Mez90], and

$$\langle \ln^2 P(x,t)\rangle - \langle \ln P(x,t)\rangle^2 = \frac{V^2}{2\Gamma}|x| \tag{5.52}$$

which appears to hold true in these same simulations only for $x < t^{2/3}$, saturating at larger values. Fisher and Huse [FH91] have sought to explain this effect by arguing that since two polymers starting with an initial separation greater than $t^{2/3}$ cannot interfere with one another, the correlation function of the effective potential $\varphi(x)$, given by (5.49), should really saturate for distances of that order. They suggest adding a mass term $m_0^2\varphi^2$ to the action, which leads in purely heuristic fashion to the result $\langle\psi(x)\psi(y)\rangle = (1/m_0)[1 - \exp(-m_0|x-y|)]$, which fits the Mezard data rather well.

As we shall see in a moment, these relations are of great utility in pinning down, for a given lattice simulation of the DPRM, the associated phenomenological parameters Γ and V^2 defined in the continuum formulation. Finally, one can also establish the asymptotic, nongaussian character of the disorder-averaged positional probability distribution, confirming Eq. (5.40)

$$\ln\langle P(x,t)\rangle \sim -(x/t^{2/3})^3, \quad \text{for } x \gg t^{2/3}. \tag{5.53}$$

Although it is numerically difficult to access this cubic behavior of the tails [see, e.g., HH91], there has been recently, confirmation by Goldschmidt and Blum [GB93].

• *Closing note:* To produce precise numbers for the amplitude prefactors, it is necessary to study the statistical properties of the toy model via computer simulation [BO90]. We simply generate the gaussian process ψ and search for the value of ξ that minimizes the toy model Hamiltonian. Averaging over 20000 realizations of ψ landscape and keeping track of the fluctuating values of the transverse extension ξ and energy ϵ of the point particle, Bouchaud and Orland deduced that

$$\langle\xi^2\rangle^{1/2} = 1.02(\Gamma V^2)^{1/3}, \quad \langle\xi^4\rangle^{1/4} = 2.35(\Gamma V^2)^{1/3}, \quad \langle\epsilon\rangle = -0.76(V^4/\Gamma)^{1/3}.$$

Unfortunately, these numbers presently disagree with existing transfer matrix data [HH91]; for example, the ratio of the even positional moments being too big. These discrepancies are most likely

due to a weak breaking of replica symmetry in the $1+1$ DPRM, which apparently leaves unaffected the exponents, but causes some minor troubles with the amplitudes.

5.4.3. Replica scaling theory and Hartree-Fock approximation

Zhang has suggested an nonperturbative means of obtaining the exponent ω analytically, based upon the *replica-scaling* method, which uses the leading n-dependence of the disorder-averaged, replicated partition function $\langle Z^n \rangle$ to obtain the free energy fluctuations via Laplace transform. Recall that our disordered DPRM model is mapped, by means of the replica technique, onto a quantum mechanical, n-body bound-state problem [Kard87a]. In anticipation of the bound-state energy result, we may express $\langle Z^n \rangle = \exp(-tE_0(n))$, where the groundstate energy is $E_0(n) \sim -n^\beta$, for asymptotically large t and n. From the knowledge of all these moments (n being finite and positive), we can reconstruct the probability distribution function [Z89b,Z90d] of the free energy $F(t) = \ln Z$ (see (5.70) for precise definition of $P(F)$ and its relation to $\langle Z^n \rangle$)

$$P(F) \sim \exp\left\{-c\frac{|F-F_0|^{\eta_\pm}}{t^{\eta/\beta}}\right\}, \quad \eta_\pm \quad \text{for } F - F_0 \gtrless 0 \tag{5.54}$$

where $\eta_+ = \beta/(\beta-1)$, with $\beta > 1$, and c being a constant. At the present, η_- cannot be evaluated analytically yet, due to the difficulties of negative moments $\langle Z^n \rangle$ ($n < 0$). From (5.54) we deduce that $\Delta F \sim t^{1/\beta}$, or the desired exponent $\omega = 1/\beta$. Note that, generally, $E_0(n)$ contains subleading terms in n, which depend on the approximation scheme employed. Nevertheless, thanks to the Laplace transform, only the leading term in n determines the scaling behavior. This is to be contrasted with the traditional replica trick where the opposite limit $n \to 0$ is assumed.

Our problem is thus reduced to finding the ground-state energy of the Schrödinger equation, where the number of particles n is assumed to be large. Here, we restrict ourselves to the $d = 1+1$ case only. For the standard DPRM, where all n particles are subject to mutual attractive interaction, we have

$$\left\{-\sum_{i=1}^{n}\partial_i^2 - \sum_{i>j}\delta(x_i - x_j)\right\}\psi(x_1,\ldots,x_n) = E_0(n)\psi(x_1,\ldots,x_n). \tag{5.55}$$

As discussed in Section 5.4.1, the $1+1$ DPRM has been solved using Bethe ansatz [Kard87a], where it was found, to leading order, that $E_0(n) \sim -n^3$. Why might we bother with approximative methods if we can solve the model exactly? The reason is that solvable cases are extremely rare, for most problems there is no hope to a solution. Nevertheless many approximations can be used to extract the leading order physics from such problems. To do this we need to calibrate our approximative tools using the available exact solution, then extend these tools to more complicated cases. Here a Hartree-Fock approximation will be invoked. For details of its application to this celebrated many-body problem (n bosons in one spatial dimension, interacting via an attractive contact potential) see a recent textbook [NO88], where comparison is made between the exact Bethe ansatz solution and that of the Hartree-Fock mean-field approximation, making manifest their agreement to leading order in n, a fact which follows from of a more general understanding within the context of a $1/n$ expansion. We outline the Hartree-Fock procedure below. Let us consider the following trial function

$$\psi = \prod_{\alpha=1}^{n} \varphi(x_\alpha), \tag{5.56}$$

the idea is to assume everybody has the same single particle wave function. The Hartree-Fock method consists in considering only one particle in a background of all the others. It is clear that the density function is just $\rho_n(x) = |\varphi(x)|^2$ and we can relate it by

$$\rho_n(x) \equiv \sum_{\alpha=1}^{n} \delta(x - x_\alpha). \tag{5.57}$$

For n attracting particles we can define a single-particle wavefunction $\varphi(x)$, which satisfies the self-consistent equation:

$$\{-\partial^2 - (n-1)|\varphi(x)|^2\}\varphi(x) = \epsilon\varphi(x), \tag{5.58}$$

with the normalization condition $\int dx|\varphi(x)|^2 = 1$, and the boundedness requirement $|\varphi(x \to \pm\infty)| \to 0$; ϵ denotes the groundstate energy of a single particle, while the many-body bound-state has energy $E_0(n) = n\epsilon$. In the above equation $n-1$ will be replaced by n, in keeping with the large-n nature of Hartree-Fock approximation. Fortunately, this nonlinear equation is well known to be integrable, possessing the normalizable soliton solution

$$\varphi(x) \sim \pm\sqrt{n}/\cosh(nx), \tag{5.59}$$

provided $\epsilon = -n^2$. We see that Eq. (5.59) agrees with the exact integration of the whole wave function. Thus we obtain the result $E_0(n) \sim -n^3$, in agreement with the exact Bethe ansatz solution [Kard87a]. From (5.59), it is easy to see that the typical size x_0 of the bound-state scales as $x_0 \sim 1/n$. We must merely note that, with n particles confined to a small region R, the total kinetic energy $\sim n(1/x_0)^2$ opposing the collapse should be of the same order of magnitude as the ground-state energy $\sim -n^3$.

Remark: *Concerning higher dimensions, the curious reader may wonder why not apply the above methods to the most interesting case for DP in $d = 2 + 1$? The difficulty is a technical one and it may well be unsurmontable. Using the replica trick, one still obtains a Schrödinger equation for a n-body pure system. The story stops here, however, since there is no Bethe Ansatz solution in higher dimensions. Proceeding with the approximative approach of Hartree-Fock, we would obtain an equation*

$$\{-\nabla^2 - n\varphi^2\}\,\varphi = \varepsilon\varphi(\boldsymbol{x}) \tag{5.60}$$

where ∇^2 is the d-dimensional Laplacian. If we assume the spherical symmetry, which is plausible for the ground state wave function, $\nabla^2 = \partial_r^2 + r^{-1}(d-1)\partial_r$ only the radial part remains. The resulting equation, though one-dimensional, has an extra term proportional to $r^{-1}\partial_r$ (representing friction force). The equation is not integrable. Even by numerical integration only for a discrete set of values of the parameters the solution exists [Zinn84].

Comment – regarding justification of the large n limit, for which we can apply Hartree-Fock approximation. *In the original formulation, the DP partition function Z is a fluctuation quantity (so*

is h through $Z = e^h$). The moments $\langle Z^n \rangle$ (n large) preferentially yield information on rare and large fluctuations, less on mild and more common ones. Physically this is desirable since large and rare fluctuations usually characterise the overall fluctuation behaviour (see discussions on power-law noise). In any case, for fluctuation information, there is no need to invoke the usual $n \to 0$ limit.

Unlike the Bethe ansatz, the replica-scaling analysis is easily generalized to handle spatially correlated disorder [Z90d]. Consider the DPRM path integral formulation (5.1), but now with random pinning potential possessing the variance $\langle V(x,t)V(x',t')\rangle = R(x-x')\delta(t-t')$, where the spatial correlation function $R(x) \sim x^\alpha$ includes the uncorrelated DPRM ($\alpha = -1$, because $\delta(x) \sim 1/x$), as well as the domain wall in the random-field problem ($\alpha = 1$). In general, we consider the entire range $-1 \leq \alpha \leq 1$. Let us set up the following scheme. Consider the replicated average over the partition function,

$$\langle Z^n \rangle = \langle \exp -nF \rangle = \int Dx_1 \cdots Dx_n \exp -H(n) \tag{5.61}$$

where

$$H(n) = \int dt \left[\sum_{i=1}^{n} \dot{x}_i^2 - \sum_{i,j} R(x_i(t) - x_j(t)) \right]. \tag{5.62}$$

Consider $-1 \leq \alpha < 0$ first. With $R(x) \sim 1/x^{|\alpha|}$, we see the above potential favors bound formations, since the n objects like to stay together in order to reduce the system's energy. Thus, the interaction energy would apparently favor complete collapse; i.e., all n directed polymers overlapping on top of each other. This is prevented by the kinetic energy (strictly speaking, entropy) term.

Instead of the Bethe ansatz method, let us find the approximate solutions by performing a Flory-type scaling analysis. Since we anticipate a bound-state, the kinetic part behaves as nt/x^2, rather than the usual form nx^2/t for unrestricted space. This is because the limited room of a bound-state induces an entropy loss, resulting in a steric repulsion between the replicas [see, e.g., MF86r]. By contrast, the interactive part behaves as $n^2 t/x^{|\alpha|}$, where the limit $n \gg 1$ is understood. Put both in the exponential,

$$\exp\left(-n\frac{t}{x^2} + n^2 \frac{t}{x^{|\alpha|}} \right) \tag{5.63}$$

For given n and t, we look for the optimal size x_0 and find,

$$x_0 \sim 1/n^{1/(2-|\alpha|)} \tag{5.64}$$

which coincides with our earlier result for the uncorrelated DPRM case $x_0 \sim 1/n$ for $\alpha = -1$. Substituting back into our original equations, we obtain the ground-state energy

$$\exp -E_0(n), E_0(n) \approx -n^\beta, \quad \beta = \frac{4-|\alpha|}{2-|\alpha|} \tag{5.65}$$

where, again, we reproduce the uncorrelated DPRM case $\alpha = -1$, $E_0(n) \approx -n^3$. Note that we take care of signs here, but pay no attention to proportionality constants.

Let us now turn to the case $0 < \alpha \leq 1$. Similar considerations show that the replicated system has repulsive interactions among the n polymers since the potential $R(x)$ now favors large separations. Therefore the above method of estimating bound states is no longer appropriate. How can one treat such repulsive interactions, where the polymers wish to escape from each other to infinity? The answer is that they all have a common initial condition at the origin – remember our earlier discussion regarding center of mass motion. Consequently, their separation is small early on, but an increasing function of t. Of course, for $t \to \infty$, the mean polymer separation diverges – that is, no translational states. For repulsive interactions, the kinetic part takes the usual form nx^2/t, so we have

$$\exp\left(-n\frac{x^2}{t} + n^2 t x^{\alpha}\right). \tag{5.66}$$

Minimizing the energy, we find

$$x_0 \sim (nt^2)^{1/(2-\alpha)} \tag{5.67}$$

and our exponential becomes

$$\exp(+n^{\beta}t^{\gamma}), \quad \beta = \frac{4-\alpha}{2-\alpha}, \quad \gamma = \frac{2+\alpha}{2-\alpha} \tag{5.68}$$

Note the positive sign in that exponential.

But how do we use the above results to infer the scaling behavior of directed polymers subject to this long-range correlated disorder? First note that in the attractive and repulsive cases, we obtain the following form,

$$\langle \exp(-nF) \rangle = \exp(n^{\beta}t^{\gamma}) \tag{5.69}$$

where the average is made on disorder samples. Suppose there exists an *effective* distribution $P(F)$, defined by the condition

$$\int P(F)\exp(-nF) \equiv \langle \exp(-nF) \rangle = \langle Z^n \rangle. \tag{5.70}$$

Inverting this Laplace transform, we find

$$P(F) \sim \exp\left\{-(\Delta F)^{\eta_+}/t^{\delta}\right\} \tag{5.71}$$

where $\eta_+ = \beta(\beta - 1)$, $\delta = \gamma(\beta - 1)$, and $\Delta F = F - F_0 > 0$. From this effective $P(F)$, we can read off the scaling behavior of the free energy,

$$\Delta F \sim t^{\delta/\eta_+} = t^{\gamma/\beta}, \quad \omega = \gamma/\beta \tag{5.72}$$

so that the replica scaling prediction [Z90d] for the correlated DPRM free energy fluctuation exponent ω reads

$$\omega = \begin{cases} \dfrac{2-|\alpha|}{4-|\alpha|}, & -1 \geq \alpha \geq 0, \\ \dfrac{2+\alpha}{4+\alpha}, & 0 \leq \alpha \leq 1 \end{cases} \tag{5.73}$$

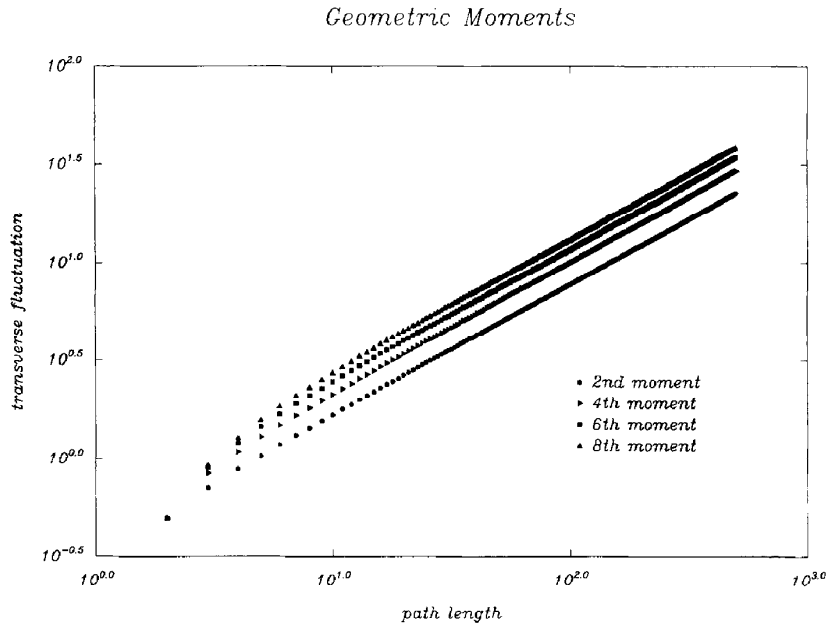

Fig. 5.8. log-log plot of the first four positional moments of the $T = 0$ 1+1 DPRM [HH91].

there being a discontinuous slope at $\alpha = 0$, where the replica interaction changes from attraction to repulsion. Thus, within the replica scaling picture, we see that attractive and repulsive interations play very different roles, as revealed in replica space, suggesting a naive application of Flory scaling theory may be inappropriate for any $\alpha < 0$. Of course, for long-range correlated disorder, $\alpha > 0$, his results coincide with the dynamic RG and DPRM functional RG predictions, since all treatments are inherently Flory-like in this regime – see Sections 4.3.1, 5.5.1.

5.4.4. *Transfer matrix studies. II. Probability distributions and amplitudes*

The general analytical predictions of the gaussian, uncorrelated 1 + 1 DPRM have been put to the wall, so to speak, by subsequent numerical transfer matrix studies [Mez90, KBM91a, HH91, KrMHH92, AF92]. Although the outcome from this confrontation between theory and numerical experiment has left the extended Bethe ansatz solution in a rather favorable light, it is also clear that it's hardly the whole story. We will address these matters separately for the geometric and free energy fluctuations of the 1+1 DPRM. Thanks to a mapping via the KPZ equation, the latter will have strong implications for dynamic scaling of kinetically roughened edges of 2d ballistic deposits and Eden clusters.

- *Geometric properties [HH91].*

(i) *Moments:* In Fig. 5.8 are shown the first four even positional moments of the globally optimal path of the 1 + 1 DPRM at zero temperature. The numerical work, performed on a SparcStation 2, involved calculating the nth root of the disorder average of x^n, resulting from 10^5 realizations of the random energy landscape traversed by directed paths of length 500 steps. As is evident from the figure, the large number of realizations have made it possible to minimize the statistical noise of the data and to obtain reasonably good scaling as soon as the walker has covered just a dozen steps or so. Performing a least squares fit to the data to pick off the critical indices,

we find 0.667 ± 0.005 in all cases, indicating that the wandering exponent ζ controls the full positional probability distribution. Indeed, if we examine the amplitude prefactors of these even moments, one discovers that the probability distribution of the globally optimal path is certainly not gaussian, possessing moments in the ratio 1.00 : 1.28 : 1.52 : 1.72.

(ii) *Positional probability distributions:* Fig. 5.9 explores the disorder-averaged positional probability distribution $\langle P(x,t)\rangle$ of the $1+1$ DPRM that is responsible for generating the above moments and comes from the very same zero temperature simulation as above, involving 10^5 realizations of randomness. In Fig. 5.9a, which plots $\ln\langle P(x,t)\rangle$, the data for three separate time slices, t=100, 200, and 500, are collapsed to a single universal curve that is evidently *symmetric* and entirely consistent with the scaling form $\langle P(x,t)\rangle \sim \exp-(|x|/t^{2/3})^{\rho}$. Taking a logarithm of these collapsed data, one finds that the distribution has some gaussian character, but the slope certainly begins to exceed two at $x/t^{2/3} \approx 1$. In fact, a least-squares fit in this regime, see Fig. 5.9b, gives an effective exponent $\rho \approx 2.2$. Unfortunately, even with 10^5 realizations of the disorder we could not access sufficiently the depth of the tail to test Eq. (5.40) with $\rho = 3$. However, more recent studies [GB93,Klafter and Zumofen, unpublished] have reported findings that do support the scaling law with $\rho = 3$, at least deep in the tail region.

As is apparent to the educated reader, the process of disorder averaging and taking the logarithm do not commute, so that $\langle \ln P(x,t)\rangle \neq \ln\langle P(x,t)\rangle$. We just discussed the latter, and now in Fig. 5.10a we show the former for a finite temperature simulation of the $1+1$ DPRM, in which the Boltzmann weights are evolved according to the prescription,

$$Z(x,t+1) = e^{-\mu(x,t)}[Z(x,t) + \gamma Z(x-1,t) + \gamma Z(x+1,t)] \tag{5.74}$$

where the polymer follows the traditional links of the upper half-plane (so-called *slab* geometry), whose vertical bonds have uncorrelated random energies $\mu(x,t)$ drawn from a uniform distribution of width s and variance $\sigma^2 = s^2/12$, and γ, the microscopic diffusion constant, is set by the elastic energy cost of transverse jumps. It is apparent that the data, rescaled and collapsed from three time slices, fall nicely on a parabola, in complete agreement with Parisi's prediction, Eq. (5.51). In fact, one can use the data to determine the renormalized macroscopic diffusion constant Γ, which is a phenomenological parameter in the continuum description, arising from a given set of input lattice quantities for the simulation at hand [KrMHH92]. Fig. 5.10b shows the quantity $\langle \ln^2 P(x,t)\rangle - \langle \ln P(x,t)\rangle^2$, which, as noted first by Mézard [Méz90], is consistent with the Parisi second result, Eq. (5.52), for small values of $x/t^{2/3}$, but eventually saturates on either side, presumably via the mechanism proposed by Huse and Fisher [HF91]. Armed with Γ from the previous figure, we can ascertain the renormalized disorder strength V^2 from this plot. As discussed by Krug, Meakin and Halpin-Healy [KrMHH92], it is necessary to pin down the values of Γ and V^2 for a particular simulation in order to extract meaningful estimates of the universal amplitudes characteristic of the strong KPZ coupling fixed point.

- *Free energy properties [KBM91a,HH91,KrMHH92,AF92].*

(i) *Finite-size effects:* In Fig. 5.11, we exhibit related data [HH91] for the disorder-averaged free energy per unit length of a finite temperature 1+1 DPRM, done in the manner of Kardar [Kard85b]. This and all available such data are in agreement with the Bouchaud-Orland prediction [BO90] which suggests that the finite-size correction vanishes as $t^{-2/3}$. It should be stressed that F/t always approaches its asymptotic value from above, i.e. wiht positive slope. This is natural because the DPRM is close kin to the SS model [TKW91], which has $\lambda < 0$,

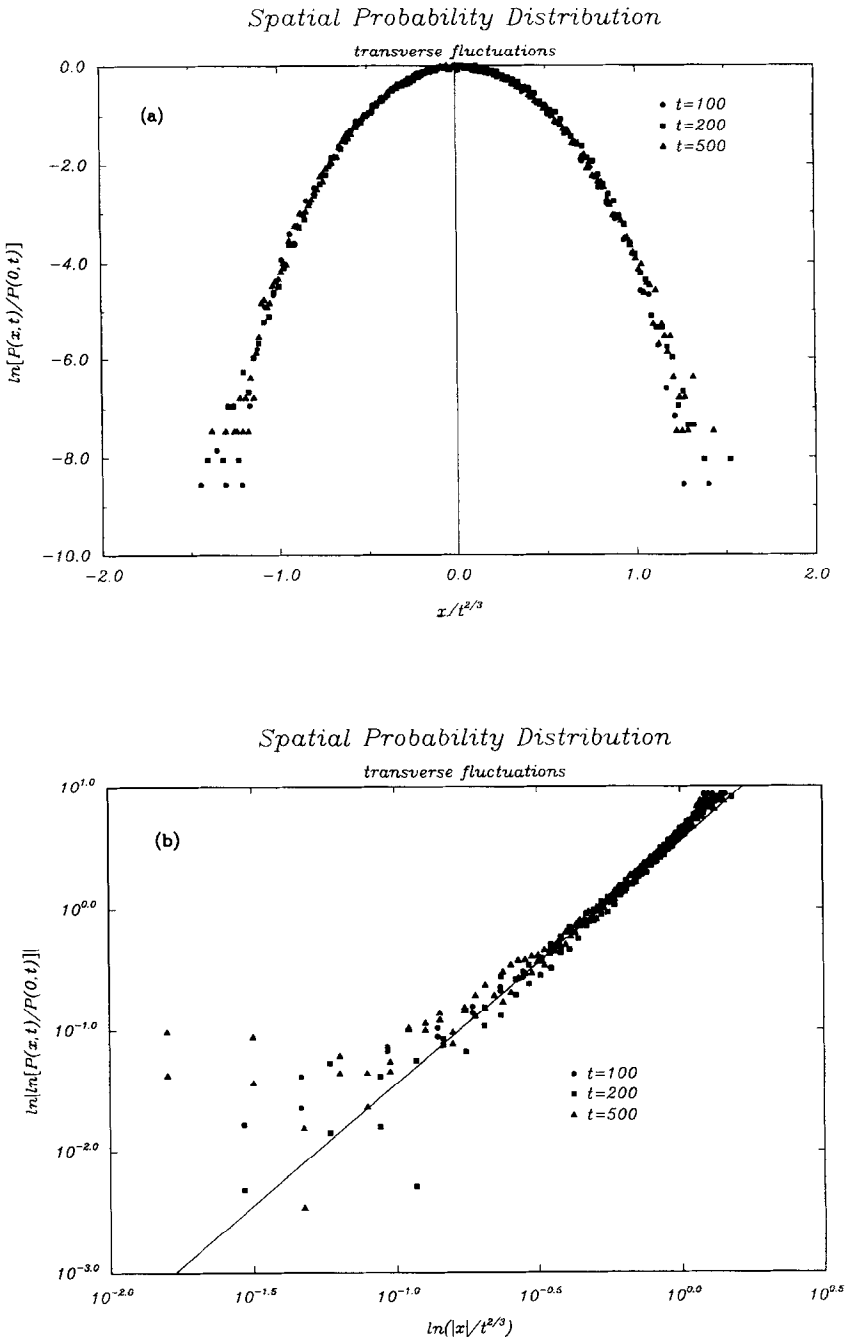

Fig. 5.9. *Symmetric* positional probability distribution $\langle P(x,t)\rangle$ for $T = 0$ 1+1 DPRM. (a) $\ln\langle P(x,t)/P(0,t)\rangle$ versus $|x|/t^{2/3}$, exhibiting data collapse for three separate time slices. (b) $\ln|\ln\langle P(x,t)/P(0,t)\rangle|$ versus $\ln(|x|/t^{2/3})$; for increasing abscissa, the data pull away from the line of slope 2, indicating nongaussian behavior [HH91].

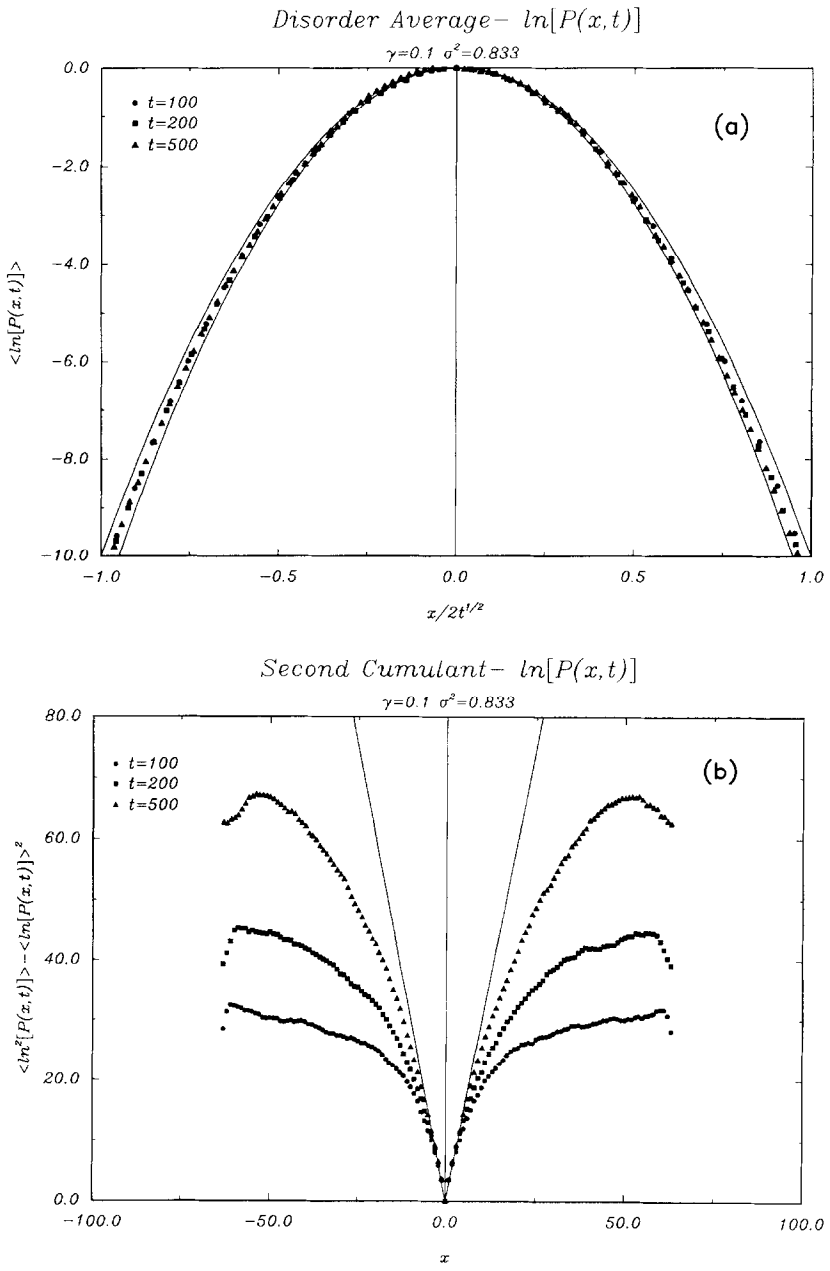

Fig. 5.10. (a) Disorder average of the logarithm of positional probability distribution, $\langle \ln P(x,t) \rangle$, for the finite temperature 1+1 DPRM (500 steps, 10^4 realizations of the random energy landscape) with microscopic input parameters $\gamma = 0.1$ and $\sigma^2 = 5/6$; data collapse for three separate time slices. The inner parabola corresponds to $\Gamma = 0.09$, while the outer one has $\Gamma = 0.10$. We therefore estimate, via (5.51), the DPRM phenomenological parameter $\Gamma(\gamma = 0.1, \sigma^2 = 5/6) = 0.095 \pm 0.005$. (b) Second cumulant of $\ln P(x,t)$ for the same time slices. The solid line corresponds to the function $3|x|$, which in view of the Parisi result (5.52), implies $V^2 = 0.57$ [KrMHH92].

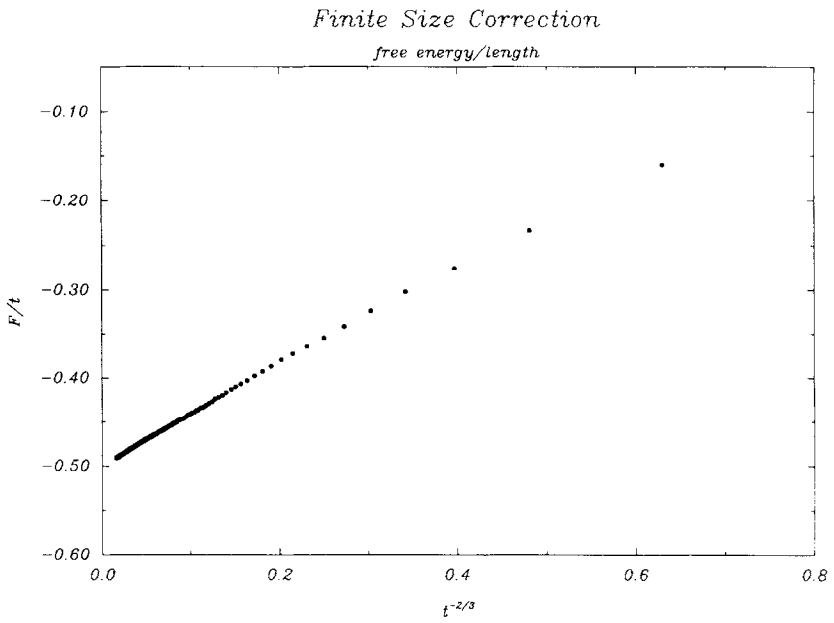

Fig. 5.11. Finite-size correction to the disorder-averaged free energy per unit length. 10^4 realizations, 500 steps, finite temperature simulation with $\gamma = 0.1$ and σ^2=5/6. This quantity is analogous to the early-time finite-size correction to the growth velocity in the kinetic roughening context, see [KrM90].

recall Fig. 3.10, it being known that KPZ nonlinearity and free-energy finite-size correction have opposite signs [KrMHH92]; see also Fig. 3.5b. Finally, with regard to the many-dimensional DPRM, it can be shown that, more generally, we expect the finite size correction to go to zero as $t^{\omega-1}$, a result which has been nicely confirmed for the d=2+1 case, where $\omega \approx 1/4$ [KBM91a].

(ii) *Cumulants:* Fig. 5.12 reveals the scaling behavior of the second and third cumulants of the free energy for a finite-temperature simulation. The numerical work here involves 5×10^4 realizations of randomness for $t = 500$. Even with the modest system sizes, f_{rms} scales nicely with an exponent $\omega = 0.333 \pm 0.003$. The third order cumulant, by contrast, while scaling with essentially the same exponent, is considerably noisier. In fact, although f_{rms} scales well for as few as 10^3 realizations of the random energy landscape, it is nearly impossible to observe proper scaling of the third-order cumulant of the free energy unless one performs exhaustive averaging. The importance of the third cumulant was unearthed for the first time in Kardar's calculation of the DPRM free energy (Section 5.4.1), but it is only within the context of the Bouchaud-Orland analysis that we see all free energy cumulants scaling properly. In particular, they show explicitly that $f_{rms} \sim t^{1/3}$, a subdominant contribution that was lost in Kardar's solution.

(iii) *Full Probability distribution:* The 1+1 DPRM possesses a free energy probability distribution [DG88,NR88,HH89b] which is clearly asymmetric and nongaussian, see Fig. 5.13. An attempt [KBM91a] has been made to fit the tails on either side of this disorder-averaged free energy probability distribution, with power laws of the form

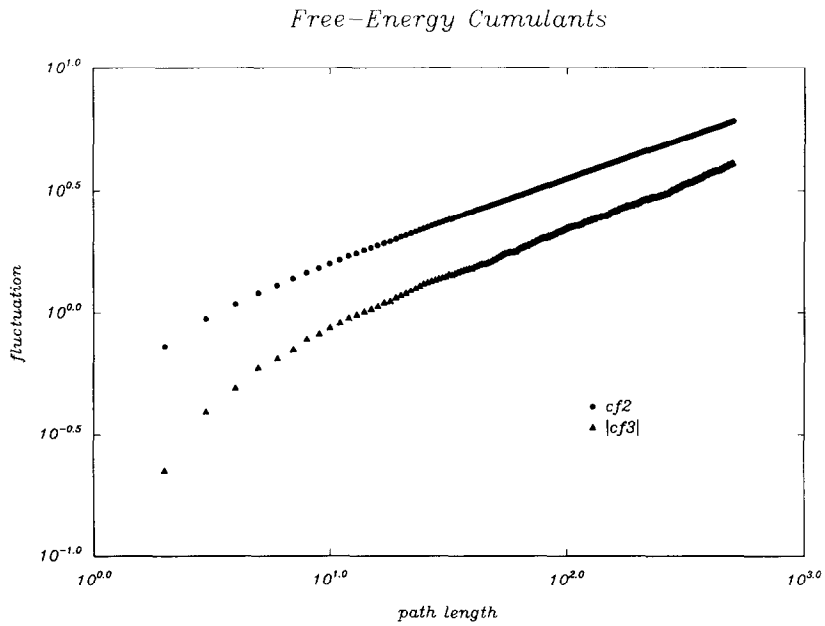

Fig. 5.12. Negative, third-order cumulant of the free energy, $c_3(f)$ scales with an exponent 0.37 ± 0.02, in agreement with, though slightly larger than Kardar's predicted value. The second-order cumulant $c_2(f)$, with $\omega = 0.333 \pm 0.003$, is in complete accord with the expectation 1/3. Finite-temperature simulation with 5×10^4 realizations of disorder required to elicit reasonable scaling of the third cumulant [HH91].

$$P(a) \simeq \begin{cases} e^{-c_-|a|^{\eta_-}}, & a < -1 \\ e^{-c_+|a|^{\eta_+}}, & a > 1 \end{cases} \tag{5.75}$$

for $1 < |a| < 5$, where $a = (F - F_0)/t^{\omega}$ is a normalized measure of the deviation from the mean and $c_{\pm}$ are constants. One finds $\eta_- = 2.4 \pm 0.2$ and $\eta_+ = 1.6 \pm 0.2$, the latter being not at all inconsistent with the replica scaling theory prediction of Zhang [Z89a,Z90d] which suggests $\eta_+ = 1/(1 - \omega) = 3/2$. For a beautiful illustration of the equivalence of the kinetic roughening phenomena and the statistical mechanics of the DPRM, make a point of examining the final figure of [KBM91a], where an explicit comparison is made between the early-time height fluctuations exhibited by the Kim-Kosterlitz RSOS growth model and the free energy fluctuations of the directed polymer. It makes a very strong case for the existence of universality across the border between stochastic growth models and the DPRM. The equivalence between the evolution algorithms and the lattice DPRM is made beautifully manifest at the microscopic level via the waiting-time formulation of growth, as discussed by Tang, Kertesz and Wolf [TKW91] for SS edges and Roux, Hansen and Hinrichsen [RHH91] for Eden clusters.

(iv) *Skewness and kurtosis:* The asymmetry of the above distribution is conveniently characterized by the normalized third and fourth cumulants, otherwise referred to as the skewness $s = c_3/c_2^{3/2}$ and kurtosis, $\hat{c}_4 = c_4/c_2^2$. The approach to asymptopia of the former is illustrated in Fig. 5.14, from which we can deduce the value $s = -0.296 \pm 0.028$ [KrMHH92]. The latter has been studied in the DPRM context by [KBM91a], attaining the universal value $\hat{c}_4 = +0.16$.

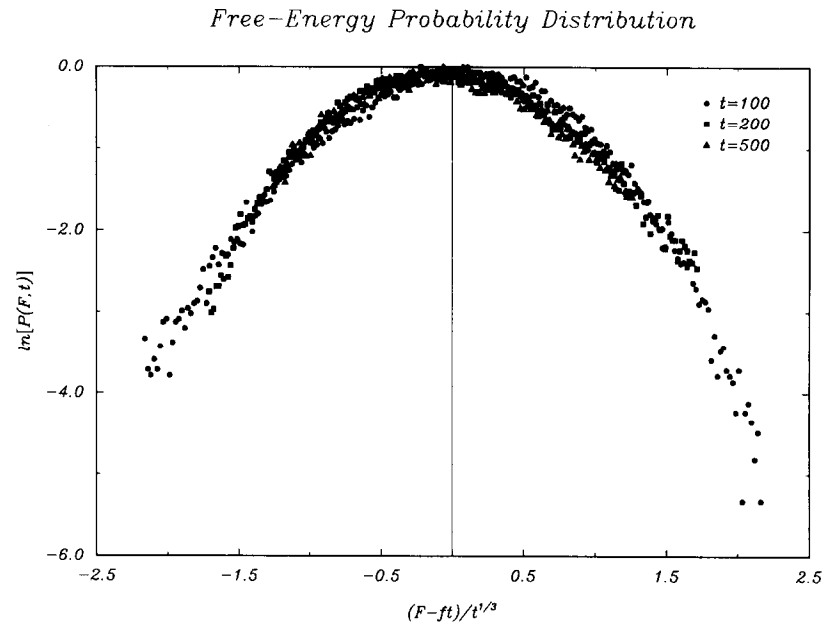

Fig. 5.13. *Skewed* free-energy probability distribution $P(F,t)$ of the 1+1 DPRM at finite temperature. Plotted is $\ln[P(F,t)]$ vs normalized deviation from the mean free energy, in data collapsed form for three separate time slices; 5×10^4 realizations of the random energy landscape [HH91].

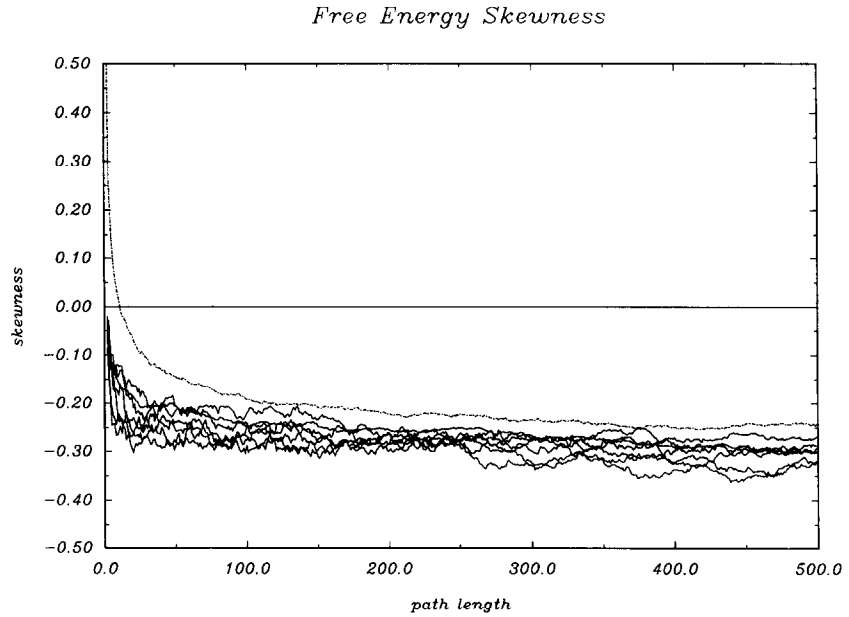

Fig. 5.14. *Skewness* of the 1+1 DPRM free energy probability distribution. The curves correspond to simulations done with different input values of the lattice diffusion constant γ and disorder strength σ^2. From these transfer matrix calculations, we estimate the skewness $s = -0.296 \pm 0.028$ [KrMHH92].

5.5. Variations on a theme

As discussed in Section 4 members of the community have considered the effects of various forms of noise upon the kinetic roughening in stochastic growth models, including power-law, correlated gaussian, and quenched varieties. Related efforts were mounted, independently, within the context of directed polymers in random media. In fact, investigations into the role of disorder that was correlated gaussian (i.e., gaussian on the sites, but correlated between neighboring sites) arose very early on because of its connection to the phenomenon of domain wall roughening in disordered magnets, such as random-bond (RB) and random-field (RF) systems, as well as models that interpolated between the two [Kard87b,N87], a subject that evolved very naturally within the broader setting of diverse manifolds in random media [HH89a]. Here, we discuss briefly the DPRM with correlated noise, where a functional RG calculation yields the same exponents as the 1-loop dynamic RG of the KPZ equation. We follow with a short treatment of the DPRM subject to power-law noise, presenting some numerical aspects and Zhang's Flory argument for the wandering exponent. We conclude with the very rich subject of directed polymers with time-independent noise, complete with possible applications to diffusion in random media, models of punctuated biological evolution, and the roughening of vortex lines in ceramic superconductors by columnar defects.

5.5.1. Correlated noise [Kard87b,N87]

Recall the DPRM partition function, but consider now the possibility that there may exist substantial *spatial* correlation between random energies at neighboring sites; for simplicity, we restrict ourselves to pinning energies that are gaussian, with zero mean, and possessing the correlator

$$\langle \mathcal{V}(x',t')\mathcal{V}(x,t)\rangle \sim |x-x'|^{2\rho-1}\delta(t-t') \tag{5.76}$$

the notation motivated by our discussion, in Section 4.3.1, of KPZ subject to spatially correlated noise, where we noted anomalous kinetic roughening. In the context of the DPRM, spatially correlated disorder leads to anomalous wandering of the directed polymer. Indeed, if the correlation becomes sufficiently long-ranged, the wandering exponent can become as large as unity; for example, it is known, see [Z86b], that for $\rho = 1$, where the DPRM corresponds to roughened interface in a 2d RF Ising model, the wandering exponent reaches this limiting value, $\zeta_{RF} = 1$ [FGIK83]. An approximate functional renormalization group calculation [HH90] for the many-dimensional DPRM indicates that

$$\zeta(\rho) = \begin{cases} 2/3, & \text{if } \rho < 1/4; \\ 3/(5-2\rho), & \text{if } 1/4 < \rho < 1. \end{cases} \tag{5.77}$$

for the 1+1 dimensional case, a result which is complete accord with the dynamic RG analysis of the KPZ equation with correlated noise [MHKZ89]. The interesting feature is the apparent existence of a short-ranged fixed point function responsible for forcing the DPRM wandering exponent to its classic value; that is, provided the spatial correlations fall off sufficiently fast ($\rho_c = 1/4$). Furthermore, the wandering exponent for $\rho > \rho_c$ is consistent with that determined via a generalized Imry-Ma arguments, familiar from the RF debacle [see GG84] and discussed in a nice paper by Kardar [Kard87b]. The functional RG notwithstanding, there exist several values of ρ for which the DPRM partition function ought to be analytically tractable, since they lead to gaussian functional integrals. In particular, for the RF case where $\rho = 1$, we obtain a (subtle) linear interaction between replicas,

while $\rho = 3/2$, the interparticle potential is quadratic. We leave the reader to pursue the slippery path associated with the former case, while we sketch out below the analysis involved in the latter.

5.5.2. A special example. Quadratic case [Pa90o,M90u]

For $\rho = 3/2$, the disorder-averaged, replicated partition function is gaussian and therefore, in principle, tractable. It is a model of n coupled harmonic oscillators. The problem has been addressed by Parisi [Pa90o], as well as Maritan [M90u]. Here we follow exactly Maritan's unpublished work. Maritan's starting point is the path integral

$$\langle Z^n \rangle = \int_{x_a(0)=0}^{x_a(t)=0} Dx_a \exp\left(-\int_0^t dt' \left[\sum_{a=1}^{n} \dot{x}_a^2(t') + \sum_{a,b=1}^{n} (x_a(t') - x_b(t'))^2 \right] \right). \tag{5.78}$$

Maritan's approach consists of direct integration of the above replicated partition function, which is clearly possible since all the terms in the exponential are of quadratic form. All we need do is proceed with the diagonalization We discretize the time axis, dividing the time interval $[0, t]$ into $T = t/\tau$ intervals of size τ, the position coordinate of the ath replica at the i^{th} time slice denoted $x_a(i)$, where $i = 0, \ldots, T$. The trajectories of the n replicas begin and end at the origin, $x_a(0) = x_a(T) = 0$. Following this regularization, we have

$$\langle Z^n \rangle = \int \prod_{a=1}^{n} \prod_{i=1}^{T-1} Dx_a(i) \exp\left(-\sum_{i=0}^{T-1} (x_a(i+1) - x_a(i))^2 \frac{1}{\tau} - \sum_{i=1}^{T-1} \sum_{a,b=1}^{n} (x_a(i) - x_b(i))^2 \tau \right). \tag{5.79}$$

Note that the argument of the exponential can be formally written as

$$-\frac{1}{\tau} \sum_{a=1}^{n} \sum_{i,j=1}^{T-1} x_a(i) T^{ij} x_a(j) - \tau \sum_{i=1}^{T-1} \sum_{a,b=1}^{n} x_a(i) V^{ab} x_b(i) \tag{5.80}$$

where the spatial matrix T and replica matrix V have the following elements,

$$T^{ij} = \begin{cases} 2, & \text{for } i = j; \\ -1, & \text{for } |i-j| = 1, \end{cases} \qquad V^{ab} = \begin{cases} 2(n-1), & \text{for } a = b; \\ -2, & \text{for } a \neq b. \end{cases}$$

The matrices T and V, since they act on different indices, can be diagonalized simultaneously. The eigenfunctions of V^{ab} are $\exp(2\pi i a p/n)$ with eigenvalue $\lambda_p = 2n(1 - \delta_{p,0})$, where the index $p = 0, \ldots, n-1$. For the kinetic piece, we have eigenfunctions $\sin(m\pi\omega/T)$ with eigenvalues $\Lambda_\omega = 2(1 - \cos\frac{\pi\omega}{T}) = 4\sin^2 \pi\omega/2T$ with $\omega = 1, \ldots, T-1$. Thus we are lead to

$$\langle Z^n \rangle = \text{const} \prod_{p=0}^{n-1} \prod_{\omega=1}^{T-1} \left(\frac{1}{\tau}\Lambda_\omega + \tau\lambda_p\right)^{-1/2} \tag{5.81}$$

so that

$$\ln Z^n = \text{const} - \frac{1}{2} \sum_{\omega=1}^{T-1} \ln\left(\frac{4}{\tau}\sin^2\frac{\pi\omega}{2T}\right) - \frac{n-1}{2} \sum_{\omega=1}^{T-1} \ln\left[\frac{4}{\tau}\sin^2\frac{\pi\omega}{2T} + 2n\tau\right]. \tag{5.82}$$

Now, so far as τ is finite, everything is well-defined and convergent, but if we consider the limit of vanishing τ, we're in trouble. We isolate the n-dependence of the above, finding

$$\ln\langle Z^n\rangle = -\frac{n-1}{2}F \tag{5.83}$$

where

$$F \equiv \sum_{\omega=1}^{T-1} \ln\left[\frac{4}{\tau}\sin^2\left(\frac{\pi\omega}{2T}\right) + 2n\tau\right] \tag{5.84}$$

Looking at the derivative,

$$\frac{dF}{dn} = \sum_{\omega=1}^{T-1} \frac{2\tau}{\frac{4}{\tau}\sin^2\left(\frac{\pi\omega\tau}{2t}\right) + 2n\tau}. \tag{5.85}$$

This sum can be evaluated in the complex plane via the integral,

$$\frac{dF}{dn} = \int_\gamma \frac{dz}{2\pi i}\frac{\operatorname{cotg} z}{z^2 + 2t^2 n}. \tag{5.86}$$

Closing the contour γ at infinity and using Jordan's Lemma, yields

$$\frac{dF}{dn} = -t^2\left[\frac{1}{2t^2 n} - \frac{\operatorname{cotg}\sqrt{2t^2 n}}{\sqrt{2t^2 n}}\right] \tag{5.87}$$

so that

$$F(n) = -\tfrac{1}{2}\ln n + \ln \operatorname{sh}\sqrt{2t^2 n} \tag{5.88}$$

which implies

$$\langle Z^n\rangle \to \exp\left[\frac{n-1}{4}\ln n - \frac{1}{\sqrt{2}}\sqrt{n}(n-1)t\right] \tag{5.89}$$

in the limit of diverging nt^2.

We will pause a moment before interpreting the physics of this solution to discuss an alternative, instructive method due to Parisi [Pa90o], who found the same result somewhat earlier using a technique reminiscent of the Bethe ansatz approach. Thus, Eq. (5.78) can be diagonalized via the Schrödinger equation, much as we did before,

$$\left\{-\sum \partial_\alpha^2 + \sum_{\alpha,\beta}(x_\alpha - x_\beta)^2\right\}\psi_0(x_1,\ldots,x_n) = E(n)\psi(x_1,\ldots,x_n). \tag{5.90}$$

The above equation describes a system of n mutually coupled harmonic oscillators. It is not hard see that the appropriate gaussian wavefunction, respectful of the symmetry of the problem, has the form

$$\psi(x_1, \ldots, x_n) \sim \exp\left\{-\frac{1}{2\sqrt{n}} \sum_{\alpha,\beta} (x_\alpha - x_\beta)^2\right\} \tag{5.91}$$

the constant being determined by trial and error. The groundstate energy is readily obtained by substitution of ψ_0 into our Schrödinger equation, yielding

$$E_0(n) = \frac{\sqrt{n}}{2}(n-1). \tag{5.92}$$

The careful reader may have noticed that this boundstate energy is not generally negative, in contrast to the Bethe ansatz solution for the case of uncorrelated noise. Nevertheless, this is the lowest energy. Thus, we see that Parisi's simple physical argument reproduces the result of Maritan's direct integration, aside from an n-dependent constant, which is irrelevant since only contributions involving both n and t matter in Zhang's replica scaling analysis [Z89a,Z90d]. According to this method, we have to invert

$$\langle Z^n \rangle \propto \exp\left[-\frac{1}{\sqrt{2}}\sqrt{n}(n-1)t\right] \tag{5.93}$$

to find the effective probability distribution for the free energy fluctuations $P(F = \ln Z)$. Curiously, there does not exist any $P(F)$ that can yield a form of $\exp(-n^\beta t^\gamma)$ with the minus sign, only the positive sign corresponds to possible existence of $P(F)$. Hence, although $n^{3/2}t$ is the leading order (n always assumed large), we ignore it, taking instead the leading contribution with the correct sign; i.e., $\exp(\sqrt{n/2}\,t)$. This form can be readily inverted to find $P(F)$, which in turn gives us the free energy fluctuation exponent,

$$\Delta F \sim t^{\gamma/\beta} = t^2. \tag{5.94}$$

We conclude that for $R(x) = x^2$ (strong correlation), a DP deviates like $x \sim t^\zeta$, $\zeta = (1+\omega)/2 = 3/2$, in other words, we have

$$x^2 \sim t^3. \tag{5.95}$$

This is the Richardson [R26] law for the fully developed turbulence where the displacement of a particle is faster than a linear function of time t. Interpreting the fully developed turbulence motion by a DP model with harmonically correlated noise is very instructive and will be elaborated elsewhere.

Note that this agrees with the replica scaling theory, which predicts

$$\frac{\gamma}{\beta} = \frac{2+\alpha}{4-\alpha} \quad \text{for } 1 \geq \alpha \geq 0 \tag{5.96}$$

where α measures the power-law increase in spatial correlations, provided we extrapolate the replica prediction to $\alpha = 2$. Then again, for all $\alpha > 0$, the replica scaling, dynamic RG and Flory predictions coincide, so the Parisi-Maritan result is a welcome confirmation, joining all other well-known exact results.

Remark: *We have, so far, two exact solutions for the* $1+1$ *DPRM: uncorrelated case,* $R(x) = \delta(x)$, *and the very correlated case* $R(x) = x^2$. *What happens to the physically relevant case when the*

correlation function is $R(x) = |x|$, relevant to disordered random field magnets [Kard87b]? In the first case we have the ground state wavefunction for n DP's $\psi_0 \sim \exp - \sum_{\alpha>\beta} |x_\alpha - x_\beta|$, and the $R(x) = x^2$ case $\psi_0 \sim \exp - \sum_{\alpha>\beta} (x_\alpha - x_\beta)^2$. It is very tantalizing to speculate that the in-between case $R(x) = |x|$, should have a similar symmetric expression. Why not $\psi_0 \sim \exp - \sum |x_\alpha - x_\beta|^{3/2}$?

Unfortunately, the straightforward Bethe ansatz type integration is presently hindered by technical difficulties [JZ92]. Nevertheless, strong, albeit indirect evidence shows that the above guess is indeed the likely answer, up to polynomial functions corrections (Zhang, unpublished). Let us sketch the physical reasoning: in the steps leading Imbrie to his proof of absence of long range order in $d = 1+1$ random field domain wall problem [I86], he found that for system size L there are degenerate ground states of linear size $l \sim L^{2/3}$. In our present context this implies that $|x_\alpha - x_\beta| \sim t^{2/3}$. Remember that for our problem at hand we know from elsewhere (RG and replica scaling) that $x \sim t^\zeta$ $\zeta = 1$. The ansatz with the motion of the center of mass is

$$\exp\left\{ -\sum_\alpha x_\alpha^2/t - \sum_{\alpha>\beta} |x_\alpha - x_\beta|^k \right\}, \tag{5.97}$$

k is the exponent to be found. Since $x_\alpha \sim t$, and the difference $|x_\alpha - x_\beta|^k \sim t$ should scale the same way as the kinetic term x_α^2/t. Thus we find $k = 3/2$, confirming the above conjecture.

Exercise: *Find the asympototic solution for two particles in potential $v(x) = |x|$, just like the solution for Eq. (5.24). Is $\exp -|x|^{3/2}$ a good approximation?*

Exercise: *Explicitly evaluate the disorder-averaged, replicated partition function for the case of linearly correlated noise. When done, submit your results to The Physical Review.*

5.5.3. Power-law noise [MZ90]

Marconi and Zhang have performed transfer matrix studies of the zero-temperature 1+1 DPRM subject to power-law noise, where the random energies are drawn independently (i.e., no correlation between neighboring sites) from the distribution

$$P(\epsilon) \sim |\epsilon|^{-(\mu+1)}, \quad \text{for } |\epsilon| \geq 1; \quad \text{zero otherwise.} \tag{5.98}$$

The fall off of the long power-law tail is controlled by the parameter μ. These authors consider only $\mu > 2$, ensuring a well-defined mean and variance. The case $\mu < 2$, related to so-called Lévy distributions, results in diverging second moments and must be handled separately. Previously, the statistical mechanics community had paid little attention to these weak tails in disorder. Indeed, the common wisdom, based solely upon experience with purely Markovian processes such as our coin-flipping random walker, would argue that as long as the variance of the microscopic disorder is finite, the scaling behavior of the physical observables on macroscopic scales, typically mean or rms quantities, would not be affected *at all* by the higher moments of the disorder. Then again, the DPRM is not a Markovian matter; we must dismiss such notions. The data of Marconi and Zhang, see Fig. 5.15, reveal the wandering exponent to be strongly μ-dependent. The globally optimal path now makes large excursions in search of rare, but dominating, large singular values buried deep in the tails of the power-law distributions. To give an indication of nature of power-law distributions, recall Fig. 4.11, which shows a random distribution of dots, whose sizes are dictated by various values of

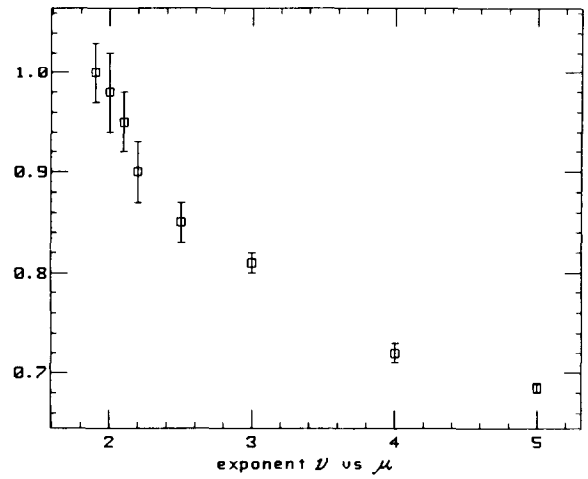

Fig. 5.15. DPRM wandering exponent as a function power-law noise parameter [MZ91].

μ. Apparently, there is a substantial, quite impressive change as $\mu \to 2^+$, where, correspondingly, the wandering exponent monotonically approaches unity.

In the DPRM context, several authors [Z90b,BH91u,Derrida, unpublished], have cooked up a Flory argument analogous to Krug's for anomalous kinetic roughening [Kr91a], see Section 4.2.1. Consider the transverse fluctuation of the directed polymer, which scales as $x \sim t^{\zeta}$. As the polymer meanders through the power-law random energy landscape, it samples a volume $x^d t$, within which the typical maximum energy on a lattice bond is $\eta_{\max} \sim (x^d t)^{1/\mu}$. Balancing this rare, but crucial extremal energy gain against the entropically generated elastic energy cost of large transverse wandering, which scales as x^2/t, we find the scaling exponent

$$\zeta(\mu) = \frac{\mu + 1}{2\mu - d} \tag{5.99}$$

which in $d = 1$ agrees rather well with the data of Marconi and Zhang all the way down to $\mu_c > 5$, where the numerics, as well as the Flory argument, suggest the directed polymer wandering exponent recovers its celebrated value 2/3. In fact, recent work by Lam and Sander [LS92,LS93b] in the stochastic growth model context argues that this simple Flory argument may exact. This contrasts with some computational efforts [BHV91] during the intervening years which had suggested a revised $\mu_c \approx 7$.

5.6. *Time-independent noise: columnar DPRM in various applications*

Suppose that the energies in the standard $(n + 1)$-dimensional DPRM are strongly correlated in the t-direction. In particular, consider the limiting case in which the bond or site energies are actually independent of t. In this situation, the globally optimal path that *maximizes* total energy becomes, literally, the spacetime trajectory of a particle diffusing in n-dimensional random medium in search of the optimal localization site of the sample! Such problems, concerning transport in random medium as well as diffusion-controlled reaction and recombination, are classical subjects that have recently

drawn renewed attention because much appreciated connections to a variety of physical, chemical and biological processes.

5.6.1. Hopping as a dynamical consequence of localization [Z86a]

As an indication of the efforts made in this direction, we note the following PDE,

$$\partial_t \psi = \nabla^2 \psi(\boldsymbol{x}, t) + \lambda V(\boldsymbol{x}) \psi(\boldsymbol{x}, t) \tag{5.100}$$

which was considered by Zhang as a prototype model of diffusion in a spatially random potential soon after the KPZ equation was introduced, and clearly represents a DPRM subject to time-independent noise. Here, $\psi(\boldsymbol{x}, t)$ represents the probability distribution which details the spatio-temporal properties of the diffusing particle, $V(\boldsymbol{x})$ is the Gaussian random potential, and λ, which gauges the strength of the disorder, can be measured in units of inverse temperature. Of course, as an imaginary time Schrödinger equation with random potential, the above is clearly relevant to matters of electrical conductivity in disordered solids and owes much to and also bears upon much antecedent literature discussing Anderson localization.

The more appropriate context of Eq. (5.100) is in biology. Imagine a population diffuses around in space, in which there is a random distribution of food (positive value of V) and poison (negative V). Food causes the local population to proliferate exponentially, while poison does the opposite. We are interested in the long term fate of the population. For instance, if the population manages to survive in this random environment, where is its relative concentration center and how fast does this center move? We shall see below that surprisingly, the population decides upon the subballistic movement as its best survival strategy.

In the present physics context, the essential and perhaps simplest question is the following: Given an initial distribution, say $\psi(\boldsymbol{x}, 0) = \delta(\boldsymbol{x})$, what statistical statements can we make regarding the motion of the localization center? Our physical intuition tells us that the origin, or its immediate neighbors, may not be the best attractor (the place where the finite spatial spread has the highest combined random energies), so the probability distribution will not remain localized there forever. Given enough time, the probability at some distant better attractor can outgrow that at the first, resulting in a dynamics characterized by intermittent hopping. Assuming an infinite sample size, it is apparent that any attractor is but a metastable potential trap. The key point is that better and better attractors can always be found over larger and larger spatial regions with longer and longer lifetimes spent at each attractor. At the heart of the problem lies a natural hierarchy of potential barrier, distance and time scales.

The strong coupling regime can be readily inferred from the study of the static problem – localization: in $d = 1$ we expect that in the static case the wave function is localized around some potential minimum, for the whole range of the coupling constant λ (related to the temperature). In the dynamic case, we expect this picture is still valid – the only difference is, that the localization center changes in time in search for deeper and deeper potential minima, while the wave function itself is a focused object that does not change in time for large times. This is the essential conjecture – hopping as a dynamic consequence of localisation.

Given the strong coupling regime's nature in 1d, we can regard the wave function as almost a point object (strongly localized, or zero temperature limit) and follow its trajectory as time goes on. For $d \geq 2$, our problem can have both strong and weak regimes, depending on parameters. In strong

coupling regime, the point-object approximation will be still valid; in the weak regime, however, the present approach is not permitted. Other approaches using RG perturbation methods have also been tried by Cates and Ball [CB89]. On the other hand, our approach is adequate for the strong coupling regime, for which no perturbative scheme can achieve physical meaningful results.

• *Subballistic motion:* Let us proceed to highlight our approach, which is essentially a variational analysis. Suppose the wave function is localized at some potential minimum (V_0, note that our notation is the negative of the energy) and regard this position as the origin. Suppose also that at some distance from the origin there is a deeper attractor, ($V_x > V_0$). It is clear, that if the gain ($V_x - V_0$) is sufficiently great, the distance x is not too far, or the time is long enough, the deeper attractor will grab the localization center from the present attractor. This can be concretely expressed in the approximate form of the wave function,

$$\psi(x,t) \sim \exp\{t(V_x - V_0) - x\bar{V}\}. \tag{5.101}$$

The first term on the exponential represents the gain which increases in time, the second is the loss where we have assumed an exponential tail (again from localization!) with an average cost $\bar{V} > 0$. In order for a given t, the localization center is already at x and no longer at the origin 0, we need that the above be optimized for a suitable x.

$$t(V_x - V_0) - x\bar{V} = \max. \tag{5.102}$$

It is clear for a x too small, even though the cost $-x\bar{V}$ is indeed not too penalizing, but possible gain $V_x - V_0$ would not be likely to be profitable – since in the close neighborhood there are not many better attractors. To proceed we need to know how large a gain can be statistically expected in a given volume. Assuming a gaussian, independent distribution, we have the probability

$$P_x = \int_{V_x}^{\infty} e^{-V^2} dV \tag{5.103}$$

and we require $p_x \cdot l_x \sim 0(1), l_x = |\boldsymbol{x}|$ is the volume ($d = 1$). Eq. (5.103) defines V_x as the best value one can find in the volume. This gives

$$V_x = [\ln(x)]^{1/2}. \tag{5.104}$$

We see by going to larger volumes the attractor can always improve. However, the above is an extremely slowly increasing function. Substituting (5.104) to (5.102) and vary x to optimize (5.102) we obtain (denote $x_c(t)$ as the winning distance of x)

$$x_c(t) \simeq t/(\ln t)^{1/2}. \tag{5.105}$$

Note that in the original reference, [Z86a], Eq. (6) contains a trivial misprint. The physical implication is rather astonishing: as a consequence of localization (i.e., strong coupling regime makes the wave function always focused), the center of mass,

$$x_c(t) = \int dx x\psi^2(x,t) \Big/ \int \psi^2(x',t)dx' \tag{5.106}$$

moves faster than that of diffusion $x \sim \sqrt{t}$! It is almost linear (sub-ballistic). For higher d, (5.105) still holds (only coefficients change) as long as the corresponding static case remains in localized

regime. Crossing possible delocalization transition lines, $t/(\ln t)^{1/2}$ will cross over to the diffusion behavior $t^{1/2}$.

The above variational analysis is nothing but a dynamic generalization of the Mott's variable-range hopping. Recently this method was rediscovered by Hansen et al. [HHR93] who discussed a similar model with various different potential distributions. What happens if the distribution is not gaussian? The above analysis can be repeated for other distributions. For instance V is uniformly distributed in [0,1]. We readily obtain

$$x_c(t) \simeq t^{1/(d+1)} \tag{5.107}$$

The motion appears to be highly sensitive to the choice of distribution. However, a moment's reflexion tells us that only the gaussian distribution yields robust behavior $t/\sqrt{\ln t}$. This is because that, although $x_c \simeq t^{1/(d+1)}$ is valid for strictly zero temperature limit, at low temperatures, the localization center may spread over quite a few lattice sites. The effective approximation should consider a sum of a finite group of V-values since the wave function covers a finite region. A sum of independent random numbers quickly approaches a gaussian variable.

• *Intermittent jumps:* Most interesting, however, is the intermittent behavior underlying the sub-ballistic motion. The above variational method does not give a hint on how x_c jumps. In order to distinguish between a smooth motion and an intermittent motion, we need to consider two (or more) possible candidates, V_x and $V_{x'}$, one is closer to the origin, the other say, is very far away. We know the closer one has a tiny gain but also costs little, the farther one has higher gain but the exponential tail may make it prohibitively expensive. Our question is, for a given time, which attractor is realized first? In other words, what is the typical gain to motivate a jump: a small gain each time (thus by small jump distances) or a large gain each time (by large jumps)? In principle, all gains (small or big) motivate jumps, the problem is, how long a time does a particular gain require to be realized. For example, a very small gain may be realized only over relatively long time t_1; a larger gain may require less time $t_2 < t_1$, in this case the smaller gain is simply skipped and never realized! To express this idea more precisely, we need a second variational method, based on the physical requirement, that only jumps (or gains) with the *shortest* time are realized.

Let us consider the temporal behavior. Suppose that we have reached the k-th attractor and the $(k+1)$th jump (at x) is about to realize. The wave function at x_{k+1} is comparable to that at the present attractor at x_k,

$$tV_{k+1} - \bar{V}(x_{k+1} - x_k) \simeq tV_k. \tag{5.108}$$

Note the same t appears on both sides. The difference with the previous variational analysis is that t counts time interval between the two successive jumps, while previously it was for the accumulated t during which many jumps may have already occured. We want the smallest t for which the above holds.

$$t \simeq \frac{(x_{k+1} - x_k)\bar{V}}{V_{k+1} - V_k}, \tag{5.109}$$

where V_k is given by Eq. (5.104), $V_k \simeq \sqrt{\ln x_k}$. By variation with respect to x_{k+1} we find that the smallest t occurs when $\partial t/\partial x_{k+1} = 0$, or

$$V_{k+1} - V_k \simeq \frac{1}{2V_k}. \tag{5.110}$$

The constant $\bar{V}$ drops out and we have used $x_{k+1} \gg x_k$. Thus we obtain

$$V_{k+1} = V_k + \frac{1}{2V_k} + O\left(\frac{1}{V_k^2}\right) \tag{5.111}$$

which implies that there is a gain (finite amount!) for each realized jump. Finite gain implies a relatively long distance jump. For d dimensions, the constant $1/2$ is replaced by $d/2$ in (5.111). The relation for the jump distance x and the time needed to prepare a jump (waiting time!) $t \sim x\sqrt{\ln x}$ can be also easily figured out [Z86a]. We conclude that in the localized regime, the center of mass of our wave function pursues the sub-ballisitic motion $x_c \sim t/\sqrt{\ln t}$ in an intermittent fashion. Jumps are motivated by a finite amount of energy gain, the successive attractors appear to have a discrete, quantized spectrum. We can iterate Eq. (5.111) to obtain the asymptotic behavior of V_k to be

$$V_k \simeq \sqrt{k}. \tag{5.111a}$$

This fast improvement of attractor is only possible by searching ever larger distance. In fact, with the help of (5.104), we obtain the kth jump's position, which is expected to be

$$x_k \simeq \exp ck, \tag{5.111b}$$

where c is a dimension-dependent constant. This prediction of exponential jump distance is consistent with our intuitive expectation that $x_{k+1} \gg x_k$. The relation between the discrete index of the jump events k is easily related to the time t_k also,

$$t_k \simeq \exp ck, \tag{5.111c}$$

up to a logarithmical correction.

Some of the above results using variational methods can be obtained via more rigorous density matrix methods [EE87]. Our approach is however, more direct and intuitive and is able to obtain essentially all the messages contained in the original problem.

5.6.2. Punctuated evolution

Eq. (5.100) can be also interpreted in biology to describe a population diffuses around an abstract space, say the geno-type space, rather than the physical space. Then the intermittent jumps can be naturally interpreted as the steps of Punctuated Evolution [GE76]. The implication is fascinating: Ebeling et al. advocates that equation (5.100) is actually a prototype model for evolution of species. In the evolutional history it is well known that the species evolve or improve in an intermittent way. This proposition is further elaborated recently by Bak and Sneppen [BS93], using a prototype inspired from the SOD interface model, recall Section 4.6. Bak and Sneppen show their model of evolution is also capable describing long quiescent transition periods, as well as sudden bursts of activity—the benchmark of biological evolution. Much exciting work has recently followed; see e.g., [PMB94,MPB94,J94] which suggest membership of Bak-Sneppen and self-organized depinning models within a single larger class tied to directed percolation. The relation between our columnar DPRM model and the others is presently being explored (Maritan, private communication).

Inspired by the previous work [EE84,Z86a,EE87], in which diffusion in a random potential meant evolution of a species subject to a fitness function in phenotype space, Krug and Halpin-Healy [KrHH93] have recently reconsidered the DPRM subject to columnar disorder with the hope of providing a unified picture capable of addressing both zero and finite temperature behaviors, as well as broader questions of universality. In striking contrast to the standard DPRM with point disorder, they find the behavior to be very different at zero temperature, where the scaling exponents depend on the details of the random energy distribution, and at finite temperature, where universality is essentially restored and the transverse wandering of the directed polymer is subballistic. We summarize the numerical findings of Krug and Halpin-Healy, as well as the associated Flory arguments, below:

• *Zero temperature:* The columnar DPRM was examined first at zero temperature. Directed paths emanate from the origin of a square lattice and proceed upwards into the half-plane $t > 0$. Transverse jumps of one unit are permitted with no energy cost; larger jumps are not allowed. Quenched random energies $\epsilon(x)$ are assigned independently to the columns of the lattice. A zero-temperature transfer matrix calculation in the substrate geometry [KBM91a] evolves the ground state energy recursively

$$E(x,t+1) = \min[E(x,t), E(x-1,t), E(x+1,t)] + \epsilon(x) \tag{5.112}$$

keeping track of the transverse positional and energy fluctuations. Several different types of probability distribution were considered; in all cases power-law scaling was obtained, but the wandering and energy fluctuation exponents, ζ and ω, indicated a very sensitive dependence upon details of the energy distribution: For example, if columnar defect energies $\epsilon \in [0,1]$ were drawn from the *bounded, continuous* distribution- $P_\nu(\epsilon) = (\nu+1)\epsilon^\nu$, it was discovered numerically that the exponents were consistent with the result $\zeta = \omega = (\nu+1)/(\nu+2)$. By contrast, for the *binary distribution* $P_b(\epsilon) = b\delta(\epsilon) + (1-b)\delta(\epsilon-1)$, with $0 < b < 1$, they found that both scaling indices essentially vanished, a result that is not too surprising since P_b can be regarded as the $\nu \to -1$ limit of P_ν.

Qualitatively, the absence of universality at $T = 0$ can be attributed to the fact that optimal configurations of the directed polymer are localized at individual columns with *exceptionally low energies.* By contrast, for the DPRM with point disorder, the optimal path encounters an extensive ($\sim t$) number of impurities, and the central limit theorem, with a wave of the hand, insures convergence to a universal distribution. The basic physical picture is entirely consistent, perhaps, with the reader's immediate intuition. The optimal path behaves trivially – starting from the origin, it travels diagonally to a favorable site at some transverse distance R and remains there up to time t. The energy of the transverse portion of the path is simply $\bar{\epsilon}R$, where $\bar{\epsilon}$ is the average of the random energy distribution. A la Flory, the total energy of the path can be estimated as

$$\Phi(R,t) = \bar{\epsilon}R + (t-R)E_{min}(R) \tag{5.113}$$

where $E_{min}(R)$ denotes the *lowest energy* anticipated in the spatial interval $[-R,+R]$, a quantity which manifests the *extremal statistics* of the energy distribution. For a given $P(\epsilon)$, the distribution of the smallest among N independently chosen random energies is

$$P_N(\epsilon) = NP(\epsilon)\left(1 - \int_{-\infty}^{\epsilon} d\epsilon P(\epsilon)\right)^{N-1} \tag{5.114}$$

so that a transverse displacement R, which necessitates exploring $N = 2R+1$ possible energies, yields an optimal energy

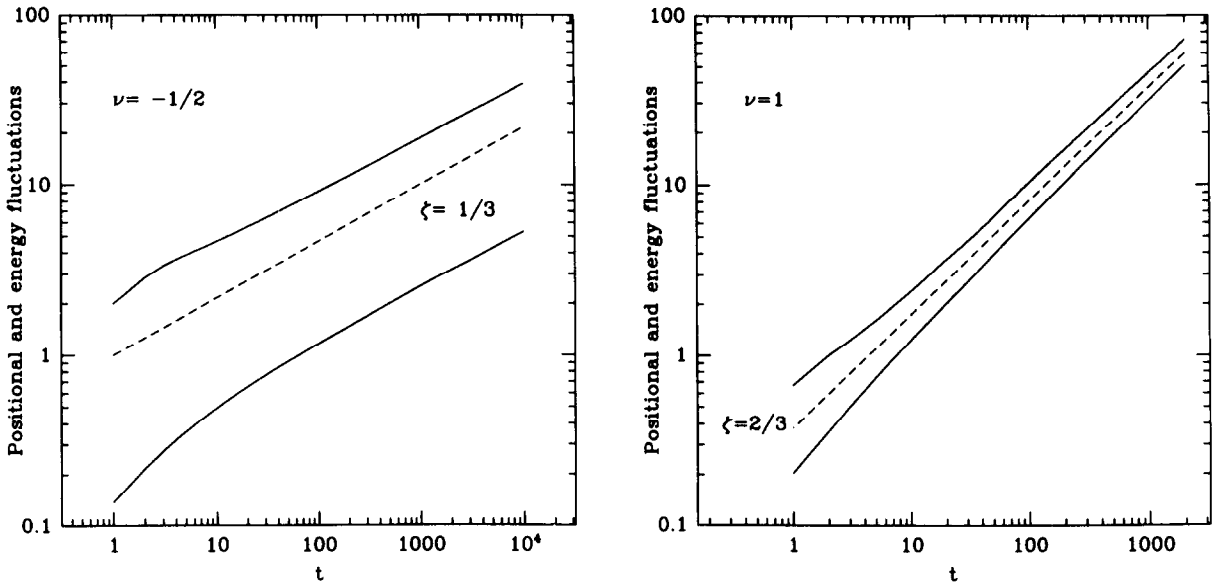

Fig. 5.16. Position and energy fluctuations for the $T = 0$ columnar DPRM, with pinning energies drawn from bounded, continuous distributions with $\nu = -1/2$ and $+1$ [KrHH93].

$$E_{min}(R) = \int_{-\infty}^{+\infty} d\epsilon P_{2R+1}(\epsilon) \tag{5.115}$$

which implies, for our family of bounded distributions P_ν above, that for large R,

$$E_{min}(R) \approx (2R)^{-1/(\nu+1)}. \tag{5.116}$$

With this in hand, we minimize the Flory expression for the energy w.r.t. R, obtaining $\zeta = (\nu+1)/(\nu+2)$, as advertised. Because E_{min} is a decreasing function of R, it is apparent that the dominant energy cost to be balanced against the energy gain tE_{min} is provided by the first term $\bar{\epsilon}R$ in (5.113). This implies that $\Phi \sim R$ for the optimal path, revealing that the energy fluctuations are of the same order as those of the position, hence $\omega = \zeta$; again, honest advertising! Finally, for the binary distribution, matters are straightforward enough – the optimal path makes a beeline to the nearest site with $\epsilon = 0$, which typically requires only a small displacement. There it remains forever, since it has no incentive to venture further away, insisting $\zeta = 0$. Simulation results for the T=0 columnar DPRM are shown in Fig. 5.16, for $\nu = -\frac{1}{2}$ and 1, confirming the anticipated power-law scaling, as well as the equal, and expected, values of the energy fluctuation and wandering exponents.

Exercise: *Consider columnar defect energies drawn from the family of power-law distributions discussed in Section 5.5.3. Show that, for these unbounded distributions,* $E_{min}(R) \sim (2R)^{1/\mu}$, *which yields a wandering exponent of unity and an energy fluctuation exponent* $\omega = 1 + 1/\mu$. *In other words, the ground-state energy per unit length diverges as* $t^{1/\mu}$! *Note that the Flory minimization for this case turns on the energy cost of the third, rather than the first, term in (5.113).*

Exercise: *For the Gaussian energy distribution,* $P_G(\epsilon) = \exp -\epsilon^2/\sqrt{\pi}$, *perform the associated extremal statistics calculation to find Eq. (5.104), that* $E_{min}(R) \sim (\ln R)^{1/2}$, *which results in* $2R \ln R \approx t$, *so that at very long times the wandering is subdiffusive with exponent* $\gamma = 1$, *as defined above. This behavior is reminiscent, though different, from the finite temperature scaling that we'll discuss shortly.*

It is intriguing to study the manner in which the transverse displacement accumulates for a single realization of disorder. Fig. 5.17a shows the time dependence of the end point of the globally optimal path $x_{opt}(t)$, while Fig. 5.17b reveals the evolution of the corresponding energy $\epsilon(x_{opt})$. The dynamics are characteristically *intermittent* – the globally optimal end point of the polymer remains fixed for long periods of time, with the transverse displacement occurring via a few abrupt jumps as the energy levels of two locally optimal paths cross. In the language of current evolutionary theory, long periods of *stasis* are punctuated by short *episodes* of rapid change, a pattern suggested by the fossil record to be typical of species evolution [Kauff93,GE93]. Interestingly, Krug and Halpin-Healy [KrHH93] have observed that, regarding this evolutionary hopping, the average number of jumps grows only *very slowly,* as $\ln t$ – see Fig. 5.18. This can be understood, in each case, in rather simple terms, if one keeps in mind, recall Fig. 5.17b, the unrelenting cascade of ever-decreasing energies. With the globally optimal path ending at a site with energy $\epsilon(x_{opt}) = \epsilon_n$, the next jump occurs to a site with energy ϵ_{n+1} chosen at random from the disorder distribution $P(\epsilon)$, subject only to the constraint that $\epsilon_{n+1} < \epsilon_n$, which implies

$$\langle \epsilon_{n+1} \rangle = \int_{-\infty}^{\epsilon_n} d\epsilon\, \epsilon P(\epsilon) \Big/ \int_{-\infty}^{\epsilon_n} d\epsilon P(\epsilon).$$

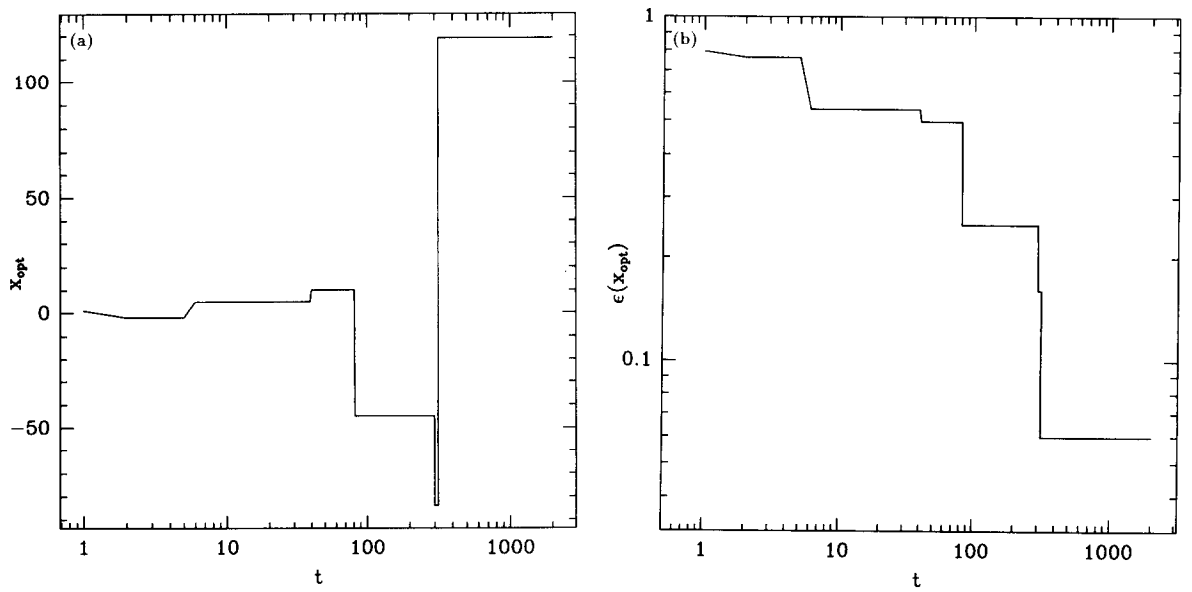

Fig. 5.17. Time evolution of the (a) endpoint $x_{opt}(t)$, and (b) energy $\varepsilon(x_{opt}(t))$ of the globally optimal path for a single realization of disorder in the columnar DPRM.

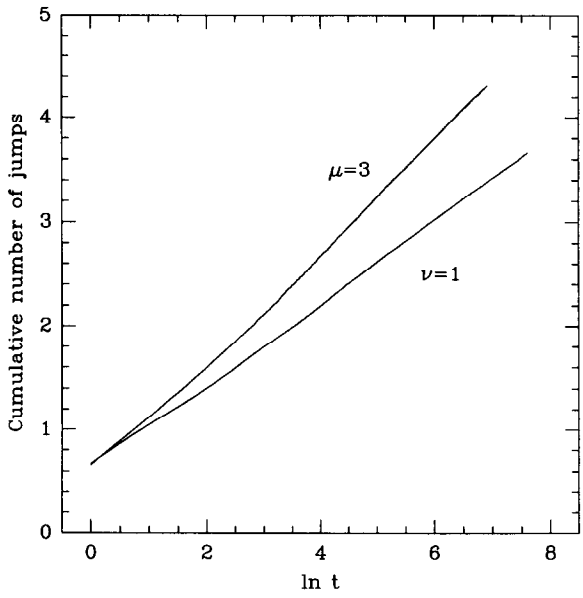

Fig. 5.18. The logarithmic nature of evolutionary hopping [KrHH93,Kauff93,F63].

For our family of bounded, continuous distributions, P_ν, this yields an average site energy that decreases *exponentially* with the number of jumps, $\langle \epsilon_n \rangle = \zeta^n$ where $\zeta = (\nu + 1)/(\nu + 2)$ is the zero-temperature wandering exponent. Quite independently, the Flory energy estimate suggests $\langle \epsilon(x_{opt}) \rangle \sim E_{min}(R) \sim t^{-(1-\zeta)}$. Equating these two expressions, we obtain

$$\langle n \rangle \approx \frac{1-\zeta}{\ln(1/\zeta)} \ln t \tag{5.117}$$

where the prefactor is not to be trusted, given the crudeness of the argument. As stressed by Krug, and indicated by Fig. 5.18, which includes results from simulations with an unbounded power-law distribution, this logarithmic behavior is extremely robust and apparently independent of the underlying distribution. We will see soon enough that it is independent of the temperature too.

Exercise: *Convince yourself of the robust, logarithmic nature of evolutionary hopping – consider the family of power-law distributions, P_μ, introduced earlier. Show that they produce an* exponential *divergence $\langle \epsilon_n \rangle = -(\mu/(\mu-1))^n$, which, when equated to the time dependence $\langle \epsilon(x_{opt}) \rangle \sim t^{1/\mu}$, gives $\langle n \rangle \sim \ln t$. For the gaussian distribution, the very same law is established in a somewhat more subtle manner – one has $\langle \epsilon_{n+1} \rangle = -\frac{1}{2} \exp -\epsilon_n^2 [\mathrm{erfc}(-\epsilon_n)]^{-1}$, with $\mathrm{erfc}(x)$ the complementary error function. Expand this function for large arguments to recover the result Eq. (5.110) $\epsilon_{n+1} - \epsilon_n \approx -1/(2\epsilon_n)$, which implies that $\epsilon_n \approx -\sqrt{n}$ for large n. Since the site energies decrease with time as $-(\ln t)^{1/2}$, we arrive once again at this interesting result. Given the apparent universality of the logarithmic nature of evolutionary hopping, construct a general proof establishing its verity.*

• *Finite temperature:* At $T > 0$, universality is essentially restored, with subballistic wandering, $x(\ln x)^\gamma \sim t$, the rule rather than the exception. Rather than tracking the sole path which is globally optimal, we update the Boltzmann weight Z, which is the restricted partition function for all paths

running from the origin to the end point (x, t), according to the usual prescription

$$Z(x, t+1) = e^{-\epsilon(x)/T}[Z(x, t) + Z(x-1, t) + Z(x+1, t)] \tag{5.118}$$

and monitor the hopping of the wavepacket as it jumps intermittently from an attractor to the next more favorable one. During this process, the distribution $Z(x, t)$ becomes momentarily bimodal, leading to substantial spreading of the wavepacket, whose thermal width peaks as the jump is made. With regard to the calculational aspects, Krug and Halpin-Healy have applied Zhang's spirit of minimalism to strip down Ebeling's bulky, but powerful machinary, generating Flory arguments very much reminiscent of the $T = 0$ case just discussed, but rather different in the details. Thanks to earlier efforts [EE84,Z86a], we realize that the attractors no longer correspond to individual lattice sites, but to *localization centers* associated with the eigenstates ψ_j of the time-independent version of the discrete, imaginary time Schrödinger equation, which themselves satisfy

$$\psi_j(x) + \psi_j(x+1) + \psi_j(x-1) = \exp \epsilon(x)/T - \lambda_j \psi_j(x) \tag{5.119}$$

where λ_j denote the quasienergies. This equation belongs to a large class of disordered one-dimensional problems, coming under the general rubric of Anderson localization, for which it is known that the low lying states that dominate $Z(x, t)$ are exponentially localized, $\psi_j(x) \approx \exp -|x - x_j|/\xi_j$, where x_j is the localization center, and $\xi_j(\lambda_j)$ is the localization length. A spectral decomposition of the constrained Green's function $Z(x, t)$ in terms of the $\psi_j(x)$ yields

$$Z(x, t) \approx \sum_j \exp[-(|x_j|/\xi_j + |x - x_j|/\xi_j + \lambda_j t)]. \tag{5.120}$$

The localization centers correspond to local maxima of Z, but we must extremize the argument of the exponential to determine which state dominates the sum- a task which requires knowledge of the *smallest eigenvalue* likely to be encountered in a region of given size. Consequently, Krug and Halpin-Healy introduce a function $\lambda_{min}(R)$, which is the finite temperature analog of $E_{min}(R)$. It can be computed from the generic extremal statistics formula, provided the bare disorder distribution $P(\epsilon)$ is replaced by the *density of states* $\rho(\lambda)$ of the Anderson tight-binding problem. Once $\lambda_{min}(R)$ and the energy dependence of the localization length ξ are known, the typical transverse hop necessary to reach the dominant localization center can be estimated by minimizing the effective Flory expression

$$\Phi(R, t) = R/\xi + t\lambda_{min}(R) \tag{5.121}$$

Note the two important changes in our formalism as we moved from zero to finite temperature:

(i) The bare disorder distribution is renormalized to the density of states ρ, opening the door to Lifschitz tail phenomena, as we calculate $\lambda_{min}(R)$.

(ii) The energy cost of a transverse jump of size R is scaled by the relevant localization length ξ.

To illustrate the method, we consider the simplest case - that of the binary distribution P_b, which as a bounded, discrete disorder distributions is known to be universally characterized by a pure Lifshitz tail in the integrated density of states $k(\lambda) = \int_{\lambda_0}^{\lambda} d\lambda \rho(\lambda)$ near the band edge $\lambda_0 = -\ln 3$:

$$k(\lambda) \approx \exp -C(\lambda - \lambda_0)^{-d/2} \tag{5.122}$$

where C is a positive constant and d the dimensionality. With this form for the integrated density of states, the extremal statistics calculation yields $\lambda_{min}(R) - \lambda_0 \sim (\ln R)^{-2/d}$. Since the kinetic energy

of a state of spatial extent l is of the order $1/l^2$, the states which dominate the partition function (5.120) occupy regions of size $(\ln R)^{1/d}$. This scale is small compared to the distance R from the origin, so the overlap of such a state with the origin, which gives rise to the first term in the Flory free energy (5.121), decays exponentially in R with localization length $\xi = O(1)$, independent of R. Hence, we have

$$\Phi(R,t) = R + t/(\ln R)^{2/d} \tag{5.123}$$

which, whence minimized w.r.t. R, yields

$$R(\ln R)^{1+2/d} \sim t \tag{5.124}$$

so that for very long times, $\gamma = 1 + 2/d$ for the binary distribution. Numerical simulations in $d = 1$ by Krug and Halpin-Healy give results consistent with (though a bit smaller than) the prediction $\gamma = 3$, in disagreement with earlier work of Nieuwenhuizen [Nh88], who used a conventional elastic energy cost R^2/t rather than the term R/ξ, resulting in $\gamma = 3/2$.

Things proceed in a different fashion for the gaussian distribution. There, since the density of states remains gaussian, which implies $E_{min}(R) \sim -(\ln R)^{1/2}$, while the localization length actually decreases with decreasing energy, $\xi(\lambda) \sim |\lambda|^{-1/2}$, so the lowest lying states are the strongest localized. The Flory expression to be minimized then reads

$$\Phi(R,t) = R(\ln R)^{1/4} - t(\ln R)^{1/2} \tag{5.125}$$

so that

$$R(\ln R)^{3/4} \sim t \tag{5.126}$$

with $\gamma = 3/4$. Here, it is conceivable that, in a lattice simulation, the decrease in ξ would saturate at some microscopic scale, implying crossover to $\gamma = 1/2$; see earlier numerics reanalyzed [Z86a,EE87].

Caveat: Ignorance of the subballistic universality at finite temperature would result in a profusion of highly nonuniversal, *effective* wandering exponents were one to force the data into straight log-log plots as we did at $T = 0$ [KrHH93].

Finally, regarding the very general logarithmic character of evolutionary hopping – it remains robust, despite the change to finite temperature, see [KrHH93]. Note, too, that the mathematics community has, recently, provided strong support [Snt93] for the ad hoc finite temperature Flory arguments of Krug and Halpin-Healy, discussed above.

5.6.3. *Point versus columnar defects [AHHK94]*

Flux-line assemblies in cuprate high temperature superconductors form a fascinating system, exhibiting a potentially broad variety of phases, including a topologically entangled liquid, proposed in the absence of disorder [Nel88], as well as possible vortex [MPAF89, FFH91] and Bose glass [NV92] states, which may arise at low temperatures as a result of the growing influence of *point* and *columnar* defects, respectively, which pin the already thermally roughened vortex lines. A correct understanding of the relevant pinning mechanisms and their implications for the global phase diagram Abrikosov flux-line lattice is of great technological importance, given the tendency of these high temperature superconductors toward giant thermal flux creep [Mal88], which greatly compromises the practical utility of these materials. In ordinary crystals of $YBa_2Cu_3O_7$, BaCuCO and the like, it

has been rather readily established [Chud90] that the oxygen vacancies are, in fact, the point-like impurities responsible for pinning down the vortex lines, preventing, at least at low temperatures, their resistive flow under the influence of an external current, via the Magnus force. More recently, efforts to overcome shortcomings associated with flux creep have relied upon the introduction of artificially created point defects by proton irradiation [Civ91], which leads to a dense distribution of point-like pinning sites that increases the critical current, beyond which superconductivity is lost, near $T = 0$ but has surprisingly little effect at liquid nitrogen temperatures, 77 K, slightly below their $T_c \approx 93.5$ K. Considerably more effective in vortex confinement has been the inclusion by Civale et al. [Civ91] of artificial columnar defects, achieved by irradiating their cuprate superconductor with highly energetic ion bombardment; more specifically, their $1 \times 1 \times 0.02$ mm^3 $YBa_2Cu_3O_7$ sample was exposed to dosages $\sim 10^{11}$ ions/cm^2 thanks to a 580 MeV Sn beam, giving rise to a geometrically random, but dense array of permanent columnar defects of length ≈ 15 μm comparable to the sample thickness, diameter roughly 50 Å, and whose density was equivalent to that a vortex array resulting from an external magnetic field of about 5 T which, for the given sample, corresponds to about 10^9 vortices with a mean spacing $\approx$ 250 Å. In contrast to the proton induced point defects which exhibited a saturation effect, the columnar defects resulted in substantially enhanced pinning at high temperatures and fields, evidenced by elevated critical currents that increased monotonically with columnar defect density, resulting in a remarkable upward shift of several Tesla in the irreversibility line. Picking up on this extraordinary experiment [Civ91], as well as related efforts by Konczykowski et al. [Kon91], Nelson and Vinokur [NV92] made an intriguing link to earlier theoretical work of Fisher et al. [FWGF89], suggesting that the physics of flux-lines in cuprate superconductors pinned by columnar defects be mapped onto the problem of boson localization in a two dimensional disordered medium. The Nelson-Vinokur mapping, based upon the profitable equivalence between classical statistical mechanics and quantum mechanics in one less dimension, predicted a wealth of states for the flux-line lattice – among them a Bose glass phase with an infinite tilt modulus and zero linear resistivity, an entangled flux liquid characterized by a unique neutron diffraction signature, and finally at the very highest densities, where the vortex line density was comparable to or exceeded that of the columnar defects, a "Mott insulator" phase signaled by infinite tilt and compressional moduli. They discussed in great detail the transport properties of these phases and tentatively identified the irreversibility line, first observed by Malozemoff et al. [Mal88], with their transition between Bose glass and entangled liquid phases, and provided clear experimental tests to distinguish the Bose glass model [NV92] from the competing vortex glass theory [MPAF89,FFH91].

The essential distinction between the the vortex and Bose glass scaling theories lay in the differing effects of point versus columnar defects – the former promoting flux-line roughening and entanglement, whereas the latter inhibits wandering and encourages localization. Indeed, the vortex glass model concentrates solely on the low temperature role of point disorder, while the Bose glass model focusses on the apparantly dominant effect of columnar disorder, ignoring entirely the influence of the point impurities. In an effort to study the competition between point and columnar defects, inevitable in any actual sample of an irradiated cuprate superconductor, Arsenin, Halpin-Healy and Krug [AHHK94] considered the extremely simplified model of the DPRM simultaneously subject to *both* time dependent and independent noise. As discussed earlier, see Section 5.3.5, an isolated vortex line roughened by point impurities was put forth by Nattermann and Lipowsky [NL88] as a physical realization of the standard DRPM with time dependent noise. The inclusion of time-independent noise then mimics, in a very natural way, the effect of the columnar microstructure induced by ion

bombardment of the sample. Keeping the model stripped down to its bare essentials, Arsenin et al. performed a zero-temperature transfer matrix calculation for the 1+1 DPRM, square lattice-substrate geometry, with the following update prescription:

$$E(x,t+1) = \min[E(x,t), E(x-1,t), E(x+1,t)] + p\eta(x,t) + c\epsilon(x) \tag{5.127}$$

where the noise terms, η and ϵ, are random variables drawn uniformly from the unit interval [0,1] and the ratio p/c gauges the relative strengths of the point and columnar defects. By construction the columnar defects of the model are everywhere present, being superposed atop the point impurities, while c would represent the condensation energy *per unit length* that a vortex line pinned to a column would gain by remaining localized. The DPRM calculation follows the evolution of the globally optimal path through this god-foresaken medium; consequently, it assumes the sparse limit of a few noninteracting vortex lines greatly outnumbered by columnar defects. Nevertheless, this simple p/c DPRM exhibits rather interesting scaling behaviors. In Fig. 5.19, we show the results of Arsenin et al. for the positional and energy fluctuations at various values of the coupling p/c. As is apparent from this double log plot, they retrieved the anticipated results at either extreme – for $p/c = 0$, where there are no point defects, but only columnar pins, $\zeta = \omega = 1/2$ as we know already from the work of Krug et al. [KrHH93, see above], while $p/c = \infty$ is the limiting case of purely point disorder, for which one expects the *unequal* exponents $\zeta = 2/3$ and $\omega = 1/3$. It is interesting to note at this stage that the wandering exponent associated with point defects exceeds that of purely columnar disorder, entirely consistent with our intuition that the columns diminish wandering and enhance localization. At finite, but nonzero values of p/c, the scaling is complex – following an initial crossover, the positional and energy fluctuations seem to scale with the same effective exponent, reminiscent of the purely columnar fixed point [KrHH93], but with a value, roughly 3/4, which is paradoxically greater than those at either endpoint! This suggests that the roughening of vortex lines subject to both point and columnar defects results in wandering that is substantially greater than either sort of disorder could induce on its own. A closer examination reveals, however, that this exponent is not the asymptotic value, for the slope continues to increase and a more appropriate plot, motivated by the finite temperature behavior of the purely columnar DPRM, sets $x(\ln x)^{\gamma=2} \sim t$, yielding a much more satisfactory fit. Thus, the net effect of adding point disorder upon the dominating role of the columnar defects, is, from the point of view of the Bose glass model, simply akin to raising the temperature! Somewhat surprisingly, this suggests that the phase diagram and renormalization group flows appropriate to the (1+1)-dimensional p/c DPRM are those indicated in Fig. 5.20, a result very much at odds with the naive expectation that everything flow to the columnar defect fixed point. Lastly, in Fig. 5.21, we show globally optimal paths through the random energy landscape for various values of p/c, which are indicative of the configurations of the directed polymer that result from the competing effects of point and columnar pins.

5.7. *Disturbing the random energy landscape: ground-state instabilities*

As it was stressed earlier [Z87], the precise trajectory followed by the globally optimal path through a given realization of the random energy landscape is quite susceptible to small changes in that random environment, there being many neighboring paths whose energies are very close to that of the ground state, but are characterized by markedly different configurations. These concerns have great physical import, of course, since true physical systems often possess quenched disorders that are actually

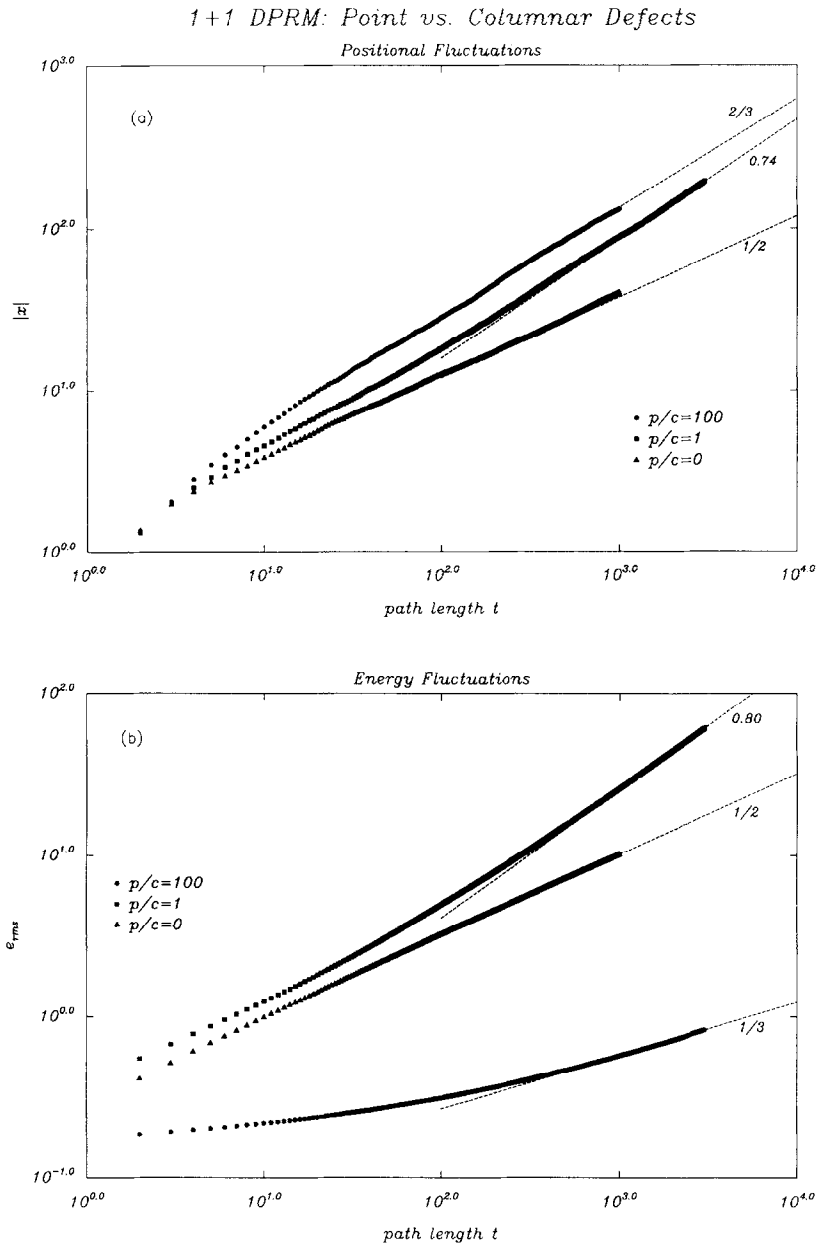

Fig. 5.19. (a) Position and (b) energy fluctuations of the zero temperature 1+1 DPRM roughened by point and columnar defects. The ratio p/c gauges the relative strengths of these two rather different types of disorder [AHHK94].

dynamical variables, albeit on rather long timescales and with very small amplitudes. In his own numerical investigation into these issues, Zhang concentrated on the effects of an uncorrelated slow drift in the random energies of the bonds; that is, he considered adding atop each random bond energy $\in [0, 1]$ an uncorrelated, tiny perturbation drawn with uniform probability between 0 and δ, with

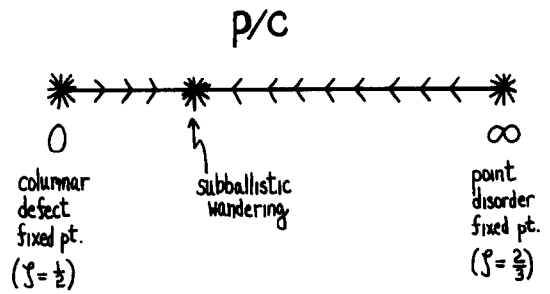

Fig. 5.20. Phase diagram for the $T = 0$ 1+1 dimensional p/c DPRM, as suggested by numerical simulations [AHHK94].

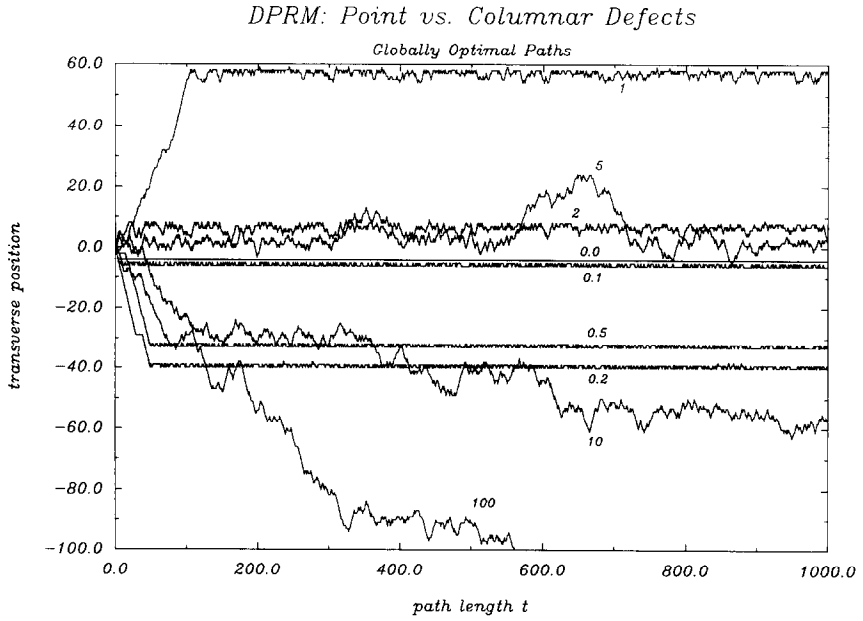

Fig. 5.21. Globally optimal trajectories of directed polymers in random media (i.e., vortex lines in cuprate superconductors!), subject to point vs. columnar defects for different values of p/c.

$\delta \ll 1$. In the context of disordered two-dimensional magnets, this corresponds to uncorrelated RB perturbations upon a RB interface. In the DPRM global optimization problem, this procedure yields two realizations of the random energy landscape that are different, though produced from similar distributions and possessing substantial overlap. Because of the work of Shapir [S91], we know that there exists a crossover length scale $t^* \sim \delta^{-1/\varphi}$, where $\varphi_{RB} = 1/6$ for random bond perturbations and $\varphi_{RF} = 1/2$ for random field perturbations, beyond which the small differences between the perturbed and unperturbed realizations of the random energy landscape manifest themselves in an asymptotic fashion. There are, however, a number of interesting scaling properties associated with ground-state instabilities of this disordered system that reveal themselves immediately. We focus our attention upon them first.

The ground state instabilities have far-reaching consequences. One such example is the lack of the continuum limit of any DPRM model or its offspring. In the surface growth chapter, we already

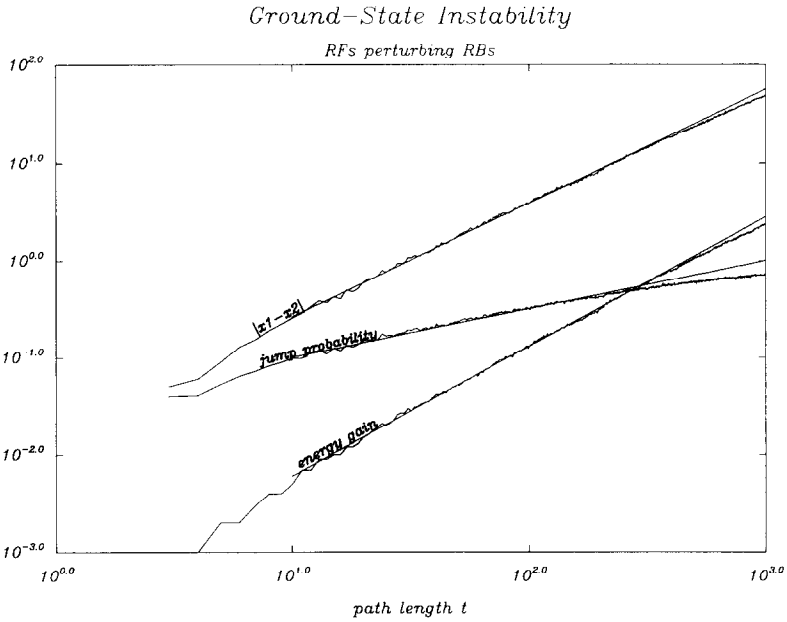

Fig. 5.22. RF perturbations of the RB DPRM. From the left – Top curve: mean jump distance. Middle curve: jump probability. Bottom curve: energy advantage of new best path over old best path [HHH93].

discussed the ambiguity of the continuum limit which can lead to spectacular experimental manifestations. In the DP context we present the problem using the following example: Imagine an optimal DP configuration in a very large lattice with very small lattice spacing. Suppose now coarse-grains the lattice by doubling the lattice, random value on each bigger cell is taken to be the average of the values the constituent original smaller cells. This procedure should not change macroscopic physics if the lattice is sufficiently big and spacing is sufficiently small provided – the continuum limit exists. After the lattice coarse-graining we shall find with probability of order unity that the global position of the new optimal DP configuration is significantly different from the original one, allbeit there may be some overlap segments. This can be readily verified on a computer, and it can also be interpreted as the consequence of the ground state instability – here the instability is not cause by shifting the random values on each site, but by taking a step in the continuum limit. This shows that even for the gaussian distribution, the continuum limit does not exist, microscopic details influence the macroscopic physics.

5.7.1. Numerical evidence [Z87,HHH93]

Consider, for example, the fact that the two globally optimal paths in the two different, but highly correlated random environments, are typically quite distinct. If x_1, x_2 denote the tranverse positions of these two best paths, then one finds [HHH93] for RFs perturbing RB interfaces that the mean jump scales with path length as, see Fig. 5.22, $|x_1 - x_2| \sim t^{\alpha=1.16\pm0.02}$, entirely consistent with Shapir's prediction [S91] that $\alpha_{RF} = \varphi_{RF} + \zeta_{RB} = 1/2 + 2/3 = 7/6$. Original data for the case of RBs perturbing RBs [Z87], are presented here for sake of comparison, shown in Fig. 5.23, corroborating the mean jump exponent $\alpha_{RB} = \varphi_{RB} + \zeta_{RB} = 1/6 + 2/3 = 5/6$. In both instances, $\delta = 0.1$ and disorder

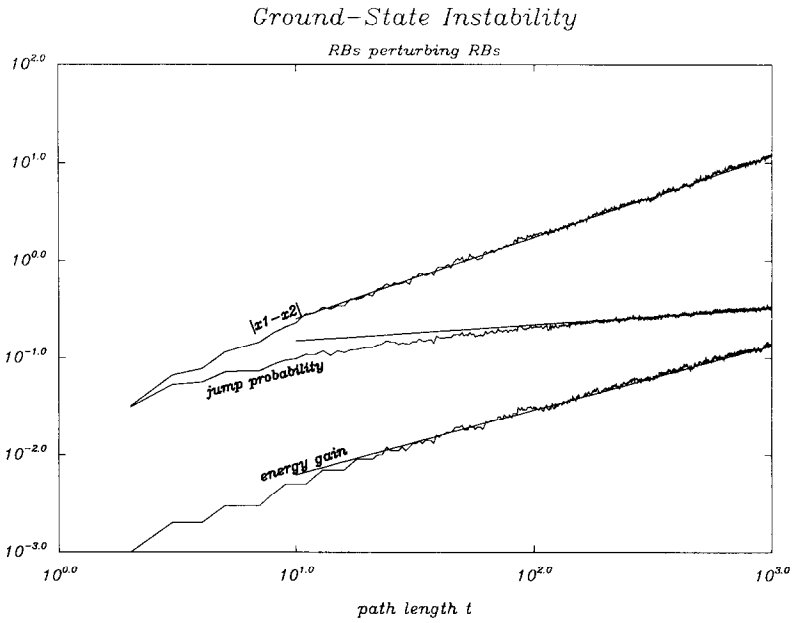

Fig. 5.23. Same as previous figure, but for RB perturbations of the RB DPRM – the case considered by Zhang [Z87].

averages have been performed over 4000 realizations of the random energy landscape. Furthermore, it is apparent that in the case of RFs perturbing RBs, where the crossover length scale $t^{\star}_{RF} \sim \delta^{-2} \sim 100$, the data begin to pull away from the straight line fit. By contrast, for RBs perturbing RBs, the data follows the line well beyond accessible system sizes since $t^{\star}_{RB} \sim \delta^{-6} \sim$ million steps (!) in this case.

Note that this mean jump scaling index is quite large because of the ultrametric structure of the ensemble of locally optimal paths, see below. The very best path in a given realization of randomness is stable with respect to its immediate family thanks to the substantial ancestry they have in common. Hence, there is an intrinsic resistance to change, which was alluded to as a Hopfield memory effect [Z87]. Nevertheless, because of the random perturbations upon the original disordered landscape, a distant relative of the original best path can accumulate enough energy gains to become the globally optimal trajectory in the perturbed landscape, incurring a large transverse jump in the process. Since the triumphant neighbor is rarely a local relative, the jumps make important contributions to the statistical averages.

In addition to the mean jump size, one can also study the probability that a jump actually happens $(x_1 \neq x_2)(t)$ for perturbations of the random energy landscape. A glance at Fig. 5.22 reveals that for paths shorter than the crossover lengthscale, the data for RFs perturbing RBs are well fit by a line of slope 1/2. For RBs perturbing RBs, the data fall along a line of slope 1/6, as explained first by Feigel'man and Vinokur [FV88]. Again, for the RB case, there is no indication, whatsoever, of incipient crossover phenomena. Note that, while there are geometric arguments [FV88,N88,Z87] that predict these jump probability exponents, for both RFs and RBs, they coincide with the crossover index φ.

Given the growing jump probability, it is natural to wonder whether the old best path in the original random energy landscape retains some honor by remaining a locally optimal path in the new

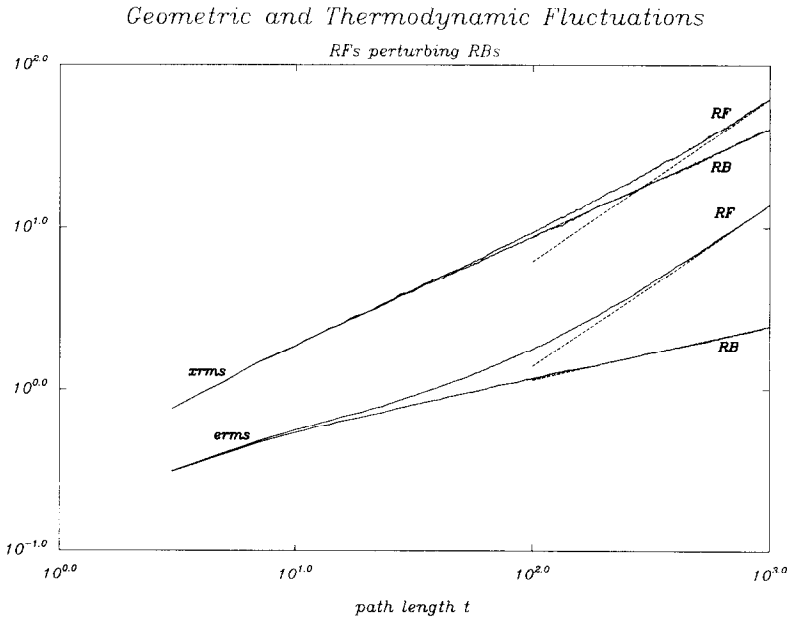

Fig. 5.24. Position (top pair) and energy (bottom pair) fluctuations of the globally optimal path. Upper curves within each pair correspond to the best path in the disordered environment perturbed by random fields. For RFs perturbing RBs, both the position and energy fluctuations eventually scale with unit slope, in agreement with Imry-Ma arguments for the 2d RF Ising model. Lower curves, associated with the original unperturbed energy landscape, exhibit standard 1+1 DPRM exponents, $\zeta_{RB} = 2/3$, $\omega_{RB}=1/3$ [HHH93].

disordered environment. Numerical studies indicate, see [HHH93], that the energy change of the old best path in the different energy environments possesses an exponent of *unity* for RFs, suggesting that the new locally optimal path does indeed overlap substantially with the old best path. Finally, one can investigate the energy advantage, in the new environment, that motivated the jump away from the old optimal path. See Figs. 5.22 and 5.23. It scales with an exponent $\omega'_{RF} = 4/3$ for RF perturbations, $\omega'_{RB} = 2/3$ for RB perturbations. These simulations provide strong support for the conjecture that the instability exponents obey a scaling relation, $\omega' = 2\alpha - 1$, analogous to that of the unperturbed problem [Z87]!

Finally, Fig. 5.24 illustrates the long term implications of RF perturbations upon the RB landscape. Whereas the data for geometric and free energy fluctuations in the original unperturbed random energy landscape scale nicely and are consistent with the exponents $\zeta_{RB} = 2/3$ and $\omega_{RB} = 1/3$, in the new environment RF perturbations incur crossover to the stronger fluctuations characteristic of correlated roughening, the exponents $\zeta_{RF} = \omega_{RF} = 1$ in agreement with the those predicted by Imry-Ma type arguments for the 2d RF Ising model, see [HH90]. Note that, while deviations manifest themselves first for the sample to sample fluctuations of the energy, the march to asymptotic scaling is well under way for both quantities once the length scale $t^*_{RF} \sim 100$ is crossed.

It is clear from our numerical studies that correlated random perturbations can incur severe ground-state instabilities in uncorrelated disordered systems. In the case of the DPRM, a RF perturbation upon the RB landscape can have increasingly drastic consequences for the configuration of globally optimal paths, causing large jumps to distant relatives beyond the immediate family. Ultimately, of course,

the scaling is controlled entirely by the RF fixed point, characterized by exponents quite different from those of the RB problem. These effects are presumably observable in 2d RB magnets that are subject to a very weak external magnetic field, giving rise to small perturbing RFs within the sample [FA79]. Thermally activated jumps of domain walls to minimal energy configurations might manifest themselves as large observable noises in measurements of the magnetization, susceptibility, etc. For the kinetic roughening of stochastically grown surfaces, the importance of a spatially correlated perturbation in the atomic beam would be dramatic, leading to radically different surface morphologies with substantially different scaling properties.

5.7.2. Back of the envelope: linear-response theory [Méz90,S91]

Much of the above numerical data can be easily understood on the basis of Shapir's scaling ansatz [S91] for the interfacial roughness $|x(t)|$,

$$|x_\delta(t)| = |x_0(t)|g(\delta t^\varphi) = |x_0(t)|\{1 + g'(0)\delta t^\varphi + \cdots\} \tag{5.128}$$

from which it follows that the displacement in the perturbed environment is given by

$$\Delta x(t) = |x_\delta(t)| - |x_0(t)| \sim |x_0(t)|g'(0)\delta t^\varphi \sim \delta t^{\varphi+\zeta} \tag{5.129}$$

whence the mean jump exponent, while

$$P(\text{jump}) \sim \Delta x(t)/|x_0(t)| \sim \delta t^\varphi. \tag{5.130}$$

For reasons that are unclear, the energy-based derivation of Feigel'man and Vinokur[FV88] for the jump probability exponent appears not to carry through for RF perturbations of the RB landscape. Nonetheless, the linear dependence of both the mean jump distance and the jump probability on the strength of the perturbation are clearly manifest in both the RB and RF simulations as the value of δ is varied [Z87,HHH93].

This is just the tip of the iceberg, Shapir has done much more, considering both uniform and random perturbations upon diverse manifolds pinned by quenched impurities. Finally, motivated by possible issues of replica symmetry breaking in the context of the DPRM, Mézard [Méz90] has performed an interesting numerical study in which he investigates consequences of a uniform field acting at the head of the polymer. His important study indicates the importance of distinguishing between the average susceptibility, which is correctly predicted by Shapir's general approach but is governed by dominant rare events, and the typical response.

5.8. Geometric properties of DPRM river basin deltas

5.8.1. Ultrametricity [KZ87,Ram86r]

Up to this point we have concentrated entirely on the statistical properties of the globally optimal path, paying little attention to its kin which possess less favorable energies. Nevertheless, the evolutionary history of the ensemble of locally optimal paths reaching a given time slice exhibit a highly nontrivial, complex geometry worthy of study in its own right, see Fig. 5.25. Kardar and Zhang [KZ87], in their preliminary foray in to the scaling behavior of the many-dimensional DPRM, paused briefly to comment upon the geometric complexity of such DPRM *river basin deltas*. Interestingly, similar patterns arise within the KPZ context, where a waiting-time formulation of the growth

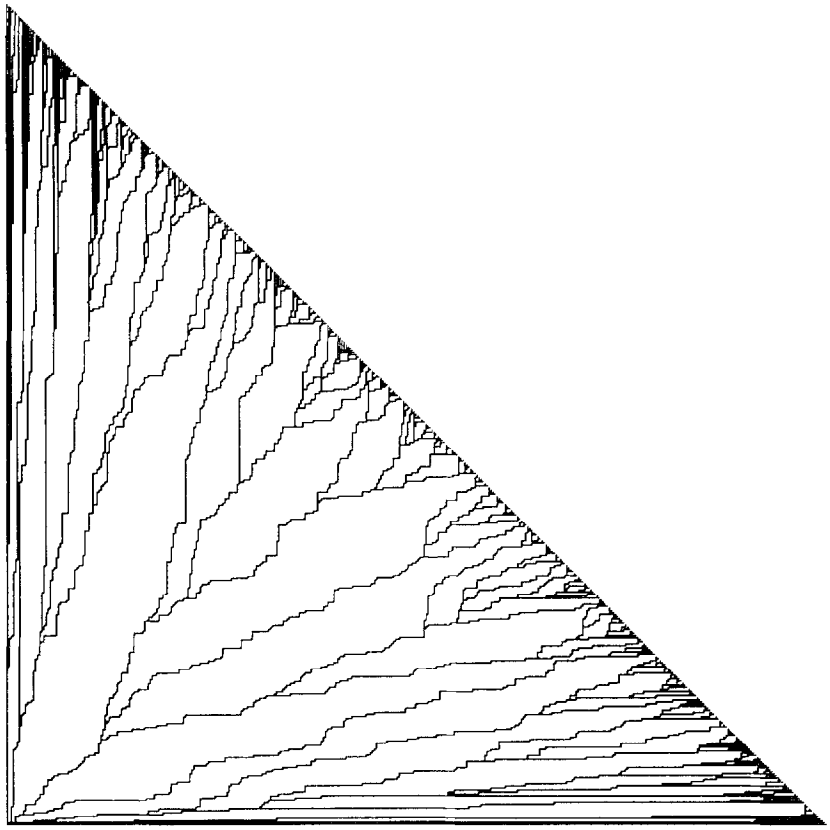

Fig. 5.25. 1+1 DPRM river basin delta, consisting of the collection of locally optimal paths to the base, for a given realization of the random energy landscape.

process permits a direct mapping to the lattice DPRM, avoiding the continuum link, see [TKW91]. Recall that the ensemble of locally optimal paths is the collection of $i + 1$ paths emanating from the origin at the apex of the triangle that optimize trajectories to the $i + 1$ specified endpoints of the ith time slice. The globally optimal path is the winning member of this elite ensemble. Visually, these geometric patterns are quite compelling and are wonderfully reminiscent of some rather well known directed formations found in Nature, such as the Nile Delta, blood vessel capillary networks, and neuronal arrays in which *optimization* processes dictate some of the more important features. In fact, the hierarchical tree structure of the DPRM deltas is rigorously *ultrametric*, indicating that the free energy landscape of the DPRM is explicitly so, which imports crucially upon our understanding of ground-state instabilities, as discussed in the previous section. Consider two locally optimal paths whose endpoints are separated by a small distance x along the base of the delta. It is clear (just check the figure!), that for large values of x, the two paths may have nearly distinct trajectories, but for smaller values of x, there is a greater likelihood that the two paths share much the same ancestry, having many bonds in common and splitting only as they approach the base. If z denotes the distance along which the paths are distinct, then the DPRM delta strongly suggests, at least on average, that for small distance x, z depends only on x and not on the total path length t. One wrong but informative possibility, noted by Kardar and Zhang [KZ87], is that the paths diverge at the latest

possible instant, which implies $\langle z \rangle \sim x$, by virtue of light cone constraints. This would result in an energy difference between the two paths that scaled as $\Delta E \sim z^{1/2} \sim x^{1/2} \sim t^{\zeta/2}$, implying $\omega = \zeta/2$ which, taken in the same breath as the scaling relation $\omega = 2\zeta - 1$, leads immediately to the correct scaling indices $\zeta = 2/3$ and $\omega = 1/3$. This would be fine for the 1+1 DPRM; unfortunately, however, the argument is independent of dimensionality and mistakenly suggests that the exponents for directed polymers in random media are superuniversal [KZ87,MM88]. An alternative suggestion, due to Imbrie [I87], has just garnered strong support thanks to recent quantitative studies [Per92,PHH93] of the DPRM river basin delta, see below. The essential idea is that the DPRM delta is a statistically self-similar geometric object, for which the global behavior continues at all scales, so that $z \sim x^{1/\zeta}$ and $\Delta E \sim z^{\omega} \sim x^{\omega/\zeta}$. This, of course, provides us no help in pinning down the precise values of ω and ζ, wrong or not (!), but the assumption, implicit in Imbrie's argument, that optimal paths constrained not to intercept behave as unconstrained paths is the simplest scenario. Nevertheless, even a quick glance at the figure leads one to believe, perhaps, that z grows faster than linearly with x.

To make more precise the mathematical notion of river basin ultrametricity, consider two destination points along the base of the DPRM delta, as well their associated locally optimal paths back to the apex. Define the *ancestral distance* between these two points as the number steps since their locally optimal paths last met at a common ancestor. Clearly, this is just the quantity z discussed above. It is easy to see, with this definition of distance and given the geometry of the DPRM river basin delta, that if one were to consider three points along the base (let us call them A, B, C), two of the ancestral distances would be equal and, furthermore, greater than the remaining separation; i.e., $z(A,C) = z(B,C) > z(A,B)$. In other words, the space and defined distance modulus require that any three points bear the relation of a tall, skinny isosceles triangle. Such spaces are termed ultrametric, and play an important role in fixing the free energy landscape in disordered statistical mechanical systems such as spin glasses. For a user-friendly introduction to such matters, see [Ram86r].

5.8.2. *Ancestry, progeny and distant relatives [Z87]*

In a study tangential to his investigation of DPRM ground-state instabilities, Zhang examined the scaling properties of the lowest excited states; that is, the locally optimal paths that were near, but slightly more costly that the globally optimal trajectory. Surprisingly, he discovered that the associated energy gaps decreased slowly with increasing path length, approaching constant values, indicating that the problem of directed polymers in random media may be characterized by a *discrete spectrum*. These constants are later known to be linearly proportional to the lattice spacing a. Upon taking a continuum limit, a can be made arbitrarily small, these low excited states are just degenerate ground states. They will be responsible for the weakly broken replica symmetry. The most interesting is the number of these degenerate states, we expect it to be an increasing function of the DP length t. This is yet to be studied. A look at how far away these lowest excited states were located, geometrically, from the ground state revealed that the mean displacements scaled with an exponent of 1/3. It was concluded that the immediate neighbors of the best path are too few to be chosen as lowest excited states – thanks to the family tree structure, we expect that the lowest excited states are among the relatives of the best path in an enlarged neighborhood. Roughly speaking, the ensemble of locally optimal paths can be divided up into families; each family having its own characteristic energy, the size of the family growing as $t^{1/3}$ and the number of families as $t^{2/3}$. Since the tree is hierarchical, families are descendents of superfamilies and so on, with the origin being the ultimate progenitor.

Thermal fluctuations may affect the best path in its own family, but as we learned in the previous section, if the random disorders undergo slow drifts, producing a slightly altered random energy landscape, the best path has a resistance to jump since its family members or close relatives are unlikely to compete with it (aptly referred to as *family protection*), though a completely different rival family which is typically far away may suddenly triumph thanks to accumulated gains, causing a long jump of the globally optimal path in the altered environment.

5.8.3. Cross-sections and branching probabilities [Per92,PHH92]

So much for organizational details. Let's get to the heart of the matter and discuss quantitative features of the DPRM river basin deltas. Perlsman and Schwartz [Per92] christened such endeavors with an investigation of the standard 1+1 DPRM subject to uncorrelated gaussian noise. Subsequent work by Pang and Halpin-Healy [PHH93], involving separate studies of linearly correlated gaussian noise, as well as uncorrelated power-law noise, established the universality of the river basin patterns, and corroborated the Perlsman-Schwartz hypothesis that many of the basic features of the network were dictated by the wandering exponent of the globally optimal path.

(i) *Cross-Section:* Consider a point p on the *central branch* of the DPRM river basin delta of Fig. 5.25; that is, the locally optimal path that connects the apex of the triangle to the center of the base. The height h of this point p is defined to be the number of steps between it and the base. In addition, we define a p-branch of this central path as the set of all bonds below p, belonging to *all* the locally optimal paths passing through p. Since locally optimal paths do not intersect, the p-branch is, apparently, also an ultrametric tree. We identify, in a very natural way, the number of base points belonging to a particular p-branch as the *cross-section* w of the central branch at that particular height. It is a direct measure of the total number of rivulets in the network that owe their existence to the central path. A glance at the DPRM river basin delta reveals that, for a single realization, w is a function that increases by discrete steps, suddenly saturating as $h \to t$, when we find ourself at the apex of the triangle. Averaging over many river basins to generate good statistics will smooth the steps, though only mildly ameliorating the abrupt saturation. Perlsman and Schwartz studied the scaling behavior of the cross-section of the center branch, as well as that of the globally optimal path, as a function of height, finding $w \sim h^{0.67}$ for $10 < h < 250$ in their river basin deltas of size $t = 1000$. In Fig. 5.26, we show the corresponding data of Pang and Halpin-Healy for the cross-section of the globally optimal path in the case of (i) uncorrelated gaussian disorder, studied in [Per92], which has $\zeta_{RB} = 2/3$, (ii) uncorrelated power-law noise characterized by $\mu = 3$, with $\zeta_{\mu=3} \approx 4/5$, and (iii) linearly correlated, gaussian disorder, well known for its $\zeta_{RF} = 1$. Statistical averages were performed over 5000 realizations of the random energy landscape, path lengths were 500 steps. In each instance, the cross-section scales with the wandering exponent characteristic of the particular form of disorder! Interestingly, it is only the value of ζ that appears to matter, since one observes, see [PHH93], nearly identical scaling behavior of the cross-section for RF and $\mu = 2$ DPRM, both of which are characterized by a wandering exponent of unity. One concludes, in concert with Perlsman and Schwartz that there is no way of deciding the size of a tree by looking at p-branches of the globally optimal path or central branch for p's of height h, provided $h \ll t$; i.e., if we stay away from the apex. Imbrie's notion [I87] of self-similarity is vindicated.

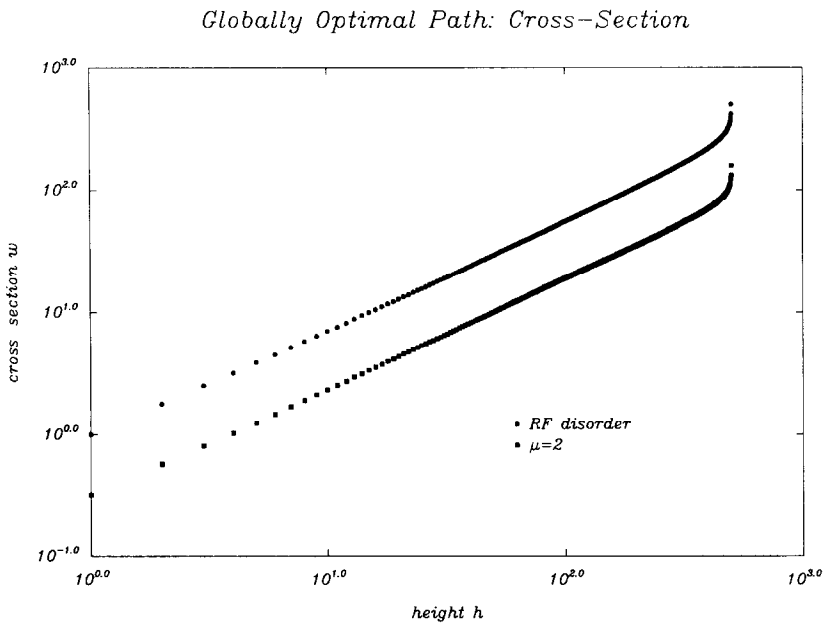

Fig. 5.26. *Cross-section* of the globally optimal path as a function of height h from the base of the river basin delta. At a particular height, w is defined as the total number of rivulets that emanate from the globally optimal path below that point. The data sets correspond to two different disorder distributions. In each case, however the cross-section scales in a manner dictated by the corresponding wandering exponent.

(ii) *Branching probability:* Perlsman and Schwartz also showed for the standard 1+1 DPRM that the total number of branches splitting off the globally optimal path grows very slowly; in fact, only *logarithmically* with the height from the base. This is easily understood as a consequence of the fact that the statistical probability $P(h)$ that the globally optimal (or central) branch splits between h and $h + dh$ must be proportional to $1/h$, a result which follows immediately from the fact that the width $w(h)$ of a branch at height h, is simply the sum of the widths of the branches that split from it at lower heights:

$$w(H) = \int_1^H w(h')P(h')dh' \tag{5.131}$$

Because the numerical studies reveal the cross-section $w(h)$ to be a power law in h, simple dimensional considerations require $P(h) \propto 1/h$. The universality of this result has been confirmed, see Fig. 5.27. Regardless of the underlying probability distribution or correlation in the disorder, the branching probability of the DPRM river basin delta falls inversely with height from the base [PHH93]. Interestingly, this general behavior has surfaced, recently, with the context of fracture statistics – see the work of Bouchaud et al. [BBL93].

Lastly, we indicate in Fig. 5.28, the *geomorphological* shifts which result in the DPRM river basin delta as one changes, in this case, the power-law tail of the distribution controlling the energies of the random landscape. The following features are readily apparent. For $\mu = 1$, which corresponds to an extreme Lévy flight case, there is a predominance of straight-line segments and a persistance

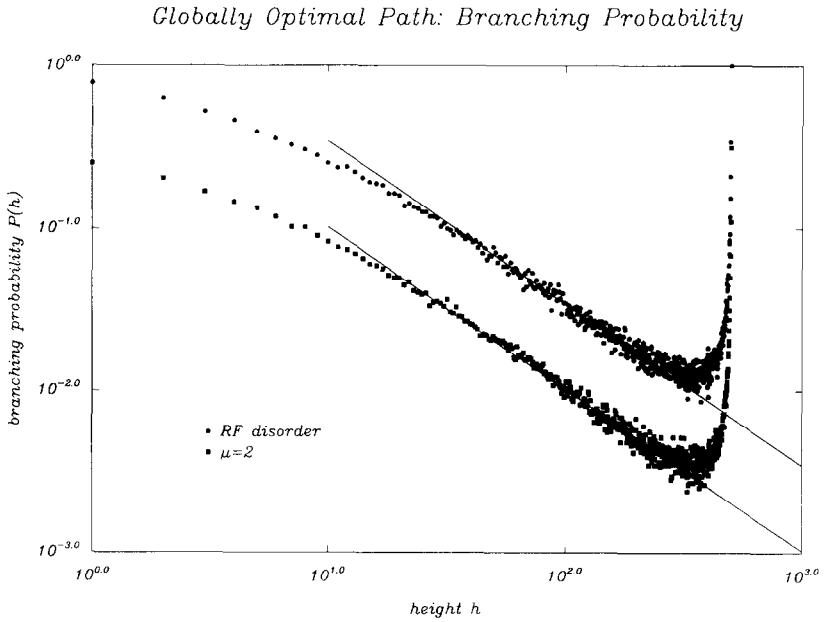

Fig. 5.27. *Branching probability* of the globally optimal path as a function of height for the RF and $\mu = 2$ DPRM. $P(h)$ is the normalized probability, here obtained by sampling 5000 realizations of the random energy landscape, that the overall best path branches at a height h above the base of the river basin delta. The straight lines have slope -1, providing strong evidence that, aside from crossover and saturation effects, this probability falls inversely with height in a universal manner, independent of the underlying noise distribution [PHH93].

of right angle vertices on *macroscopic* scales that appear lost, or at least greatly weakened, as μ is increased beyond 2 or 3. This substantive qualitative change is also manifest as $\mu \to 3$ in an increased jaggedness of the trajectories and an enhanced meandering in the middle of the delta. By contrast, a comparison of the deltas for μ=3 and μ=7 reveals a change that is much more modest, being one of degree rather than kind. In other words, the important geometric characteristics gleaned from the μ=3 delta are maintained, and merely amplified, as the range of the power-law tail is decreased.

5.9. The many-dimensional DPRM

Since its introduction by Kardar and Zhang [KZ87] a few years back, the many-dimensional DPRM has had, either directly or via its incarnation within the KPZ kinetic roughening context, a rather colorful history with much debate raging over the dimensionality dependence of the strong-coupling exponents, as well as the possible existence of a finite-temperature phase transition.

5.9.1. Strong-coupling exponents

Let it be said that the early numerical work [KZ87] suggested that the zero-temperature wandering exponent was superuniversal; that is, $\zeta_{n+1} = 2/3$ regardless of the number of transverse dimensions n. Indeed, there was even a rough proof sketched out that corroborated this notion [MM87]. Nevertheless, it soon became clear that this was not the case – simulations by Wolf and Kertész in Eden growth [WK87], when translated into the language of the DPRM, confirmed the decrease of exponents with

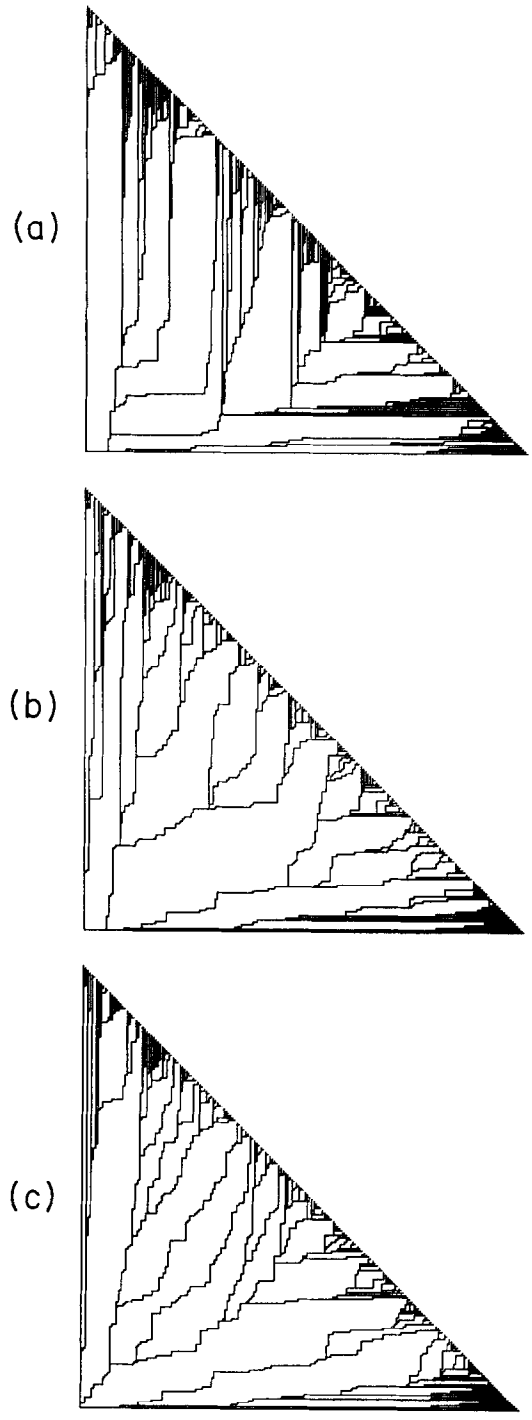

Fig. 5.28. River basin deltas associated with the power-law DPRM : (a) $\mu = 1$, (b) $\mu = 3$, and (c) $\mu = 7$. The patterns were all generated from the same seed, but evolve differently when the tail of the distribution is changed [PHH93].

dimensionality, finding $\zeta_{2+1} \approx 0.60$, a value not at all inconsistent with an approximate 1-loop functional renormalization group calculation of Halpin-Healy [HH90]. A more extensive simulation soon thereafter by Kim and Kosterlitz [KK89] on an RSOS version of ballistic deposition furnished the community with a more refined estimate for the wandering exponent, $\zeta_{2+1} = 0.625 \pm 0.005$; this value, coupled to the known result for the 1+1 DPRM and their estimates in higher dimensions, led to the famed KK conjecture, which for the many-dimensional DPRM, read $\zeta_{n+1} = (n+3)/2(n+2)$. The careful reader should note the monotonic decrease of this exponent with increasing n; in fact, as $n \to \infty$, we retrieve, perhaps not surprisingly, purely entropic wandering in the limit of infinite dimensionality. Despite the immediate appeal of the KK conjecture (a simple rule yielding rational exponents!), more recent numerical studies [FT90,TFW92,AV94], which yield $\zeta_{2+1} = 0.624 \pm 0.001$, have resulted in its demise (RIP!), though not without some modest death-bed protest [KBM91a]. The best direct estimates to date for the 3+1 DPRM are to be found in unpublished data of Nattermann and Renz [NR90] which indicate $\zeta_{3+1} \approx 0.585$, consistent with the KPZ growth model value $\beta_{3+1} = 0.180 \pm 0.002$ [AHKV92], recall Section 3.4. Regarding the wandering exponent of the $T = 0$ many-dimensional DPRM, it should be stressed that the quoted uncertainties are a highly subjective matter, becoming a lighting rod of sorts when friendly, though serious discussions between the relevant groups are had. Since a distinction in the third decimal place necessarily involves a bit of black magic and may be a divisive matter for specialists in the art of numerics, we will be content in this review to avail ourselves frequently of the KK values, which serve well enough on most occassions.

5.9.2. DPRM phase diagrams

Simply put, the many-dimensional DPRM possesses a very phase rich structure when the model is extended to finite temperatures. Recall that at $T = 0$, the DPRM is essentially a global optimization problem in which energy considerations reign, entropy is irrelevant, and a single path dominates the partition function. By contrast, for $T > 0$, all paths are weighted by the appropriate Boltzmann factor, giving rise to a competition between energy and entropy that may yield, for sufficiently great temperatures in large enough dimensionalities, a high temperature phase where the wandering of the polymer is dictated by thermal fluctuations, rather than being disorder-induced. It is now well understood that this is the case for all $n > 2$, so that the 3+1 DPRM has a finite-temperature phase transition, whereas the 1+1 DPRM does not – its wandering always being controlled by the zero-temperature strong-coupling fixed point. These facts can be appreciated by various arguments, including a simple physical picture based on standard quantum mechanical arguments, a Harris criterion specifically tailored to the DPRM problem, and a rigorous mathematical proof.

(i) *Physical picture [LL62]:* The $n+1$ DPRM can be viewed as the world line of a point particle moving in n spatial dimensions. Replicating the partition function N times, performing the disorder average leads to the quantum mechanical problem of N bosons in n dimensions interacting via a short-ranged potential $R(x-x')$. In $n = 1$, we take $R(x) = \delta(x)$ explicitly and the ground state dominating the large t-behavior is an N-body bound-state. For $n > 2$, however, the delta function attractive potential is not well-defined, see [LL62] or your favorite graduate QM text, and one must consider a potential well of finite depth and width. It is standard quantum mechanical lore that there is no bound state if the well is too shallow, though a bound state betweeen the replicas can be formed upon raising the strength of the potential. It is the replica

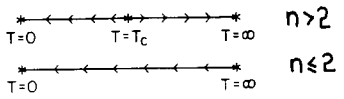

Fig. 5.29. RG flows in temperature space for the $n+1$ DPRM, as determined by a Harris criteron [HH90].

bound state that dictates the physics of the strong coupling fixed point. If you lose the bound state, you lose the physics.

(ii) *Harris criterion [HH90]:* Given the elastic piece of the DPRM hamiltonian,

$$Z = \int Dx \exp -\frac{1}{T} \int \left(\frac{dx}{dt}\right)^2 ,$$

it is apparent that, upon infinitesimal rescaling, the temperature renormalization flow equation reads

$$\frac{dT}{dl} = (\tfrac{1}{2} - \zeta)T \tag{5.132}$$

to first order in a perturbation expansion in T, which forms the basis of the functional RG approach to the DPRM [HH90]. This recursion for T indicates that the zero-temperature, strong-disorder fixed point is *stable* against a finite-temperature perturbation provided the wandering exponent exceeds its simple entropic value. As discussed previously, this is apparently the case for all finite dimensionalities, which implies that the RG flow always runs into the $T = 0$ fixed point, regardless of dimension, see Fig. 5.29. To establish the simplest overall phase diagram topology, it is necessary to address the issue of stability at the $T = \infty$ fixed point against disorder perturbations. A Harris criterion,

$$\alpha = 2 - \nu_{\|} d_{\|} - \nu_{\perp} d_{\perp} = 2 - 1 - \tfrac{1}{2}n = 1 - \tfrac{1}{2}n > 0 \tag{5.133}$$

reveals that the infinite temperature fixed point, characterized by purely entropic wandering $\zeta = 1/2$, is indeed *unstable* for $n < 2$, giving rise to the RG flows in temperature space shown in Fig. 5.29. Note the existence of a finite-temperature phase transition for $n > 2$, separating disorder-induced and thermal wandering. More on this in Section 5.9.4.

(iii) *Rigor [IS88]:* Imbrie and Spencer have established that for all $n > 2$, there is a finite temperature beyond which the free energy of the many-dimensional DPRM is given by an annealed, $\ln\langle Z\rangle$, rather than quenched average, $\langle \ln Z\rangle$, implying an entropic wandering exponent. Similar arguments have been advanced and utilized, with somewhat lighter mathematical baggage, by Derrida and coworkers [DG89].

The marginal case $n = 2$, resistant to the above arguments and once a source of debate [DG90,PJ90], requires special care. Nevertheless, it has been convincingly shown that the 2+1 DPRM is, like its counterpart in one less dimension, devoid of a finite temperature phase transition, though it does possess *excruciatingly* long crossovers before exhibiting asymptotic scaling characteristic of the strong coupling fixed point. We now focus our attention on this interesting case.

5.9.3. *Slow crossovers in* $2+1$ *[TNF90,KBM91b]*

In endeavoring to establish the existence of a possible high-temperature phase of the many-dimensional DPRM, one is very naturally led to consider the thermal properties of the quantity

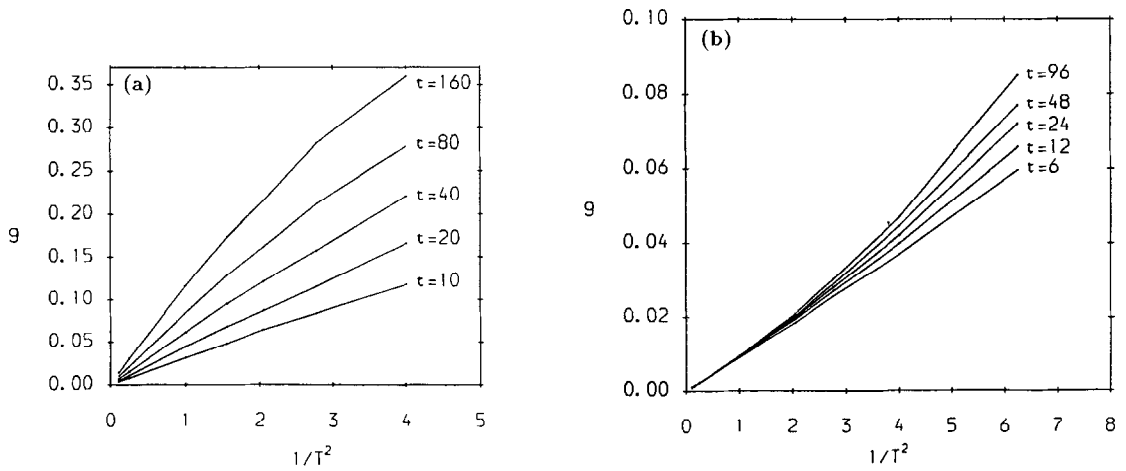

Fig. 5.30. $g(T,t)$ vs. $1/T^2$ for directed polymers of various lengths in (a) 1+1, and (b) 2+1 dimensions [KBM91b].

$g(T,t) = \langle\bar{x}\rangle^2/\langle\bar{x^2}\rangle$, which depends on both the temperature T and the length t of the polymer, and is inspired by Binder's g factor defined for spin glasses [Bin81]. Here the overbar refers to the disorder average, while angular brackets denote thermal averages, taken with respect to the Boltzmann weight. At the infinite temperature fixed point, $g = 0$ because $\langle x\rangle$ vanishes by symmetry, even before the disorder average is taken. By contrast, for T=0, $\langle x^2\rangle = \langle x\rangle^2$, which implies that $g = 1$. Within a finite-temperature formulation of the many-dimensional DPRM, Kim, Bray and Moore [KBM91b] performed a weak-disorder/high-temperature expansion, finding to first order in σ^2/T^2,

$$g(T,t) = \frac{2\sigma^2[e^{\gamma/T} + 2(d-1)]^{(d-1)/2}}{(5-d)(8\pi)^{(d-1)/2}T^2}\, t^{(3-d)/2} \tag{5.134}$$

where σ^2 gauges the disorder strength and γ is the energy cost against a single transverse step, left or right, made by the polymer; recall the standard variables in a finite temperature DPRM transfer matrix calculation. Immediately, one notes:

$d = 1 + 1$: For fixed T, g increases with t, indicating the absence of a high-temperature phase. A transfer matrix analysis of the DPRM devoted to extracting the behavior of g has confirmed the quartic dependence of the crossover length scale $t^*(T) \sim T^4$, beyond which the scaling is controlled by the strong coupling fixed point, yielding a wandering exponent $\zeta = 2/3$. For path lengths $t \ll t^*$, the wandering is entropic in nature. Fig. 5.30a shows the scaling plot of $g(T,t)$ in this dimensionality for a range of temperatures.

$d = 2 + 1$: The subtle, marginal dimension. Including the next order term in the high temperature expansion for g, one has

$$g(T,t) \sim \frac{\sigma^2}{T^2}\left(1 + C\frac{\sigma^2 \ln(t/t_0)}{T^2}\right) \tag{5.135}$$

where C is a positive constant and t_0 is a cutoff length. Since g grows logarithmically with path length, it is apparent that the $T = \infty$ fixed point is, in fact, unstable, though the crossover length scale has a very strong dependence on temperature, $t^* \sim e^{T^2}$, a feature which has been noted in the growth

model context by Tang, Nattermann and Forrest [TNF90]. Kim, Bray and Moore [KBM91b] have strong numerical evidence supporting this scaling form for $g(T, t)$. Consequently, the 2+1 DPRM, like the 1+1 DPRM, exhibits no high temperature phase, the scaling at any finite T ultimately controlled by the zero-temperature, strong coupling fixed point. A glance at Fig. 5.30b suggests the numerical subtleties induced by this enormous crossover length scale – although the curves corresponding to different polymer path lengths appear to meet at $T = 1$ and stick together for higher temperatures, a careful examination reveals an increase in $g(T = 1, t)$ for increasing t. In fact, the increase agrees precisely with the logarithmic behavior dictated above in the high temperature expansion! The sly behavior of this quantity was responsible for, and no doubt ameliorates a mistaken assertion, by several groups, concerning a finite-temperature phase transition in this dimensionality [PJ90,DG90].

5.9.4. Transfer matrix studies. III. Phase transition in $3 + 1$ *[PJ90,DG90]*

The first thorough numerical study of the dimension dependent properties of the finite temperature DPRM was due to Derrida and Golinelli, [DG90] whose transfer matrix analysis concentrated on the finite size scaling of the specific heat, as well as its derivative. Their starting point was the recursion relation for the Boltzmann weight Z connecting successive time slices. They considered systems that were very long, of length L in the longitudinal direction, but of finite extent n in the transverse dimensions, with periodic boundary conditions suitably imposed. Thermal properties of the true system ($n = \infty$) were established by noting the n dependence of the relevant physical quantities as the system size increased. For finite size lattices, determination of the free energy of the finite-temperature d-dimensional DPRM amounts to finding the largest Lyapunov exponent of a product of L random matrices of size $n^d x n^d$.

In the case of the 3+1 DPRM at finite temperature, Derrida and Golinelli considered a single random sample of length $L = 10^4$ for transverse system sizes $n = 2, 4, 8, 16, 32$, and with bond energies drawn from a gaussian distribution $\rho(\epsilon) = (2\pi)^{-1/2} e^{-\epsilon^2/2}$. Disorder-averaging over many realizations of the random energy landscape (here a slab) is not necessary because, for finite n, the system is one-dimensional, which means that for sufficiently large L, all thermal quantities are self-averaging. In Fig. 5.31 is shown the specific heat

$$c_n = \frac{d}{dT}\left(T^2 \frac{d}{dT} \frac{\ln Z(L)}{L}\right)$$

and the third derivative, $a_n = d^3/d\beta^3 (\ln Z(L)/L)$, of the 3+1 DPRM free energy w.r.t. $\beta = 1/T$. Note, see Fig. 5.31a, that the specific heat sharpens as the system size is increased, a necessary but not sufficient signature of a phase transition singularity. Beyond the incipient peak, the specific heat falls inversely as T^2, consistent with the notion that the free energy of the high temperature phase is dictated by an annealed average over the gaussian disorder,

$$\frac{\ln Z_L}{L} = \frac{\ln\langle Z_L\rangle}{L} = \ln[2d\langle e^{-\epsilon/T}\rangle] = \ln 2d + \beta^2 \tag{5.136}$$

which also requires that $a_n(T)$ vanish there, see Fig. 5.31b. Indeed, as we mentioned above, it is a general and rigorous result due to Imbrie and Spencer [IS88] that for T sufficiently large, the free energy of the finite temperature DPRM in dimensionality $d+1>2+1$ is given with probability 1 by the annealed, rather than quenched, average. For the case at hand, with gaussian distributed energies,

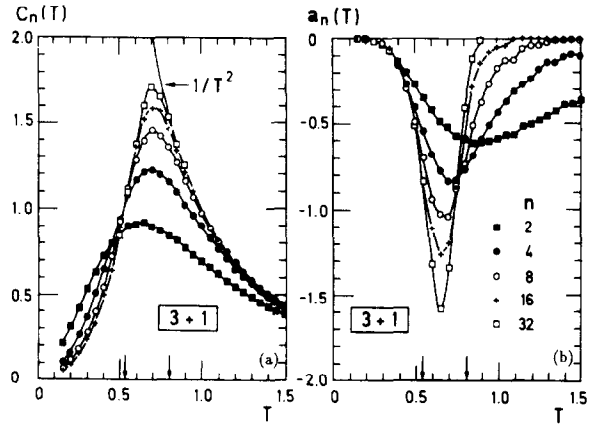

Fig. 5.31. (a) Specific heat $c_n(T)$, and (b) third derivative $a_n(T)$ of the free energy, as a function of temperature for 3+1 DPRM. The path length $L = 10^4$, the transverse system sizes $n = 2, 4, 8, 16, 32$, and the arrows indicate analytical bounds derived by [DG90] for the transition temperature.

Derrida and Golinelli showed that the ratio $\langle Z_L^2\rangle/\langle Z_L\rangle^2$ had a finite limit as $L \to \infty$ for temperatures $T > T_2(d) = [\ln(1 + 2/J_d]^{-1/2}$, where

$$J_d = \int_0^{2\pi} \frac{dq_1}{2\pi} \cdots \int_0^{2\pi} \frac{dq_d}{2\pi} (d - \sum_{\mu=1}^{d} \cos q_\mu)^{-1},$$

permitting them an *upper* bound on the phase transition temperature. In particular, $T_2(d = 3) = 0.790$, see Fig. 5.31. A *lower* bound on T_c can be had, as well, by noting that the entropy associated with the annealed free energy goes negative for temperatures $T < T_0(d) = (2\ln 2d)^{-1/2}$, which implies $T_c > 0.528$ for $d = 3$. It is satisfying indeed that the observed critical temperature of the 3+1 DPRM sits comfortably between these bounds! Lastly, finite-size scaling analysis yields a specific heat exponent $\alpha = -0.10 \pm 0.10$, characterizing the singular part of the free energy at $T_c = 0.60 \pm 0.03$ from below. There is no singularity as $T \to T_c^+$ because the free energy there is given by its annealed value, as discussed earlier. This finite-temperature phase transition was observed, simultaneously, in the KPZ kinetic roughening context via the beautiful work of Pellegrini and Jullien [PJ90].

5.9.5. Hierarchical lattices [DG89,HH89b,HH90,FH91,MK93]

The Derrida-Griffiths RSRG, [DG89], a variant of the Migdal-Kadanoff method specifically adapted to situations with quenched random disorder, is a procedure that is, at least in principle, exact upon hierarchical lattices – those carefully crafted lattices whose connectivity is such that bond moving incurs no approximation, see Fig. 5.32. If one considers the ith generation of the b-branch hierarchical lattice illustrated in the figure, there are b^{i-1} possible directed paths between the points A and C, each of which has length $L = 2^{i-1}$. For the zero-temperature DPRM on the hierarchical lattice, we associate, as usual, random energies with each of the bonds and search for the globally optimal path of least energy. Averaging over many realizations of randomness and studying the statistical properties of the optimal path's energy as a function of the trajectory length L, we can ascertain the energy fluctuation exponent ω, since rms deviations from the mean will scale as L^ω. Within the context of the Derrida-Griffiths RSRG, the fundamental object of interest is the probability

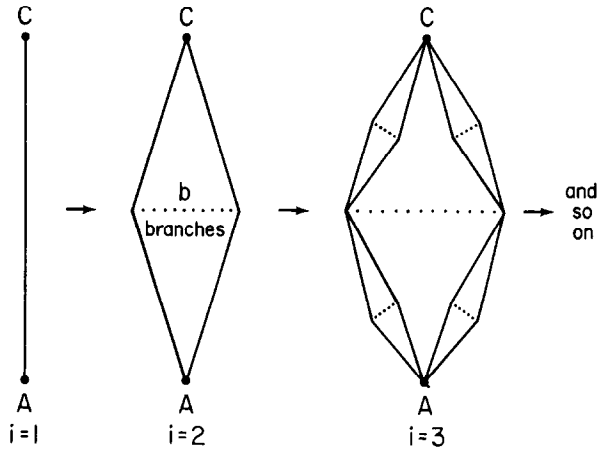

Fig. 5.32. b-branch hierarchical lattice, connecting the points A and C, shown through the third generation ($i = 3$). A succeeding generation is obtained from the previous one by splitting each bond in half, followed by b-fold replication.

distribution $P(x)$, from which the uncorrelated random bond energies are drawn. The crucial feature of the method is a functional recursion relation which dictates the manner in which this probability distribution is transformed after successive generations, as we look at effectively larger and larger length scales. With P_i denoting the functional form of the probability distribution at the ith generation, the renormalized distribution at the next generation is obtained via a multistep process. First, splitting each bond in two (i.e., doubling the path length $L \rightarrow 2L$) necessitates a self-convolution of the probability distribution

$$Q_i(x) = \int P_i(x-y)P_i(y) \tag{5.137}$$

while the b-fold replication of the branch requires

$$\int_x^\infty P_{i+1}(y)\,dy = \left(\int_x^\infty Q_i(y)\,dy\right)^b \tag{5.138}$$

so that the probability distribution at the $(i+1)$th generation is given by

$$P_{i+1}(x) = bQ_i(x)\left(\int_x^\infty Q_i(y)\,dy\right)^{b-1} \tag{5.139}$$

which, in fact, is the form of the functional recursion utilized most naturally in practice. The appropriateness of the second step was made particularly manifest by the observation of Derrida and Griffiths that, in order for the optimal path's energy not to exceed a certain value, it must not do so in each of the newly created b branches. Hence, it is the b^{th} power of the partially integrated convolution that is relevant and must be equated to a similar integration of the renormalized distribution. For a given hierarchical lattice (that is, for a specific value of b), one determines the energy fluctuation exponent ω following from the Derrida-Griffiths RSRG by iterating the functional recursion relation for P and noting the evolution of its width after successive generations. As the path length doubles from one

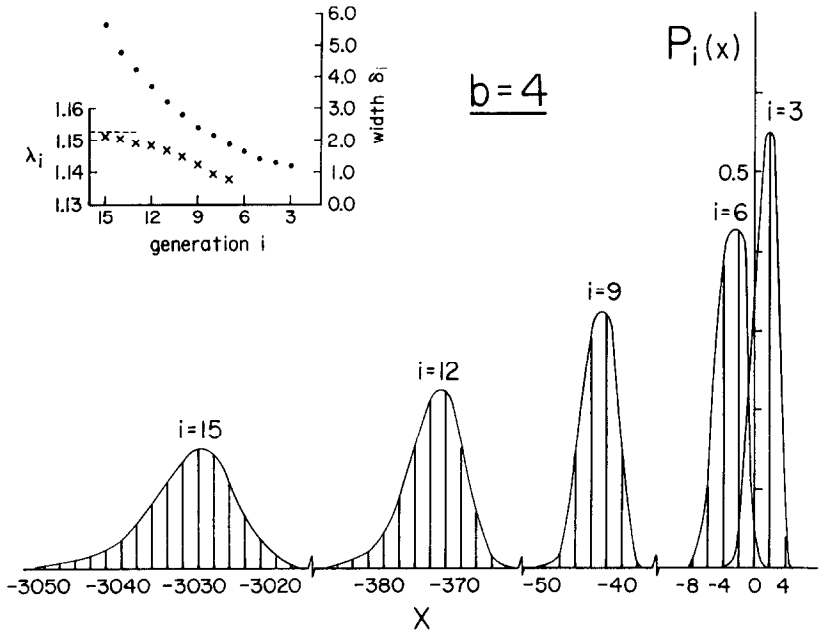

Fig. 5.33. Renormalized probability distributions $P_i(x)$ at generations i=3,6,9,12,15, using the Derrida-Griffiths RSRG for the DPRM on a $b = 4$ disordered hierarchical lattice. The inset shows the absolute rms width δ_i of the iterated distribution, as well as the width renormalization factor $\lambda_i = \delta_i/\delta_{i-1}$, which asymptotically approaches the value $\lambda \approx 1.152$ [HH90].

generation to the next, the width of P ought to increase by a factor that asymptotically approaches a value $\lambda = 2^{\omega}$.

Guided by a strong faith in the principle of universality and motivated by calculational convenience, one concentrates on initial (or, using the language of the renormalization group, bare) probability distributions of the form

$$P_i(x) = p\delta(x-1) + (1-p)\delta(x+1) \tag{5.140}$$

with $p \approx 1^-$ sufficiently large, for the dimensionalities of interest, to guarantee that the (-1) bonds do not percolate across the lattice, while simultaneously maximizing smooth, quick convergence of the successive λ_i. Iteration of the functional recursion leads in this manner to an ever growing collection of δ–function spikes whose coefficients and center of mass are altered with each new generation. The numerical aspects of this procedure are handled with relative ease on a computer. In Fig. 5.33 are illustrated typical results for the particular case $b = 4$, indicating the form of the renormalized probability distribution for generations $i = 3, 6, 9, 12, 15$. The most transparent features are the decreasing height and increasing width of successive iterates as the renormalized distribution runs off in the direction $-\infty$. The accompanying inserts document the absolute width δ_i and the width renormalization factor $\lambda_i = \delta_i/\delta_{i-1}$ as a function of the generation i. After a dozen iterations, the RG procedure is well enroute to asymptopia (easily so for b this small), and we obtain $\lambda = \lim_{i\to\infty} \lambda_i \approx 1.152$, which implies an energy fluctuation exponent $\omega(b = 4) = \ln_2 \lambda \approx 0.0204$, there being an uncertainty of ± 2 in the last digit if one terminates the iteration process at $i = 15$. In Fig. 5.34 is summarized results for ω for $b \leq 12$, using the Derrida-Griffiths RSRG. With

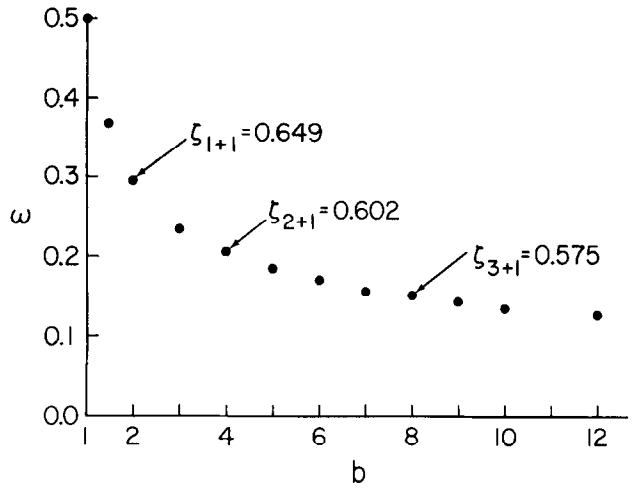

Fig. 5.34. Energy fluctuation exponent $\omega = \ln_2 \lambda$ for general b, calculated via the RSRG. Using the relation, $b = 2^{d-1}$, sanctified by tradition permits us to translate our results into RSRG estimate for the many-dimensional wandering exponent ζ_d [HH90].

the standard, but approximate correspondence between b–branch hierarchical and d–dimensional hypercubic lattices, $b = 2^d - 1$, we connect immediately to the physically relevant cases, showing explicitly estimates for the many-dimensional DPRM wandering exponent $\zeta = (\omega+1)/2$. The validity of the correspondence notwithstanding, the general trend concerning the dimensionality dependence of the scaling indices is clear. For $d = 1$, the exact value $\omega = 1/2$ is retrieved, followed by a steady decline toward zero as d is increased. As pointed out by Derrida and Griffiths, the result for $d = 2$ is a bit below the known wandering exponent $\zeta = 2/3$, which is where the RSRG estimate belongs presumably [BK92], a recent conjecture [RH91] notwithstanding. There is great interest, of course, regarding higher dimensionalities, which have thus far eluded exact analysis. Whereas a 1-loop functional RG analysis [HH90] gives $\zeta_{2+1} = 3/5$, the Derrida-Griffiths RSRG yields 0.602, both methods clearly underestimating the accepted value $\zeta_{2+1} \approx 0.62$ [FT90,TFW92,AV94]. A more powerful implementation of this method, investigating the large dimension limit can be found in the paper of Fisher and Huse [FH91]. Nevertheless, the RSRG method is intrinsically unsuited to settle matters regarding a possible upper critical dimension, see Section 6.4 for alternative techniques. On a different front, Medina and Kardar have managed an insightful application of the Derrida-Griffiths RSRG to study the validity of the continuum approximation for the 1+1 DPRM, see [MK93]. Their work makes explicit efforts to pin down the size of the replica bound state as a function of the lattice disorder σ^2, diffusion constant γ, and temperature T employed in numerical transfer matrix calculations. Finally, as we discuss in section 6.2.3, Tang and Lyuksyutov [TLv93], as well as Balents and Kardar [BK94], have employed the Derrida-Griffiths RSRG to study delocalization of directed polymers from line defects on the hierarchical lattice.

6. DPRM extensions

In this brief, final chapter, we address several topics naturally related to the problem of directed polymers in random media. We start with a presentation of a DP model in a *vector* potential, related to the well-known problem of passive scalars in turbulent fluids. In this context, we apply the replica scaling theory to obtain the relevant probability distribution function (PDF). We then discuss disorder-induced delocalization from extended defects, a subject of great relevance to vortex-line wandering in superconducting materials possessing columnar pins and grain boundaries, in addition to point impurities. Next, we consider directed polymers with complex weights, where interesting interference effects between coincident paths can arise. Nevertheless, at the day's end, the numerics will indicate a single DPRM universality class there. Lastly, we conclude with a short word on the statistical mechanics of diverse manifolds in random media, paying particular attention to domain-wall roughening, though emphasizing the utility of this unifying picture, where various functional renormalization group and variational approaches have been applied with some measure of success.

6.1. Passive scalars [Z90c]

We shall see that the passive scalar equation can be interpreted as a natural generalization of the DP models discussed in Chapter 5. Instead of scalar quenched random potential, it is replaced by a vector field-the random fluid velocity. The wave function now is interpreted as the concentration of a scalar field-e.g. temperature. We want to use the previously developed non-perturbative DP tools here to be able to predict the distribution of the concentation field. Below, we briefly outline the background of the problem.

Before starting, the reader should be aware of the more direct approach using the geometrical measure theory, developed by Constantin and Procaccia [PC93,CP93]. The approach offered below is less realistic for the moment in the sense we still need the unjustified assumption about the velocity distribution field. In any case, this approach can be potentially important if further breakthrough in handling the velocity distribution is achieved. From theoretical point of view the DP method described below gives unique insight into the higher moments in a nonperturbative manner.

Passive scalar fields in turbulent fluids are of great general interest in physics; indeed, much experimental and theoretical work has been devoted to them. A passive scalar field may represent, for example, temperature or, perhaps, the concentration of a dye in a background random fluid. Recently, it has been pointed out that the passive scalar field may follow some singular distribution. Indeed, Sinai and Yakhot [SY89] have argued in favor of a universal distribution. They were able to relate the distribution for the spatial gradient of temperature $(\nabla T)^2$ to that of the temperature T itself. For the first time they have derived a power law distribution. While the above authors consider the static limit $(t \to \infty)$, we shall concern ourselves here with dynamical relaxation processes. We consider the initial value problem of a conserved passive scalar field. We find that while the passive scalar field relaxes from the initial inhomogeniety towards its final equilibrium state, its fluctuation, or probability distribution function has two distinct behaviors depending on the correlation function of the background fluid. First, there is a diffusive region where the PDF is sharply concentrated; second, a turbulent region where the PDF obeys a power law $P(\theta) \sim 1/\theta$ under rather general conditions.

The equation of motion of a passive scalar field $\theta(\boldsymbol{x}, t)$ is

$$\dot{\theta} = (D\nabla^2 - \boldsymbol{u}\cdot\nabla)\theta(\boldsymbol{x},t) \tag{6.1}$$

where $\boldsymbol{x}$ is a vector in a d-dimensional space, the random velocity field $\boldsymbol{u}(\boldsymbol{x},t)$ is subject to the incompressibility condition $\nabla\cdot\boldsymbol{u}=0$. It looks like (5.1), but now the wave function is coupled to the vector potential. The fluid velocity field can be regarded as "quenched" since it influences θ and not the other way. Note that this equation enjoys translation ($\theta\to\theta+c$), inversion ($\theta\to-\theta$), and dilation ($\theta\to c\theta$) symmetries – the last would imply a scale-invariant PDF, $P(\theta)\,d\theta\sim d\theta/\theta$. However, the initial and boundary conditions do not respect these symmetries. In the following we shall show that the dilation symmetry is in fact broken in the diffusive region, whereas in the turbulent region (to be specified below) it is only very weakly broken so as to allow a very broad range of θ in which $P(\theta)$ is approximately $1/\theta$. We restrict ourselves here to an investigation of the simplest initial value problem, $\theta(\boldsymbol{x},t=0)=\delta(\boldsymbol{x})$. The space is continuous and infinite. The static limit of our present problem is trivial: $\theta(\boldsymbol{x},t\to\infty)\to 0$.

Our strategy here is to study the disorder averaged moments $\langle\theta^n\rangle$, which in turn will enable us to find an effective $P(\theta)$, like we have outlined in Section (5.4.3). For this purpose we need to rewrite the differential equation (6.1) in Feynman path integral form, which we shall see later is particularly suitable for evaluating the moments. Note that (6.1) linear in θ and it is of first order, consequently it admits a path integral solution. Following the original steps of Feynman, we find

$$\theta(\boldsymbol{x},t)=\int_{(\mathbf{0},0)}^{(\boldsymbol{x},t)} D\boldsymbol{x}\exp-\frac{1}{4D}\int_0^t d\tau(\dot{\boldsymbol{x}}-\boldsymbol{u})^2. \tag{6.2}$$

The above expression implies a sum over all the line configuration directed in the time direction. The initial condition requires that all configurations start from the same point $(\mathbf{0},0)$. The action, a terminology from quantum physics, has simple physical meaning: when the diffusion constant D, the analog of Planck's constant h, or temperature T in statistical mechanics, approaches zero, the dominant paths are those that satisfy the equation of Lagrangian motion [Vul89]:

$$d\boldsymbol{x}/dt=\boldsymbol{u}(\boldsymbol{x},t) \tag{6.3}$$

which is traditionally used to describe the classical motion of marker particles. The above path integral formulation (6.2) falls into the category of so-called directed polymers, recall chapter 5.

The above average is over random fluid, hence we must specify its space-time correlation function,

$$\langle u_\mu(\boldsymbol{x},t)u_\nu(\boldsymbol{x},t)\rangle = 2R_{\mu,\nu}(\boldsymbol{x}-\mathbf{x}',t-t') \tag{6.4}$$

where $\langle\ldots\rangle$ denotes an ensemble average, while the greek index μ refers to the μth component of a d-dimensional vector. Such a correlation function can be regarded as being generated by the gaussian measure

$$\frac{1}{\sqrt{\det\boldsymbol{R}}}\int D\boldsymbol{u}\exp-\tfrac{1}{4}\boldsymbol{u}\cdot\boldsymbol{R}^{-1}\cdot\boldsymbol{u} \tag{6.5}$$

where $\boldsymbol{R}^{-1}$ is the inverse matrix of $\boldsymbol{R}$. The matrix has space-time indices, as well as tensor component indices, and below we shall also introduce latin letters as replica indices. Summation over continuous variables is understood as integration. Often we shall suppress these subscripts for the sake of simplicity.

By assuming the gaussian measure we have done gross injustice to the background turbulent fluid whose space-time velocity correlation functions are known not to be gaussian [Oz73]. Ignoring higher moments implies that our theory at this stage does not take into account many important aspects of the fluid itself, such as intermittancy in fluid velocity; or line-like, sheet-like and multifractal objects [HP82]. However as we will see below, even the gaussian behavior of the background fluid velocity can generate singular distributions for the passive scalar; that is, a distribution with a long tail. Therefore, our simple assumption serves to single out what is responsible for the singular distribution of passive scalars. Eventually when our theory is extended to include higher moments, to account also for the intermittant behavior of the fluid itself, we expect that our qualitative conclusions will not change.

In this work we consider the correlation function R to be of the form $R \sim x^{\alpha}$ and examine what value of α corresponds to physical reality. The energy spectrum of the fluid is defined through the second moment only,

$$E(k) = k^{d-1} \int d^d \boldsymbol{x} e^{i\boldsymbol{k}\cdot\boldsymbol{x}} R_{\mu,\mu}(\boldsymbol{x}) \tag{6.6}$$

where R is at equal time, $x = |\boldsymbol{x}|$ and repeated greek indices are summed. If the fluid is driven at sufficiently high wave numbers, i.e. at molecular levels, the energy spectrum at low wave numbers [FNS77] is $E(k) \sim k^{d-1}$, with the corresponding scaling behavior $R \sim x^{-d}$. At the other extreme, for fully developed isotropic turbulence, we have the homogeneous Kolmogorov law $E(k) \sim k^{-5/3}$, which implies that R has the scaling behavior and $R \sim x^{2/3}$. Procaccia and Zeitak [PZ89] have found that for the convective turbulence [Cas89] $R \sim x^{2/5}$. For the convenience of our analysis, we assume $R \sim x^{\alpha}$, with α lying continuously between $(-d, 2/3)$.

Now we first want to analyze the typical path integral solution of (6.2) in a given random fluid (without averaging). The path in (6.2) can be regarded as the trajectory of a marker particle in a random fluid, whose typical distance away from the origin at time t can be easily estimated. Note that (6.2) behaves as

$$\theta \approx a(t) \exp \frac{1}{4D}(-x^2/t + 2xu - u^2 t). \tag{6.7}$$

Since θ is conserved, the factor $a(t) \sim 1/t^{d/2}$ is there to make the spatial integral $\int d^d \boldsymbol{x}\, \theta$ normalizable. According to (6.4), we typically have $u^2 = R \sim x^{\alpha}$, or $u \sim x^{\alpha/2}$. (6.7) reaches a maximum when $x^{1-\alpha/2} = t$ for a given time t. This reproduces the Richardson law $x^{2/3} \sim t$ for fully developed turbulence $\alpha = 2/3$. This relation implies that thanks to the background velocity, a marker particle can be transported around much faster than by diffusion alone. For a very negative α on the other hand, if $1 - \alpha/2 > 2$, the diffusion mechanism dominates ($x^2 \sim Dt$) and the transport effect the flow is negligible. In all cases, we can express this relation via the so-called dynamical exponent z,

$$x^z \sim t \tag{6.8}$$

where

$$z = \min(1 - \alpha/2, 2)$$

so we see that the dividing value is $\alpha_o = -2$.

In order to study the θ-distribution, we consider the moments, $\langle\theta^n\rangle$, whose knowledge will allow us to find the full probability distribution $P(\theta)$. The analysis here follows closely the techniques [Z90d] developed for directed polymers in random media. The moment $\langle\theta^n\rangle$ is evaluated with the help of Eqs. (6.2) and (6.5):

$$\langle\theta^n\rangle = \int Dx N(\tilde{\boldsymbol{R}}, \boldsymbol{R}) \exp -\frac{1}{4D}\left[\sum_{i=1}^{n}\int d\tau\, \dot{x}_i^2 - \frac{1}{D}\sum_{i,j}^{n}\int d\tau\, d\tau'\, \dot{\boldsymbol{x}}_i(\tau)\cdot\tilde{\boldsymbol{R}}_{i,j}(\boldsymbol{x}_i(\tau)-\boldsymbol{x}_j(\tau'),\tau-\tau')\cdot\dot{\boldsymbol{x}}_j(\tau')\right]. \tag{6.9}$$

It describes n interacting paths, originating with the same initial condition. The mutual interaction kernel $\tilde{\boldsymbol{R}}$ (including interactions of the same path at different times) is induced by averaging over random velocities with the gaussian measure (6.5). Note that in the above expression $\langle\theta^n\rangle$ is considered only at the origin $(\boldsymbol{x}=\boldsymbol{0}, t)$. Due to the complication of the quadratic term u^2 in the action, the kernel $\tilde{\boldsymbol{R}}$ cannot, in general, be obtained in closed form; rather, it is the solution of the following integral equation,

$$\tilde{R}_{(i,j);(\mu,\nu)}(\boldsymbol{x}-\boldsymbol{x}', t-t') = R_{(i,j);(\mu,\nu)}(\boldsymbol{x}-\boldsymbol{x}', t-t') - \frac{1}{D}\sum_{k=1}^{n}\int d\tau\, R_{(i,k);(\mu,\gamma)}(\boldsymbol{x}_i(t)-\boldsymbol{x}_k'(\tau), t-\tau')\tilde{R}_{(k,j);(\gamma,\nu)}(\boldsymbol{x}_k(\tau)-\boldsymbol{x}_j'(\tau),\tau-t'). \tag{6.10}$$

Note that $\tilde{\boldsymbol{R}}$ is symmetrical in its indices and also satisfies the incompressibility condition $\nabla\cdot\tilde{\boldsymbol{R}}=0$. The presence of the factor $N(\tilde{\boldsymbol{R}}, \boldsymbol{R})$ in (6.9) is necessary because, in carrying out the $\boldsymbol{u}$-integration, we have used the kernel $\tilde{\boldsymbol{R}}$ instead of $\boldsymbol{R}$, resulting in the incomplete cancellation of the determinant in the measure. The full expression for N is too complicated to write down explicitly. For our purpose we need only consider scaling forms of (6.9) and (6.10). Another simplification comes from the fact that the spatial-temporal correlation function, $\boldsymbol{R}$ can be expressed as a function of space variable $\boldsymbol{x}$ only, this is due to the so-called frozen turbulence hypothesis that velocities at different times can be brought to an equal time upon a linear transformation.

After these considerations, $\tilde{R}$ of equation (6.10) takes the much simplified scaling form, $\tilde{R} = R - (nt/D)R\tilde{R}$, so

$$\tilde{R} = \frac{R}{1+Rnt/D}, \quad N(\tilde{R}, R) \sim \frac{1}{\sqrt{1+Rnt/D}}. \tag{6.11}$$

If $ntR/D \sim x^\alpha t \ll 1$ for large x, then we have $\tilde{R} \simeq R$ and $N(\tilde{R}, R) \simeq 1$. This happens when $\alpha < -2$. With the help of (6.8), we see this in this case $z=2$, so a marker particle follows diffusive motion. For $\alpha < -2$, the interaction energy's contribution (the second piece in the exponential of Eq. (6.9)) can be estimated,

$$\exp\left[\frac{n^2}{4D^2}\frac{1}{x^{|\alpha|-2}}\right]. \tag{6.12}$$

This implies an *attractive* interaction among the n paths, since the above factor favors the situation when the typical interpath distance x is small. Such an attractive force, however, is counteracted by

the appropriate kinetic energy contribution, $\exp[-nt/4Dx^2]$. (Note that the kinetic term takes the form $-t/x^2$, rather than $-x^2/t$ for attractive interactions when $x < \sqrt{t}$; see [Z89ab]). Balancing the two terms, we find a saddle point solution with

$$\langle \theta^n \rangle \simeq a^n(t) e^{(n/D)^{\beta}/t^{\gamma}} \tag{6.13}$$

where $\beta = (6 - |\alpha|)/(4 - |\alpha|)$ and $\gamma = (|\alpha| - 2)/(4 - |\alpha|)$. Note that the above analysis is valid only for $-4 < \alpha < -2$. Define an effective PDF $P(\theta)$ through

$$\int_0^{\infty} d\theta\, \theta^n P(\theta) = \langle \theta^n \rangle. \tag{6.14}$$

Substituting (6.13) into (6.14) allows us to find $P(\theta)$ for large t via steepest descend methods [Z89ab],

$$P(\theta)) \sim \frac{a(t)}{\theta} \exp[-|D \ln[\theta/a(t)]|^{\eta} t^{\omega}] \tag{6.15}$$

where $\eta=(6 - |\alpha|)/2$ and $\omega = (|\alpha| - 2)/2$. From the above result, we would have $P(\theta) \sim 1/\theta$ if not for the logarithmic "correction". However, it is the latter which makes the PDF sharply restricted in the range

$$\Delta \ln[\theta/a(t)] \sim \frac{1}{D} t^{-(|\alpha|-2)/(6-|\alpha|)} \tag{6.16}$$

and as $t \to \infty$, it shrinks to zero. For example, when $-\alpha = d = 3$, where the energy spectrum $E(k) \sim k^{d-1} = k^2$, we have $\Delta \ln[\theta t^{3/2}] \sim 1/(Dt^{1/3})$. This implies that θ is concentrated on

$$\theta \simeq a(t) \simeq 1/t^{d/2}. \tag{6.17}$$

Around this center value the fluctuation (6.16) is ever smaller with increasingly larger time t. Note also that the fluctuation around the center value is symmetrical. The above result may not be surprising since a pure diffusion mechanism would yield (6.17). We conclude that, when $-4 < \alpha < -2$, disorder has only very weak effect on the $P(\theta)$-distribution, compared to the disorder-free diffusion case. It is not clear what will happen for the marginal case when α is exactly -2.

Let us now consider the case $\alpha > -2$, which includes fully developed turbulence ($\alpha = 2/3$) as a special case. Now we consider $x^{\alpha} tn/D \gg 1$ for large t and x: from (6.11), we see that the leading order of $\tilde{R}$ does not depend on R. Indeed it can be shown when the indices in (6.10) are carefully considered, that the leading order cancels the kinetic term in (6.9) exactly! In a sense this makes the whole category of turbulent fluids a marginal case. Nevertheless, the sub-leading order contributes to the moment (6.9),

$$\exp\left\{-\frac{nx^2}{4Dt} + \frac{x^2 n^2}{4D^2} \frac{x^{\alpha}}{1 + ntx^{\alpha}/D}\right\} \simeq \exp -\frac{x^{2-\alpha}}{4t^2}. \tag{6.18}$$

Therefore, x is restricted to its physical value $x \sim t^{1/z}$ when the exponential factor is order $O(1)$ and it does not depend on n. The leading n-dependent contribution to $\langle \theta^n \rangle$ comes from the factor $N(\tilde{R}, R) \sim 1/\sqrt{1 + ntx^{\alpha}/D}$ where x is to be replaced by $t^{1/z}$. Finally, we have

$$\langle \theta^n \rangle \sim a^n(t) \frac{1}{\sqrt{1 + (n/D) t^{(2+\alpha)/(2-\alpha)}}}. \tag{6.19}$$

Note that now the moment has only a relatively weak dependence on n, as compared to the exponential dependence in (6.13). Using a Mellin integral transform and the definition (6.14), we can invert (6.19) to yield the PDF

$$P(\theta) \sim \frac{a(t)}{\theta} \frac{1}{\sqrt{|\ln \theta / a(t)| t^{(2+\alpha)/(2-\alpha)}}}. \tag{6.20}$$

Now the logarithm gives only negligible correction, in contrast to the previous case. $P(\theta)$ contains an extra time dependent factor which decreases with large t. In a broad range we can now say that the distribution of θ is approximately $1/\theta$. Note that at larger times it is more likely to find smaller θ, due to the extra time factor.

Our $P(\theta)$ has ensemble average meaning. Ensemble average is not easy to realize in laboratory conditions, in particular our ensemble is time dependent so that the measurements at at given time cannot be compared with those of another time. To circumvent this difficulty we may assume, as it is generally believed, that the ensemble average is equivalent to the spatial average on a particular set of spatial points. For example we can take measurements simultaneously on points which are equi-distant from the origin where the initial inhomogeniety was placed. In this sense the $P(\theta)$ gives approximate spatial distribution which is much more easily accessible.

Let us summarize our results. Using a Feynman path integral representation we study an initial value problem of a passive scalar in a random velocity field. Our starting point is the two point correlation function of the background velocity fields. We show that even the gaussian bahavior of the fluids can result in non trivial PDF for the passive scalar. Our strategy is to find the nth moment in a closed form, by a scaling approximation. Then this moment can be inverted to find the PDF. When the velocity is sufficiently short-range correlated the passive scalar is distributed not very differently from that of the pure diffusion mechanism. For long range correlated velocities, on the other hand, the PDF is approximately $P(\theta) \sim 1/\theta$ over a broad range of θ.

We expect our results for this initial value problem can be extended to more general cases. Our initial value problem can be clearly implemented experimentally. However, the most interesting case is when there is a static PDF which is only possible when there is a nontrivial spatial distribution of the passive scalar. It is clear that any initial inhomogeneity will relax to a smooth equilibrium state in a random fluid. To have interesting distribution one has to maintain some inhomogeneity constantly in time. This is a boundary condition problem, the mean gradient of the passive scalar is non-zero. The recent experiment on temperature fluctuation in convective turbulence can be an example. We suspect our $1/\theta$ law may still be valid. A boundary condition problem can be considered as an infinite series of initial conditions, the PDF in question should also be some sort of superposition of our present result at different times. However, future investigation in this direction is needed.

The above is only a prototype calculation using unjustified gaussian ansatz (6.5). In order to confront with experiments we need to consider more realistic correlation functions. This will complicate much of the present calculation. We expect to return this point elsewhere.

6.2. Depinning by quenched randomness

6.2.1. Edge defect: replica calculation of liberation exponent [Kard87a]

Kardar considered an interesting variant of the standard 1+1 DPRM in which the directed polymer trajectories are confined to a half-space with a row of particularly favorable bonds running along the edge. If the variance of the random bonds in the bulk is sufficiently small, the polymer stays localized near the edge, taking advantage of the lower energy available there. Nevertheless, as the variance in the bulk is augmented, the polymer will make ever greater excursions into the bulk, eventually liberating itself from the pinning potential at the edge. This phase transition, involving depinning of the polymer by quenched randomness in the bulk, is the ill-condensed matter analog of critical wetting, [A80] a novel surface critical phenomena with a recent, though venerable history [MF86r], in which an interface is freed from an edge by purely thermal fluctuations [BHL83, FH85,LF86].

Kardar's starting point is the replicated partition function for the 1+1 DPRM, which leads to the n-body Hamiltonian,

$$\mathcal{H}_n = (\bar{\mu} - \tfrac{1}{2}V^2 - 2\gamma)n + \sum_{\alpha=1}^{n}\left[-\gamma\frac{\partial^2}{\partial x_\alpha^2} + \mathcal{V}_s(x_\alpha)\right] - V^2\sum_{\alpha>\beta}\delta(x_\alpha - x_\beta) \tag{6.21}$$

which is the same as before, aside from the external localization potential $\mathcal{V}_s$ that acts on the bosons, causing the wave function of a captured particle to fall off as $e^{-\lambda x}$, where $\lambda = 0$ indicates the ordinary thermal depinning transition. Although there was no precedent for a Bethe ansatz solution of interacting particles in an external potential, Kardar made the most natural choice for his many-body wave function: $\Psi_D \sim \exp(-\sum_\alpha \kappa_\alpha x_\alpha)$, with a string of momenta, $\kappa_\alpha = \lambda + 2(\alpha - 1)\kappa$, that ensures proper derivative discontinuities when two particles are exchanged and permits the particle closest to the edge to have the required exponential tail. Recall that $\kappa = V^2/4\Gamma$. With the kinetic energy equal to $\gamma\sum\kappa_\alpha^2$ as before, see Section 5.4.1, calculation of the total energy of the n-particle bound state is straightforward:

$$E_D = (\bar{\mu} - \tfrac{1}{2}V^2 - 2\gamma)n - \gamma[(\lambda^2 - 2\lambda\kappa + \tfrac{2}{3}\kappa^2)n + 2\kappa(\lambda - \kappa)n^2 + \tfrac{4}{3}\kappa^2 n^3] \tag{6.22}$$

and we find that the free energy difference between bound and unbound ($\kappa = 0$) states of the directed polymer vanishes quadratically, $\Delta f = -\Gamma(\lambda - \kappa)^2$, indicating a discontinuous interfacial specific heat, which is, coincidently, the same as in the case of thermal depinning. It should be stressed that Kardar's analysis rests upon a finite-temperature treatment and the depinning transition can be induced by increasing bulk bond randomness or equally well by raising the temperature.

Perhaps the most interesting feature of Kardar's depinning transition concerns the *quadratic* divergence of the mean interface position. It is here that depinning by quenched randomness has a unique signature. His calculation, involving an occassional deft sleight of hand, is a veritable gem – we wish to determine the mean localization length:

$$l = \lim_{n\to 0}\langle x_\alpha\rangle = \lim_{n\to 0}\left\langle \frac{1}{n}\sum_\alpha x_\alpha \right\rangle \tag{6.23}$$

which assumes, for better or worse, an unbroken replica symmetry. (All replicas equivalent!) Note that disorder average has already been performed, we are already within the replica framework and

the angular brackets refer to *thermal* expectation values calculated with the n-body wave function Ψ_D; in other words,

$$\left\langle \sum_\alpha x_\alpha \right\rangle = \int_0^\infty \prod_\alpha dx_\alpha \left(\sum_\alpha x_\alpha \right) \Psi_D(\{x_\alpha\})/N(\lambda) \tag{6.24}$$

where, as we shall soon see, the entire computation of the localization length will ride upon determining the normalization factor $N(\lambda)$, given by the sum of $n!$ equal contributions from the different orderings of the particles,

$$N(\lambda) = n! \int_0^\infty dx_1 e^{-\lambda x_1} \int_{x_1}^\infty dx_2 e^{-(\lambda+2\kappa)x_2} \cdots \int_{x_{n-1}}^\infty dx_n e^{-(\lambda+2(n-1)\kappa)x_n} \tag{6.25}$$

where the limits on the individual integrals reflect the assumed ordering $0 < x_1 < x_2 < \cdots < x_n$. Performing the integrals sequentially right to left, we obtain

$$\begin{aligned} N(\lambda) &= n! \prod_{\alpha=1}^{n} \{\alpha\lambda + [2\alpha n - \alpha(\alpha+1)]\kappa\}^{-1} \\ &= \exp\left\{ -\sum_\alpha \ln[\lambda + (2n - \alpha - 1)\kappa] \right\}. \end{aligned} \tag{6.26}$$

A moment's reflection reveals that all the necessary information is encoded in the normalization; with

$$\left\langle \sum_\alpha x_\alpha \right\rangle = -\frac{\partial}{\partial\lambda} \ln N(\lambda),$$

we have the beast in hand,

$$\left\langle \sum_\alpha x_\alpha \right\rangle = \sum_\alpha \frac{1}{\lambda + (2n - \alpha - 1)\kappa} \tag{6.27}$$

which can be rewritten,

$$l = \sum_\alpha \int_0^\infty dy\, e^{\{-[\lambda+(2n-\alpha-1)\kappa]y\}}. \tag{6.28}$$

Evaluating the sum, and bringing the resulting expression into a form that can be analytically continued in n we find,

$$l = \int_0^\infty dy \exp\{-[\lambda + (2n-1)\kappa]y\} \frac{e^{n\kappa y} - 1}{e^{\kappa y} - 1}, \tag{6.29}$$

an expression that is amenable to the possibly dangerous limit $n \to 0$, which we require to obtain our final answer:

$$l = \int_0^\infty dy\, \kappa y \frac{\exp[-(\lambda - \kappa)y]}{[1 - \exp(-\kappa y)]} \tag{6.30}$$

from which we elicit the advertised asymptotics. For very weak disorder, $\kappa \ll \lambda$, $l \sim \lambda^{-1}$ and we have the temporary linear divergence reminiscent of thermal depinning, but as the quenched randomness in the bulk is augmented, $\kappa \to \lambda$, the liberation of the directed polymer becomes characteristically quadratic, $l \sim \kappa/(\lambda - \kappa)^2$.

6.2.2. *Edge defect: numerical confirmation [ZHH91,WL91]*

Somewhat surprisingly, when Kardar sought to confirm his replica prediction for the liberation exponent via numerical transfer matrix caculations, he discovered only an *approximately linear* divergence, which he attributed to an inability to reach the asymptotic scaling regime. Using somewhat greater computational power and casting their results in terms of more appropriate scaling variables, Zapotocky and Halpin-Healy [ZHH91] managed to gain access to the true critical behavior, thereby observing the elusive *quadratic* divergence. Contemporary, but independent and somewhat more broadly focussed efforts by Wuttke and Lipowsky [WL91] were also successful in this same regard. In the simulation of Zapotocky and Halpin-Healy, based upon Kardar's SOS model in the presence of random bonds, the interface (i.e., directed polymer) runs parallel to the x-axis on a square lattice with $y \geq 1$, one end being pinned to $(0, 1)$ and a particular configuration described by the set of integer heights $\{y(x)\}$. Whenever $y(x + 1) = y(x) \pm 1$, the interface jumps vertically, incurring an elastic energy cost K, with associated Boltzmann weight $\gamma = \exp(-K)$. The horizontal segments along the edge are *weaker* ($\Rightarrow$ more favorable) than the mean of the random bond energies in the bulk, which are drawn from a uniform distribution of variance $\sigma^2 = s^2/12$. For very small values of s, the interface rather quickly attains its equilibrium distance from the edge, see Fig. 6.1, which shows the average position of polymer as a function of path length. Nevertheless, as the variance of bulk disorder strength is increased, the directed polymer wanders further and further from the edge in search of optimal energy configurations. Very long simulations become necessary as the variance is pushed toward its critical value s_c^2. Eventually, the critical value is reached and the polymer is liberated. For values $s^2 > s_c^2$, the interface very quickly frees itself, exhibiting a nearly unadulterated, characteristic wandering exponent $\zeta = \frac{2}{3}$. Fig. 6.2 shows the inverse localization length versus s^2, the latter, rather than s, being the most appropriate abscissa since the replica theory predicts $l^{-1} \sim (\text{const} - \kappa)^2$, where $\kappa^{-1} \propto \gamma/s^2$. It is important to observe that although the *quadratic* behavior clearly manifests itself as $s^2 \to s_c^2$, it is inevitably so thanks only to the inclusion of the final three data points, which required path lengths nearly 10^5 long to equilibrate, indicating the extreme numerical difficulty of the problem. For more discussion regarding depinning by quenched randomness in various guises, see the papers by Lipowsky and Fisher [HFL89,MF86r].

6.2.3. *Extended defects in the bulk [BK93,TLv93,BK94]*

Motivated by the Civale experiment [Civ91] and related efforts [Lssa93], which observed enhanced pinning of the vortex lines in ceramic superconductors irradiated by a high energy particle beam (recall Sections 5.3.5, 5.6.3), there has been much interest recently to understand the competing effects upon DPRM wandering of point disorder in the bulk versus an *isolated* extended defect, such as an ion track, dislocation line, grain boundary, or twin plane. We have just discussed the disorder-induced

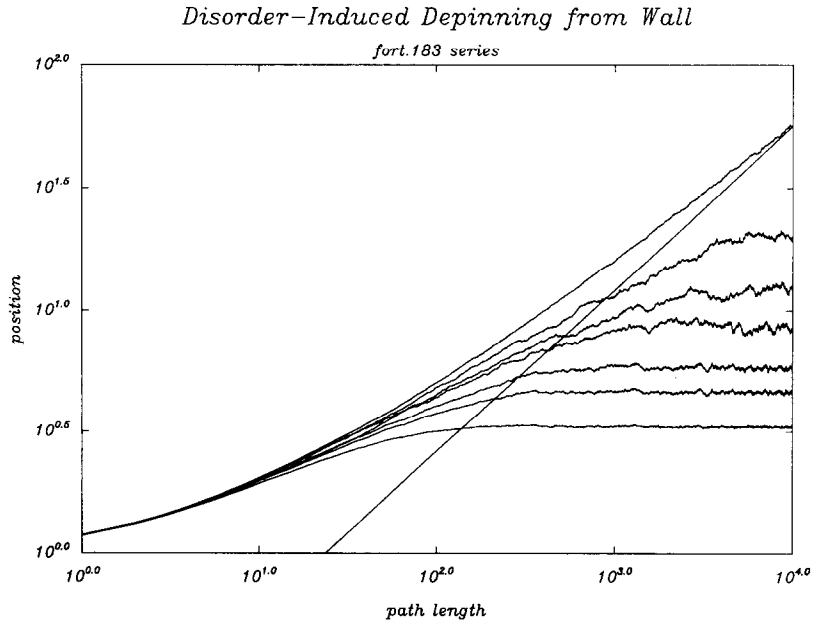

Fig. 6.1. Mean position of the 1+1 DPRM subject to an edge pinning potential, as a function of path length, for increasing values of the bulk disorder variance. Beyond a critical value, the directed polymer frees itself from the localizing potential and exhibits unadulterated disorder-induced wandering with scaling index 2/3. [ZHH91]

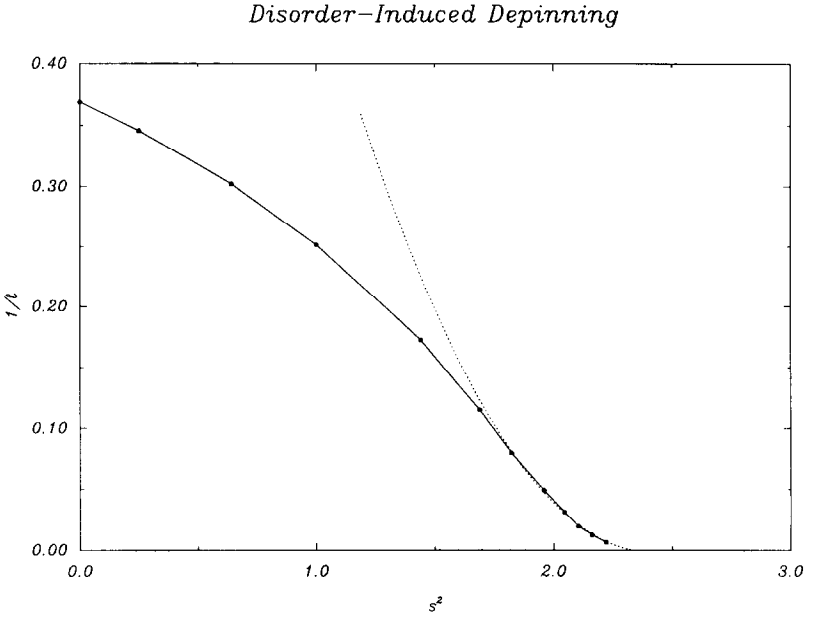

Fig. 6.2. Interfacial delocalization by quenched randomness from an edge contact potential. The inverse localization length, given by the mean position of the interface, vanishes quadratically as the variance of the bulk disorder strength attains its critical value [ZHH91].

delocalization transition in two dimensions for a linear defect running along the *edge*. Initially, it was proposed [Kard85a] that an identical transition took place from a linear defect in the *bulk*; indeed, the best numerics appeared to confirm this notion [ZHH91,LW91], despite the absence of corresponding Bethe ansatz. Nevertheless, subsequent renormalization group calculations [BK93,TLv93,HN94] have revealed that d=2 is tricky, for it is the marginal dimension for this problem; in fact, the 1+1 DPRM remains bound to a linear defect in the bulk for any finite well depth. The same is apparently true for the 2+1 DPRM localized by a planar defect [BK93,TLv93], which corresponds to the physically compelling case of a vortex line localized by a grain boundary in an actual superconducting sample. More generally, a simple power-counting argument [BK93] shows that a directed polymer remains pinned to an n-dimensional extended defect, provided the bulk dimensionality $d \leq d_c$, where the lower critical dimension (beyond which a nontrivial delocalization transition exists) is determined by the self-consistency condition

$$(d_c - n)\zeta = (1 - \omega) \tag{6.31}$$

where ζ and ω are the DPRM wandering and energy fluctuation exponents, respectively. Clearly, for a linear defect (n=1), we have $d_c(n = 1) = 2$, as advertised, since the exponents are known exactly, $(\zeta, \omega)=(\frac{2}{3}, \frac{1}{3})$. By contrast, for a planar defect, $3 < d_c(n = 2) < 4$, since $\zeta_{2+1} = \frac{5}{8}$, with the wandering exponent monotonically decreasing. For $d < d_c$, the transverse localization length diverges as the well depth vanishes with the "liberation" exponent [BK93,94],

$$\nu^{\perp} = \frac{\zeta}{1 - \omega - \zeta(d - n)} \tag{6.32}$$

which yields, for the DPRM and planar defect problem, $\nu_{\perp} \approx 4.43$ [TLv93] assuming $\zeta_{2+1} = 0.62$ [FT90], though it should be stressed that the precise value depends very sensitively on the numerical estimate employed for the wandering exponent. Numerical work by Tang and Lyuksyutov [TLv93], using a hypercubing stacking model with excess particle deposition along a line (i.e., the relevant inhomogeneous surface growth analog in the KPZ kinetic roughening context [WT90]), indicates results entirely consistent with this value. Unfortunately, direct transfer matrix simulations of the 2+1 DPRM and planar defect by Balents and Kardar [BK93,BK94] produce a lower estimate, but are subject to strong finite size effects.

Finally, regarding the second physically interesting case of a vortex line localized by a solitary columnar pin, n=1, $d = 3 > d_c$, we have the interesting possibility of a delocalization transition at finite well depth. For the 2+1 DPRM & columnar defect problem, Tang and Lyuksyutov [TLv93] extract (again, indirectly, via the growth model, but this time with deposition excess at one point,...) the liberation exponent ψ_{2+1}^{bulk}=1.8±0.6, which agrees with the functional RG analysis of Balents and Kardar [BK94], who find ≈ 1.4, a value consistent with their own numerical estimate, 1.3 ± 0.6, from transfer matrix studies of the directed polymer. Furthermore, these authors, reviving the DPRM tradition of Nattermann and Lipowsky [NL88], work very hard to connect the directed polymer to actual experiments, discussing the applicability of the single flux line limit, estimating physically relevant quantities such as pinning energies of point defects (oxygen vacancies) and well depths associated with columnar pins (ion tracks, dislocation lines) and even suggest implications for I–V characteristics. In any case, both groups confirm the absence of a similar transition in $d = 2$, with the numerics (KPZ stochastic growth [TLv93] and DPRM [BK94]) suggesting an exponentially

diverging localization length, consistent with expectations for this marginal dimension. A later RG analysis by Hwa and Nattermann [HN94], taking advantage of the mapping to the noisy Burgers equation, supports all these findings in $d = 2, 3$ and reports $\psi_{2+1}^{bulk} = 1.25$. In addition, they explain the technical difficulties that arise from an attempted replica analysis. Lastly, we mention that much of the structure (phase diagrams, fixed points, renormalization group flows,...) underlying the disorder-induced delocalization transition of the DP from a linear defect in the *bulk* can be understood by means of the Derrida-Griffiths RSRG (recall Section 5.9.5), as elegantly implemented by Tang and Lyuksyutov [TLv93, but see BK94, as well], who use it as a testing grounds to motivate their own novel RG approach which, operating in the critical regime, apparently side-steps the issue of finite-size effects.

6.3. The DPRM revisited: complex weights [Z89a-c,MKSW89]

Recall the standard DPRM is phrased via the Feynman path integral form,

$$Z(x,t) = \int_{(0,0)}^{(x,t)} \mathcal{D}x \exp\left\{ -\int d\tau \left[\frac{1}{2}\left(\frac{dx}{d\tau}\right)^2 + V(x(\tau),\tau) \right] \right\}. \tag{6.33}$$

An interesting generalization can be had by considering the complex random amplitude $\exp[-iV(\boldsymbol{x}, t)]$ in place of $\exp[-V(\boldsymbol{x}, t)]$, which renders the quantity of interest $|Z(x,t)|^2$, rather than $Z(x,t)$. For the special case where $V = 0, \pi$ randomly, we have the random amplitude ± 1. A lattice realization of the path integral would then imply a sum over directed paths with bond values assuming real, but random $\pm$ signs. It is clear that since paths terminating at the same endpoint may have opposite signs, frequent cancellations are expected in this sum; in other words, *quantum interference* is present. This is the characteristic feature of the complex directed polymer (CDP) problem, numerical evidence suggesting that the DPRM with random signs ($V = 0$ or π) and the DPRM with random phases (V drawn uniformly from the interval $[0, \pi]$) belonging to a single CDP universality class [Z89,MKSW89]. The physical motivation underlying the CDP model concerns electronic transport properties of strongly disordered metals, where the Mott variable range hopping conductivity connecting two distant points is dictated by multiple random scattering events from intervening impurities [NSS86,SW87]. In these materials, the tunneling amplitude dies exponentially with path length, so only the shortest paths are taken into account. This leads quickly to an approximation in which no backtracking is allowed, the architectural signature of the directed polymer. Extension of the CDP to situations of nonzero magnetic field, resulting in an increased localization length and a positive magnetoconductance [MKSW90], as well as the inclusion of spin-orbit effects [MK91], has been nicely summarized in a long paper by Medina and Kardar [MK92], which makes a careful presentation of the general subject of quantum interference exhibited by strongly localized electrons, possesses a healthy dose of pertinent experimental references, and proposes a *universal* probability distribution for tunneling events associated with the statistics of forward scattering paths. Somewhat surprisingly, the CDP also surfaces in a discussion of the high-temperature expansion for the spin-spin correlation function of the nearest-neighbor $\pm J$ Ising spin-glass [MKSW89]. An additional application can be found in the rich subject of light transmission in anisotropic random media, where each scatterer is represented by a random index of refraction, producing random phase shifts in the deflected coherent beam [FGZ90]. Discussion of such directed classical waves in a random medium is postponed till

Section 6.3.2, however, where a subtle unitarity constraint reveals this problem to be of a rather different ilk.

Exercise: *CDP is a generalization DP by considering complex weights, thus interference effect comes in. We may consider a further generalization: instead of a weight (complex or real) on each bond, now we have a matrix on each bond. The product of matrices in general does not commute, thus we arrive a model of non-abelian DP model. In Eq. (5.1) the integral on the exponent should have a well specified order. On a lattice this model is well defined. We expect that the interference effect still stays, but with an additional complication of non-commuting matrices. Find the scaling behavior of this generalized DP model for random SU(2) matrices.*

6.3.1. Lattice CDP [Z89a,MKSW89,MK92]

Let us consider, first, the ± problem, letting $J(x,t)$ denote the sum over all paths commencing at the origin, terminating at the point (x,t), each path contributing ± 1, depending upon the product of signs associated with sites visited along the way. The weights are constructed recursively, using the transfer matrix method,

$$J(x,t) = \eta_{x,t}[J(x+1,t-1) + J(x-1,t-1)] \tag{6.34}$$

where $\eta_{x,t}$ is the random sign at site (x,t). We are interested in the statistical properties of the fluctuating variable $\ln|J(t)|$, upon averaging over many realizations of the ± landscape. Since we would like to regard $\ln|J(t)|$ as a free energy variable, fluctuating from sample to sample, we expect $\langle \ln|J(t)| \rangle$ to behave as an extensive quantity, growing linearly with t; indeed, Medina *et al.* [MKSW89] have verified this behavior, obtaining $\langle \ln|J(t)| \rangle = (0.322 \pm 0.001)t$, for system sizes $t = 2000$, and disorder-averaging over 2000 realizations of the random energy landscape, assuming equal probability of ± signs. Interestingly, an analysis [MK92] of the finite-size correction to this quantity suggests agreement with expectations from the ordinary directed polymer [BO90,KrMHH92] and KPZ contexts [KrM90]. In analogy with the standard DPRM, the "free-energy" fluctuations, $\langle \ln|J(t)|^2 \rangle - \langle \ln|J(t)| \rangle^2$, should grow as a power t^{ω}; Medina et al. find, upon fitting their data to the asymptotic region, see Fig. 6.3, that $\omega = 0.33 \pm 0.05$. Note the rather large uncertainty, which is due to the tough statistics associated with the CDP. Even so, the evidence in favor of the standard DPRM energy exponent $\omega = 1/3$ is strong. Their analysis of the positional fluctuations confirm this picture. Plotted in Fig. 6.4 can be found $\langle [x^2]_{av} \rangle$ and $\langle [x]_{av}^2 \rangle$, which measure the transverse fluctuations of the *center* of the distribution $|J(x,t)|^2$, as well as their difference which gauges the *spread* of that distribution. Here $[\cdots]_{av}$ refers to an average over the distribution, similar to the procedure for the standard DPRM at finite temperature. From these data, Medina et al. extract the wandering exponent $\zeta = 0.68 \pm 0.05$, consistent with the known DPRM value $2/3$ for random positive weights. Furthermore, the diffusive spreading of the distribution $|J(x,t)|^2$ about its center, indicated by the scaling $t^{1/2}$, is highly reminiscent of that observed and understood within the context of the finite temperature DPRM [SVBO88,FH91]. The theoretical question of interest here concerns whether the CDP universality class differs from the standard DPRM with real, positive weights. A replica-scaling Hartree-Fock approach introduced by Zhang [Z89bc] suggested a negative response to this query, while a statistical argument by Medina et al. [MKSW89] for the CDP problem led them right back to the standard DPRM exponents! Medina and Kardar [MK92] examine the complex DPRM on

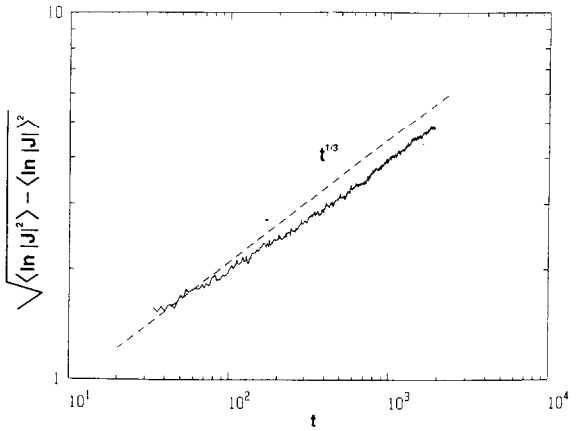

Fig. 6.3. Root mean square deviation of the "free energy" for the (1+1)-dimensional complex DPRM. Dashed line has slope $\omega = 1/3$, the value expected for the standard DPRM. Angular brackets denote disorder average [MK92].

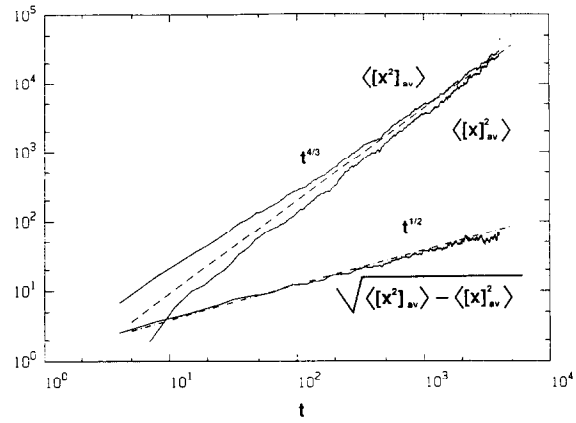

Fig. 6.4. Transverse fluctuations of the (1+1)-dimensional complex DPRM, as measured by $\langle [x^2]_{av} \rangle$ and $\langle [x]^2_{av} \rangle$. Square brackets refer to an average over lateral coordinate at a fixed t, using the weight $|J(x,t)|^2$, while angular brackets denote disorder average. The dashed line has slope $2\zeta = 4/3$. The difference between the two curves grows linearly in t, a fact used by Gelfand [Gel91] to study the universality class of the complex directed polymer. The dashed-dotted line has slope 1/2.

increasingly wider strips, showing the expected crossover from ω=1/2 (the anticipated value for the 0+1 DPRM) to ω=1/3. Finally, their very modest simulation of the 2+1 complex DPRM yields $\omega \approx 1/5$. All this indicates a single universality class.

Initial numerical results were somewhat contradictory. A few years after, the consensus reached by all parties suggests that the energy exponent in both DP and CDP is probably the same. Accepting this would jeopardize Zhang's initial position who concluded that the energy exponent $\omega = 1/2$, from the well-known exponent relation $\zeta = (1 + \omega)/2$. The ultimate answer could be a happy ending for all parties; i.e., $\omega = 1/3$ as for DP, but ζ perhaps unrelated to ω. As a matter of fact, the characteristic KPZ exponent identity need not hold for CDP, since there is no associated Galilean invariance in the complex context. One should instead directly measure the ζ exponent. In Zhang's original calculation

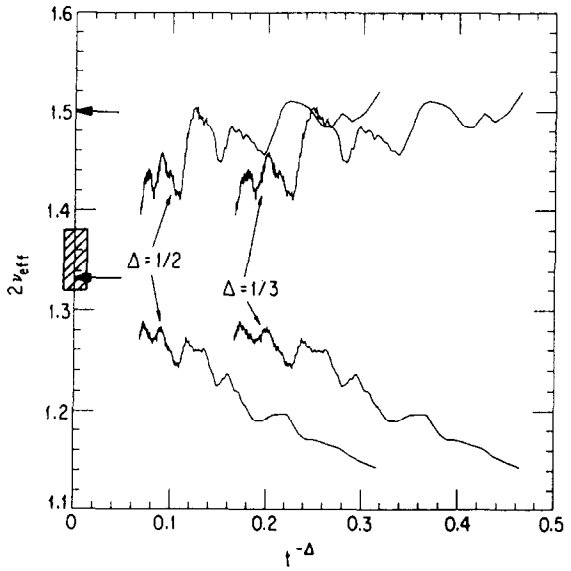

Fig. 6.5. Gelfand's careful analysis of the corrections to scaling for the complex DPRM. Here, $\Delta = 2\zeta - 1$ is the correction to scaling exponent whose value depends on the choice $\zeta = 3/4$, upper arrow [Z89a], or $\zeta = 2/3$, lower arrow [MKSW89,MK92]. Either way, Gelfand's asymptotics point to the latter, the hatched region indicating his uncertainty [Gel91].

[Z89a], with rather lengthy polymers (t_{max}=10000) to avoid potentially troublesome finite size effects, he estimated $\zeta \simeq 0.73 \pm 0.01$, leading him to conjecture $\zeta = 3/4$. As discussed above, Medina et al [MKSW89] found ζ slightly larger than the DP value 2/3. There the matter sat, awaiting third party clean up. Subsequent systematic work of Gelfand [Gel91] appears to have done just that, see Fig. 6.5, though some might object to his small system sizes (t_{max}=500), despite the exhaustive sample averaging- 100000 realizations of the random energy landscape. Nevertheless, more recent exhaustive averaging on larger samples ($t_{max} = 2000$) by Blum and Goldschmidt [BG92s] appears to confirm, once again, the notion of a single universality class.

The weak point in Zhang's replica scaling approach is usually attributed to the assumption that the physics of the DPRM is controlled by the large n limit, since the simple arguments made above suggest that the replica ground-state becomes increasingly more tightly bound, eventually invalidating the continuum limit. Indeed, recent work by Friedberg and Yu [FY94a] has tried to examine precisely this issue of lattice versus continuum versions, finding agreement between the two descriptions for sufficiently small $n = 2, 3$. Complementary work by Medina and Kardar [MK93, see also MK92], using the Derrida-Griffiths RSRG to investigate scaling properties of higher moments $\langle Z^n \rangle$ for the standard DPRM on a hierarchical lattice, seems to confirm such suspicions. For small n, their fixed point characteristic function $f^*(n) = \ln\langle Z^n \rangle$ is of universal form, while the behavior at $n > 10$, depends entirely upon the details of the bare distribution assumed, which is precisely what we would expect when the replica-bound state shrinks down to a single lattice spacing.

Admittedly, there is vast evidence in support of the thesis that CDP and DP yield identical scaling behavior. While majority maintains that DP and CDP belong to the same universality class, in spite of the interference feature; a minority (e.g. Zhang) still holds out, maintaining some difference between

the two must exist. Hint comes from the replicated model where CDP is mapped into a model of oppositely charged particles [Z89b], without necessarily the need of the large n limit. Blum, Shapir and Koltun [BSK91] has undertaken to study the nature of the boundstate of $2n$ particles. They considered the $2n$-body model proposed in [Z89b] seriously and numerically evaluated the bound-state energy for the range $0 < n < 5$, covering the range $n = 2, 3$ studied by Friedberg and Yu [FY94]. They found that the (ground) bound-state energy as a function of n scales markably well with the Zhang's earlier prediction ($\beta = 2$): $E(n) \simeq n^{\beta}$, $\beta \simeq 1.952$. One subtlety must be borne in mind here is that Friedberg and Yu used the $\pm$ amplitude model, while the $2n$ charge gas model derives from the full fledged complex weight model. General view is that these two models are identical. Recall also that for the real DP's the bound-state has $\beta = 3$. While the bound-state calculation of Blum et al.[BSK91] provides precious information for the nature of the boundstate, showing the qualitative difference with the real DP counterpart, Zhang cannot claim victory since all attempts so far to directly measure the free energy fluctuations fail to reveal significant deviations in scaling from the real DP case. However, the qualitative difference in replica boundstate's nature cannot be reconciled with the majority's point of view either. We may even be led to doubt some fundamentals that we should not doubt: Is the replica mapping always faithful? How can such qualitative difference (if any) show up in the original model? In almost all the simulations, people based their conclusions by calculating the second moment of the transverse deviation and the free energy. Maybe only some weird high moments can show much wanted the difference? Or the the replica picture is not relevant at all for any n, and CDP and DP models are but one. But this possibility will upset everybody since all camps use the replica approach. The comprehensive understanding is still out in the wild, maybe some subtle point has not been appreciated so far. In further research the reader may have the chance to put a final word.

6.3.2. Directed waves in random media: unitary versus nonunitary case [FGZ90,MKS91,SKR92]

Recall that the standard DPRM [KZ87] can be viewed as diffusion in a dynamically random potential, with restricted partition function $\Psi(x, t)$ governed by the equation

$$\partial_t \Psi = [\Gamma \nabla^2 + V(x, t)]\Psi \tag{6.35}$$

with $V(x, t)$ a random, but *real* function, typically assumed uncorrelated in space and time. Allowing V to be imaginary, we obtain the complex DPRM, apparently in the same universality class, see Section 6.3.1. Permitting Γ to be imaginary as well leads us literally to the Schrödinger equation for a particle in a time-dependent random potential, which is, however, an altogether different beast. This last problem was introduced to the kinetic roughening community by Feng, Golubović and Zhang [FGZ90] who, interested in interference effects arising from the propagation of multiply-scattered, but entirely directed waves in random media, suggested a possible link to the complex directed polymer. Their motivation was to model light propagation in a medium with random index of refraction – a situation of great practical importance, but inherently *nonunitary* since it involves a total amplitude that decreases in the propagation direction; in other words, probability is not conserved.

Interestingly, it was quickly pointed out by Medina, Kardar, and Spohn [MKS91] that the distinct *unitary* directed wave problem was fundamentally distinct from the complex DPRM, thanks to special unitary properties of the Schrödinger equation, associated with the conserved norm $\int dx|\Psi(x, t)|^2$, which precludes the possibility of a replica bound-state ever forming. By rigorously imposing the

unitarity condition, they obtained numerics indicating that the transverse wandering of the beam center of mass was *subdiffusive*, scaling as $t^{\approx 0.3}$ in 1+1 dimensions, in marked contrast to the superdiffusive behavior characteristic of the DPRM, where the known exponent is 2/3. Subsequent, more refined numerical work by Bouchaud, Touati, and Sornette [BTS92] suggested that the wandering exponent was closer to 1/4, while the width of the wave packet scaled diffusively- the wavefunction, itself, possessing novel multifractal properties. Later numerical efforts by Saul, Kardar, and Read [SKR92], based upon a novel S-matrix approach rather than brute force, but properly unitary, integration of the Schrödinger equation [MKS91,BTS92], confirmed unambiguously that the exponent was 1/4 in 1+1 dimensions. By contrast, for the physically relevant case of 2+1 dimensions, they discovered logarithmic behavior. The method of Saul, Kardar and Read is noteworthy because it employs a numerical discretization for which unitarity is manifestly preserved and, furthermore, permits certain disorder averages to be computed exactly. Finally, [SKR92] show, in a very natural way, how these scaling laws emerge from a simple arguments based upon two interacting random walkers. Friedberg and Yu [FY94b] have fully developed these analytical matters, explicitly calculating the asymptotics, coefficients, and leading corrections, in addition to considering more general interactions between the walkers.

6.4. *Diverse manifolds in random media [HH89a,HH90,MP91]*

Consider an n-component vector field $z(x)$ of d'-dimensional support, subject to the competing effects of elasticity and disorder-induced roughening. Many recent outstanding problems in ill-condensed matter are naturally incorporated within such a general framework, including domain-wall roughening in random-field (RF) and random-bond (RB) Ising models of magnetism (n=1, d' arbitrary), the wandering of directed polymers in random media (n arbitrary, $d' = 1$), as well as the impurity-induced distortion of the Abrikosov flux-line lattice in dirty superconductors. Halpin-Healy, motivated by work of Kardar [Kard87b] and Nattermann [N87] on models of correlated disorder interpolating between RF and RB magnets, and the many-dimensional DPRM [KZ87], proposed a unified treatment of diverse manifolds in random media [HH89a, 90], focussing his attention upon the critical index $\zeta_{d',n}$ defined by the scaling relation $\langle |z| \rangle \sim |x|^{\zeta}$. Using an approximate one-loop *functional* RG calculation, adapted to the ill-condensed matter context by Fisher [DF86], he generalized the notions of Imry-Ma [IM76,GM83] to the category of arbitrary elastic manifolds governed by disorder of arbitrary correlation, determined the range of validity of such naive scaling arguments, and finally, for the case of quenched, short-range correlated random media, determined the roughening exponent to be $\zeta_{d',n} = 2(4 - d')/(8 + n)$. Analytical fallout from Halpin-Healy's functional RG included:

(i) Corroboration of the exact (?) wandering exponent for the (1+1)-dimensional DPRM with correlated disorder, $\zeta_{1+1}(\beta \leq \frac{1}{2}) = 3/(4 + \beta)$; $\zeta_{1+1}(\beta \geq \frac{1}{2}) = 2/3$, first obtained by Kardar [Kard87b] and Nattermann [N87] using an entirely different, 1-loop dynamic RG approach for the KPZ equation; recall Section 4.3.1, where β dictates the tail of the correlated disorder.

(ii) Determination of the roughening exponent for domain walls in random-bond Ising magnets. Halpin-Healy's estimate: $\zeta_{RB} = \frac{2}{9}\epsilon$, where $\epsilon = (4 - d')$, provides a counterpoint to the celebrated Imry-Ma value [IM76], $\zeta_{RF} = \frac{\epsilon}{3}$, for the random-field Ising model and yields the correct value, with $d' = 1$, for the 1+1 DPRM wandering exponent. Using the functional RG, he found $\zeta(\beta)$ for arbitrarily correlated disorder, there being, interestingly, a short-ranged fixed point function that controls the scaling for all $\beta \geq \frac{1}{2}$, see Fig. 6.6. It should be stressed that the "exactness" of

these values remains, very much, an open question. Even the Imry-Ma index for the RF Ising model, basking for the past decade in its victory over the ill-fated and incorrect supersymmetry prediction $\zeta_{RF} = \epsilon/2$ (see [GG84], for an excellent history of associated experimental and theoretical controversies), is only known with certainty for $d' = 1$, where a rigorous proof due to Imbrie [I84] had established this to be the lower critical dimension of the model, corroborating earlier numerical work [FGIK83] that had indicated $\zeta_{RF}(d' = 1) = 1$. Indeed, Fisher's own estimate for the random-bond exponent, $\zeta_{RB} \approx 0.2083\epsilon$ [DF86], based upon a numerical implementation of the functional RG, has received some additional support from a subsequent, but truncated three-parameter version of the RG by Nattermann and Leschhorn [NL91]. Clearly, for both RF and RB cases, high precision numerical work needs to be done for the most physically compelling dimensionality $d' = 2$! Such a project was initiated by Kardar and Zhang [KZ89], leading to the effective values $\zeta_{RF} = 0.59 \pm 0.07$ and $\zeta_{RB} = 0.50 \pm 0.08$, where the generalized transfer matrix techniques evolved a world-sheet through the random medium. Unfortunately, however, their efforts suffered somewhat from some finite-size effects. Even so, this stubborn numerical matter may yield its secrets to the next generation of computers.

(iii) To understand properly the troublesome phenomena of "giant flux creep" in ceramic superconductors, we must appreciate the collective effects of disorder on the roughening of the vortex lattice. In the long-wavelength limit, the most natural description invokes continuum elasticity theory with a 2d distortion field $z(x)$ describing the local displacement of the flux-line lattice (FLL) in 3d space, a collection of elastic moduli, and a random pinning potential meant to model the FLL interaction with defects – precisely one of the scenarios alluded to above! For this case, Halpin-Healy's functional RG approach predicts the FLL roughening exponent $\zeta_{3,2} = \frac{1}{5}$, a result obtained later via entirely independent arguments by Feigel'man, Geshkenbein, Larkin, and Vinokur [FGLV89]. Knowledge of $\zeta_{3,2}$ permits us to characterize the nature of flux-creep phenomena in the case of collective pinning of the lattice by disorder, including the scaling properties of the activation barrier heights, average bundle size and hopping distance [for details see, FGLV89, Milne94r].

(iv) For the many-dimensional DPRM ($d' = 1$), Halpin-Healy's functional RG approach [HH90] yields $\zeta_{n+1} = 6/(8 + n)$, which captures the exact result for the 1+1 DPRM, correctly mimics, though slightly overestimates the monotonic decline of the wandering exponent with increasing n (as noted explicitly in the Derrida-Griffiths RSRG [HH89b]), though mistakenly (?) predicts a finite upper critical dimension $n_c = 4$, whereas the prevailing wisdom maintains (and the high precision KPZ growth model simulations [AHK92] confirm), $\zeta_{1,n}$ drops gently, asymptotically approaching its entropic value $\frac{1}{2}$ in the limit $n \to \infty$. The truncated functional RG of Nattermann and Leschhorn [NL91] gives $\zeta_{1+1} \approx 0.633$, but exacerbates the false issue of a finite UCD, producing $n_c \approx 2.6$, an unfortunate value also obtained via Fisher's numerical implementation of the functional RG [GL91]. Interestingly, various approximate implementations of the mode-coupling approach [HF91] to the KPZ equation by Schwartz and Edwards [SE92], Bouchaud and Cates [BC93], and Doherty et al. [DMKB94] produce $n_c \approx 3.25$, 3.75, and 3.6, respectively, see however [Tu94]. Even so, an intriguing argument by Bouchaud and George [BG91] suggests that the directed percolation provides a lower bound to the DPRM wandering exponent, indicating that $n = 4$ may be a special value after all.

More recently, the functional RG has been applied to other instances of elastic media subject to quenched random disorder, such as pinned charged density waves [NF92], localization of elastic

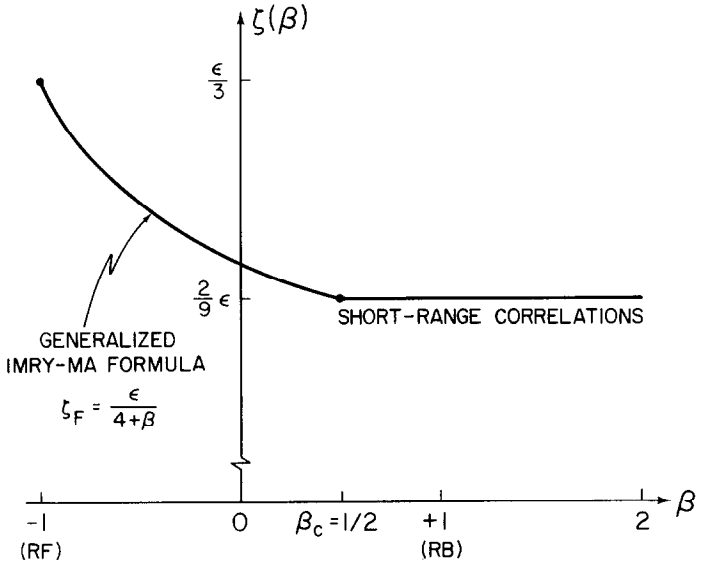

Fig. 6.6. Interfacial roughening exponent ζ as a function of β, which describes the decay of impurity correlations. A generalized Imry-Ma argument is only correct for sufficiently long-ranged correlations; for example $\beta = -1$ corresponds to the RF Ising model, where it is known that $\zeta_{RF} = \epsilon/3$. Beyond the critical value $\beta_c = 1/2$, however, a single SR FPF dictates the scaling properties and ζ sticks to the RB value.

layers by correlated disorder [B93], and diverse manifolds in the large n limit [BF93]. This last effort is of particular interest because the authors obtain the very same roughness exponent as Mezard and Parisi [MP91], who have employed a gaussian variational ansatz to investigate possible consequences of replica symmetry breaking (RSB) within a field theoretic formulation of the diverse manifold problem. This variational replica field theory, despite being calculationally formidable, has the virtue of providing, perhaps, some additional physical insight, since the hierarchical breaking of symmetry permits one to handle, in a potentially natural way, the many metastable states of the manifold. Moreover, Mezard and Parisi show that the inclusion of RSB converts the incorrect supersymmetry prediction [PS79], $\zeta_{RF} = (4-d')/2$ into the proper Imry-Ma value, $\zeta_{RF} = (4-d')/3$. Unfortunately, however, the variational treatment yields the Flory expression $\zeta_{d',n} = (4-d')/(4+n)$ for uncorrelated disorder, which is wrong in general and certainly so for the 1+1 DPRM, where it predicts 3/5. Even so, the method has inspired later efforts, including a variational RSB approach to various pinning effects on vortex lattices [BMY91,BG92], as well as a growing appreciation of the random energy landscape in the directed polymer context, where rare, but dominating events [HF94] can control disorder averages.

Acknowledgments

This review started with a suggestion by Itamar Procaccia a couple of years ago. While the deadlines for its delivery have been repeatedly missed, in compensation we were able to benefit from the considerable knowledge accumulated in the last few years. We are indebted to many colleagues and friends who have shared with us their insights, enthusiasm, and offered us help. In particular,

we want to mention Jean-Philippe Bouchaud, Bernard Derrida, Deephak Dhar, Terry Hwa, Mogens Jensen, Mehran Kardar, Mike Kosterlitz, Amos Maritan, Thomas Nattermann, Giorgio Parisi, Itamar Procaccia, Gene Stanley, Chao Tang, Lei-Han Tang, Dietrich Wolf and Po-zen Wong. One of us, Y.-C.Z. has benefitted from the long time, fruitful collaboration with Parisi and Kardar. The other, T.H.-H., is much indebted to Joachim Krug for a careful reading of an earlier manuscript, many constructive criticisms, as well as a recent profitable stay in Cologne. In carrying out this work in different stages, the authors have been visiting scientists for extensive periods and received important support from various institutions: T.H.-H. is grateful to the Isaac Newton Institute, Cambridge University; Y.-C.Z. thanks Nordita, Copenhagen and Phys. Dept of Aarhus University, especially Hans Fogedby, for the kind hospitality. Finally, the efforts of T.H.-H. have been supported by the Troisième Cycle en Suisse Romande, the National Science Foundation (NSF DMR 92-1140), and the Petroleum Research Fund of the American Chemical Society, and those of Y.-C.Z. by INFN, CNRS, and Swiss National Foundation.

References

Relevant review articles and books:

[JHP94] C. Jayaprakash, F. Hayot, and R. Pandit, Phys. Rev. Lett. **72**, 308 (1994).

[F88r] J. Feder, *Fractals*, (Plenum Press, New York, 1988).

[FLN91r] G. Forgacs, R. Lipowsky and T. Nieuwenhuizen, "Behavior of Interfaces in Ordered and Disordered Systems," in *Phase Transitions and Critical Phenomena*, Volume 14, C. Domb and J. L. Lebowitz, eds. (Academic Press, London, 1991).

[FV91r] F. Family and T. Vicsek, eds., *Dynamics of Fractal Surfaces*, (World Scientific, Singapore, 1991).

[HR90r] H. J. Herrmann and S. Roux, eds., *Statistical Models for the Fracture of Disordered Media*, (Elsevier, Amsterdam, 1990).

[Kr90r] J. Krug, *Die Entstehung fraktaler Oberflachen* (Harri Deutsch, Frankfurt, 1990).

[KrS91r] J. Krug and H. Spohn, in *Solids Far From Equilibrium: Growth, Morphology and Defects*, C. Godreche, ed. (Cambridge University Press, Cambridge, 1991).

[KV94r] J. Kertész and T. Vicsek, "Self-Affine Interfaces," in *Fractals & Disorder 2*, S. Havlin and A. Bunde, eds. (Springer-Verlag, Berlin, 1994).

[JKMW92r] R. Jullien, J. Kertész, P. Meakin and D. E. Wolf, eds., *Surfaces Rugueuses*, 1992 Les Houches Winter School, France (Nova-Science, New York, 1993).

[M86r] P. Meakin, in *On Growth and Form*, H. E. Stanley and N. Ostrowsky, eds. (M. Nijhoff, Dordrecht, 1986).

[M88r] P. Meakin, in *Phase Transitions and Critical Phenomena*, Volume 12, C. Domb and J. L. Lebowitz, eds. (Academic Press, London, 1988).

[M93r] P. Meakin, "The Growth of Rough Surfaces and Interfaces," Phys. Rep. **235**, 191 (1993).

[Man82r] B. B. Mandelbrot, *Fractal Geometry of Nature*, (Freeman, San Francisco, 1982).

[MF86r] M. E. Fisher, "Interface Wandering in Pure and Impure Media," J. Chem. Soc., Faraday Transactions, II **82**, 1569 (1986).

[Milne94r] G. Blatter, M. V. Feigel'man, V. B. Geshkenbein, A. I. Larkin, and V. M. Vinokur, "Vortices in High Temperature Superconductors," Rev. Mod. Phys. **66**, no. 4 (1994).

[MPV87r] M. Mézard, G. Parisi and M. Virasoro, *Spin Glass Theory and Beyond*, (World Scientific, Singapore, 1987).

[Ram86r] R. Rammal, G. Toulouse, and M. A. Virasoro, "Ultrametricity for Physicists," Rev. Mod. Phys. **58**, 765 (1986).

[SZ95r] B. Schmittmann and R.K.P. Zia, "Statistical Machanics of Diffusion Driven Systems" in *Phase Transitions and Critical Phenomena*, eds. C. Domb and J.L. Lebowitz (Academic Press, London, 1995).

References:

[A80] D. Abraham, Phys. Rev. Lett. **44**, 1165 (1980).
[A87] S. R. Anderson, Phys. Rev. B**36**, 8435 (1987).
[ABS94] L. A. N. Amaral, A.-L. Barabasi, and H. E. Stanley, Phys. Rev. Lett. **73**, 62 (1994).
[AC79] S. M. Allen and J. W. Cahn, Acta Metall. **27**, 1085 (1979).
[AF90] J. Amar and F. Family, Phys. Rev. A**41**, 3399RC (1990).
[AF91] J. Amar and F. Family, J. Phys. A**24**, L79 (1991).
[AF92] J. Amar and F. Family, Phys. Rev. A**45**, 5378 (1992).
[AF93] J. Amar and F. Family, Phys. Rev. E**47**, 1595 (1993).
[AFG93] M. Albrecht, H. Fritzsche, and U. Gradmann, Surf. Sci. **294**, 1 (1993).
[AHHK94] I. Arsenin, T. Halpin-Healy, and J. Krug, Phys. Rev. E **49**, R3561 (1994). to appear.
[AHHR89] L. de Arcangelis, A. Hansen, H. J. Herrmann, and S. Roux, Phys. Rev. B**40**, 877 (1989).
[AHK92] T. Ala-Nissila, T. Hjelt, and J. M. Kosterlitz, Europhys. Lett. **19**, 1 (1992).
[AHKV93] T. Ala-Nissila, T. Hjelt, and J. M. Kosterlitz, and O. Venäläinen, J. Stat. Phys. **72**, 207 (1993).
[ALF91] J. Amar, P.-M. Lam, and F. Family, Phys. Rev. A**43**, 4548RC (1991).
[ARH85] L. de Arcangelis, S. Redner, and H. J. Herrmann, J. Physique Lett. **46**, 585 (1985).
[AV94] T. Ala-Nissila and O. Venäläinen, "Scaling Exponents for Driven 2d Surface Growth," J. Stat. Phys. **76**, 1083 (1994).
[B74] J. M. Burgers, *The Nonlinear Diffusion Equation,* (Riedel, Boston, 1974).
[B90] G. S. Bales, et al., Science **249**, 264 (1990).
[B93] L. Balents, Europhys. Lett. **24**, 489 (1993).
[BA84] R. Bruinsma and G. Aeppli, Phys. Rev. Lett. **52**, 1547 (1984).
[Bau81] R. Bausch, V. Dohm, H. K. Janssen and R. K. P. Zia, Phys. Rev. Lett. **47** 1837 (1981).
[BBL93] J.-P. Bouchaud, E. Bouchaud, G. Lapasset, J. Planes, Phys. Rev. Lett. **71**, 2240 (1993).
[BBS91] V. Ben-Avrahm, R. Bidaux and L. S. Schulman, Phys. Rev. A**43** 7093 (1991).
[BC93] J.-P. Bouchaud and M. E. Cates, Phys. Rev. E**47**, 1455RC (1993); erratum, *ibid*, **48**, 635E (1993).
[BF93] L. Balents and D. S. Fisher, Phys. Rev. B**48**, 5949 (1993).
[BF94] A. Berera and L.-Z. Fang, Phys. Rev. Lett. **72**, 458 (1994).
[BG91] J.-P. Bouchaud and A. Georges, private communication.
[BG92] J.-P. Bouchaud and A. Georges, Phys. Rev. Lett. **68**, 3908 (1992).
[BG92s] T. Blum and Y. Y. Goldschmidt, Nuc. Phys. B**380**, 588 (1992).
[BH91] A. J. Bray and K. Humayan, J. Phys. A**24**, L1185 (1991).
[BH91u] J.-P. Bouchaud and D. A. Huse, unpublished.
[BH93] A. Bunde and S. Havlin, *Percolations*, to appear.
[BHK91] S. Buldyrev, A.-L. Barabasi, S. Havlin, J. Kertész, H. E. Stanley, T. Vicsek, Phys. Rev. A**43**, 7113 (1991).
[BHL83] E. Brézin, B. I. Halperin, and S. Leibler, Phys. Rev. Lett. **50**, 1387 (1983).
[BHV91] R. Bourbonnais, H.J. Herrmann and T. Vicsek, Int. J. Mod. Phys. C**2**, 719 (1991).
[Bin81] K. Binder, Z. Phys. B**43**, 119 (1981).
[BK92] L. Balents and M. Kardar, J. Stat. Phys. **67**, 1 (1992).
[BK93] L. Balents and M. Kardar, Europhys. Lett. **23**, 503 (1993).
[BK94] L. Balents and M. Kardar, Phys. Rev. B **49**, 13030 (1994).
[BKS85] H. van Beijeren, R. Kutner, and H. Spohn, Phys. Rev. Lett. **54**, 2026 (1985).
[BKW91] R. Bourbonnais, J. Kertész, and D.E. Wolf, J. Phys. II France **1**, 493 (1991).
[BLP90] E. Bouchaud, G. Lapasset, and J. Planès, Europhys. Lett. **13**, 73 (1990).
[BMY91] J.-P. Bouchaud, M. Mézard and J. Yededia, Phys. Rev. Lett. **67**, 3840 (1991).
[BO90] J.-P. Bouchaud and H. Orland, J. Stat. Phys. **61**, 877 (1990).
[BRZ89] G. S. Bales, A. C. Redfield, and A. Zangwill, Phys. Rev. Lett. **62**, 776 (1989).
[Boston92] S. V. Buldyrev, A.-L. Barabasi, F. Caserta, S. Havlin, H. E. Stanley, T. Viscek, Phys. Rev. A**45** 8313RC (1992).
[BS93] P. Bak and K. Sneppen, Phys. Rev. Lett. **71**, 4083 (1993).

[BS94] A.-L. Barabasi and H. E. Stanley, *Fractal Concepts in Surface Growth* (Cambridge Univ. Press, Cambridge, 1995).
[BSK91] T. Blum, Y. Shapir and D. S. Koltun, J. de Physique I **1**, 613 (1991).
[BTS92] J.-P. Bouchaud, D. Touati and D. Sornette, Phys. Rev. Lett. **68**, 1787 (1992).
[BTW87] P. Bak, C. Tang and K. Wiesenfeld, Phys. Rev. Lett. **59**, 381 (1987).
[BU91] S. Havlin, A.-L. Barabasi, S. V. Buldyrev, C. K. Peng, M. Schwartz, H. E. Stanley, T. Viscek, in Proceedings of Granada Conf., Spain (Oct.7-11, 1991), ed. by J. M. Garcia-Ruiz et al. (Plenum, New York, 1993).
[Bud92] R. C. Budhani, M. Swenaga, and S.-H. Liou, Phys. Rev. Lett. **69**, 3816 (1992).
[CD89] J. Cook and B. Derrida, J. Stat. Phys. **57**, 89 (1989).
[Chev91] J. Chevrier, V. Le Thanh, R. Buys, and J. Derrien, Europhys. Lett. **16**, 737 (1991).
[CHSVV93] Z. Csahok, K. Honda, E. Somfai, M. Vicsek, T. Vicsek, Physica **A200**, 136 (1993).
[Chud90] E.M. Chudnovsky, Phys. Rev. Lett. **65**, 3060 (1990).
[Civ91] L. Civale, et al., Phys. Rev. Lett. **67**, 648 (1991).
[Cot93] M. Cotta, et al., Phys. Rev. Lett. **70**, 4106 (1993).
[CP93] P. Constantin and I. Procaccia, Phys. Rev. E **47**, 3307 (1993).
[CR88] M. Cieplak and M. O. Robbins, Phys. Rev. Lett. **60**, 2042 (1988); Phys. Rev. B**41**, 11508 (1990).
[CS80] J. L. Cardy and R. L. Sugar, J. Phys. A**13**, L423 (1980).
[CSV93] A. Czirók, E. Somfai, and T. Vicsek, Phys. Rev. Lett. **71**, 2154 (1993).
[CV92] Z. Csahók and T. Vicsek, Phys. Rev. A**46**, 4577 (1992).
[D85] D. Dhar, Phys. Rev. Lett. **54**, 2058 (1985).
[D87a] D. Dhar, Phase Transitions **9**, 51 (1987).
[D87b] D. Dhar, in *Proceedings of the Solid State Physics Symposia*, Vol. **30A**, Trombay, India, 27-31 December 1987 (Dept. Atomic Energy, India).
[DDM92] B. Derrida, E. Domany, and D. Mukamel, J. Stat. Phys. **69**, 667 (1992).
[DE93] B. Derrida and M. R. Evans, J. Phys. I France **3**, 311 (1993).
[DE94] B. Derrida and M. R. Evans, preprint.
[DEHP93] B. Derrida, M. Evans, V. Hakim, and V. Pasquier, J. Phys. A**26**, 1493 (1993).
[DEM93] B. Derrida, M. Evans, and D. Mukamel, J. Phys. A**26**, 4911 (1993).
[DF86] D. Fisher, Phys. Rev. Lett. **56**, 1964 (1986).
[DG89] B. Derrida and R. B. Griffiths, Europhys. Lett. **8**, 111 (1989).
[DG90] B. Derrida and O. Golinelli, Phys. Rev. A**41**, 4160 (1990).
[DH75] U. Deker and F. Haake, Phys. Rev. A**11**, 2043 (1975).
[DHHT93] H. Diratzouian, T. Halpin-Healy, and B. Tamminga, unpublished work.
[DK92] C. Doty and J. M. Kosterlitz, Phys. Rev. Lett. **69**, 1979 (1992).
[DMKB94] J. P. Doherty, M. A. Moore, J. M. Kim, and A. J. Bray, Phys. Rev. Lett. **72**, 2041 (1994).
[DMVW94r] M. Droz, A. J. McKane, J. Vannimenus, and D. E. Wolf, eds., *Scale Invariance, Interfaces and Nonequilibrium Dynamics*, (Plenum Press, New York 1995).
[DS88] B. Derrida and H. Spohn, J. Stat. Phys. **51**, 817 (1988).
[DS89] P. Devillard and H. E. Stanley, Physica A**160**, 298 (1989).
[DST91] S. Das Sarma and P. Tamborenea, Phys. Rev. Lett. **66**, 325 (1991).
[DV83] B. Derrida, J. Vannimenus, Phys. Rev. B**27**, 4401 (1983).
[DZ92] G. Deitler and Y.-C. Zhang, Physica A**191**, 2133 (1992).
[E58] M. Eden, in *Symposium on Information Theory in Biology*, H.P. Yockey, ed. (Pergamon Press, New York, 1958).
[E61] M. Eden, in *Proc. Fourth Berkeley Symposium on Mathematical Statistics and Probability*, F. Neyman, ed., Vol. IV (UC-Berkeley, 1961).
[E64] S. F. Edwards, J. Fluid Mech. **18**, 239 (1964).
[EBJ94] E. Ben-Jacob et al., Fractals **2**, 15 (1994).
[EE84] W. Ebeling, A. Engel, B. Esser, and R. Fiestel, J. Stat. Phys. **37**, 369 (1984).
[EE87] A. Engel and W. Ebeling, Phys. Rev. Lett. **59**, 1979 (1987).
[EG92] D. Eaglesham and G. Gilmer, in *Surfaces Rugueuses*.
[EH66] G. Ehrlich and F. G. Hudda, J. Chem. Phys. **44**, 1039 (1966).

[EK92] D. Ertas and M. Kardar, Phys. Rev. Lett. **69**, 929 (1992).
[Ekl91] E. Eklund, R. Bruinsma, J. Rudnick, R. S. Williams, Phys. Rev. Lett. **67**, 1759 (1991); also, Surf. Sci. **285**, 157 (1993).
[Ern94] H.-J. Ernst, F. Fabre, R. Folkerts, and J. Lapujoulade, Phys. Rev. Lett. **72**, 112 (1994).
[Ess88] J. W. Essam, A. J. Guttmann, K. De'Bell, J. Phys. A**21**, 3815 (1988).
[EW82] S. F. Edwards and D.R. Wilkinson, Proc. Roy. Soc. London A**381**, 17 (1982).
[F63] W. Feller, An Introduction to Probability Theory and its Applications (Wiley, New York, 1963).
[F82] J. Finn, et al., Phys. Rev. Lett. **49**, 1321 (1982).
[F86] F. Family, J. Phys. A**19**, L441 (1986).
[F88r] J. Feder, *Fractals*, (Plenum Press, New York, 1988).
[F94] E. Frey and U. C. Tauber, Phys. Rev. E **50**, 1024 (1994); see also [SP94].
[F95] E. Frey and U.C. Tauber, work in progress.
[FA79] S. Fishman and A. Aharony, J. Phys. C**12**, L729 (1979).
[FCA92] F. Family, K. Chan, and J. Amar, in *Surfaces Rugueuses*.
[FFH91] D. S. Fisher, M. P. A. Fisher, and D. A. Huse, Phys. Rev. B**43**, 130 (1991).
[FGIK83] J. F. Fernandez, G. Grinstein, Y. Imry, and S. Kirkpatrick, Phys. Rev. Lett. **51**, 203 (1983).
[FGLV89] M. V. Feigel'man, V. B. Geshkenbein, A. I. Larkin, and V. M. Vinokur, Phys. Rev. Lett. **63**, 2303 (1989).
[FGZ90] S. Feng, L. Golubović, and Y.-C. Zhang, Phys. Rev. Lett. **65**, 1028 (1990).
[FH85] D. S. Fisher and D.A. Huse, Phys. Rev. B**32**, 247 (1985).
[FH91] D. S. Fisher and D.A. Huse, Phys. Rev. B**43**, 10728 (1991).
[FLN91r] G. Forgacs, R. Lipowsky and T. Nieuwenhuizen, "Behavior of Interfaces in Ordered and Disordered Systems," in *Phase Transitions and Critical Phenomena,* Volume 14, C. Domb and J. L. Lebowitz, eds. (Academic Press, London, 1991).
[FM89] H. Fujikawa and M. Matsushita, J. Phys. Soc. Jpn. **58**, L3875 (1989); Physica A **168**, 493 (1990).
[FNS77] D. Forster, D. R. Nelson, and M. J. Stephen, Phys. Rev. A**16**, 732 (1977).
[FT90] B. M. Forrest and L.-H. Tang, Phys. Rev. Lett. **64**, 1405 (1990).
[FV85] F. Family and T. Vicsek, J. Phys. A**18**, L75 (1985).
[FV88] M. V. Feigel'man and V. M. Vinokur, Phys. Rev. Lett. **61**, 1139 (1988).
[FV91r] F. Family and T. Vicsek, eds., *Dynamics of Fractal Surfaces*, (World Scientific, Singapore, 1991).
[FWGF89] M. P. A. Fisher, P. B. Weichman, G. Grinstein, and D. S. Fisher, Phys. Rev. B**40**, 546 (1989).
[FY77] H. Fujisaka and T. Yamada, Prog. Theor. Phys. **57**, 734 (1977).
[FY94a] R. Friedberg and Y.-K. Yu, "The Replica Model at Low Integer N For DPRM," Phys. Rev. E **49**, 4157 (1994).
[FY94b] R. Friedberg and Y.-K. Yu, "Directed Waves in Random Media: An Analytical Calculation," Phys. Rev. E **49**, 5755 (1994).
[FZ94] G. Foltin et al., Phys. Rev. E **50**, R639 (1994).
[G84] N. Goldenfeld, J. Phys. A**17**, 2807 (1984).
[Gam91] P. L. Gammel, L. F. Schneemeyer, and D. J. Bishop, Phys. Rev. Lett. **66**, 953 (1991).
[GB93] Y. Y. Goldschmidt and T. Blum, Phys. Rev. E**47**, 2979RC (1993).
[GE93] S.J. Gould and N. Elridge, Nature **366**, 223 (1993).
[Gel91] M. P. Gelfand, Physica A**177**, 67 (1991).
[GG84] G. Grinstein, J. Appl. Phys. **55**, 2371 (1984).
[GGN83] D. G. Green, A. M. Gill, and I. R. Noble, Ecolog. Modeling **20**, 33 (1983).
[HR90r] H. J. Herrmann and S. Roux, eds., *Statistical Models for the Fracture of Disordered Media*, (Elsevier, Amsterdam, 1990).
[GKGG84] E. T. Gawlinski, K. Kaski, M. Grant, and J. D. Gunton, Phys. Rev. Lett. **53**, 2266 (1984).
[GL91] S. Grotehans and R. Lipowsky, unpublished.
[GM83] G. Grinstein and S.-K. Ma, Phys. Rev. B**28**, 2588 (1983).
[GS85] G. S. Grest and D. J. Srolovitz, Phys. Rev. B**32**, 3014 (1985).
[GS92a] L.-H. Gwa and H. Spohn, Phys. Rev. Lett. **68**, 725 (1992).
[GS92b] L.-H. Gwa and H. Spohn, Phys. Rev. A**46**, 844 (1992).
[GW88] D. J. Gates and M. Westcott, Proc. Roy. Soc. London A**416**, 443, 463 (1988).

[GZ94] S. Galluccio and Y.-C. Zhang, preprint May 1994.
[Han91] A. Hansen, E. L. Hinrichsen, and S. Roux, Phys. Rev. Lett. **66**, 2476 (1991).
[Hay93] F. Hayot, C. Jayaprakash, and Ch. Josserand, Phys. Rev. E**47**, 911 (1993).
[HB91] K. Humayun and A. J. Bray, J. Phys. A**24** 1915 (1991).
[He92] Y.-L. He, H.-N. Yang, T.-M. Lu, and G.-C. Wang, Phys. Rev. Lett. **69**, 3770 (1992).
[Her92] P. Herrasti, et al., Phys. Rev. A**45**, 7440 (1992).
[HF91] T. Hwa and E. Frey, Phys. Rev. A**44**, 7873RC (1991).
[HF94] T. Hwa and D. Fisher, Phys. Rev. B**49**, 3136 (1994).
[HFL89] M. Huang, M.E. Fisher, and R. Lipowsky, Phys. Rev. B**39**, 2632 (1989).
[HFV91a] V. K. Horváth, F. Family and T. Vicsek, J. Phys. A**24**, L25 (1991).
[HFV91b] V. K. Horváth, F. Family and T. Vicsek, Phys. Rev. Lett. **67**, 3207 (1991).
[HH89a] T. Halpin-Healy, Phys. Rev. Lett. **62**, 445 (1989).
[HH89b] T. Halpin-Healy, Phys. Rev. Lett. **63**, 917C (1989).
[HH90] T. Halpin-Healy, Phys. Rev. A**42**, 711 (1990).
[HH91] T. Halpin-Healy, Phys. Rev. A**44**, 3415RC (1991).
[HH92] T. Halpin-Healy and A. Assdah, Phys. Rev. A**46**, 3527 (1992).
[HH93] T. Halpin-Healy, unpublished.
[HHH93] T. Halpin-Healy and D. Herbert, Phys. Rev. E**48**, 1617RC (1993).
[HHR93] A. Hansen, E. L. Hinrichsen, and S. Roux, J. Phys. I France **3**, 1569 (1993).
[HL92] T. C. Halsey and M. Liebig, Phys. Rev. A**46**, 7793 (1992).
[HN94] T. Hwa and T. Nattermann, "Disorder-Induced Depinning Transition," Phys. Rev. B **51**, 455 (1995).
[HNV93] T. Hwa, D. Nelson, and V. M. Vinokur, Phys. Rev. B**48**, 1167 (1993).
[HP82] G. E. Hentschel and I. Procaccia, Phys. Rev. Lett. **49**, 1158 (1982).
[HuH85] D. A. Huse and C. Henley, Phys. Rev. Lett. **54**, 2708 (1985).
[HuHF85] D. A. Huse, C. Henley, and D. S. Fisher, Phys. Rev. Lett. **55**, 2924 (1985).
[Hwa92] T. Hwa, Phys. Rev. Lett. **69**, 1552 (1992).
[Hy86] J. M. Hyman, B. Nicolaenko, and S. Zaleski, Physica D**23**, 265 (1986).
[I84] J. Z. Imbrie, Phys. Rev. Lett. **53**, 1747 (1984).
[I86] J. Z. Imbrie, Physica A**140** 291 (1986).
[I87] J.Z. Imbrie, unpublished.
[IM76] Y. Imry and S.-K. Ma, Phys. Rev. Lett. **35**, 1399 (1976).
[IS88] J. Z. Imbrie and T. Spencer, J. Stat. Phys. **52**, 609 (1988).
[J94] B. Jovanović et al., Phys. Rev. E **50**, R2403 (1994).
[JB85a] R. Jullien and R. Botet, Phys. Rev. Lett. **54**, 2055 (1985).
[JB85b] R. Jullien and R. Botet, J. Phys. A**18**, 2279 (1985).
[JHP93] C. Jayaprakash, F. Hayot, and R. Pandit, Phys. Rev. Lett. **71**, 12 (1993).
[JKMW92r] R. Jullien, J. Kertész, P. Meakin and D. E. Wolf, eds., *Surfaces Rugueuses*, 1992 Les Houches Winter School, France (Nova-Science, New York, 1993).
[JM87] R. Jullien and P. Meakin, Europhys. Lett. **4**, 651 (1987).
[John94] M. Johnson, et al., Phys. Rev. Lett. **72**, 116 (1994).
[JR91] H. Ji and M. O. Robbins, Phys. Rev. A**44**, 2538 (1991).
[JR92] H. Ji and M. O. Robbins, Phys. Rev. B**46**, 14519 (1992).
[JZ92] E. Jacquet and Y.-C. Zhang, unpublished.
[K84] Y. Kuramoto, *Chemical Oscillations, Waves, and Turbulence*, (Springer, Berlin, 1984).
[Kard85a] M. Kardar, Phys. Rev. Lett. **55**, 2235 (1985).
[Kard85b] M. Kardar, Phys. Rev. Lett. **55**, 2923 (1985).
[Kard87a] M. Kardar, Nucl. Phys. B**290** [FS20], 582 (1987).
[Kard87b] M. Kardar, J. Appl. Phys. **61**, 3601 (1987).
[Kauff93] S. Kauffman, *The Origins of Order*, (Oxford Univ. Press, New York, 1993).
[KBM91a] J.M. Kim, A.J. Bray, and M.A. Moore, Phys. Rev. A**44**, 2345 (1991).
[KBM91b] J.M. Kim, A.J. Bray, and M.A. Moore, Phys. Rev. A**44**, 4782 (1991).
[Keb93] P. Keblinski, Phys. Rev. Lett. **71**, 805C (1993).

[KHHB93] J. Krim, I. Heyvaert, C. van Haesendonck, and Y. Bruynseraede, Phys. Rev. Lett. **70**, 57 (1993).
[KK89] J.M. Kim and J.M. Kosterlitz, Phys. Rev. Lett. **62**, 2289 (1989).
[KL85] J. Koplik and H. Levine, Phys. Rev. B**32**, 280 (1985).
[KL92] M. Kotrla, A.C. Levi and P. Smilauer, Europhys. Lett. **20**, 25 (1992).
[KLS92] D. Kessler, H. Levine, and L. Sander, Phys. Rev. Lett. **69**, 100 (1992).
[KLT91] D. A. Kessler, H. Levine, and Y. Tu, Phys. Rev. A**43**, 4551 (1991).
[KM92] D. Kandel and D. Mukamel, Europhys. Lett. **20**, 325 (1992).
[KMr92] S. Kramer and M. Mardar, Phys. Rev. Lett. **68**, 205 (1992).
[Ko89] R. H. Koch, et al., Phys. Rev. Lett. **63**, 1511 (1989).
[Kon91] M. Konczykowski, et al., Phys. Rev. B**44**, 7167 (1991).
[KPZ86] M. Kardar, G. Parisi, and Y.-C. Zhang, Phys. Rev. Lett. **56**, 889 (1986).
[Kr87] J. Krug, Phys. Rev. A**36**, 5465 (1987).
[Kr89] J. Krug, J. Phys. A**22**, L769 (1989).
[Kr90r] J. Krug, *Die Entstehung fraktaler Oberflachen* (Harri Deutsch, Frankfurt, 1990).
[Kr91a] J. Krug, J. Phys. I France **1**, 9 (1991).
[Kr91b] J. Krug, Phys. Rev. A**44**, 801RC (1991).
[Kr91c] J. Krug, Phys. Rev. Lett. **67**, 1882 (1991).
[Kr94] J. Krug, "Turbulent Interfaces," Phys. Rev. Lett. **72**, 2907 (1994).
[Kr94u] J. Krug, unpublished work.
[KrHH93] J. Krug and T. Halpin-Healy, J. Phys. I France **3**, 2179 (1993).
[KrM89] J. Krug and P. Meakin, Phys. Rev. A**40**, 2064 (1989).
[KrM90] J. Krug and P. Meakin, J. Phys. A**23**, L987 (1990).
[KrM91] J. Krug and P. Meakin, Phys. Rev. Lett. **66**, 703 (1991).
[KrMHH92] J. Krug, P. Meakin, T. Halpin-Healy, Phys. Rev. A**45**, 638 (1992).
[KrPS93] J. Krug, M. Plischke, and M. Siegert, Phys. Rev. Lett. **70**, 3271 (1993).
[KrS88] J. Krug and H. Spohn, Phys. Rev. A**38**, 4271 (1988).
[KrS89] J. Krug and H. Spohn, Europhys. Lett. **8**, 219 (1989).
[KrS90] J. Krug and H. Spohn, Phys. Rev. Lett. **64**, 2232 (1990).
[KrS91r] J. Krug and H. Spohn, in *Solids Far From Equilibrium: Growth, Morphology and Defects*, C. Godreche, ed. (Cambridge University Press, Cambridge, 1991).
[KrT94] J. Krug and L.-H. Tang, Phys. Rev. E **50**, 104 (1994).
[Ktsz92] J. Kertész, Physica A**191**, 208, (1992).
[Ktsz93] J. Kertész, V. K. Horváth, and F. Weber, Fractals **1**, 67 (1993).
[KV94r] J. Kertész and T. Vicsek, "Self-Affine Interfaces," in *Fractals & Disorder 2*, S. Havlin and A. Bunde, eds. (Springer-Verlag, Berlin, 1994).
[KW88] J. Kertész and D. E. Wolf, J. Phys. A**21**, 747 (1988).
[KZ87] M. Kardar and Y.-C. Zhang, Phys. Rev. Lett. **58**, 2087 (1987).
[KZ89] M. Kardar and Y.-C. Zhang, Europhys. Lett. **8**, 233 (1989).
[L62] I. M. Lifshitz, Sov. Phys. JETP **15**, 939 (1962).
[L85] T. Liggett, *Interacting Particle Systems*, (Springer-Verlag, Berlin, 1985).
[L93] H. Leschhorn, Physica A**195**, 324 (1993).
[LDS91] Z.-W. Lai and S. Das Sarma, Phys. Rev. Lett. **66**, 2348 (1991).
[LF86] R. Lipowsky and M. E. Fisher, Phys. Rev. Lett. **57**, 2411 (1986); Phys. Rev. B**36**, 2126 (1987).
[LLPP93] V. S. L'vov, V. V. Lebedev, M. Paton, and I. Procaccia, Nonlinearity **6**, 25 (1993).
[LP88] D. Liu and M. Plischke, Phys. Rev. B**38**, 4781 (1988).
[LP92] V. S. L'vov and I. Procaccia, Phys. Rev. Lett. **69**, 3543 (1992).
[LP94] V. S. L'vov and I. Procaccia, Phys. Rev. Lett. **72**, 307 (1994).
[LR91] D. Lely and S. Roux, J. Phys. III France **1**, 1675 (1991).
[LS92] C.-H. Lam and L. M. Sander, Phys. Rev. Lett. **69**, 3338 (1992).
[LS93a] C.-H. Lam and L. M. Sander, Phys. Rev. Lett. **71**, 561 (1993).
[LS93b] C.-H. Lam and L. M. Sander, Phys. Rev. E**48**, 979 (1993).
[Lssa93] M. Leghissa, et al., Phys. Rev. B**48**, 1341 (1993).

[LSW92] C.-H. Lam, L. M. Sander, and D. E. Wolf, Phys. Rev. A**46**, 6128RC (1992).
[LT93] S. Liang and C. Tang, Phys. Rev. Lett. **71**, 2769 (1993).
[LT94] H. Leschhorn and L.-H. Tang, Phys. Rev. E**49**, 1238 (1994).
[Lv92] I. F. Lyuksyutov, Europhys. Lett. **20**, 273 (1992).
[M59] W. W. Mullins, J. Appl. Phys. **30**, 77 (1959).
[M81] P. Manneville, Phys. Lett. A**84**, 129 (1981).
[M86r] P. Meakin, in *On Growth and Form*, H. E. Stanley and N. Ostrowsky, eds. (M. Nijhoff, Dordrecht, 1986).
[M87] P. Meakin, J. Phys. A**20**, L1113 (1987).
[M88r] P. Meakin, in *Phase Transitions and Critical Phenomena,* Volume 12, C. Domb and J. L. Lebowitz, eds. (Academic Press, London, 1988).
[M90u] A. Maritan, unpublished.
[M93r] P. Meakin, "The Growth of Rough Surfaces and Interfaces," Phys. Rep. **235**, 191 (1993).
[Ma94] A. Maritan et al., Rev. Mod. Phys., in preparation.
[Mal88] A. P. Malozemoff, T. K. Worthington, Y. Yeshurun, and F. Holtzberg, Phys. Rev. B**38**, 7203 (1988).
[Mål92] K. Måløy, A. Hansen, E. Hinrichsen, and S. Roux, Phys. Rev. Lett. **68**, 213 (1992).
[Man82r] B. B. Mandelbrot, *Fractal Geometry of Nature*, (Freeman, San Francisco, 1982).
[Mark84] R. E. Mark, ed., *Handbook of Physical and Mechanical Testing of Paper and Paperboard,* Vol. 1, (Marcel Dekker, New York, 1984).
[Méz90] M. Mézard, J. Physique (Paris) **51**, 1831 (1990).
[MCR91] N. Martys, M. Cieplak, M. O. Robbins, Phys. Rev. Lett. **66**, 1058 (1991); Phys. Rev. B**44**, 12294 (1991).
[MF86r] M. E. Fisher, "Interface Wandering in Pure and Impure Media," J. Chem. Soc., Faraday Transactions, II **82**, 1569 (1986).
[MHKZ89] E. Medina, T. Hwa, M. Kardar, and Y.-C. Zhang, Phys. Rev. **A 39**, 3053 (1989).
[Mi94] S. Mukherji, Phys. Rev. E **50**, R2407 (1994).
[Mill92] D. Miller, K. Gray, R. Kampwirth, and J. Murduck, Europhys. Lett. **19**, 27 (1992).
[Milne94r] G. Blatter, M. V. Feigel'man, V. B. Geshkenbein, A. I. Larkin, and V. M. Vinokur, "Vortices in High Temperature Superconductors," Rev. Mod. Phys., to appear.
[MJ87] P. Meakin and R. Jullien, J. Physique (Paris) **48**, 1651 (1987).
[MJB86] P. Meakin, R. Jullien, and R. Botet, Europhys. Lett. **1**, 609 (1986).
[MK91] E. Medina and M. Kardar, Phys. Rev. Lett. **66**, 3187 (1991).
[MK92] E. Medina and M. Kardar, Phys. Rev. B**46**, 9984 (1992).
[MK93] E. Medina and M. Kardar, J. Stat. Phys. **71**, 967 (1993).
[MKS91] E. Medina, M. Kardar, and H. Spohn, Phys. Rev. Lett. **66**, 2176 (1991).
[MKSW89] E. Medina, M. Kardar, Y. Shapir, and X. R. Wang, Phys. Rev. Lett. **62**, 941 (1989).
[MKSW90] E. Medina, M. Kardar, Y. Shapir, and X. R. Wang, Phys. Rev. Lett. **64**, 1816 (1990).
[MM88] A.J. McKane and M.A. Moore, Phys. Rev. Lett. **60**, 527 (1988).
[MM92] S. Matsuura and S. Miyazima, Physica A**191**, 30 (1992).
[MM93] T. Matsuyama and M. Matsushita, Crit. Rev. Microbiol. **19**, 117 (1993).
[Mo72] D. Mollison, Nature **240**, 467 (1972).
[MP90] M. Mézard and G. Parisi, J. Phys. A**23**, L1229 (1990).
[MP91] M. Mézard and G. Parisi, J. Phys. France I **1**, 809 (1991).
[MP94] S. Maslov and M. Paczuski, Phys. Rev. E **50**, 643AC (1994).
[MPAF89] M. P. A. Fisher, Phys. Rev. Lett. **62**, 1415 (1989).
[MPB94] S. Maslov, M. Paczuski and P. Bak, Phys. Rev. Lett. **73**, 2162 (1994).
[MPV87r] M. Mézard, G. Parisi and M. Virasoro, *Spin Glass Theory and Beyond,* (World Scientific, Singapore, 1987).
[MRSB86] P. Meakin, P. Ramanlal, L. Sander, and R. Ball, Phys.Rev. A**34**, 5091 (1986).
[MS63] W. W. Mullins and R. F. Sekerka, J. Appl. Phys. **34**, 323 (1963); *ibid,* **35**, 444 (1964).
[MTKB92] A. Maritan, F. Toigo, J. Koplik, and J. R. Banavar, Phys. Rev. Lett. **69**, 3193 (1992).
[MW90] A. Margolina and H. E. Warriner, J. Stat. Phys. **60**, 809 (1990).
[MW92] K. Moser and D. E. Wolf, *Surfaces Rugueuses*; also, K. Moser, J. Kertész and D. E. Wolf, Physica A**178**, 215 (1991).
[MW94] K. Moser and D. E. Wolf, J. Phys. A **27**, 4049 (1994).

[MZ90] U. M. B. Marconi and Y.-C. Zhang, J. Stat. Phys. **61**, 885 (1990).
[N85] T. Nattermann, Phys. Stat. Sol. b**132**, 125 (1985).
[N87] T. Nattermann, Europhys. Lett. **4**, 1241 (1987).
[N88] T. Nattermann, Phys. Rev. Lett. **60**, 2701 (1988).
[Nel88] D. R. Nelson, Phys. Rev. Lett. **60**, 1973 (1988); also, D. R. Nelson and H. S. Seung, Phys. Rev. B**39**, 9153 (1989).
[Nel92] D. R. Nelson and V. M. Vinokur, Phys. Rev. Lett. **68**, 2398 (1992).
[NF92] O. Narayan and D. Fisher, Phys. Rev. Lett. **68**, 3615 (1992); Phys. Rev B**46**, 11520 (1992).
[Nh88] T. M. Nieuwenhuizen, J. Phys. A**21**, L567 (1988).
[NKMR93] C. S. Nolle, B. Koiller, N. Martys, and M. O. Robbins, Phys. Rev. Lett. **71**, 2074 (1993).
[NL88] T. Nattermann and R. Lipowsky, Phys. Rev. Lett. **61**, 2508 (1988).
[NL91] T. Nattermann and H. Leschhorn, Europhys. Lett. **14**, 603 (1991).
[NO88] J. N. Negele and H. Orland, *Quantum Many Particle Systems*, (Addison-Wesley, New York, 1988).
[NR88] T. Nattermann and W. Renz, Phys. Rev. B**38**, 5184 (1988).
[NR90] T. Nattermann and W. Renz, unpublished.
[NSS86] V. L. Nguyen, B. Z. Spivak, and B. I. Shklovskii, JETP Lett. **41**, 42 (1986).
[NSTL92] T. Nattermann, S. Stepanow, L.-H. Tang, and H. Leschhorn, J. Phys. II France **2**, 1483 (1992).
[NT92] L.-H. Tang and T. Nattermann, Phys. Rev. A**45**, 7156 (1992).
[NZ94] S. Nechaev and Y.-C. Zhang, preprint (1994), to appear in Phys. Rev. Lett.
[OMM92] M. Ohgiwari, M. Matsushita and T. Matsuyama, J. Phys. Soc. Japan **61**, 816 (1992).
[OPZ94] Z. Olami, I. Procaccia, and R. Zeitak, Phys. Rev. E**49**, 1232 (1994).
[OPZ94r] Z. Olami, I. Procaccia, and R. Zeitak, Weizmann preprint (1994).
[Oz77] S. A. Orszag, "Fluid Dynamics," in Proceedings-Les Houches 1973, R. Balian and J.-L. Peube, eds. (Gordon and Breach, London, 1977).
[P92] I. Procaccia, et al., Phys. Rev. A**46**, 3220 (1992).
[Pa90] G. Parisi, J. Physique (Paris) **51**, 1595 (1990).
[Pa90o] G. Parisi, Rend. Acad. Naz. Lincei, **XI-1**, 277 (1990).
[Pa91] G. Parisi and L. Pietronero, Europhys. Lett. **16**, 321 (1991).
[Pa92] G. Parisi, Europhys. Lett. **17**, 673 (1992).
[PC93] I. Procaccia and P. Constantin, Phys. Rev. Lett. **70**, 3416 (1993).
[Per92] E. Perlsman and M. Schwartz, Europhys. Lett. **17**, 11 (1992).
[PHH93] N.-N. Pang and T. Halpin-Healy, Phys. Rev. E**47**, 784RC (1993).
[PHSS91] C.-K. Peng, S. Havlin, M. Schwartz, and H. E. Stanley, Phys. Rev. A**44**, 2239RC (1991).
[PJ90] Y. P. Pellegrini and R. Jullien, Phys. Rev. Lett. **64**, 1745 (1990).
[PK94] G. Palasantzas and J. Krim, Phys. Rev. Lett. **73**, 3564 (1994).
[PMB94] M. Paczuski, J. Maslov and P. Bak, Europhys. Lett. **27**, 96 (1994).
[Poi92] C. Poirier, M. Ammi, D. Bideau, and J.-P. Troadec, Phys. Rev. Lett. **68**, 216 (1992).
[PPP84] Y. Pomeau, A. Pumir, and P. Pelce, J. Stat. Phys. **37**, 39 (1984).
[PR85] M. Plischke and Z. Rácz, Phys. Rev. A**32**, 3825 (1985).
[PRL87] M. Plischke, Z. Rácz and D. Liu, Phys. Rev. B**35**, 3485 (1987).
[PS79] G. Parisi and N. Sourlas, Phys. Rev. Lett. **43**, 744 (1979).
[PSW93] M. Plischke, et al., Phys. Rev. Lett. **71**, 2509 (1993).
[PYHH94] N.-N. Pang, Y.-K. Yu and T. Halpin-Healy, work in progress.
[PZ84] G. Parisi and Y.-C. Zhang, Phys. Rev. Lett. **53**, 1791 (1984).
[PZ85] G. Parisi and Y.-C. Zhang, J. Stat. Phys. **41**, 1 (1985).
[PZ86] G. Parisi and Y.-C. Zhang, Brookhaven Internal Report, BNL38274 (1986).
[PZ89] I. Procaccia and R. Zeitak, Phys. Rev. Lett. **62**, 2128 (1989).
[R73] D. Richardson, Proc. Camb. Phil. Soc. **74**, 515 (1973).
[Ram86r] R. Rammal, G. Toulouse, and M. A. Virasoro, "Ultrametricity for Physicists," Rev. Mod. Phys. **58**, 765 (1986).
[RF86] R. Friedberg, Ann. Phys. (NY) **171**, 321 (1986).
[RH91] S. Roux and A. Hansen, J. Stat. Phys. **65**, 183 (1991).

[RH94] S. Roux and A. Hansen, J. de Physique **I4**, 515, (1994).
[RHG87] S. Roux, A. Hansen, and E. Guyon, J. Phys. (Paris) **48**, 2125 (1987).
[RHH91] S. Roux, A. Hansen, E. L. Hinrichsen, J. Phys. A**24**, L295 (1991).
[RRR93] A. Rinaldo, I. Rodriguez-Iturbe, R. Rigon, E. Ijjasz-Vasquez and R. L. Bras, Phys. Rev. Lett. **70**, 822 (1993).
[RSLP91] Z. Rácz, M. Siegert, D. Liu, and M. Plischke, Phys. Rev. A**43**, 5275 (1991).
[Rubio89] M. A. Rubio, C. A. Edwards, A. Dougherty, and J. P. Gollub, Phys. Rev. Lett. **63**, 1685 (1989).
[S77] G. I. Sivashinsky, Acta. Astron. **4**, 1177 (1977); *ibid*, **6**, 560 (1979).
[S80] G. I. Sivashinsky and D. M. Michelson, Prog. Theor. Phys. **63**, 2112 (1980).
[S88] M. Schroeder, *Fractals, Chaos, and Power-Laws* (Freeman, San Francisco, 1991).
[S91] Y. Shapir, Phys. Rev. Lett. **66**, 1473 (1991).
[S93] G. W. Smith, et al., J. Cryst. Growth **127**, 966 (1993).
[Salv92] R. C. Salvarezza, et al., Europhys. Lett. **20**, 727 (1992).
[Sch90] B. Schmittmann, Int. J. Mod. Phys. B**4**, 2269 (1990).
[SE92] M. Schwartz and S. Edwards, Europhys. Lett. **20**, 301 (1992).
[SGG89] T. Sun, H. Guo, and M. Grant, Phys. Rev. A**40**, 6763 (1989).
[Shap87] J. A. Shapiro, J. Bacteriol. **169**, 142 (1987).
[SJ93] K. Sneppen and M. Jensen, Phys. Rev. Lett. **70**, 3833 (1993); *ibid*, **71**, 101 (1993).
[SK94] P. Smilauer and M. Kotrla, Phys. Rev. B **49**, 5769RC (1994).
[SKR92] L. Saul, M. Kardar, and N. Read, Phys. Rev. A**45**, 8859 (1992).
[Sne92] K. Sneppen, J. Krug, M. H. Jensen, C. Jayaprakash and T. Bohr, Phys. Rev. A**46**, 7352RC (1992).
[Snp92] K. Sneppen, Phys. Rev. Lett. **69**, 3539 (1992).
[Snt93] A.S. Sznitman, Prob. Th. Rel. Fields **95**, 155 (1993); Comm. Pure Appl. Math, in press.
[SP92] M. Siegert and M. Plischke, Phys. Rev. Lett. **68**, 2035 (1992).
[SP94] T. Sun and M. Plischke, "Field-Theory Renormalization Approach to KPZ," Phys. Rev. E **49**, 5046 (1994); M. Siegert and M. Plischke, Phys. Rev. Lett **73**, 1517 (1994).
[SPD93] J. Stroscio, D. Pierce, and R. Dragoset, Phys. Rev. Lett. **70**, 3615 (1993).
[SS66] R. Schwoebel and E. Shipsey, J. Appl. Phys. **37**, 3682 (1966); also, R. Schwoebel, J. Appl. Phys. **40**, 614 (1969).
[Sud92] J. Sudijono, M. D. Johnson, C. Snyder, M. Elowitz, and B. G. Orr, Phys. Rev. Lett. **69**, 2811 (1992); also, Surf. Sci. **280**, 247 (1993).
[SVBO88] U. Schulz, J. Villain, E. Brézin, and H. Orland, J. Stat. Phys. **51**, 1 (1988).
[SWP93] M. Schroeder, et al., Europhys. Lett. **24**, 563 (1993).
[SW87] Y. Shapir and X. R. Wang, Europhys. Lett. **4**, 1165 (1987).
[SY89] Ya. G. Sinai and V. Yakhot, Phys. Rev. Lett. **63**, 1962 (1989).
[SZ93] D. Sornette and Y.-C. Zhang, Geophys. J. Int. **113**, 382 (1993).
[T86] D. Turcotte, J. Geophys. Res. B**91**, 1921 (1986).
[T94] L.-H. Tang, "Two-Repulsive Lines on Disordered Lattices," J. Stat. Phys. **77**, 581 (1994).
[TFW92] L.-H. Tang, B. M. Forrest, and D. E. Wolf, Phys. Rev. A**45**, 7162 (1992).
[TH64] P. A. Tydeman and A. M. Hiron, B.P. & B.I.R.A. Bulletin **35**, 9 (1964).
[Tha83] J. Thacker, Rev. Mod. Phys. **54** (1983).
[TI92] H. Takayasu and H. Inaoka, Phys. Rev. Lett. **68**, 966 (1992).
[TKW91] L.-H. Tang, J. Kertész, D. E. Wolf, J. Phys. A**24**, L1193 (1991).
[TL92] L.-H. Tang and H. Leschhorn, Phys. Rev. A**45**, 8309RC (1992).
[TL93] L.-H. Tang and H. Leschhorn, Phys. Rev. Lett. **70**, 3832 (1993).
[TLv93] L.-H. Tang and I. F. Lyuksyutov, Phys. Rev. Lett. **71**, 2745 (1993).
[TN91] L.-H. Tang and T. Nattermann, Phys. Rev. Lett. **66**, 2899 (1991).
[TNF90] L.-H. Tang, T. Nattermann, and B. Forrest, Phys. Rev. Lett. **65**, 2422 (1990).
[Tu94] Y. Tu, Phys. Rev. Lett. **73**, 3109 (1994).
[TW94] W.M. Tong et al., Phys. Rev. Lett. **72**, 3374 (1994).
[V84] J. Villain, Phys. Rev. Lett. **52**, 1543 (1984).
[V91] J. Villain, J. Phys. I France **1**, 19 (1991).
[VCH90] T. Vicsek, M. Cserzö, and V. K. Horváth, Physica A**167**, 315 (1990).

[Vul89] A. Vulpiani, Physica D**38**, 372 (1989).
[W87] D. E. Wolf, J. Phys. A**20**, 1251 (1987).
[WB72] T. Williams and R. Bjerknes, Nature **236**, 19 (1972).
[WK87a] D. E. Wolf and J. Kertész, Europhys. Lett. **4**, 651 (1987).
[WK87b] D. E. Wolf and J. Kertész, J. Phys. A**20**, L257 (1987).
[WL91] J. Wuttke and R. Lipowsky, Phys. Rev. B**44**, 13042 (1991).
[Wong85] P.-z. Wong, Physics Today, **41**, 24 (1988).
[Wong92a] G. Kahanda, X. Zou, R. Farrell, and P.-z. Wong, Phys. Rev. Lett. **68**, 3741 (1992).
[Wong92b] S. He, G. Kahanda, and P.-z. Wong, Phys. Rev. Lett. **69**, 3731 (1992).
[Wong92c] P.-z. Wong, private communication.
[Wong93] G. Kahandra and P.-z. Wong, Phys. Rev. Lett. **71**, 806C (1993).
[WS81] T. Witten and L. Sander, Phys. Rev. Lett. **47**, 1400 (1981).
[WT90] D. E. Wolf and L.-H. Tang, Phys. Rev. Lett. **65**, 1591 (1990).
[WV90] D. E. Wolf and J. Villain, Europhys. Lett. **13**, 389 (1990).
[WVZ92] M. R. Wilby, D. D. Vvedensky, and A. Zangwill, Phys. Rev. B**46**, 12896RC (1992); *ibid*, B**47**, 16068E (1993).
[WW83] D. Wilkinson and J. Willemsen, J. Phys. A **16**, 3365 (1983).
[Y81] V. Yakhot, Phys. Rev. A**24**, 642 (1981).
[Y92] H. Yan, Phys. Rev. Lett. **68**, 3048 (1992).
[YPHH94] Y.-K. Yu, N.-N. Pang, and T. Halpin-Healy, Phys. Rev. E **50**, 511 (1994).
[You93] H. You, R. Chiarello, H. Kim, and K. Vandervoort, Phys. Rev. Lett. **70**, 2900 (1993).
[Z86a] Y.-C. Zhang, Phys. Rev. Lett. **56**, 2113 (1986).
[Z86b] Y.-C. Zhang, J. Phys. A**19**, L941 (1986).
[Z87] Y.-C. Zhang, Phys. Rev. Lett. **59**, 1979 (1987).
[Z88] Y.-C. Zhang, Phys. Rev. Lett. **60**, 2702 (1988).
[Z89a] Y.-C. Zhang, Phys. Rev. Lett. **62**, 979C (1989).
[Z89b] Y.-C. Zhang, Europhys. Lett. **9**, 113 (1989).
[Z89c] Y.-C. Zhang, J. Stat. Phys. **57**, 1123 (1989).
[Z90a] Y.-C. Zhang, J. Physique **51**, 2129 (1990).
[Z90b] Y.-C. Zhang, Physica A**170**, 1 (1990).
[Z90c] Y.-C. Zhang, Rome preprint 1990, unpublished.
[Z90d] Y.-C. Zhang, Phys. Rev. B**42**, 4897 (1990).
[Z92] Y.-C. Zhang, J. Phys. I France **2**, 2175 (1992).
[Z94u] Y.-C. Zhang, unpublished work.
[Zal85] S. Zaleski and P. Lallemand, J. Physique Lett. **46**, L793 (1985).
[Zal89] S. Zaleski, Physica D**34**, 427 (1989).
[ZHH91] M. Zapotocky and T. Halpin-Healy, Phys. Rev. Lett. **67**, 3463C (1991).
[Zinn84] J. Zinn-Justin, in *Recent Advances in Field Theory and Statistical Mechanics*, J.-B. Zuber and R. Stora, eds. (North-Holland, Amsterdam 1984).
[Zt92] T. Zaitsev, Physica A**189**, 411 (1992).
[ZZAL92] J. Zhang, Y.-C. Zhang, P. Alstrom and M. T. Levinsen, Physica A**189**, 383 (1992).